THE DEFORMATION OF INHOMOGENOUS MATERIALS AND CONSEQUENT GEOLOGICAL IMPLICATIONS

by

NICHOLAS CHARLES GAY

A thesis submitted for the degree of Doctor of Philosophy at the University of London

August, 1966.

ABSTRACT

This thesis is a theoretical and experimental study of the deformation of inhomogenous materials by simple and pure shear. The model adopted is that of a homogenous, Newtonian fluid matrix, in which are embedded rigid or deformable inclusions. The inclusions are ellipsoidal or elliptical in shape and the deformable ones are also assumed to be Newtonian bodies, but they may differ from the matrix in coefficient of viscosity.

Published work on rock deformation is reviewed to show that rock does, in certain geological environments, approximate closely to a Newtonian body.

Equations are derived to describe the motion and changes in shape of the inclusions (or particles as they are called) during deformation of the model. These equations are checked experimentally and, within the limits of the experimental error, the results agree satisfactorily with the theory.

The behaviour of systems containing a large number of particles is discussed and the strains developed in the matrix around the inclusions are examined.

The application of the theoretical concepts to certain problems in structural geology, such as the rotation of crystals, the development of preferred orientations and the deformation of conglomerates, is considered. Particular emphasis is laid on the use of the theoretical equations to determine the finite strain in rock.

TABLE OF CONTENTS

		Page
CHAPTER I	INTRODUCTION	
A.	GENERAL STATEMENT	1
B.	ACKNOWLEDGEMENTS	5
C.	LIST OF SYMBOLS	6
CHAPTER II	VISCOSITY AND THE VISCOUS FLOW OF ROCKS	
A.	INTRODUCTION	9
B.	RHEOLOGICAL MODELS AND THE TIME-STRAIN OF ROCKS	10
C.	TERMS USED TO DESCRIBE FLOW IN ROCKS	15
D.	CALCULATIONS OF COEFFICIENTS OF VISCOSITY FOR GEOLOGICAL MATERIALS	16
E.	THE REYNOLDS NUMBER AND THE TYPE OF VISCOUS FLOW IN ROCKS	25
F.	SUMMARY AND CONCLUSIONS	27
CHAPTER III	THE EXPERIMENTAL PROGRAMME	
A.	INTRODUCTION	29
B.	APPARATUS AND MATERIALS	30
C.	THE EXPERIMENTAL PROGRAMME	48
D.	ACCURACY AND PRECISION OF THE RESULTS	56
CHAPTER IV	THEORETICAL AND EXPERIMENTAL ANALYSIS OF THE MOTION OF PARTICLES DURING DEFORMATION OF THE PARTICLE-MATRIX SYSTEM	
A.	INTRODUCTION	58
B.	THE BEHAVIOUR OF RIGID PARTICLES DURING DEFORMATION BY SIMPLE SHEAR	63
C.	THE BEHAVIOUR OF RIGID PARTICLES DURING DEFORMATION BY PURE SHEAR	78
D.	THE DEFORMATION OF NON-RIGID PARTICLES DURING PURE SHEAR	93

E. PURE SHEAR DEFORMATION OF AN ELLIPTICAL PARTICLE WITH ITS AXES NOT NECESSARILY PARALLEL TO THE STRAIN AXES 106

F. SIMPLE SHEAR DEFORMATION OF NON-RIGID CIRCULAR PARTICLES 118

G. THE DEFORMATION OF SYSTEMS CONTAINING A LARGE NUMBER OF PARTICLES IN A VISCOUS MATRIX 127

H. STRAINS DEVELOPED IN THE MATRIX AROUND A SINGLE PARTICLE DURING DEFORMATION BY PURE OR SIMPLE SHEAR 140

CHAPTER V GEOLOGICAL APPLICATIONS

A. ROTATED CRYSTALS AS QUANTITATIVE STRAIN INDICATORS 146

B. THE DEVELOPMENT OF PREFERRED ORIENTATIONS IN ROCKS 159

C. THE USE OF DEFORMED PEBBLES AS QUANTITATIVE STRAIN INDICATORS 171

D. A PROCEDURE FOR ANALYZING DEFORMED CONGLOMERATES 180

E. COMMENTS ON SOME DEFORMED CONGLOMERATES 181

SUMMARY AND CONCLUSIONS 186

REFERENCES 192

APPENDIX I THE EXPERIMENTAL RESULTS 200

CHAPTER I INTRODUCTION

A. GENERAL STATEMENT

Structural geologists working in both igneous and metamorphic rocks have for many years now recognized the importance of small, marker particles such as gas bubbles, phenocrysts, pebbles and fossils in elucidating the state of strain in rocks. This approach is a kinematic one and involves relating the present geometrical position of particles to possible movement paths during the deformation of the whole rock mass. In other words, it should be possible to estimate the strain in a body of rock from the changes in shape and position of individual objects in the rock, provided the initial shapes of these objects and the physical properties of the rock and its components during deformation are known.

This is no new concept. One hundred and forty years ago Scrope (1825) described gas bubbles in lavas " drawn out, or elongated, in the direction of motion ....". In 1839 Naumann recognized the importance of lineation in lavas and gneisses and made a careful mathematical analysis of changes in the lineation positions with tilting of the planes in which they are contained. Deformed fossils were described by Phillips (1843); and Sharpe (1846), Haughton (1856) and Wettstein (1886) used the changes in shape to calculate the amount of strain. Slaty cleavage and its relation to deformed spots, oolites and crinoid stems was studied by Sorby (1853, 1855). The deformation of pebbles was clearly recognized and analyzed by Hitchcock, Hitchcock and Hager (1861). Heim (1878) explained external rotations and orientation of minerals and Reusch (1887) described elongation of pebbles by a rolling mechanism.

Moreover, following on these early papers, there is now available a vast amount of literature on the subjects mentioned above. Cloos (1946, 1947) reviews most of the work

up to 1945; in addition, Knopff and Ingerson (1938), Sander (1930, 1950) and Turner and Weiss (1963) also contain detailed bibliographies.

In all this work, no one, so far as the writer is aware, has suggested a general method using all the available evidence for determining the states of strain in rock. The total finite strain has been calculated from objects of known original shape which have deformed homogenously with the surrounding material. However, no attempt has been made to relate the degree of preferred orientation of rigid or non-rigid, deformed particles to the finite strain. And, similarly, where there has been a competence difference between an object and its surroundings, the change in shape of the object has not been used to estimate the finite strain in the rock.

This thesis is particularly concerned with finding methods to solve problems such as these. To do so it is assumed that under certain conditions a rock may be considered as an inhomogenous mass of extremely viscous fluid. By inhomogenous is meant that the mass of material differs from point to point in its physical properties; in particular the coefficient of viscosity may vary from zero to infinity. In detail, the model is a large body of homogenous viscous material in which are embedded much smaller spherical or ellipsoidal bodies with different physical properties. The bulk of the material will be referred to as the matrix and the inhomogeneities as the particles. The particles may be either rigid or non-rigid with coefficients of viscosity greater than, equal to or less than that of the matrix.

The types of deformation assumed are pure shear and simple shear. These are both plane strains in which there is no volume change and both have a triaxial strain ellipsoid with an intermediate axis equal to unity. Simple shear also has a component of rigid body rotation. General strains can always be considered as three mutually perpendicular simple shears of different magnitudes and so the analysis presented

here can be applied to more complex examples of strain, if necessary.

After these opening paragraphs an explanatory list of the more important symbols appearing in the text is given. In addition to those explained in the list, all symbols are defined when they are first introduced. As far as possible the writer has followed Nadai's (1950, 1963) symbols for strain analysis.

In the second part of this introductory section, some basic concepts of rheology are outlined and applied to the change with environment in the physical properties of rock. In particular, the assumption of rocks behaving as viscous fluids is examined in the light of published data obtained from field, experimental and theoretical work and an attempt is made to define the physical conditions under which the assumption is valid. Coefficients of viscosity for different rock types are tabulated and expected changes in these values with temperature and pressure discussed. Finally, the kind of flow occurring in extremely viscous materials is discussed. The Reynolds Number is used to show that rocks normally deform by laminar flow.

Chapters III and IV form the main part of the thesis. In them the mathematical theory relating the finite strain to the changes in shape and orientation of the particle during pure and simple shear deformations of the particle-matrix system is presented together with its experimental verification.

The theory is based on the fundamental equations of viscous fluid dynamics for slow-motion laminar flow and the mathematical techniques involved are similar to those used by other workers in the fields of suspensions and emulsions. The analysis is divided into sections; the first deals with the behaviour of single, rigid spheres and ellipsoids in the two types of deformation field. Single non-rigid particles are then considered and an analytical solution is obtained

for the pure shear deformation of an ellipse with its axes parallel to the strain axes. The more general problems of elliptical particles not aligned parallel to the strain axes during pure shear are solved numerically with the aid of a computer. The behaviour of multiparticle systems is then discussed in the light of this theory. Finally, the strains in the matrix surrounding the particles are examined.

Wherever possible the theoretical equations are plotted as graphs to clarify their meaning and are compared directly with the experimental results. For the sake of convenience, therefore, the basic experimental apparatuses and methods are described first and followed by the theoretical and experimental work.

Applications of the theory to geological problems are described in Chapter V of the thesis. Rigid crystals which have rotated during the deformation are used to calculate the amount of finite strain; their use in analyzing styles of folding is also discussed. The development of preferred orientations during simple and pure shear of initially random and regular assemblages of particles is correlated with the total strain in the rock. Deformed pebbles are also used to determine finite strain; the significance of the original shape of these particles, their position relative to the deforming forces and the competence difference with the matrix are discussed and techniques suggested to assess and overcome these factors. A method is suggested for determining finite strains in deformed conglomerates and the thesis ends with a discussion on two well-known deformed conglomerates.

Appendix I contains the detailed experimental results.

B. ACKNOWLEDGEMENTS

A large number of people have helped me with various aspects of this thesis. They include the Staff of the Geology Workshop who constructed the experimental apparatuses; Mr. J. Gee and Miss M. Doe who gave advice on photographic techniques and produced the final plates appearing in this thesis; and Mr. A. Hill and Mrs. A. Johns who supplied ideas on overcoming practical difficulties in the laboratory.

Mr. R. Whorlow of the Department of Physics, Battersea College of Technology, allowed me to use his department's cone - plate viscometer to determine the viscosity coefficients of the ethyl cellulose solutions and also gave advice on some rheological problems. Mr. L. Sowerby of the Department of Mathematics reviewed an early draft of the mathematical theory. Mr. C.J. Dixon helped me with the preparation of the computer programmes.

My fellow post-graduate students all helped me at one time or another. I would particularly like to thank David Elliot who has read and criticized this thesis completely.

I was fortunate to have two supervisors, Dr. J.G. Ramsay and Dr. N.J. Price, both of whom were extremely helpful and encouraging. Without their advice and guidance I could not have completed this work.

While living in England, I have been financed by a bursary from the South African Council for Scientific and Industrial Research, which I gratefully acknowledge.

My wife, Diana, drafted most of the diagrams. For this practical help and for the support she gave to me by her presence, I am deeply grateful. This thesis is dedicated to her.

C. LIST OF SYMBOLS

a - length of major semi-axis of an ellipsoid; radius of a disc.

b - length of intermediate semi-axis of an ellipsoid; length of minor semi-axis of an ellipse.

c - length of minor semi-axis of an ellipsoid.

a/b - axial ratio of an ellipse.

a_i, b_i - initial semi-axial lengths of a non-rigid ellipse.

a_o, b_o - semi-axial lengths of the infinitesimal strain ellipse.

a_1, b_1 - semi-axial lengths of an ellipse after deformation.

$\bar{a}$ - axial ratio of an elliptical cross-section through an ellipsoid of revolution.

$\underline{a}$, $\underline{b}$, $\underline{c}$, $\underline{f}$, $\underline{g}$, $\underline{h}$, ξ, η, ν - components of distortion and rotation of a fluid.

A, B, C - constant terms which may have different meanings in different equations; C is also used to denote the rate of natural strain.

A_{-3}, B_{-3}, A_2, B_2 - constant terms determined by the boundary conditions during deformation of a non-rigid particle.

A, B, A_1, B_1 - symbols in the computer programmes for the principal reciprocal quadratic elongations of an elliptical particle.

C, D, C_1, D_1 - symbols in the computer programmes for the principal reciprocal quadratic elongations of the infinitesimal strain ellipse.

C_v - volume concentration of particles in a particle-matrix system.

e - eccentricity of an ellipse; $e^2 = (a^2 - b^2)/a^2$.

exp - exponential term.

f - subscript denoting final angle or length after deformation.

i - subscript denoting initial angle or length.

J_1, J_2 - strain invariants.

k - constant of integration; also a term to describe the interference in a uniform laminar flow because of the presence of a particle.

ℓ - linear term in formula to calculate the Reynolds Number.

ln - natural logarithm.

l_1, l_2, l_3, m_1, m_2, m_3, n_1, n_2, n_3 - direction cosines between two sets of coordinate axes.

M, M_f - moments of couples acting on two-dimensional particles in simple shear.

p - mean pressure.

p_n - solid harmonic function of degree n.

$\mathcal{Q}$ - activation energy.

$r = \sqrt{(x^2 + y^2)}$

R - viscosity ratio between a particle and the matrix; also the gas constant.

R_e - Reynolds Number.

R_m - viscosity ratio between a particle and the particle-matrix system.

t - time; also thickness of a folded layer measured perpendicular to the layering.

T - absolute temperature; also thickness of a folded layer measured parallel to the axial plane.

T_m - absolute melting temperature.

u, v, w - components of fluid velocity parallel to the X, Y, Z axes.

u', v', w' - components of fluid velocity parallel to the X', Y', Z' axes.

X, Y, Z - coordinate axes fixed parallel to the particle semi-axes a, b, c.

X', Y', Z' - coordinate axes for strain or flow.

α - apical angle in the irrotational strain box.

α' - polar angle of an ellipse.

γ_s - unit of simple shear; = $\tan \delta$.

$\dot{\gamma}_s$ - rate of simple shear.

δ - angle of shear.

ε - conventional unit of strain

$\dot{\varepsilon}$ - rate of strain.

$\bar{\varepsilon}$ - natural strain; = $\ln(1 + \varepsilon)$

$\dot{\bar{\varepsilon}}$ - rate of natural strain.

θ - angle of plunge of particle major axis with respect to the deformation plane.

θ' - complement of θ.

θ', φ', ψ - Euler angles.

$\sqrt{\lambda_1}$ - length of major semi-axis of the strain ellipse.

$\sqrt{\lambda_2}$ - length of minor semi-axis of the strain ellipse.

$\sqrt{\lambda_1/\lambda_2}$ - axial ratio of the strain ellipse.

μ - coefficient of viscosity of a particle.

μ' - coefficient of viscosity of the matrix.

μ_m - coefficient of viscosity of the particle-matrix system.

ρ - density; also length of any line in an ellipse.

σ - compressive stress.

σ_{rx}, σ_{ry}, σ_{rz}, - components of stress acting on a unit area of the surface of the particle.

φ - angle between the particle major axis and the Y' coordinate axis in the deformation plane.

φ' - complement of φ.

φ_n - solid harmonic function of degree n.

Φ - interaction factor representing the interaction between regions of disturbance around individual particles in a multiparticle system.

ω - angular velocity.

$\omega_1, \omega_2, \omega_3$ - angular velocities about X, Y, Z axes.

$\cdot$ - a dot placed above a symbol indicates differentiation with respect to time.

$a \cdot b$ - dot indicates multiplication; it is only used when required to eliminate ambiguity.

a/b - the slash indicates division.

CHAPTER II VISCOSITY AND THE VISCOUS FLOW OF ROCKS

A. INTRODUCTION

In this chapter, the viscous flow of rock will be discussed in an attempt to determine the conditions under which rock will deform as a Newtonian fluid and to evaluate coefficients of viscosity during flow. Continuous deformation by flow can be observed directly in molten or unconsolidated materials such as lavas or mudflows but it is not so apparent in deep-seated igneous or metamorphic rocks. Nevertheless, phenomena such as oriented xenoliths and phenocrysts have been interpreted as evidence for flow in magmas (e.g. Balk,1937) and the presence of rheomorphic structures such as folds in deformed rocks is evidence for flow of material in an apparently solid condition (e.g. Carey, 1953). Moreover, it has been shown theoretically by Haskell (1937) that crystalline rocks under dynamic metamorphic conditions can deform by viscous flow.

The geological examples discussed in the light of the results obtained in this thesis are all concerned with deformed and metamorphosed rocks. Therefore, the possibility of viscous flow of rock at temperatures below the melting point is examined in detail and the chapter opens with a discussion on rheological models and the time strain of rock under different environmental conditions. After this, coefficients of viscosity for geological materials at temperatures above and below their melting points are tabulated. The effect of pressure and temperature on these coefficients is considered and finally, the Reynolds Number is used to define the probable type of flow during rock deformation.

B. RHEOLOGICAL MODELS AND THE TIME - STRAIN OF ROCKS

Rheologists use three ideal rheological materials to describe the behaviour of real substances. They are:

(i) The Hooke elastic body which can be represented symbolically by the spring in figure 1a and described by the equation

$$\tau = G\gamma \quad ...(II.1)$$

(τ is the shearing stress, γ the shear strain and G the modulus of rigidity)

(ii) The St. Venant plastic body, symbolized by the weight in figure 1b and defined by the equation

$$\tau = \tau_o \quad ...(II.2)$$

(τ_o is the yield strength of the body)

(iii) The Newtonian viscous body which is simulated by a dashpot (figure 1c) and defined by the equation

$$\tau = \mu\dot{\gamma} \quad ...(II.3)$$

($\dot{\gamma}$ is the rate of shear and μ the coefficient of viscosity)

Each of these models has by definition one rheological property only, in contrast to real substances which have all properties in varying degrees. However, by combining the models in different ways it is possible to represent the observed strain behaviour of actual materials.

A generalized time - strain curve for rocks subjected to a constant stress is illustrated in figure 2.

As soon as a directed load is applied to a test specimen, there is an instantaneous elastic deformation, represented by OA; this is followed by a period of primary creep, AB, during which the rate of strain decreases; a secondary creep stage, BC, in which the strain rate is constant; and a tertiary creep stage, CD, when the rate of strain increases until the specimen fails. If the load is released before the tertiary creep stage (at time t_o in figure 2) there is an immediate strain recovery corresponding to the elastic deformation, followed by

Figure 1 Symbolic and graphical representations of the ideal rheological materials:
a) Hooke body, b) St. Venant body, c) Newtonian body; τ - shearing stress, γ - shear strain, $\dot{\gamma}$ - rate of shear strain, G - modulus of rigidity, τ_o - yield strength, μ - coefficient of viscosity.

Figure 2 Theoretical time - strain curve for rocks:
OA - instantaneous elastic strain; AB - primary creep stage; BC - secondary creep stage;
CD - tertiary creep stage, failure occurs at D;
t_o - time at which applied load is released;
X - permanent deformation.

Figure 3 Rheological models to simulate the time - strain of rock (after Price, 1964):
a) Viscoelastic or Burgers body; b) B - V body;
c) Relationship between stress and rate of secondary creep for viscoelastic body;
d) Relationship between stress and rate of secondary creep for B - V body.
E_i - elastic strain; $\overline{E_t \mu_K}$ - Voigt unit;
μ_M - Maxwell viscosity; w - yield strength;
σ - compressive stress; $\dot{\varepsilon}$ - rate of strain.

1/

a/

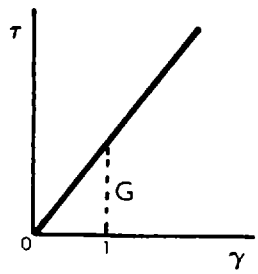
τ
G
0
1
γ

b/

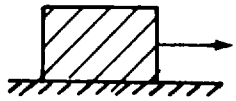

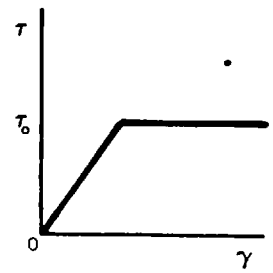
τ
τ₀
0
γ

c/

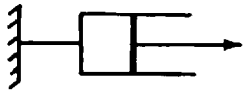

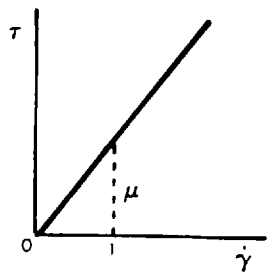
τ
μ
0
1
γ̇

2/

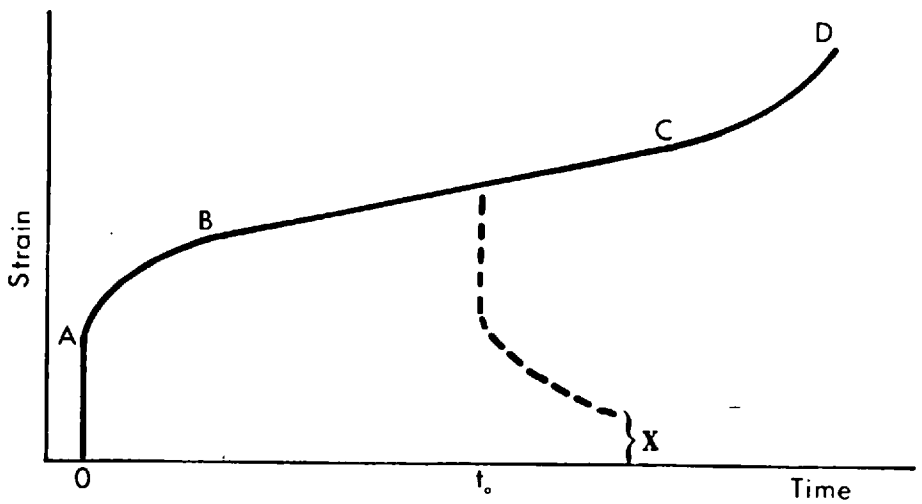
Strain
A
B
C
D
X
0
t₀
Time

3/ a/

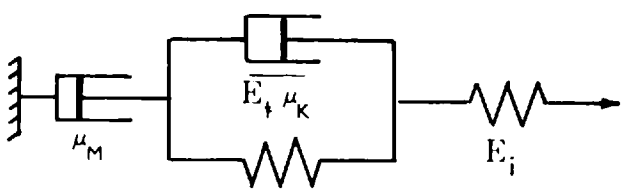
μM
Et μK
Ei

b/

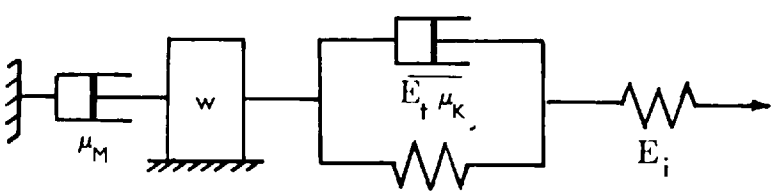
μM
w
Et μK
Ei

c/

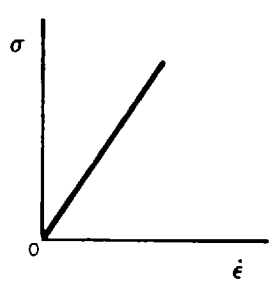
σ
0
ε̇

d/

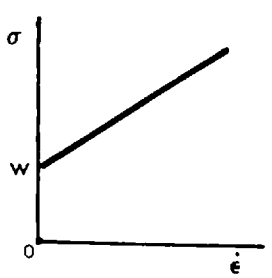
σ
w
0
ε̇

the gradual relaxation of the strain during the primary creep; the secondary creep deformation is not recovered. Primary creep is often called 'delayed elastic deformation' or 'elastic flow'. Secondary creep, on the other hand, is referred to as 'pseudoviscous flow' because the strain rate is constant and the deformation permanent.

Various empirical equations have been suggested to describe the above deformation pattern in rocks. They are reviewed by Murrell and Misra (1962) and Robertson (1964) and are in general similar to that proposed by Griggs (1939, p. 228)

$$\varepsilon = A + B \log t + C t \quad ...(II.4)$$

where ε is the total strain; t is the time; A, B and C are constants and A denotes the elastic strain component, B log t the primary creep and Ct the pseudoviscous flow. This relationship can not apply for very small or very large values of t since log t tends to $\mp$ infinity as t tends to zero or infinity.

Time - strain behaviour can also be visualized in terms of models constructed by combining the ideal rheological bodies (e.g. Price, 1964). One such model is the viscoelastic or Burgers body, illustrated in figure 3a, in which the spring (E_i) represents the elastic strain component; the Voigt unit comprising the spring and dashpot in parallel ($\overline{E_t \mu_K}$) the primary creep component and the dashpot (μ_M) the secondary creep component. For long periods of time this body simulates a Newtonian liquid of high viscosity (μ_M) which deforms permanently when subjected to any stresses (see figure 3c). It displays in effect the long term behaviour envisaged by Gignoux (1950) and Carey (1953) for rocks.

A model which considers a yield strength in rocks is the B - V (Bingham - Voigt) body proposed by Price (1964) and illustrated in figure 3b. It consists of a dashpot (μ_M) in series with a weight (w), a Voigt unit ($\overline{E_t \mu_K}$) and a spring

(E_i). The spring and the Voigt unit represent the elastic and primary creep components of the strain but before secondary creep can commence the resistance of weight w has to be overcome. Once this has been achieved, pseudoviscous flow controlled by dashpot μ_M occurs. The model therefore represents a substance which when subjected to stresses greater than its yield strength, w, for long periods of time, deforms as a Newtonian liquid of high viscosity.

From this discussion it is clear that time is an important controlling factor in the deformation of rocks. Over short time periods strains are elastic and recoverable. Permanent deformation occurs by viscous flow only when stresses are applied for a long time.

Environment also influences the deformation of rock and a number of tests have been carried out by various people to assess the effect of factors such as temperature, pressure and the rate of strain. The results of these tests will not be discussed in detail but for more information than is presented here, the reader can consult any of the available comprehensive reports on rock deformation such as Griggs and Handin (1960), Murrell and Misra (1962) and Robertson (1964). Generally, the effect of these variables on the creep of rock can be summarised as follows:

(i) The rate of primary creep is increased by increases in temperature and stress difference but decreased by an increase in confining pressure.

(ii) The rate of secondary creep is increased by increases in temperature and stress difference.

More specifically, Misra and Murrell (1965) have suggested that the primary creep predominates at temperatures below 0.22 T_m (T_m is the absolute melting temperature of the material) and Dorn (1957, p.264) has concluded from work on metals that secondary creep occurs at temperatures above 0.5 T_m.

Price's (1964) results clearly show the effect of stress differences. He found that for the rocks tested there is a minimum stress below which only primary creep is possible. The value of this minimum stress, which is termed the long-term yield strength, varies between 20 and 60 per cent of the instantaneous strength of the rocks. Secondary creep takes place at stresses greater than the long-term yield strength. In other words, the rocks conform to the deformation pattern of the B - V model.

The effect of temperature on the long-term yield strength can be deduced from the results of Misra (1962); these suggest a slight reduction in strength with increasing temperature.

Constant strain rate tests such as those used by Heard (1963) on Yule Marble provide information about the influence of the rate of strain on deformation. At low temperatures, slow rates of strain are required for pseudoviscous flow but with increase in temperature faster rates are possible. For example, Yule marble deforms by secondary creep at 400°C when strained at a rate less than $3 \cdot 10^{-5}$ sec^{-1} but at 500°C the required rate can be as high as $3 \cdot 10^{-4}$ sec^{-1}.

Therefore, it appears that at temperatures below the melting point, rock approximates to an ideal Newtonian body only when the deforming stresses operate for a long period of time or the rate of strain is very slow. Increase in temperature enhances the pseudoviscous flow but the deforming stresses must be great enough to overcome the long-term yield strength of the material.

C. TERMS USED TO DESCRIBE FLOW IN ROCKS

It has been shown that flow in rocks is very complicated and that Newtonian viscous flow as defined by equation II.3 is only active as a deforming mechanism under special conditions. The question therefore arises: Should one apply the term viscosity, in its strict Newtonian and hydrodynamic sense, to the flow of complex materials such as rock?

Goranson (1940) suggested that the basic differences between the ideal and complex bodies should be emphasised by introducing a new term for flow in solids. He proposed the word 'mobility' with the reciprocal poise as a unit. However, this term or its synonym 'fluidity' is already used by rheologists to describe flow in Bingham bodies and other complex systems (Reiner, 1960a, pp. 116, 124-129). Some workers (Handin and Hager, 1958; Donath, 1963) have used the word 'ductility' particularly to avoid implying any definite flow relationship; and Robertson (1964, pp. 215-217) has suggested a completely new parameter, the 'logarithmic viscosity'. It is defined as $\sigma/\log \dot{\varepsilon}$, where σ is the compressive stress and $\dot{\varepsilon}$ the rate of strain, and has dimensions similar to those of internal friction.

There is definitely a need for a general term to describe the phenomenon of flow in rock in view of the importance of this type of deformation in structural geology and all the above terms are preferable to the much abused 'viscosity'. However, in this thesis the assumption is made that rocks are Newtonian bodies and therefore in the theoretical section viscosity has its precise meaning as defined by equation II.3. Similarly, when applying the theory to geological examples in which the rocks appear to have been in a Newtonian condition during deformation, the term is used in its exact sense. For rocks deformed by flow which was probably not Newtonian,

however, the meaning of viscosity is used in the same sense as Handin and Hager (1958) used 'ductility'.

D. CALCULATIONS OF COEFFICIENTS OF VISCOSITY FOR GEOLOGICAL MATERIALS

In this section theoretical and experimental determinations of coefficients of viscosity of geological materials will be examined so that some idea of the value of these coefficients for different rock types may be obtained. As will be shown in the theoretical section of this thesis, the viscosity ratio between two rock types being deformed simultaneously must be known if the finite strain in the rocks is to be calculated. The results discussed here may be of use in determining this ratio.

The theoretical work deals with viscosity in the crust and upper mantle of the earth. Experimental data is available on melts of natural rocks under conditions applicable to lavas at the surface and magmas at depth; these results can be compared with measurements on lavas in the field. There is also information on the pseudoviscous flow of rocks at temperatures below their melting point and under various pressures.

(a) Theoretical calculations

The theory of diffusion creep has been applied by Gordon (1965) to the flow in the earth's mantle. The results suggest that at slow strain rates the mantle is a Newtonian body but they predict a marked change in viscosity with depth. At shallow depths in the earth's crust the viscosity decreases due to the rapid rise in temperature and relatively low pressures; as the depth increases, the viscosity rises because of the effect of the increasing pressure on the atomic mobility. Zharkov (1960) also predicts

an increase in Newtonian viscosity with increasing pressure in the mantle. These results are listed in table Ia.

(b) Calculations from natural melts.

Newtonian flow in granitic magmas has been demonstrated experimentally by Shaw (1963) who worked on obsidian - water melts at pressures of 1000 to 2000 bars. Moreover, a large number of viscosity determinations at very low pressures and therefore applicable to surficial lava flows have been made on melts of natural rocks. These results are summarized by Volarovich and Korcemkin (1937) and Birch, Schairer and Spicer (1942, pp. 131-137). They show that viscosity can be correlated with composition and that acid melts are more viscous than basic ones.

Calculations of the viscosity of two Hawaiian basic lava flows were made by Nichols (1939) assuming laminar flow. The results are similar in value to those quoted by Volarovich and Korcemkin (1937). Likewise, Friedman, Long and Smith (1963) found that their laboratory determinations of viscosity of melts of rhyolite glass and water agreed well with the viscosity of the 1953 Trident rhyodacite flow in Alaska, as calculated from the rate of flow of the lava. These and other results for viscosity coefficients of molten rocks are listed in table Ib.

(c) Calculations from tests on the pseudoviscous flow of rocks.

Unfortunately, details on the pseudoviscous flow of rocks at temperatures below their melting point are not so abundant. This is because relatively few workers on the time - strain of rocks have extended their tests into the field of secondary creep. They include Griggs (1939, 1940) who worked on Solenhofen limestone, halite and alabaster;

Roux and Denkhaus (1954) who tested quartzite; Heard (1963) who studied deformation of Yule Marble; Price (1964) who obtained data on sandstone; and Le Comte (1965) who also worked on Halite.

The formula used to calculate the equivalent viscosities during pseudoviscous flow is

$$\mu = \sigma/3 \quad \ldots(II.5) \quad \text{(Griggs, 1939, p.230)}$$

The values of μ as calculated by the authors concerned or by the present writer from the data presented in the original papers are listed in table Ic with relevant experimental conditions.

The viscosities of the sandstones, alabaster and Solenhofen limestone as determined by the present writer, were made assuming that the B - V rheological model proposed by Price (1964) and discussed above was applicable. The experimental rates of strain during secondary creep were plotted against the differential stress. The resultant graph was a straight line which then extrapolated to zero rate of strain intersected the stress axis at some positive value, equivalent to the long term yield strength for the rock under the particular experimental conditions. The viscosity was calculated from the slope of the graph using equation II.5 in the form

$$\mu_M = (\sigma - \sigma_o)/3$$

where μ_M is the Maxwell coefficient of viscosity and σ_o represents the long term yield strength.

Comparison of μ_M for Solenhofen limestone with the results of Griggs (1939) shows that μ_M is much lower than the reported viscosities. Similarly, μ_M for wet alabaster is less than most of Griggs's (1940) values. However, the two results obtained by Griggs at the highest differential stresses are less than μ_M. These two points did not fall on the straight line from which μ_M was calculated but indicated that the

Table I Viscosity coefficients for rocks under varying physical conditions.

a) Theoretical values: viscosities in the crust and mantle

Basis for calculation	μ (poise)	Reference
Diffusion creep at 1 km depth	$10^{16} - 10^{24}$	Gordon (1965)
Diffusion creep at 3 km depth	$10^{24} - 10^{28}$	Gordon (1965)
Diffusion creep in mantle	$10^{15} - 10^{22}$	Zharkov (1960)

b) Determinations on natural melts

Material	T, P conditions	μ (poise)	Reference
Olivine basalt	1400°C	$1.2 \cdot 10^{2}$	Volarovich and Korcemkin (1937)
Andesite	1400°C	$1.2 \cdot 10^{3}$	do.
Obsidian	1400°C	$1.7 \cdot 10^{5}$	do.
Hornblende granite	1400°C	$2.0 \cdot 10^{6}$	do.
Rhyolite glass	350-850°C, surface pressures	$3.1 \cdot 10^{9} - 3.1 \cdot 10^{14}$	Friedman, Long and Smith (1963)
Obsidian - water melt	800-900°C, 1000-2000 bars	$7.5 \cdot 10^{5} - 3.2 \cdot 10^{6}$	Shaw (1963)

Material	μ (poise)	Reference
Alika basalt flow, Hawaii	$4.3 \cdot 10^{4}$	Nichols (1939)
1887 basalt flow, Hawaii	$4.7 \cdot 10^{4}$	Nichols (1939)
Trident rhyodacite flow, Alaska	$6.3 \cdot 10^{10}$	Friedman, Long and Smith (1963)

μ - viscosity
T - temperature
P - pressure

Table I, continued

c) Determinations from pseudoviscous flow

i) Creep tests

Material	T	C.P.	σ	t	μ	Reference
Halite	20	-	60	42.0	2600	Griggs (1939)
Solenhofen limestone	20	10133	5400	0.1	13	do.
do.	20	10133	6600	0.2	2	do.
Alabaster (dry)	23	-	98	30.0	20000	do.
Alabaster (wet)	23	-	98	20.0	800	do.
do.	24	-	122	308.0	1400	Griggs (1940)
do.	24	-	147	110.0	640	do.
do.	24	-	162	285.0	600	do.
do.	24	-	177	133.0	510	do.
do.	24	-	201	48.0	260	do.
do.	24	-	245	13.5	160	do.
do.	24	-	294	2.5	42	do
Quartzite	20	-	330	21.0	26000	Roux and Denkhaus (1954)

ii) Constant strain-rate tests

Material	T	C.P.	$\dot{\varepsilon}$	μ	Reference
Yule marble	25	5000	10^{-14}	10^{9}	Heard (1963)
do.	400	5000	10^{-14}	10^{5}	do.
do.	500	5000	10^{-14}	300	do.
do.	600	5000	10^{-14}	5	do.
do.	800	5000	10^{-14}	0.02	do.

T - temperature ^{o}C; C.P. - confining pressure, bars;
$\dot{\varepsilon}$ - strain rate, sec^{-1}; μ - viscosity, 10^{14}poise;
t - time, days; σ - stress, 10^{6}dyn/sq cm.

Table I, continued

iii) B - V model

Material	T	C.P.	σ_o	t	μ	Reference
Pennant sandstone	23	-	49	12	50	Price (1964)
Wolstanton sandstone	23	-	230	30	500	Price (1964)
Solenhofen limestone	20.	10133	5100	0.2	0.5	Griggs (1939)
Alabaster (wet)	24	-	100	308	200	Griggs (1940)

T - temperature ^{o}C; C.P. - confining pressure, bars;
μ - viscosity, 10^{14} poise; t - time, days;
σ_o - long term yield strength, 10^{6} dyn/sq cm.

viscosity had decreased. This suggests that stresses of this magnitude are too large to allow any pseudoviscous flow but cause rapid onset of tertiary creep. Examination of Griggs's (1936, fig. 10) original curves supports this idea; there is no significant straight line portion of the curves and only an inflection point marks the secondary creep stage.

(e) The effect of pressure and temperature on viscosity coefficients

The data in table I show that the experimental conditions do affect the value of the viscosity coefficients. Therefore, before comparing coefficients for different rock types and so estimating viscosity ratios, the effect of variables such as pressure and temperature must be determined. One way of doing this is to use suitable theoretical equations.

For example, the possible influence of pressure on Newtonian viscosity can be assessed from an equation suggested by Andrade (1934):

$$\mu_p/\mu_1 = (v_1/v_p)^{\frac{1}{6}}(k_1/k_p)^{\frac{1}{2}}\exp(C/T(1/v_p - 1/v_1)) \quad \text{..(II.6)}$$

The subscripts 1 and p refer to atmospheric pressure and the desired working pressure respectively; v is the molar volume; k the compressibility; and T the absolute temperature. The equation implies that viscosity increases with increasing pressure.

A relationship between temperature and viscosity was derived by Becker (1925) using basic statistical mechanics. It is

$$\mu = A \exp(Q/RT) \quad \text{..... (II.7)}$$

in which A is a constant, Q is the activation energy and R the gas constant. The equation shows that viscosity should decrease with increasing temperature. Moreover, because

temperature also appears in II.6, the effect of increasing pressure should be less marked at higher temperatures than at lower ones.

Both these equations have been verified by workers using geologically significant materials. For example, Dane and Birch (1938) worked on boric anhydride glass and found that the ratio of viscosity at 1000 bars to the viscosity at 1 bar was 4.5 at 359°C, but only 1.6 at 516°C. More recently, Shaw (1963) has shown that an increase in pressure on obsidian - water melts under magmatic conditions (800-850°C, 1000-2000 bars) results in a very slight decrease in viscosity.

However, available information on the pseudoviscous flow of rocks suggests that the effect of the variables is more complicated. Griggs' (1939, 1940) data on Solenhofen limestone and alabaster show a decrease in viscosity with increasing pressure, which is contrary to equation II.6. Robertson (1964) has extrapolated Heard's results for Yule marble and finds a similar reduction in viscosity, and Heard, himself, points out that the differential stress required to maintain a particular strain rate is very sensitive to temperature variations.

These observations can be explained using the relationship between activation energy and pressure determined by Zharkov (1960, equation 5). This predicts a decrease in energy with increasing pressure. From equation II.7, it can therefore be deduced that, at a particular temperature, viscosity will also decrease with increasing pressure.

Nevertheless, it is obviously very difficult to assess with any precision, the effect of the two variables, pressure and temperature, on viscosity during pseudoviscous flow. One can only generalize that increases in either, or both, of them will probably result in a decrease in the coefficient of viscosity. This is, unfortunately, not sufficient information to allow recalculation of the experimental data,

so that ratios of viscosity between rocks deforming under the same pressure and temperature conditions may be evaluated.

(f) The use of activation energies to calculate coefficients of viscosity

It may be possible to overcome the difficulties in calculating coefficients of viscosity by using fundamental theoretical equations such as that for the variation of viscosity with temperature (equation II.7). Work on metals has shown that secondary creep at high temperatures begins when the activation energies for creep and diffusion are equal; this occurs at temperatures greater than 0.5 T_m (Dorn, 1957, p. 264). Therefore, as more data on activation energies for diffusion become available, they can be used in II.7 to calculate, directly, viscosities for pseudoviscous flow at suitable temperatures, provided the constant A can be assessed.

Some idea of the value of A for Yule marble can be obtained from Heard's (1963) results which provide information on both activation energies and viscosities. The activation energy varies between 45,700 and 62,400 cal/mole depending on the orientation of the test specimens but the mean value agrees well with the activation energy for diffusion in calcite crystals which is 58,000 cal/mole (Haul and Stein, 1955). Substituting this last figure for Q in II.7 and using Heard's coefficients of viscosity at a particular temperature, A can be calculated as follows:

At 800°C, $\mu = 2 \cdot 10^{12}$ poise; therefore

$$2 \cdot 10^{12} = A \exp(58{,}000/1.987 \cdot 1073)$$

which reduces to: $A \sim 3$. Similarly, at 600°C, $A \sim 1.5$ and at 500°C, $A \sim 1.2$.

These results indicate that, for Yule marble, A is small and roughly constant.

Le Comte (1965) has determined the activation energy of rock salt during creep tests and finds that at 265°C ($0.5T_m$) the value for Q is approximately 30,000 cal/mole. Substituting this in II.7 gives $\mu = 1.54A \cdot 10^{12}$ poise. This is significantly lower than the result obtained by Griggs (1939) if A is of the same order of magnitude as for Yule marble. However, the activation energies for diffusion of the Na and Cl ions are greater than Le Comte's energy of creep, the mean value being 36,000 cal/mole. If this value is used for Q in II.7, the resultant viscosity is approximately $2A \cdot 10^{14}$ poise, 10^3 times less than that determined by Griggs. This difference is probably due to the very much higher temperatures at which Le Comte worked.

Unfortunately the writer knows of no similar theoretical work relating pressure, activation energy and viscosity. As mentioned above, Zharkov (1960) predicts a decrease in energy with increasing pressure. This is supported by Misra's (1962) results for marble which indicated a decrease in the activation energy from $3.9 \cdot 10^8$ dyn/sq cm. Therefore, at higher pressures one would expect a decrease in the viscosity as calculated from II.7.

E. THE REYNOLDS NUMBER AND THE TYPE OF VISCOUS FLOW IN ROCKS.

Fluid flow is generally recognized as being of two types: laminar, or turbulent. Laminar flow is very smooth and, using Reiner's (1960b, p. 196) definition, there is no visible separation of the parts of the liquid. Turbulent flow, on the other hand, is erratic and irregular and separation of parts of the fluid can be observed.

The Reynolds Number is a dimensionless parameter which can be used to determine whether the flow is laminar or turbulent. It is defined as the ratio of inertial to viscous forces in the particular experiments; i.e.

$$R_e = \rho \ell \dot{\varepsilon} / \mu \quad \ldots(II.8)$$

where ℓ is the linear size of the fluid body and ρ the density of the material. If R_e is small (less than 1), the flow is laminar; if it is large (greater than 1000), the flow is turbulent. For values of R_e in between these limits, initial turbulence is possible but it will be damped out and the flow will become laminar with time.

To decide the type of flow prevailing during conditions of regional metamorphism, values for the variables appearing in II.8 must be assumed. From measurements along the San Andreas fault, Heard (1963, p. 178) suggests a value of $3 \cdot 10^{-14}$ sec^{-1} for a geologic strain rate. The velocity of the westward drift of America is estimated by Orowan (1965, p. 304) to be $3 \cdot 10^{-6}$ cm/sec. The rate of strain would be less than this. Suitable values for the viscosity vary from $10^{12} - 10^{18}$ poise (table 1c). Therefore, for the present calculation, assume the following values for the variables in II.8

$$\rho \sim 3, \quad \dot{\varepsilon} \sim 10^{-10} \text{ sec}^{-1}, \quad \mu \sim 10^{15} \text{ poise}$$

Hence

$$R_e = 3 \cdot 10^{-25} \ell$$

which is extremely small, no matter what the value of ℓ. Therefore, the inertial forces can be ignored and the type of flow will always be laminar.

Similarly, using Friedman, Long and Smith's (1963) data for the Trident rhyodacite flow, R_e is of the order of $3 \cdot 10^{-12} \ell$. The type of flow is again laminar. However, for the much less viscous Alika basalt flow, which moved at 11 m.p.h. (Nichols, 1939), the Reynolds Number is 0.15 . This suggests a dominance of laminar flow with a possibility of turbulence, depending upon the value of ℓ. It is important to note when discussing less viscous materials with rapid

strain rates that turbulence can easily be achieved in large bodies.

These results corroborate those of previous workers who have used dimensional analysis to show laminar flow in lavas and dykes (Nichols, 1939; Spry, 1953) and in metamorphic rocks (Charlesworth and Lambert, 1964). It seems unlikely that Schmidt's (1918, p. 296) suggestion of turbulent flow for metamorphic rocks containing snowball garnets is tenable.

In this thesis turbulent flow is not considered at all and the basic equations of laminar flow are assumed to hold for all types of deformation examined.

F. SUMMARY AND CONCLUSIONS

The object of this chapter was to investigate the possibility of Newtonian flow in rocks, and it was found that rocks do behave as viscous fluids under certain physical conditions.

For molten rock material, experimental and field evidence suggests that both surficial lavas and deep-seated magmas are Newtonian liquids.

At temperatures less than the melting point, it is possible to get rock to deform by flow under most pressures and temperatures. However, Newtonian viscosity is probably only achieved if the stresses are applied for a long time or the rate of strain is slow. High temperatures (greater than $0.5\ T_m$) and pressures facilitate the onset of pseudoviscous, Newtonian flow. In geological terms, rocks undergoing regional metamorphism are probably in a Newtonian fluid condition.

Calculated theoretical and experimental values of the coefficients of viscosity vary between 10^2 and 10^{10} poise for molten rock, the composition of the melt, temperature and pressure being the main controlling factors. For rock

in the solid state, viscosity ranges between 10^{12} and 10^{24} poise, depending on composition and the experimental conditions. Increases in temperature and pressure reduce the value of the viscosity coefficient but it is not possible to correct the experimental results for these factors, and so compare viscosity coefficients of different rock types directly.

Calculations of the Reynolds Number for viscous flow in rocks show that deformation will generally occur by laminar flow.

CHAPTER III THE EXPERIMENTAL PROGRAMME

A. INTRODUCTION

As explained previously, the development and experimental verification of the theory will be discussed together as the one follows logically from the other. It is therefore convenient to describe the apparatus and techniques used for the experimental work before describing the mathematical theory.

The object of the experimental programme was to test the behaviour of rigid and non-rigid particles in a viscous matrix during pure and simple shear deformations. To do this the writer designed and had constructed two simple pieces of apparatus capable of imparting the desired deformations to material placed inside them. The simple shear apparatus worked very successfully but, unfortunately, that for pure shear did not. It was found that when this apparatus was filled with the matrix and the straining initiated, the frictional resistance set up was so great that it locked the box before the run was properly underway. Lubricating the moving components did reduce the resistance slightly but to ensure that the apparatus worked reliably would have involved redesigning it completely. Unfortunately, the writer did not have sufficient time to do this and instead recourse was had to a piece of apparatus which, like that for pure shear, imparted an irrotational strain but did not maintain a constant area, as required by pure shear. This simpler strain box gave very satisfactory results.

The instruments used for measuring changes in shape and orientation were also simple ones. A pair of dividers and a ruler graduated in fiftieths of an inch were used to measure particle dimensions and a protractor marked out in half degrees served for angular measurements. More sophisticated instruments capable of achieving greater orders of accuracy were not necessary in view of the relatively large strains

Figure 4 Plan of the simple shear apparatus.

A - aluminium "U" pieces (only half shown)
B - fixed perspex plate
C - moveable perspex plate
D - retaining bars
E - guide posts
F - scale, in units of $0.1\gamma_s$
G - threaded brass rod
H - connecting nut
I - platform in which H sits and moves freely
J - rubber barrel coupling
K - motor drive shaft and gear box
L - electric reversible motor
M - aluminium "U" piece in cross-section

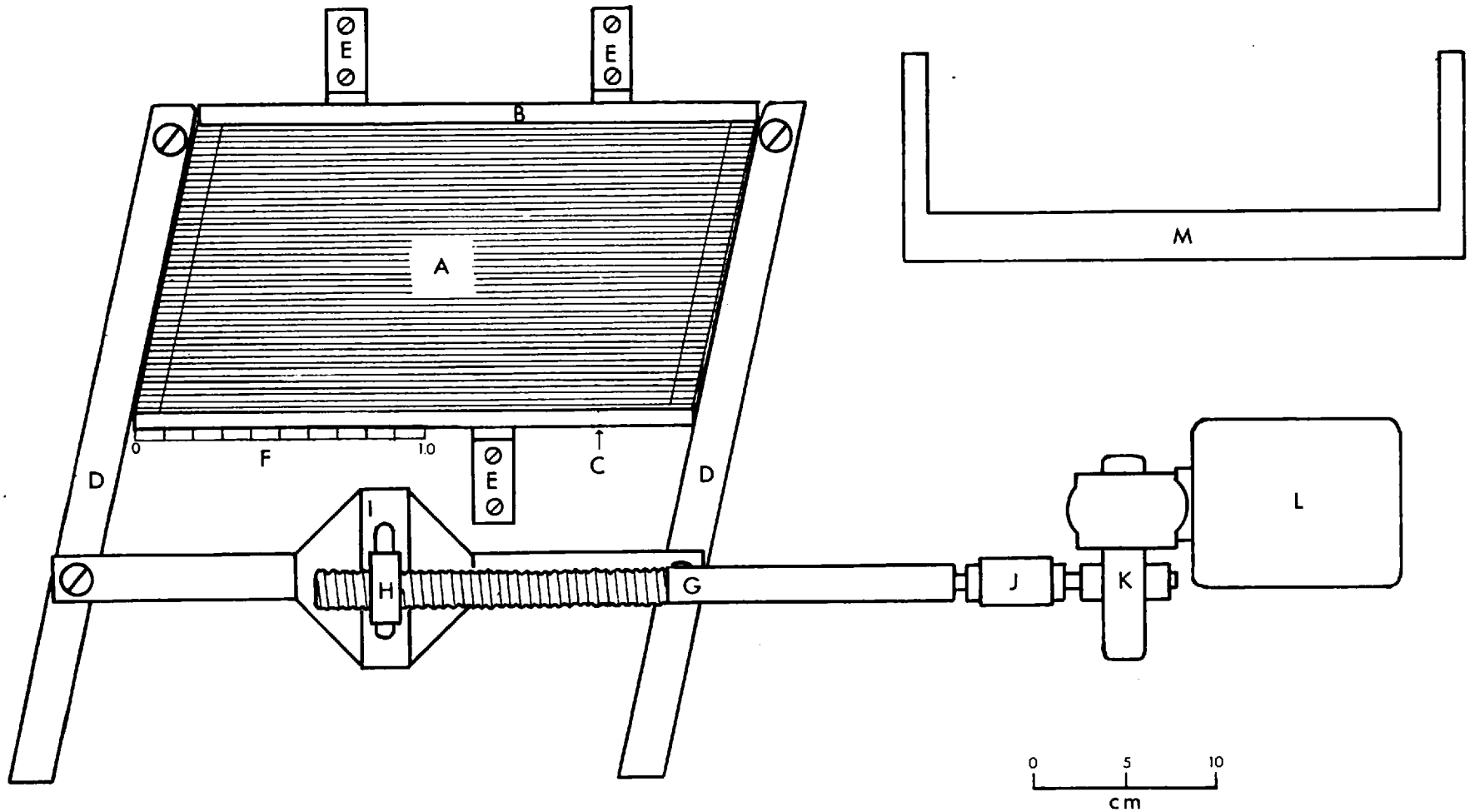
E
E
B
A
M
0
F
1.0
E
C
D
D
I
H
G
J
K
L
0
5
10
cm

obtained.

The material used for the matrix was a solution of ethyl cellulose in benzyl alcohol because it was easy to prepare and a wide range of viscosities could be obtained by varying the ratio of solvent to solute. The non-rigid particles were also prepared from this material; rigid particles were made of aluminium or glass.

Detailed descriptions of the apparatuses and materials used are given in the subsequent paragraphs. These are followed by the experimental method, which was basically the same for all the experiments. Finally, the accuracy of the method is discussed.

B. APPARATUS AND MATERIALS.

(a) The simple shear box.

The simple shear box, the essential features of which are shown in figure 4, worked on the same principle as Becker's (1904) "scission engine" and Ramberg's (1959, p.124) shearing apparatus. It consisted of 96 pieces of 1.6 mm. thick aluminium sheeting cut into "U" shapes and clamped together to form a hollow box by two 0.67 cm. thick plates of perspex. One of these perspex plates was fixed to a baseboard and the other, together with the aluminium "U"s, was constrained to slide past it by guide posts. Two retaining bars held the ends of the "U"s and the perspex plates together and served to transmit the shearing motion.

A small electric reversible motor able to rotate at 3 r.p.m. was attached to the baseboard to obtain constant rates of shear. Threaded brass rods connected the driving shaft of the motor to the retaining bars of the shear box. In this way, the bars were moved towards or away from the motor, causing the aluminium "U" plates to slide past each other. Different rates of shear were obtained by varying the number of threads per inch on the brass rods.

Figure 5 Simple shear deformation of a rectangle to a parallelogram. Amount of simple shear

$$\gamma_s = \tan \delta$$

(After Nadai, 1950, p. 146)

Figure 6 Diagram to illustrate the method of repositioning a particle at the end of a run in the simple shear box.

A - final position at the end of the run;

B - equivalent position for the start of a new run by shearing in the opposite direction.

5

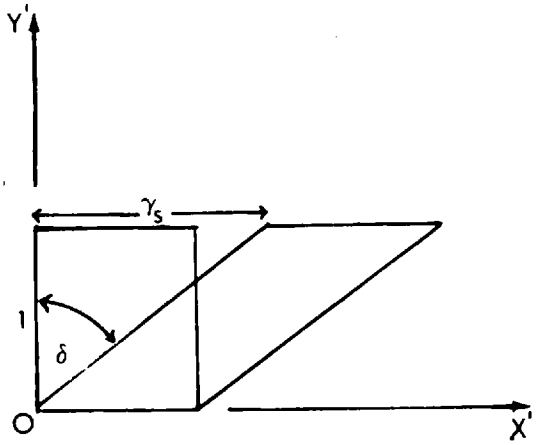

6 A

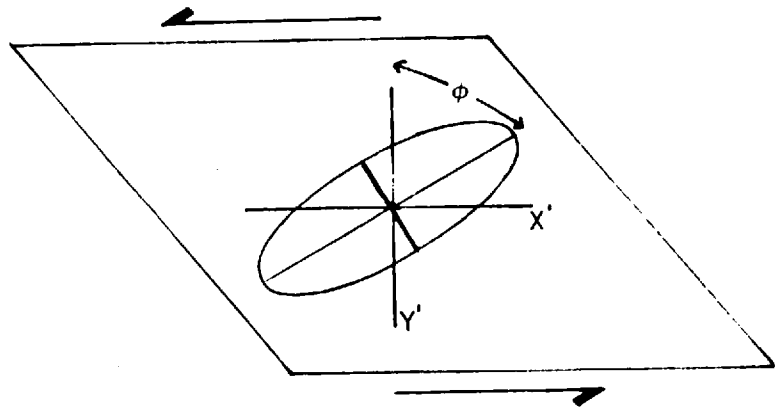

6 B

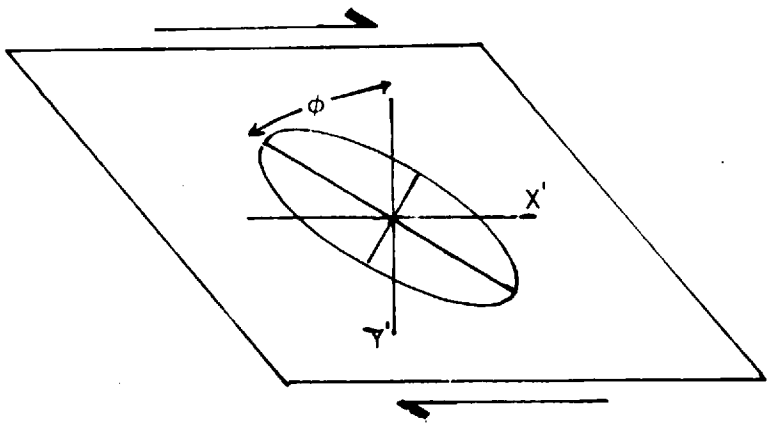

A scale, graduated in divisions of $0.1\gamma_s$, where γ_s is the unit of shear strain as defined by Nadai (1950, p. 146) and illustrated in figure 5, was placed on the baseboard, adjacent to the moveable perspex plate. When the motor was in use the maximum shear during one run was $0.7\ \gamma_s$, but $1.2\gamma_s$ was possible without the motor. Greater shears were obtained by removing the particle after a run, replacing it in the equivalent but opposite final position (see figure 6) and repeating the run in the reverse direction. By summing the individual strains, the effects of large shear deformations could be studied.

Plate 1 shows the apparatus set up for an experiment.

The geometry of any deformation in the apparatus is given by the transformations.

$$x_1 = x + \gamma_s y, \quad y_1 = y \quad \ldots(III.1)$$

An initial unit circle stamped on the material in the box has the equation

$$x^2 + y^2 = 1$$

If the circle is transformed by equations III.1, it becomes the strain ellipse

$$x^2 + 2\gamma_s xy + y^2(1 + \gamma_s{}^2) = 1$$

The lengths $(\sqrt{\lambda_1}, \sqrt{\lambda_2})$ of the major and minor semi-axes of this ellipse can be determined using standard geometrical methods (eg. Jaeger,1962, p.27-28). The resultant equations are

$$\sqrt{\lambda_1}, \sqrt{\lambda_2} = \sqrt{(\gamma_s/2)^2 + 1} \pm \gamma_s/2 \quad \ldots(III.2)$$

which give

$$\sqrt{\lambda_1/\lambda_2} = [\sqrt{(\gamma_s/2)^2 + 1} + \gamma_s/2]/[\sqrt{(\gamma_s/2)^2 + 1} - \gamma_s/2] \quad \ldots(III.3)$$

Plate I The simple shear apparatus set up for an experiment; the matrix is already in the box.

Plate II The irrotational strain box ready for use; the matrix encloses a non-rigid particle which is to be deformed. Also in the picture to the left of the box are some of the ancillary tools used in the experiments, namely: the cake cutter and the large and small plungers and open-ended test tubes, which were used for shaping the non-rigid particles.

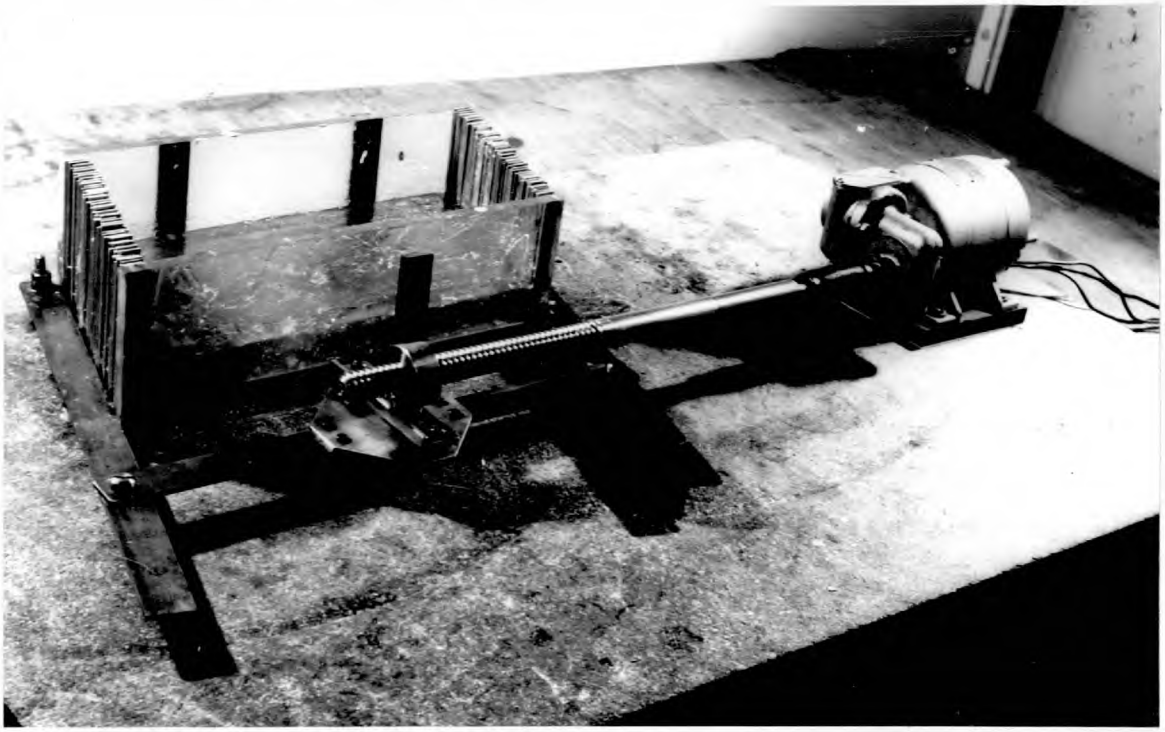

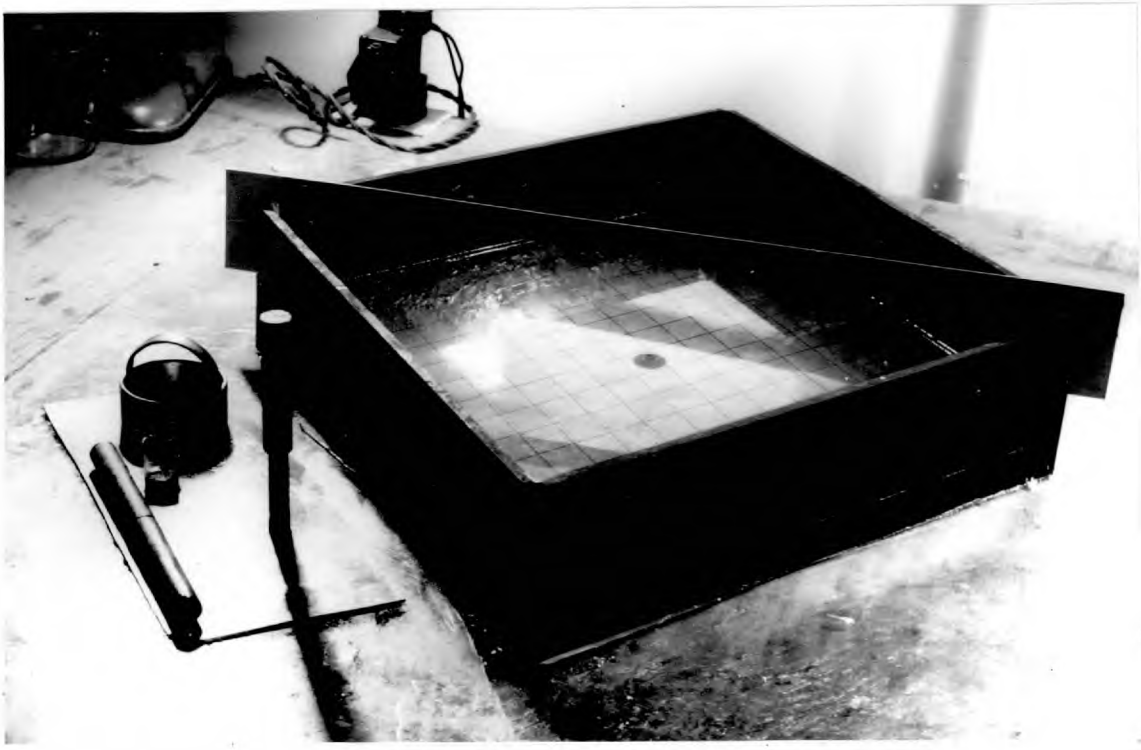

Figure 7 Graphs of equations III.3 - III.5, showing the variation, with simple shear (γ_s), of the axial ratio ($\sqrt{\lambda_1/\lambda_2}$); the orientation of the major axis (φ); and the natural strain ($\bar{\varepsilon}$).

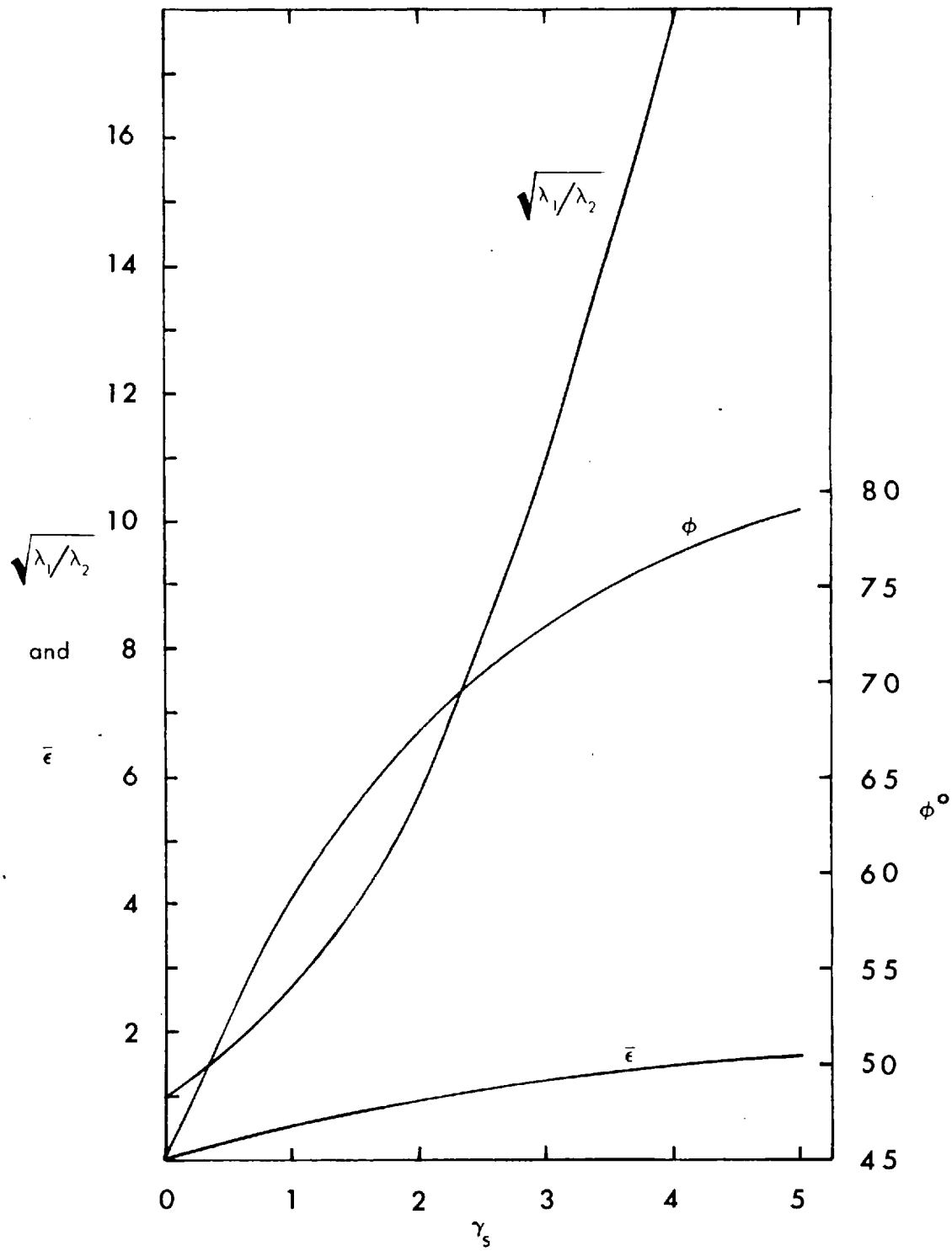
16
14
12
10
8
6
4
2
$\sqrt{\lambda_1/\lambda_2}$
$\sqrt{\lambda_1/\lambda_2}$
and
$\bar{\epsilon}$
ϕ
$\bar{\epsilon}$
80
75
70
65
60
55
50
45
$\phi°$
0
1
2
3
4
5
γ_s

The orientation of the major axis with respect to the OY ordinate of the simple shear is given by

$$\varphi = \pi/4 + (1/2)\tan^{-1}\gamma_s/2 \quad \ldots(III.4)$$

It is also convenient to have a relationship between natural strain and simple shear. This is

$$\gamma_s = 2\sinh \bar{\varepsilon} \quad \ldots.(III.5)$$

Equations III.3 - III.5 are represented graphically in figure 7.

End effects in the apparatus are negligible since the deformation conforms exactly to a theoretical simple shear. The plates forming the shear box and the material contained in them all move as one body during the shearing.

(b) The irrotational strain box.

The irrotational strain box, similar in principle to the wire net used by Cloos (1955) in his experiments on clay, was built from a design by Dr. J.G. Ramsay. The essential features of it are shown in figure 8. It consisted of four rigid tufnol boards hinged together so that they formed a rhombus with variable apical angles. Small holes were drilled at equally spaced intervals near the base of each board. Strong cotton was threaded through these holes to ensure even transmission of strain throughout the material in the apparatus. The whole box was placed on a heavy level glass base-plate which was well greased with vaseline. U-shaped clamps which fitted over the box and connected two opposite hinges served to keep the rhombus in a particular position. The strain was imparted by applying pressure on diagonally opposite corners of the apparatus. Plate II shows the box set up and ready for use.

The geometry of any deformation in this apparatus is complicated because the surface area in the box varies systematically with the apical angle, α, from a maximum value when

Figure 8 Plan of the irrotational strain box.

A - rigid tufnel sides

B - clamp

C - cotton, threaded through holes near the base of the sides

D - glass base-plate

E - hinges

Figure 9 Diagram to illustrate a finite pure shear transformation in the irrotational strain box.

8/

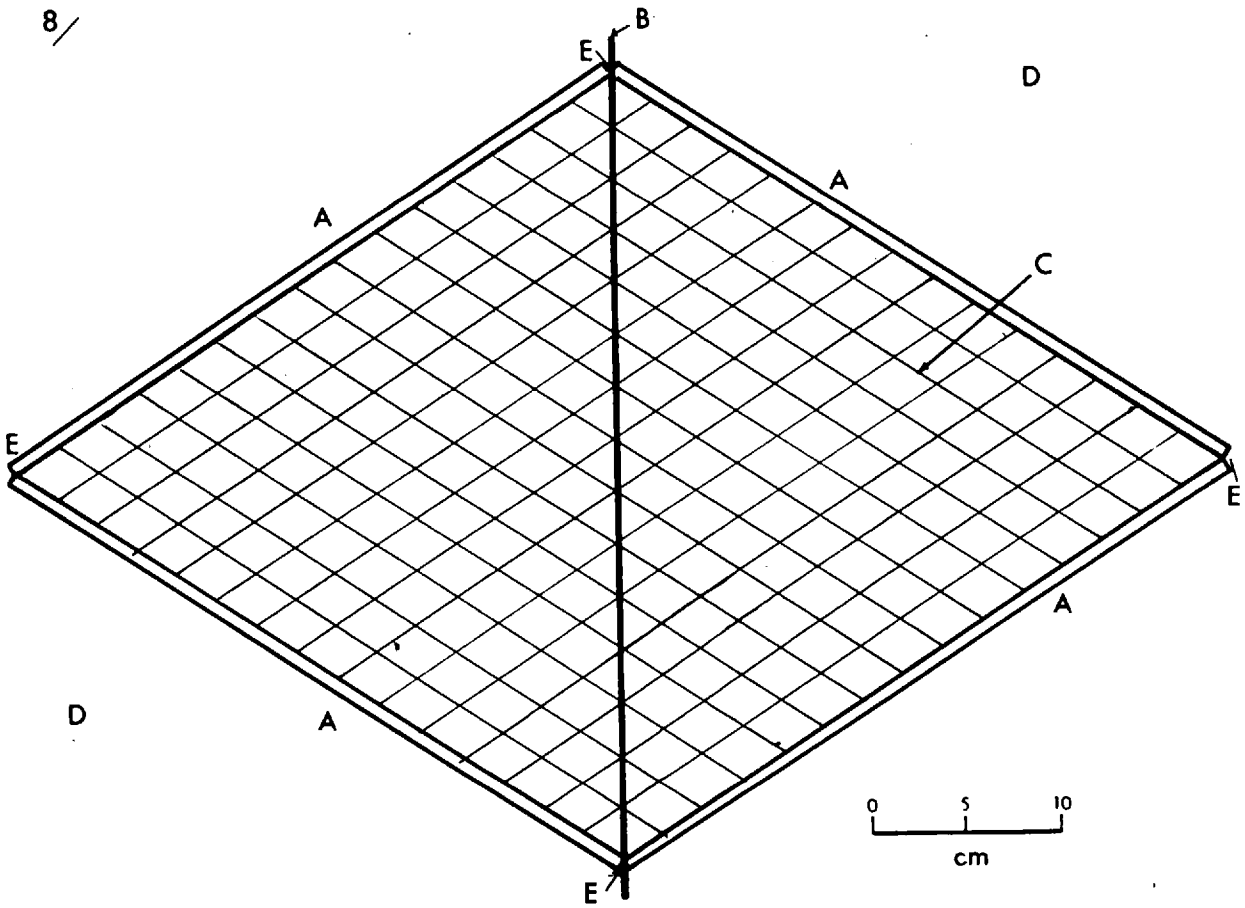

9/

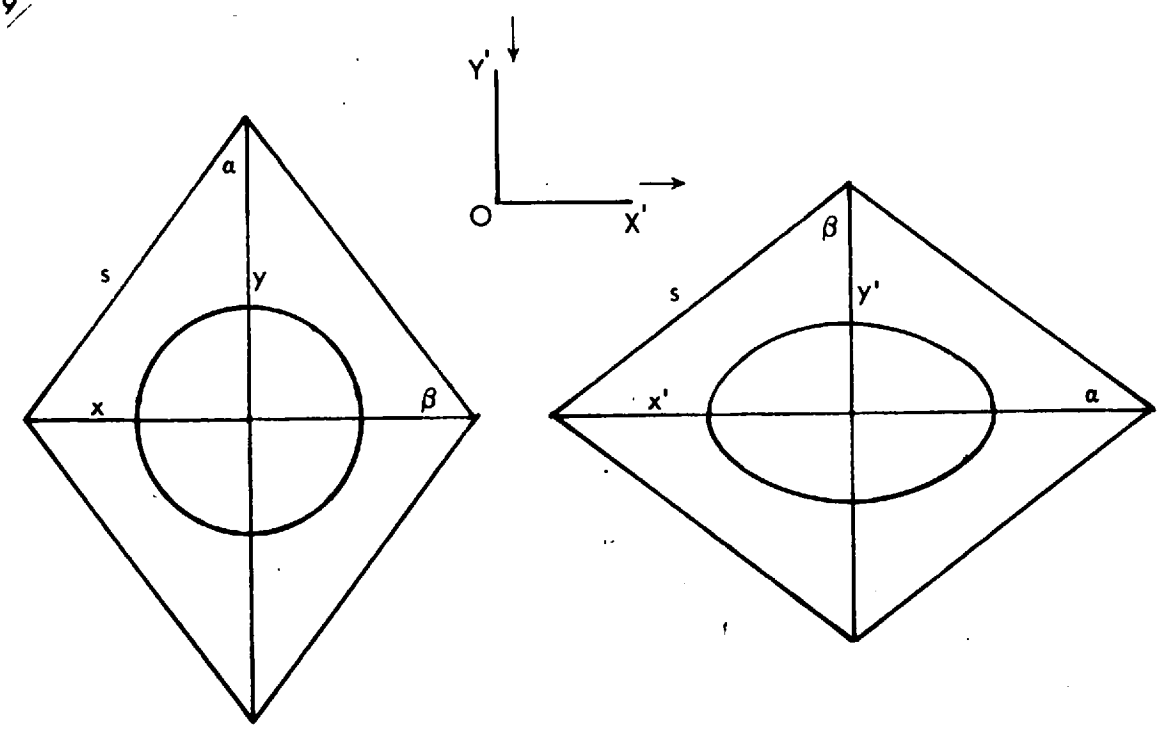

$\alpha = 90^{\circ}$ to zero when $\alpha = 0^{\circ}$. Because of this area change, it is not possible to achieve a true progressive pure shear, though one can obtain a finite pure shear transformation between the initial and final positions by ensuring that the initial and final areas are equal. It is this particular transformation which is of most interest and consequently its geometry will be considered in detail.

Referring to figure 9, the initial lengths along OX and OY are given, respectively, by

$$x = s \cdot \sin \alpha, \quad y = s \cdot \cos \alpha \quad \ldots(III.6)$$

The final lengths are

$$x' = s \cdot \sin \beta, \quad y' = s \cdot \cos \beta \quad \ldots(III.7)$$

Consider an initial unit circle stamped in the matrix with the equation

$$x^2 + y^2 = 1$$

After deformation, this circle becomes the strain ellipse

$$x^2/\lambda_1 + y^2/\lambda_2 = 1$$

From equations III.6 and III.7, the lengths of the semi-major and semi-minor axes are given by

$$\sqrt{\lambda_1} = \sin \beta / \sin \alpha, \sqrt{\lambda_2} = \cos \beta / \cos \alpha \quad \ldots(III.8)$$

and

$$\sqrt{\lambda_1/\lambda_2} = \tan \beta \cdot \cot \alpha \quad \ldots(III.9)$$

If the initial and final areas are to be equal, α and β must be complementary angles. Hence

$$\sqrt{\lambda_1} = \cot \alpha, \sqrt{\lambda_2} = \tan \alpha \quad \ldots(III.10)$$

and

$$\sqrt{\lambda_1/\lambda_2} = \cot^2 \alpha \quad \ldots(III.11)$$

Equations III.10 and III.11 are expressed graphically in figure 10.

Figure 10 Graphs of the equations III.10 and III.11, showing the theoretical changes in axial lengths, $\sqrt{\lambda_1}$ (curve B) and $\sqrt{\lambda_2}$ (curve A), and axial ratio, $\sqrt{\lambda_1/\lambda_2}$ (curve C), with the apical angle, α, of the finite pure shear transformation, in the irrotational strain box. Curve D shows the variation in axial ratio with apical angle determined experimentally by the finite pure shear transformation of a circle of diameter 6.3 cm.

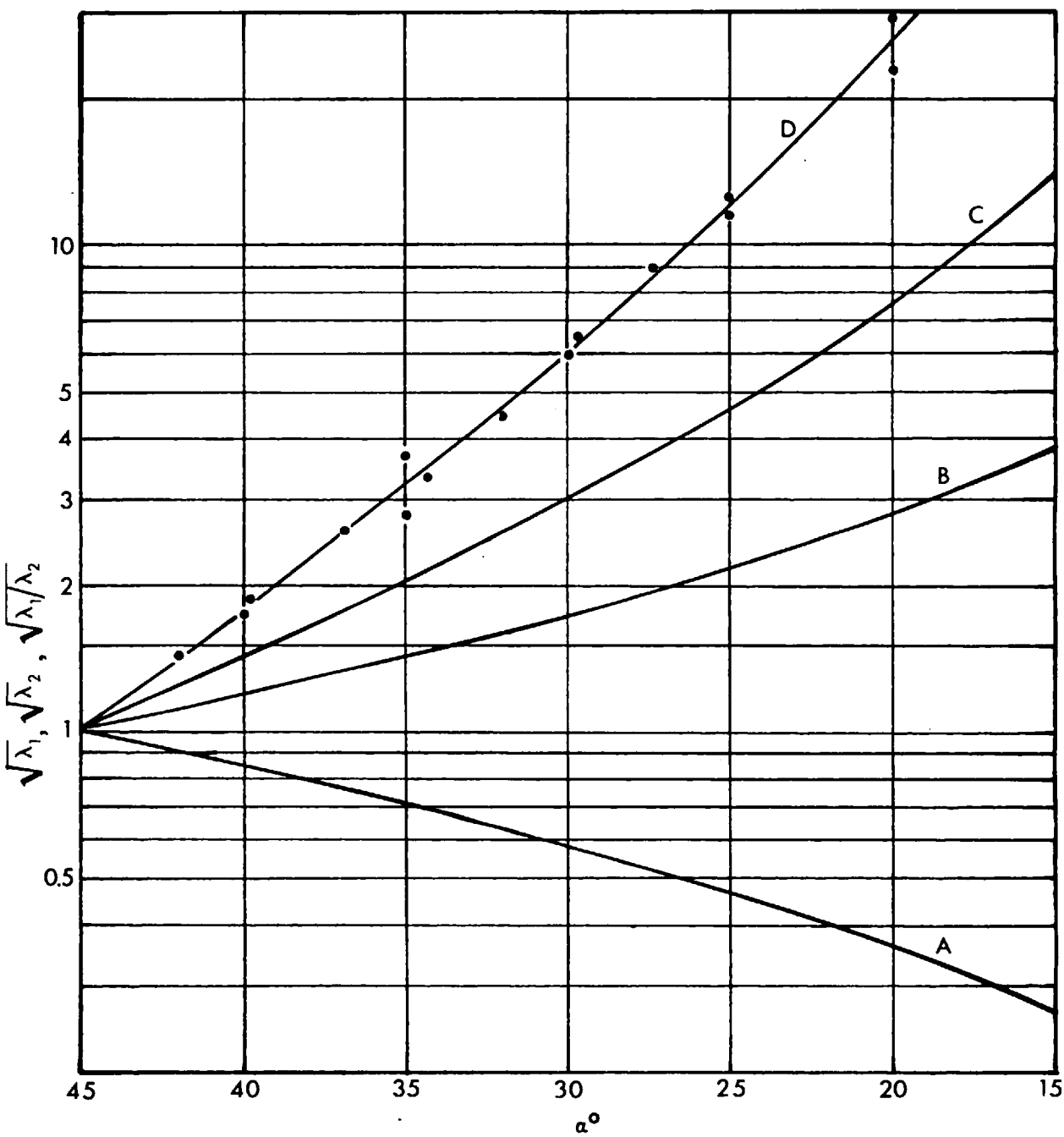
D
C
B
A
10
5
4
3
2
1
0.5
45
40
35
30
25
20
15
α°
$\sqrt{\lambda_1}, \sqrt{\lambda_2}, \sqrt{\lambda_1/\lambda_2}$

End effects, unlike those in the simple shear apparatus, are quite large in the irrotational box. This is mainly due to the area change during deformation and, since the volume remains constant, the resultant friction between the matrix solutions and the sides and base of the box. Hence, the strain varies throughout the apparatus, as is evident from figure 11 which shows the strain at different points on the surface of the solution in the box after a theoretical transformation of $\sqrt{\lambda_1/\lambda_2} = 1.42$. From the shape of the deformed circles, it appears that the strain is not even homogenous at the sides of the box.

To determine approximately the variation of the strain in the centre of the box with the change in apical angle, an initial circle of diameter 6.3 cm. was stamped onto the surface of the matrix. The circle was then deformed over the range of possible apical angles and the axial ratios of the resultant strain ellipses measured. The variation of these axial ratios with apical angle is plotted in figure 10, curve D. The graph shows that the finite strain in the centre of the box varies systematically with the change in angle and is always greater than that predicted theoretically by equation III.11.

It is possible to reduce the end effects by lubricating the sides of the box with vaseline. This is evident from the following table which contains data showing a significant, but not large, reduction in the axial ratio of the strain ellipse in the centre of the box if the sides are greased.

a°	$\sqrt{\lambda_1/\lambda_2}$ th	$\sqrt{\lambda_1/\lambda_2}$ exp	
		ungreased	greased
40	1.42	1.80, 1.80	1.65, 1.70
30	3.00	6.00, 6.05	4.85, 5.30

The importance of end effects can also be reduced by working as far away as possible from the walls and preferably the distance between the walls and the area of interest should

Figure 11 Variation of strain in the irrotational strain box after a finite pure shear transformation of $\sqrt{\lambda_1/\lambda_2} = 1.42$. The ellipses were initially circles of diameter 5 cm. The diagram was traced from a photograph

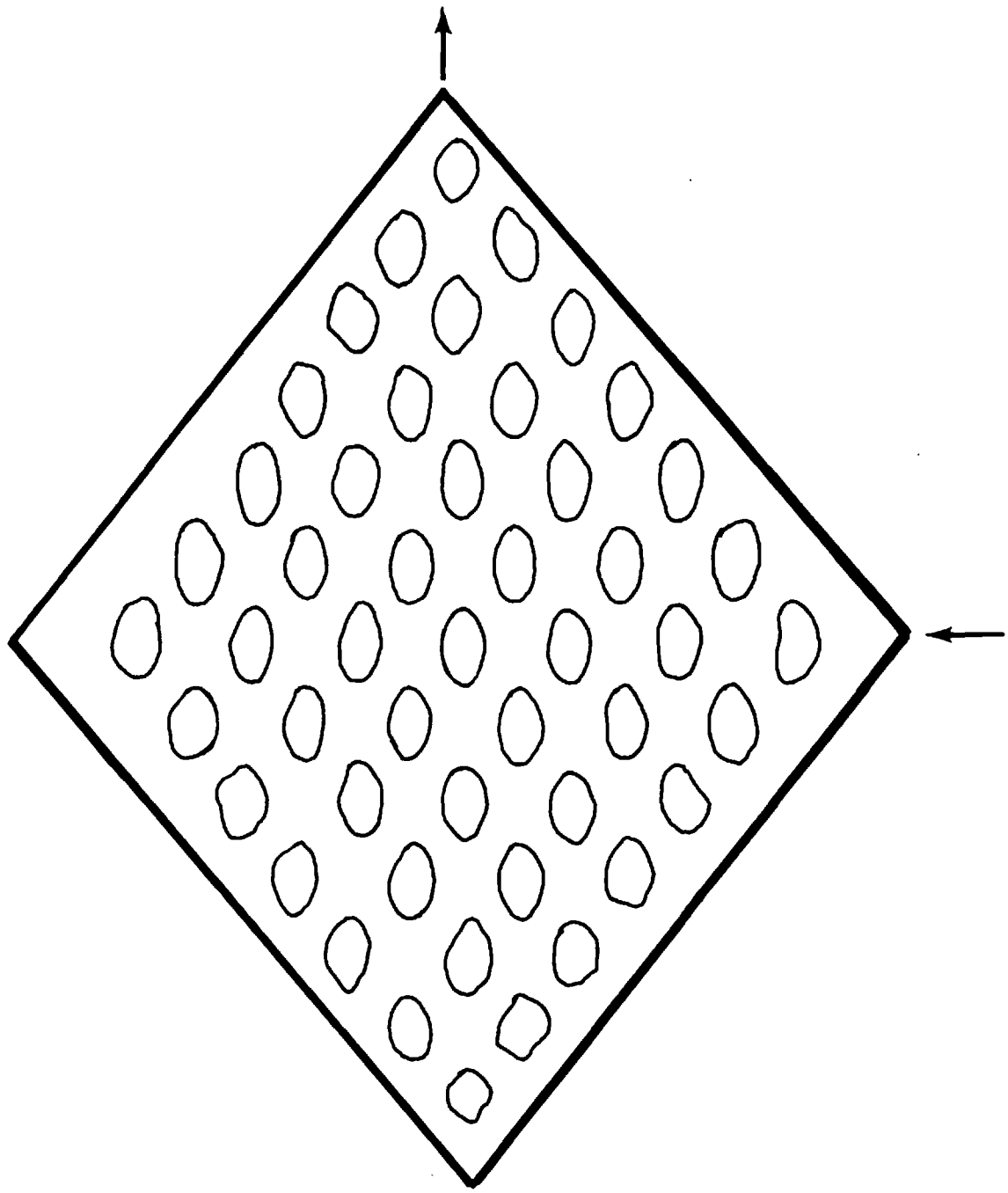

Figure 12 Graphs showing the change, with apical angle, of the distance between the sides of the box and the particle (curve x), and the ratio of distance to particle diameter (x/d).

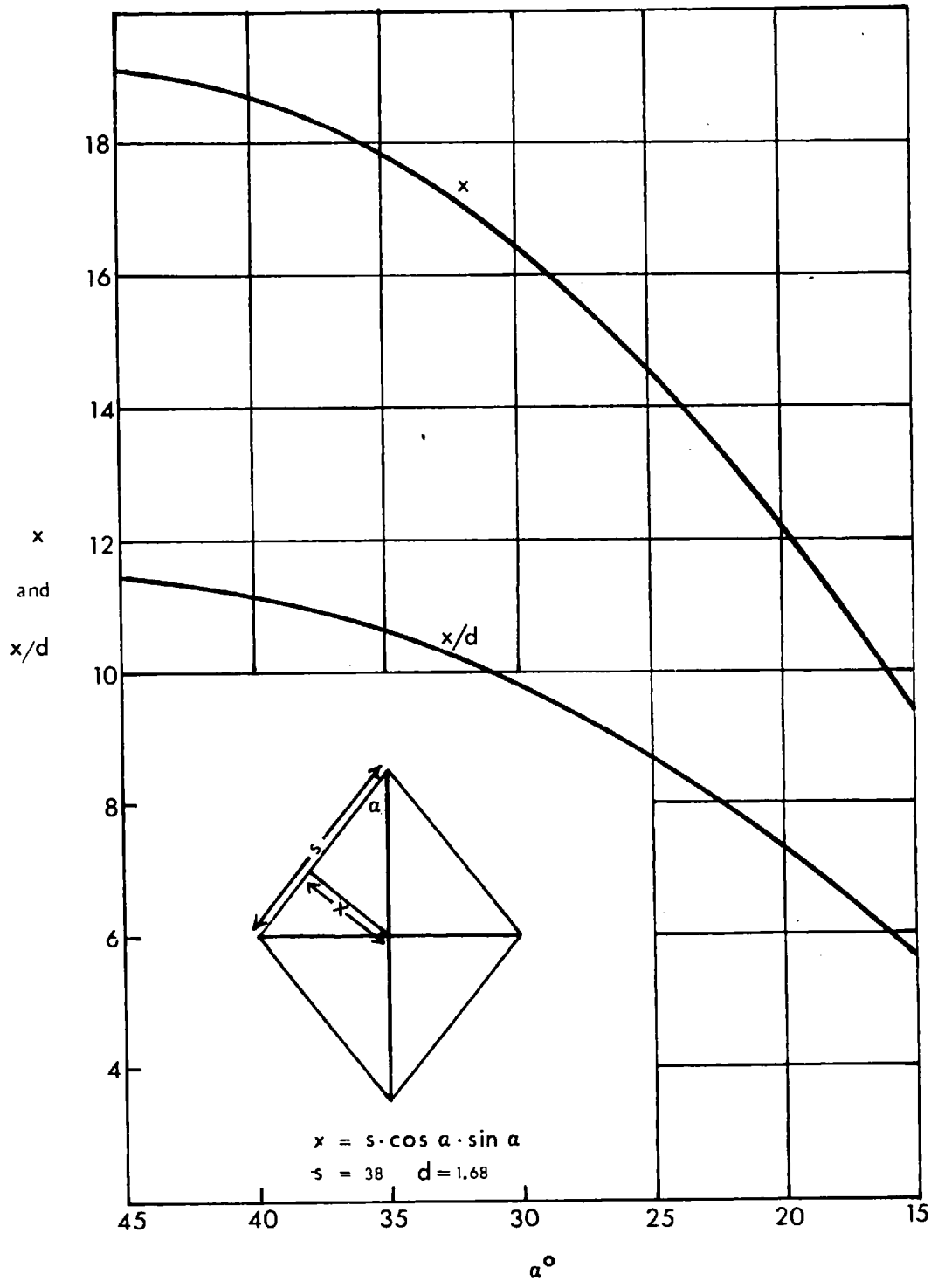
x
and
x/d
18
16
14
12
10
8
6
4
x
x/d
α
s
x
x = s · cos α · sin α
s = 38 d = 1.68
45
40
35
30
25
20
15
α°

be at least ten times the diameter of the area (Price, personal communication). Since the side of the box is approximately 38 cm long, the distance between the nearest point of the walls and the centre of the box, in the position of maximum area, is approximately 19 cm. The diameter of the particles normally used in the experiments was 1.7 cm and this gives 11.4 as the maximum value for the ratio of the distance from the walls to the diameter of the area of interest. Figure 12 shows the change in distance from the wall with change in the apical angle and the corresponding reduction in the ratio between distance and particle diameter. The value of this ratio becomes less than ten for angles smaller than 30°. Therefore, when working with these deformations, smaller particles were used.

(c) Ancillary apparatus.

Additional pieces of apparatus were designed to meet specific requirements in the experiments. These included glass test tubes which had their bases ground away and were used for shaping the non-rigid particles. Wooden plungers which just fitted inside these tubes served for inserting the particles into the matrix.

A circular metal cake cutter of diameter 7.5 cm was used to re-position the non-rigid particles being deformed by simple shear.

A similar cutter, which had a piece of stiff wire netting attached to its base, was used to impress rectangular grids on the surface of the matrix solutions in the experiments to determine the strains around a particle.

(d) Matrix material

Solutions of ethyl cellulose in benzyl alcohol were used for the viscous matrix. The rheological properties of these solutions have been determined in detail Osokina et al (1960). At concentrations of less than 15

per cent solute, the mixtures are Newtonian liquids. At higher concentrations they are non-Newtonian liquids with not very pronounced anomalous viscosities; and only small hysteresis effects and thixotropy are observed under varying deformation rates.

The viscosity coefficient increases with concentration of ethyl cellulose and ranges between 10^2 and 10^6 poise. For a particular solution, the viscosity remains constant for some time after preparation of the solution but decreases exponentially with rising temperature. Depending on the grade of ethyl cellulose used different viscosities will be obtained for the same concentration.

A strain - time curve for ethyl cellulose - benzyl alcohol solutions has been published by Bell and Currie (1964, fig. 4b) which shows that an initial elastic deformation achieved through rapid loading is quickly relieved by a viscous creep component, during which most of the elastic strain energy disappears. The small amount of energy remaining is sufficient to allow the use of photoelastic methods for stress analysis. However, this property was not required in the present work. The residual elasticity is unlikely to have affected the experimental results obtained because the relaxation time of the solutions is extremely small (10^0 - 10^1 sec; Gzovsky, 1959).

The ethyl cellulose used for the preparation of the solutions was that marketed by the Dow Chemical Company under the trade name "Ethocel" (standard ethoxy content, viscosity grade 200). The E.P. grade Benzyl Alcohol manufactured by W.J. Bush and Co. was used as solvent.

To prepare the solutions, the required proportions of ethocel and alcohol were mixed together in a large beaker which was heated on a sand bath. Best results were obtained if only small quantities of solvent and solute were mixed together at one time. Bell and Currie (1964, p. 41) state that to get a fluid free of entrapped air bubbles it is

necessary to heat the mixture in a vacuum at 70° to 80°C for 5 to 12 hours. However, the writer prepared solutions sufficiently free from air bubbles by dissolving the ethocel completely, covering the beaker to prevent evaporation of the solvent and allowing the mixture to digest on a low flame for a day and then cool gradually overnight. A longer period of digestion and cooling was required for the more viscous fluids.

To construct a graph relating the coefficient of viscosity of a solution to the proportion of ethyl cellulose dissolved in it, several solutions covering a concentration range of 15 to 35 per cent solute were carefully prepared. The viscosity coefficients were then determined using a Ferranti-Shirley cone-plate viscometer. This instrument measures the viscous traction exerted by the fluid during shearing at a constant rate and can be used for viscosities up to 10^5 - 10^6 poise. However at the very high values, cracking of the liquid may occur at even the slowest rates of shear, thus giving anomalously low results. McKennell (1960) discusses the principles of this and other types of viscometer in detail.

The results of the viscosity - concentration determinations are plotted graphically in figure 13 together with those of Osokina et al (1960) as calculated by the present writer from their figure 2, for comparison. Note that these workers used ethyl cellulose of a greater viscosity grade than the present writer and made their determinations with a constant shear stress viscometer.

Figure 13 was used as a working curve to correlate the concentration of ethyl cellulose with the viscosity coefficient of the solution. Normally solutions containing 22, 25 and 30 per cent ethocel were used for the matrix in the experiments.

Figure 13 The relationship between viscosity and concentration for ethyl cellulose - benzyl alcohol solutions. Graph A is taken from Osokina et al (1960, fig. 2) for 290 grade ethyl cellulose, at a shear stress τ = 10 gm/cm^2. Graph B was obtained by the present writer for 200 grade ethyl cellulose at 18°C and at a constant shear rate $\dot{\gamma}$ = 0.1 r.p.m.

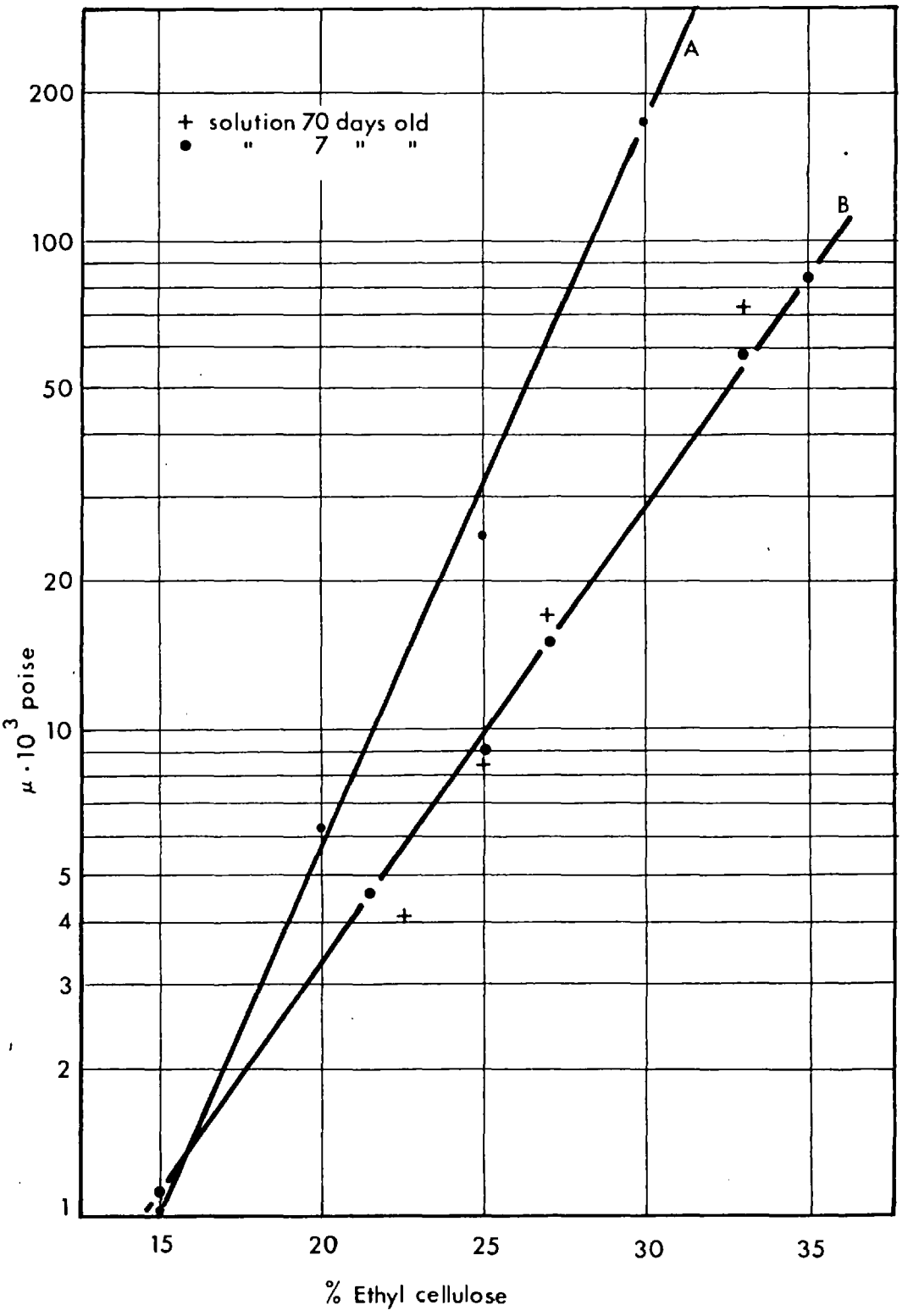
+ solution 70 days old
● " 7 " "
A
B
200
100
50
20
10
5
4
3
2
1
μ · 10³ poise
15
20
25
30
35
% Ethyl cellulose

(c) Particles

The rigid two-dimensional particles were made from 1.6 mm thick aluminium sheeting; they were circular and elliptical in shape and had the following axial ratios, eccentricities and surface areas:

a/b	e	area (sq cm)	a/b	e	area (sq cm)
1.01	0.14	5.20	2.85	0.94	4.14
1.36	0.70	3.88	3.66	0.96	5.28
1.51	0.75	3.50	3.84	0.96	10.43
1.92	0.85	5.33	4.39	0.98	5.74
1.96	0.86	2.60	4.71	0.98	2.37
2.70	0.93	5.76			

The eccentricity e is defined by $e = \sqrt{(a^2-b^2)/a^2}$ where a and b are the lengths of the major and minor particle semi-axes.

The rigid particles used for three-dimensional experiments were hollow glass prolate spheroids with axial ratios approximately 4 : 1 : 1. These ellipsoids were prepared by sealing off the ends of thin-walled, soft glass tubing and then rounding them to shape with emery paper. The dimensions of the air bubble inside it were such as to ensure that the particle had the same density as the matrix and therefore was not acted on by body forces during the experiments.

Solutions of ethyl cellulose and benzyl alcohol, coloured with methylene blue dye, were used for the non-rigid particles. These particles were disc-shaped with diameters of 1.1 or 1.7 cm and thicknesses of 1.6 mm. The open-ended glass test tubes and wooden plungers were used to shape them and great care was taken to ensure that they enclosed no air bubbles. Their compositions, viscosity coefficients and corresponding ratios with the viscosity of a 22 per cent ethyl cellulose matrix solution are tabulated below.

% ethocel	μ (poise)	R	% ethocel	μ (poise)	R
22.0	$5.0 \cdot 10^3$	1.0	31.5	$37.5 \cdot 10^3$	7.5
26.5	$12.5 \cdot 10^3$	2.5	32.5	$50.0 \cdot 10^3$	10.0
29.5	$25.0 \cdot 10^3$	5.0	34.5	$75.0 \cdot 10^3$	15.0

(R is the ratio between the viscosity of the particle and the viscosity of the matrix)

C. THE EXPERIMENTAL PROGRAMME

(a) Preparation of the apparatus

Before beginning any work, the apparatus to be used was thoroughly greased with vaseline. The main purpose of this greasing was to spread a thin, impermeable seal over the surface of the apparatus and so prevent the matrix solutions of ethyl cellulose from seeping through possible openings. Moreover, it also served to reduce the friction between the solutions and the sides of the irrotational strain box. To achieve a satisfactory seal, all 96 "U" pieces and the perspex end pieces in the simple shear box had to be carefully greased and in the irrotational strain box, great care was taken to ensure a strong seal between the glass base-plate and the tufnel sides.

In addition to lubricating the boxes, other pieces of equipment which were used to prepare and manipulate the non-rigid particles were lightly greased with vaseline before use. This was done to prevent the adhesion of the particle solutions to these tools.

After the box had been set up, the ethyl cellulose solution which acted as the matrix was placed in it and left to settle for some time so that any air bubbles could escape. In the simple shear apparatus, the layer of matrix was at least 2.5 cm deep, and in the irrotational strain box, enough solution was used to ensure that, in the position of maximum area, the cotton grid was covered by a layer of matrix 1.5 cm thick. When the matrix had settled, the irrotational

strain box was adjusted to a suitable apical angle and clamped in this position.

Once the apparatus had been set up with the matrix, it was used for many experiments until the matrix required changing.

(b) Experiments on single particles in the simple shear and irrotational strain boxes.

i) Insertion of the particles

Initial positioning of the particles being studied was carried out as follows. The rigid two dimensional particles were placed on the surface of the matrix so that they floated horizontally. Their major axes (or reference direction in the case of the disc) were set at right angles to the shear direction in the simple shear box, or, at a small angle, φ, to the direction of compression in the irrotational strain box (see figures 14a, b). In the three dimensional experiments, the glass ellipsoids were similarly positioned though at some angle of plunge, θ, to the deformation plane (i.e. the surface of the matrix) as shown in figures 14c, d. Photographs, from which θ could be calculated, were then taken vertically above the ellipsoids.

Placing the non-rigid particles in the matrix was more complicated. The particles were prepared shortly before they were required and were transferred to the matrix in the glass tube used to shape them. The plunger was then used to force them into the desired positions. The procedure had to be carried out rapidly to prevent distortion of the discs but, if this did occur, the circular shape could usually be corrected after insertion. Nevertheless, the initial shapes were photographed to record any deviations from circularity.

Figure 14 Initial positions of an ellipse and an ellipsoid in (a, c) the simple shear box and (b, d) the irrotational strain box. Only the major axes of the particles are shown; φ is the angle in the deformation plane between the major particle axis and the CY' coordinate axis; θ is the angle of plunge of the major particle axis to the deformation plane.

Figure 15 Diagram to show that the error involved in ignoring the refraction at the air - matrix interface is negligible. Using the data given in the figure

$$\tan i = a''/2h \sim 0.02 \sim \sin i$$

The refractive index of benzyl alcohol is 1.54. Therefore, by Snell's Law

$$\sin r = 1.54 \sin i = 0.013$$

and $r = 45'$

If the ellipsoid is at a depth of 1 cm below the fluid surface

$$\delta = \tan r \sim 0.013$$

which can be ignored. Similarly, δ' is very small and can be ignored. Therefore

$$a'' \sim a'$$

and the effects of the refraction at the interface can be ignored.

Figure 16 Diagram to illustrate the method of calculating the plunge, θ, of ellipsoidal particles from the apparent length, a', of the major particle axis.

14

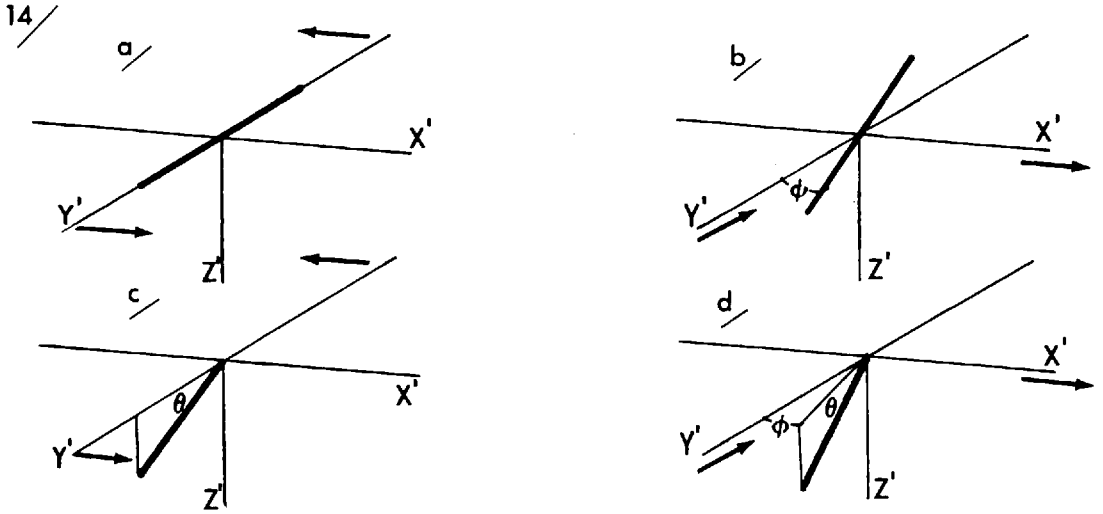
a
X'
Y'
Z'
b
X'
Y'
φ
Z'
c
θ
X'
Y'
Z'
d
X'
Y'
φ
θ
Z'

15

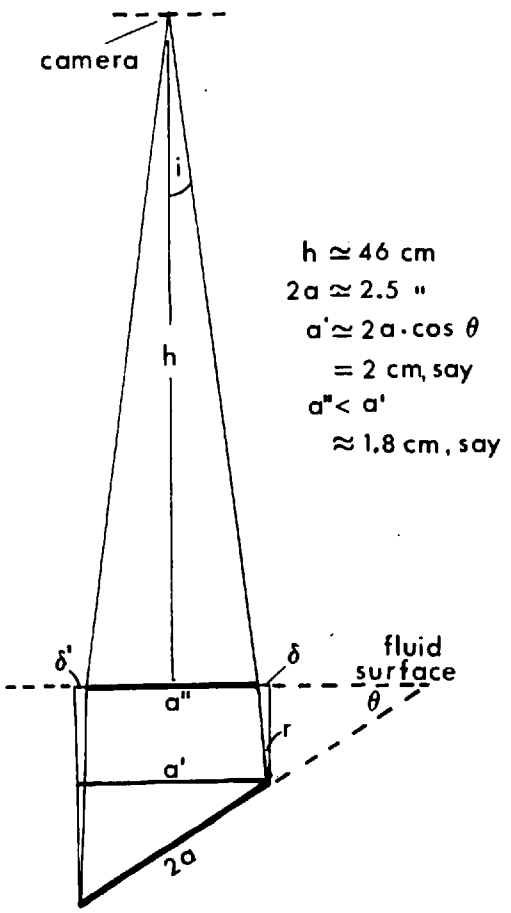
camera
i
h
h ≃ 46 cm
2a ≃ 2.5 "
a' ≃ 2a · cos θ
= 2 cm, say
a" < a'
≈ 1.8 cm, say
δ'
δ
fluid surface
θ
a"
r
a'
2a

16

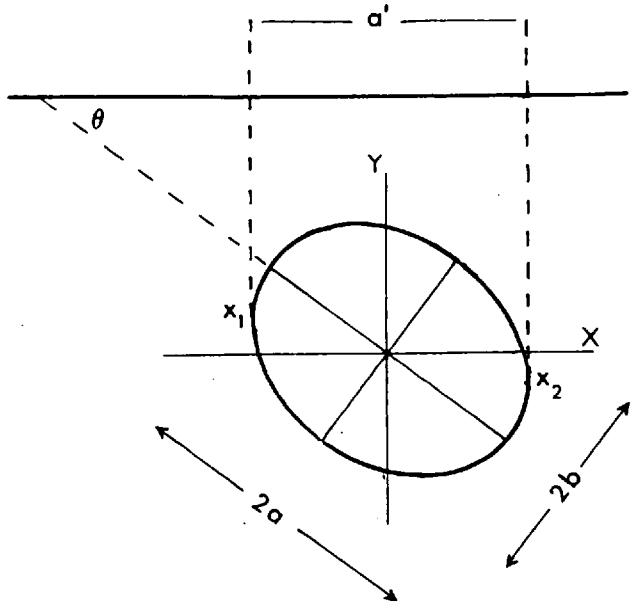
a'
θ
Y
X
x1
x2
2a
2b

ii) Deformation procedure

Having positioned the particle, the deformation was started. The simple shearing was generally carried out slowly by hand unless constant strain rates were required when the motor was used. Similarly, in the irrotational strain box, the deformation was allowed to proceed very slowly so that the level of the matrix remained horizontal despite the change in surface area. Moreover, care had to be taken to ensure that the forces causing the change in shape of the box always acted along the same line. The deformation was stopped after reaching the required apical angle for a finite pure shear transformation. Runs in the simple shear apparatus normally continued for $1\gamma_s$ shear.

iii) Recording changes in particle shape and position

During the deformation runs, the rotation and distortion of the particles were recorded at regular intervals. For the two dimensional rigid particles this was done by measuring the change in orientation of the particles directly during the experiments. However, changes in shape and position of the rigid ellipsoids and non-rigid particles were recorded photographically.

The particle axial lengths and the orientation of the major axes were measured directly from the photographs. However, the plunge of the ellipsoids had to be calculated from the apparent length of the ellipsoid major axis. This was done assuming that the effects of refraction at the matrix - air interface can be ignored. Reference to figure 15 shows that this assumption is valid for the present experiments because the photographs were taken vertically above the particles at a height great enough to reduce the angles of incidence and refraction to negligible amounts. The formula relating the apparent length, a', of the particle major axis to the angle of plunge, θ, is then derived as follows:

In figure 16, the equation of the ellipse with respect to X, Y coordinates is

$$x^2(a^2\sin^2\theta + b^2\cos^2\theta) + 2xy(a^2 - b^2)\sin\theta\cdot\cos\theta + y^2(a^2\cos^2\theta + b^2\sin^2\theta) = a^2b^2 \quad ...(III.12)$$

The length a' is equal to twice the abscissa of the point of vertical tangency x_2. To obtain the coordinates of x_2 differentiate III.12 with respect to y and let dx/dy equal zero. Then

$$y = -x(a^2 - b^2)\sin\theta\cdot\cos\theta/(a^2\cos^2\theta + b^2\sin^2\theta)$$

Substituting this for y in III.12 and simplifying gives

$$x = \pm\sqrt{a^2\cos^2\theta + b^2\sin^2\theta}$$

Hence the apparent length

$$a' = 2\sqrt{a^2\cos^2\theta + b^2\sin^2\theta}$$

which can also be written

$$a' = 2a\sqrt{1 - e^2\sin^2\theta} \quad ...(III.13)$$

Therefore

$$\sin\theta = \sqrt{4a^2 - a'^2}/2ae \quad ...(III.14)$$

Equation III.14 was used to calculate the angle of plunge θ of the major axes of the ellipsoidal particles from the apparent and true lengths of the major axis (a' and a respectively) and the eccentricity of the particle.

iv) Repositioning particles at the end of a deformation run

At the end of each run in the simple shear apparatus the particles were removed from the matrix and replaced in the equivalent position for shearing in the opposite direction, as shown in figure 6.

For non-rigid particles, however, this repositioning process was rather complicated. First, the approximate major and minor particle axial lengths and the orientation of the major axis were measured. The particle and its

immediate matrix environment were then isolated from the rest of the material in the box by enclosing them in a large cake-cutter. Finally, by turning the cutter slowly, the particle and matrix were rotated into the required position. The cutter was carefully removed and the shape and orientation checked to ensure that it agreed with the measurements before repositioning. If there was a discrepancy between these initial and final measurements, the particle was gently pushed into the correct shape. It was found that this procedure ensured the minimum amount of particle distortion during repositioning. However, particles which were elongated to such an extent that the lengths of their major axes nearly equalled that of the diameter of the cutter could not be repositioned in this way, because the distortion during rotation was too great and the particle acquired a sigmoidal shape. When this stage was reached, the experiment was discontinued.

Rigid particles in the irrotational strain box were also removed at the end of each pure shear transformation and replaced in equivalent positions for the deformation in the opposite direction. However, deformed non-rigid particles were removed and replaced by undeformed ones after the box had been adjusted to a new apical angle. The new particles were then subjected to another finite pure shear transformation.

v) Terminating the experiments

The experiments were stopped after sufficient information had been obtained to check the theoretical equations. In the simple shear tests on two dimensional rigid particles enough runs were carried out to rotate the particles through 180°. Similarly, in the irrotational strain experiments, the two dimensional particles were studied until they had approached close to the stable position parallel to the direction of elongation. The behaviour of the rigid ellipsoidal particles was not examined in such detail as

these experiments were difficult to perform and very time-consuming. As mentioned above, the simple shear tests on non-rigid particles were stopped when the particles became too elongated to be repositioned. In the irrotational strain box, the maximum deformation applied to the non-rigid particles was that corresponding to an apical angle of 15°. Working with smaller angles than this was very difficult.

(c) Deformation of a large number of non-rigid particles by simple shear

It will be shown in the theory chapter that the relative concentration of particles with respect to matrix controls the viscosity ratio between the particle and particle-matrix system and that the ratio decreases with increasing particle concentration. To test the importance of this factor, a series of experiments was performed in the simple shear box on particle - matrix systems with the following particle concentrations (in volume per cent): 3, 6, 9, 12, 15, 23. The detailed experimental method is outlined below.

1/ A rectangular grid was laid out on the base of the empty shear box. This grid was used as a guide during the insertion of the particles to ensure that they were regularly distributed throughout the matrix.

2/ A known volume of matrix solution (22 per cent ethyl cellulose in benzyl alcohol) was placed in the box and allowed to settle.

3/ The required number of particles were prepared from a 29.5 per cent ethyl cellulose - benzyl alcohol solution, giving a particle - matrix viscosity ratio equal to 5 at very low particle concentrations. The particles were cylindrical in shape and had a constant volume.

4/ The particles were inserted in the previously planned positions using the method for single discs as described above.

5/ Photographs were taken vertically above the particles to record any initial deviations from circularity in their shape. The height at which the photographs were taken was 4 feet above the box; this was sufficient to make negligible any apparent eccentricity due to the particle not being directly beneath the camera.

6/ The system was then deformed slowly by shearing through an amount of $1\gamma_s$. Photographs were taken after $0.5\gamma_s$ shear and at the final position.

7/ From the photographs the change in particle shape and the orientation of the major particle axis were determined.

(d) Determination of the strains developed in the matrix around a single particle during deformation

A series of experiments was carried out to determine the strains developed in the matrix around rigid and non-rigid particles, during deformation in the simple shear and irrotational strain boxes. The purpose of the experiments was to relate the strain pattern around the particle to the type of deformation which had produced it and to correlate the respective distortions in the particle and the matrix with the viscosity ratio. The experiments were performed using non-rigid particles with viscosity ratios of 2.5, 5.0 and 10.0, a rigid disc and a rigid 2 : 1 ellipse. The method was as follows.

1/ The required apparatus was set up and the matrix solution emplaced. The irrotational strain box was adjusted to an apical angle of 32°.

2/ If a non-rigid particle was being tested, it was inserted into the matrix in the normal manner.

3/ The wire netting attached to the base of a cake cutter was lightly sprayed with slow-drying white paint. It was then firmly and quickly pressed against the surface of the

matrix and the particle, so that the particle was roughly in the centre of the resultant grid.

4/ If a rigid particle was being used, it was now placed in the centre of the grid.

5/ Photographs were taken of the initial position.

6/ The system was then deformed through an amount of $1\gamma_s$ in the simple shear box or to the equivalent apical angle of 32° require for a finite pure shear strain in the irrotational apparatus. These deformations impart approximately the same finite strain ($\sqrt{\lambda_1/\lambda_2} = 2.6$) to the particle - matrix system and hence the results from the two boxes can be compared directly.

7/ Photographs were taken of the final position.

8/ From the distortion of the grids, the strain at different points around the particles was calculated using the Mohr construction. "Flow vectors" showing the direction of movement of the matrix during the deformation were also determined from the undistorted and distorted grids.

D. ACCURACY AND PRECISION OF THE RESULTS

The order of accuracy in the experiments is not high, mainly because of the simple measuring instruments used. Linear dimensions were determined with a pair of dividers and a ruler divided into fiftieths of an inch (equivalent to 0.5 mm). Therefore it was quite easy to estimate to 0.25 mm and the minimum experimental error is suggested to be $\pm$ 2.5 per cent for a particle axis 1 cm long. Obviously the error will be smaller for axes with lengths greater than 1 cm.

The protractor used for angular measurements was graduated in half degrees but it is unlikely that the experimental error is as small as this. Probably $\pm 1^\circ$ is a better estimate, especially for the measurements made directly during the

experiments and not taken off photographs. This means that when small changes in orientation were measured the proportional error was very large. The determination of the plunge of the ellipsoids involved several assumptions which probably increased the error; in these experiments therefore it was assumed to be $\pm 3^{\circ}$. Moreover, a larger error, estimated to be $\pm 2^{\circ}$, occurred in the determination of the orientation of non-rigid particles which had not been highly deformed because it was very difficult to find the exact position of the major axes in these particles.

The precision of the experimental method was determined from the results of a number of experiments carried out on two-dimensional rigid particles during simple shear. The results were treated statistically and are tabulated in Appendix I. From these tables it is seen that the mean value of 33 measurements of the angular rotation of a disc during $1\gamma_s$ shear was 27.5°. The range was 1° and the coefficient of variation 1.7 per cent. The number of measurements on elliptical particles was much less (n = 4 to 8) and the corresponding coefficient of variation and range much larger. The maximum value of the range in any one set of measurements is 4° but the mean value of all the ranges is only 1.3°. This is less than the range due to an experimental error of $\pm 1^{\circ}$ and therefore it is concluded that the precision of the method is satisfactory.

None of the other groups of experiments was repeated as often as those for rigid particles in simple shear. However, all of them were repeated at least twice and it is suggested that the order of accuracy and precision discussed above are applicable to their results.

CHAPTER IV THEORETICAL AND EXPERIMENTAL ANALYSIS OF THE MOTION OF PARTICLES DURING DEFORMATION OF THE PARTICLE-MATRIX SYSTEM

A. INTRODUCTION

In this chapter, the behaviour of rigid and non-rigid particles in a matrix, during deformation by pure and simple shear is examined theoretically and experimentally, assuming that both particles and matrix are viscous fluids.

The theory is developed along the lines of previous work on suspensions and emulsions, especially that of Jeffery (1922) and Taylor (1932, 1934). Jeffery derived equations of motion for rigid ellipsoidal particles in a viscous fluid, during deformation of the suspension by laminar flow. His method, which gives results for a simple shear deformation, is extended by the present writer to a pure shear type of flow. Taylor considered the deformation of drops of one viscous fluid suspended in another, assuming that the drops were so small that they remained nearly spherical under the action of surface tension forces. This assumption is not made in the present work and the resultant equations are applicable to larger particles and greater deformations. Many people (e.g. Cerf, 1951; Trevalyan and Mason, 1951; Bartok and Mason, 1958, 1959; Rumscheidt and Mason, 1961) have extended and tested experimentally the results of Jeffery and Taylor. However, good agreement with the theory was only obtained for rigid spherical particles and for small deformations of non-rigid particles.

Moreover, the approach adopted in this previous work was different from that in the present thesis, being mainly concerned with the effect the presence of the particles had on the properties of the suspension, particularly the viscosity. Although this factor is considered here, the main emphasis is placed on the kinematical behaviour of a particle during

deformation and its dependence on the finite strain involved.

(a) Assumptions and basic equations

In the section on the viscous flow of rock it was shown that rock can under certain conditions behave as a highly viscous fluid and deform by laminar flow with a small Reynolds Number. Therefore, in the theoretical analysis to follow, it is assumed that both particles and matrix are extremely viscous fluids and as such obey the fundamental equations of viscous fluid dynamics. These include the Navier-Stokes equations of fluid motion and the equation of continuity, which express, respectively, the relations of conservation of momentum and conservation of mass of the fluid.

It is also necessary to assume that there is no slipping at the particle - matrix interface, non-rigid particles deform into ellipses of constant area; and that normal and tangential stresses are continuous across the surface of the non-rigid particles.

The systems of coordinate axes used to describe the deformation by fluid flow and the particle motions during the deformation are illustrated in figure 17. The three rectangular, cartesian coordinate axes X, Y, Z have their origin at the centre of the particle and are fixed parallel to the particle axes. They, therefore, move with the particle during the deformation. The X', Y', Z' coordinate axes, also with their origin at the centre of the particle, describe the undisturbed motion of the fluid.

Relationships with respect to either of these coordinate systems can be transferred from one to the other by the following system of direction cosines:

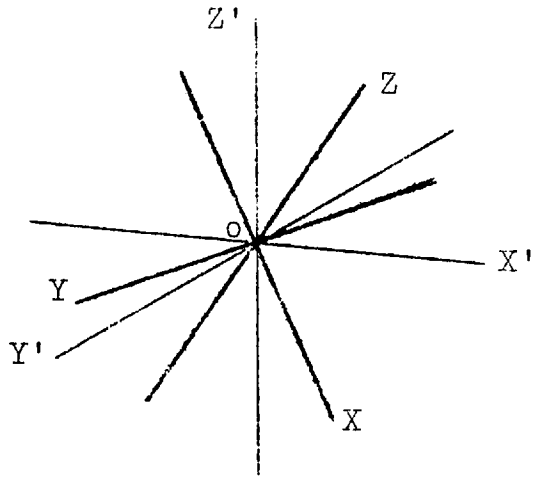

Figure 17 The two systems of rectangular coordinate axes used in the theoretical analysis.

X', Y', Z' - axes for describing the undisturbed fluid motion; they remain fixed in direction throughout the deformation.

X, Y, Z - axes fixed parallel to the particle axes and rotating with it during the deformation.

O - the origin for both sets of axes; it is situated at the centre of the particle.

$$\begin{array}{c|ccc} & X & Y & Z \\ \hline X' & l_1 & l_2 & l_3 \\ Y' & m_1 & m_2 & m_3 \\ Z' & n_1 & n_2 & n_3 \end{array} \quad \ldots\ldots(IV.1)$$

i.e.
$$x = l_1x' + m_1y' + n_1z'$$
$$y = l_2x' + m_2y' + n_2z' \quad \ldots\ldots(IV.2)$$
$$z = l_3x' + m_3y' + n_3z'$$

For each point in the fluid, the components of velocity parallel to the X', Y', Z' axes are

$$u' = dx'/dt, \; v' = dy'/dt, \; w' = dz'/dt \quad \ldots\ldots(IV.3)$$

In terms of these velocity components, a simple shear deformation is described by the equations

$$u' = \dot{\gamma}_s y', \; v' = 0, \; w' = 0 \quad \ldots\ldots(IV.4)$$

Similarly the equations for pure shear are

$$u' = Cx', \; v' = -Cy', \; w' = 0 \quad \ldots\ldots(IV.5)$$

where C is a constant. The significance of this constant is found by integrating equations IV.5 for a point in the fluid with initial coordinates (1, 1, 1), i.e.:

$$C\int_0^t dt = \int_1^{x'} dx'/x' = -\int_1^{y'} dy'/y'$$

Therefore,

$$Ct = \ln x' = -\ln y'$$

During pure shear, the area in the deformation plane remains constant, i.e. $x'y' = 1$, and so

$$C = (1/t)\ln x'$$

The term $\ln x'$ is equivalent to the natural strain and C therefore represents the rate of natural strain, $\dot{\bar{\varepsilon}}$. Equations

IV.5 can be written

$$u' = \dot{\varepsilon}x', \quad v' = -\dot{\varepsilon}y', \quad w' = 0 \quad \text{.....(IV.5a)}$$

The first assumption made above is that the deformations will satisfy the basic equations of viscous fluid dynamics. The general Navier-Stokes equations for fluid motion are very complicated (see Pai, 1956, pp. 36-41) but for flows at very small Reynolds Number, they can be greatly simplified by ignoring the body forces and assuming a slow-moving viscous, incompressible fluid. Then the equations are

$$\mu\nabla^2 u' = \partial p/\partial x', \quad \mu\nabla^2 v' = \partial p/\partial y', \quad \mu\nabla^2 w' = \partial p/\partial z' \quad \text{.....(IV.6)}$$

where p is the mean pressure and

$$\nabla^2 = \partial^2/\partial x'^2 + \partial^2/\partial y'^2 + \partial^2/\partial z'^2$$

The other fundamental equation of interest is the equation of continuity of fluid motion:

$$\partial u'/\partial x' + \partial v'/\partial y' + \partial w'/\partial z' = 0 \quad \text{.....(IV.7)}$$

It is easily shown that the simple and pure shear flows (equations IV.4, IV.5) satisfy these fundamental equations.

The layout of the rest of this chapter is as follows. First rigid particles are dealt with in a simple and then a pure shear field. Then, the deformation during pure shear of a non-rigid ellipse with its axes parallel to the strain axes is analyzed. An ellipse not aligned parallel to these axes is considered after this and finally the deformation of non-rigid discs during simple shear is examined.

The equations for single particles are then applied to systems containing a large number of particles and the chapter ends with an examination of the strains in the matrix around a particle during deformation.

Experimental results for tests on the validity of the theoretical equations are described at the end of each section.

B. THE BEHAVIOUR OF RIGID PARTICLES DURING DEFORMATION BY SIMPLE SHEAR

Einstein (1906, 1911) and Jeffery (1922) have previously investigated this problem and obtained general solutions to describe the motion of particles completely. However, to get their results, these writers had to resort to a complicated mathematical analysis which there seems little point in reproducing here. Instead an elementary, less exact, approach will be adopted and applied to specific examples of the problem.

(a) Motion of a disc

Consider first the case of a disc of small but finite thickness, floating in the deforming viscous matrix (figure 18). The fluid forces acting on the disc can be resolved into normal and tangential forces. Clearly, the sum of the normal forces is zero and, therefore, there is no translation of the disc relative to the fluid. However, the tangential forces set up a couple causing the disc to rotate about its centre O.

The area on which these tangential forces act is πa (arc AB + arc CD), if the disc is of unit thickness. The length of arm of the couple is 2a and the shearing stress of the fluid is $\tau = \mu\dot{\gamma}_s$. The moment of the couple acting on the disc is therefore:

$$M \propto \text{area} \cdot \text{length of arm} \cdot \text{shear stress}$$

i.e. $$M = 2\pi a^2 \tau = 2\pi a^2 \mu \dot{\gamma}_s$$

This moment M must equal the moment of the frictional couple acting on a disc, radius a, which is rotating in the fluid with constant angular velocity ω. Lamb (1932, p. 588, equation 4) gives this moment as

$$M_f = -4\pi\mu a^2 \omega$$

Figure 18 Rotation of a disc floating in the X'Y' deformation plane during simple shear. The radius of the disc is a and the length of arm of the couple acting on the disc is 2a. The angle φ lies between the reference direction in the disc and the OY' flow axis.

Figure 19 Rotation of an ellipse floating in the deformation plane during simple shear. The length of the couple arm, 2L, changes as the ellipse rotates, from 2b, when $\varphi = 90^{\circ}$, to 2a, when $\varphi = 0^{\circ}$.

a, b - semi-axial lengths of the major and minor axes of the ellipse.

18

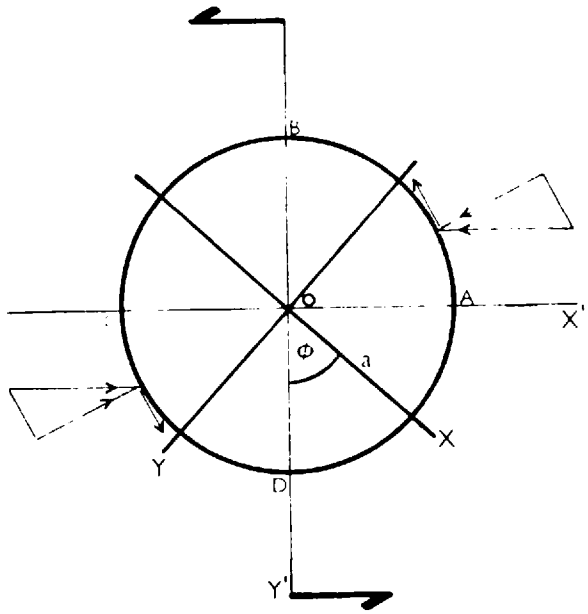

19

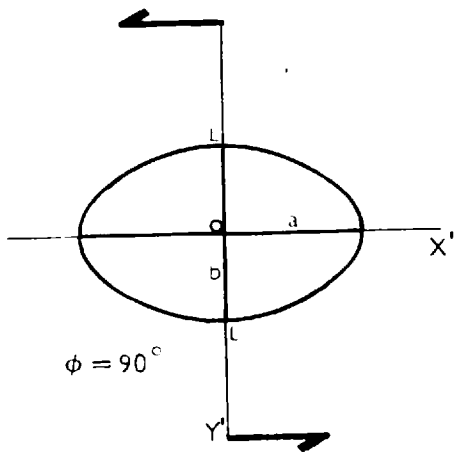

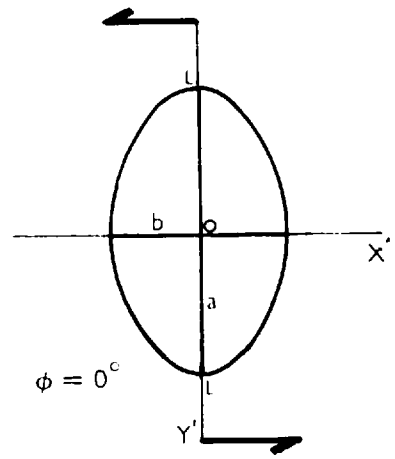

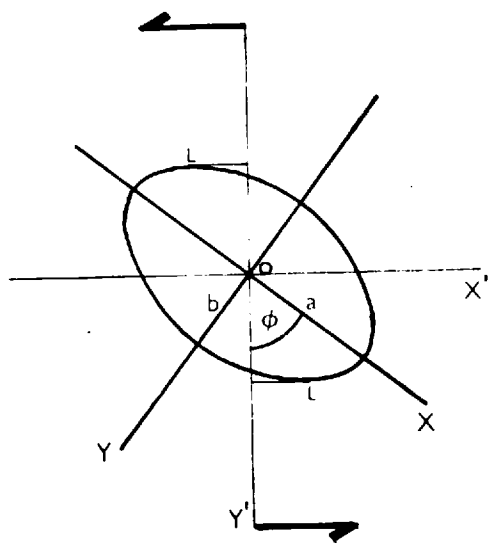

The negative sign can be ignored as it only indicates the retarding action of the fluid on the disc. Then, equating M and M_f results in

$$\dot{\gamma}_s = 2\omega$$

i.e. $$d\dot{\gamma}_s/dt = 2\, d\varphi/dt \quad \ldots.(IV.8)$$

which, if the time factor is eliminated, gives on integration:

$$\gamma_s = 2\varphi \quad \ldots.(IV/9)$$

Equation IV.8 is the same as that derived initially by Einstein (1906, 1911) for small spheres. However, equation IV.9 is of more practical use because it relates finite shears and rotations instead of rates of these displacements.

(b) Motion of an ellipse

The motion of a thin elliptical cylinder can be determined in the same way as above. Again, the tangential shearing forces of the fluid set up a couple on the cylinder but the length of couple arm varies as the ellipse rotates, as shown in figure 19. At any orientation φ the length of the couple arm is calculated as follows.

The equation of the ellipse with respect to the moving coordinate axes is

$$x^2/a^2 + y^2/b^2 = 1 \quad \ldots.(IV.10)$$

The relationship between the fixed and moving axes is

$$\left.\begin{aligned} X &= X'\sin\varphi + Y'\cos\varphi \\ Y &= X'\cos\varphi - Y'\sin\varphi \end{aligned}\right\} \ldots.(IV.11)$$

Substituting IV.11 in IV.10 and rearranging gives

$$x'^2(1 - e^2\sin^2\varphi) + y'^2(1 - e^2\cos^2\varphi)$$

$$- 2e^2x'y'\cos\varphi\cdot\sin\varphi = a^2(1 - e^2) \quad \ldots.(IV.12)$$

The length of the couple arm is twice the ordinate of the point L (i.e. $2y'_L$) at which the tangent to the surface of the ellipse is horizontal. To obtain this, differentiate IV.12 with respect to x' and set dy'/dx' equal to zero. Then IV.12 becomes

$$x' = y'e^2\sin\varphi\cdot\cos\varphi/(1 - e^2\sin^2\varphi) \quad ....(IV.13)$$

Substituting IV.13 in IV.12 and simplifying gives

$$y'_L = a\sqrt{1 - e^2\sin^2\varphi} \quad .....(IV.14)$$

The length of arc, S, and hence the area on which the fluid acts positively is proportional to y'_L, i.e.:

$$S = Ky'_L \quad ....(IV.15)$$

where K is a constant.

There is no exact formula for the perimeter or length of arc of an ellipse. Normally these quantities are evaluated from elliptic integrals of the second kind (Legendre's E function) which cannot be solved analytically but may be computed numerically. Tables of values for E functions are available (e.g. Jahnke and Emde, 1943) which can be used to evaluate lengths of arc for particular ellipses. However, the present analysis requires a general solution for any ellipse and so to solve the problem assume, arbitrarily, that the constant K in IV.15 is equal to $\pi/2$. Then

$$S = (\pi/2)a\sqrt{1 - e^2\sin^2\varphi} \quad ....(IV.16)$$

This implies that at any instant during rotation of the particle the fluid acts on a rectangular segment of a circle with radius y'_L and that the mean value for S during rotation of the particle through 90^0 will be one quarter the perimeter of the ellipse.

Assuming unit particle thickness, the area exposed to the fluid is 2S and the moment of the couple acting on the ellipse is

$$M \propto \text{area} \cdot \text{length of arm} \cdot \text{shear stress}$$

i.e. $$M = 2\pi a^2(1 - e^2\sin^2\varphi)\mu\dot{\gamma}_s$$

This moment must equal the moment of the frictional couple, M_f, retarding an elliptical cylinder rotating in a viscous fluid with angular velocity ω. Goodier (1934) has shown M_f to consist of two parts:

$$\text{a pressure torque} = 2\pi\mu\omega(a - b)^2$$

$$\text{and a viscous torque} = 4\pi\mu\omega ab$$

Therefore, the total torque is

$$M_f = 2\pi\mu\omega(a^2 + b^2)$$

Equating M and M_f gives

$$\omega = [a^2/(a^2 + b^2)]\dot{\gamma}_s(1 - e^2\sin^2\varphi)$$

i.e. $$\int_0^{\varphi} d\varphi/(1 - e^2\sin^2\varphi) = [a^2/(a^2 + b^2)]\int_0^{\gamma_s} d\gamma_s \quad ..(IV.17)$$

Performing the integration results in

$$[1/\sqrt{1 - e^2}] \text{ arc tan } [(1 - e^2)\tan\varphi]$$

$$= [a^2/(a^2 + b^2)]\gamma_s$$

which can be rearranged to

$$\tan\varphi = (a/b)\tan[ab\gamma_s/(a^2 + b^2)] \quad ....(IV.18)$$

This is the same equation as that derived by Jeffery (1922, equation 43) for an ellipsoid with its Z axis parallel to the Z' axis of flow. It relates the change in orientation φ to the finite simple shear γ_s.

Figure 20 Rotation of an ellipsoid of revolution during simple shear.

θ - the angle of plunge of the major axis of the ellipsoid to the deformation plane.

φ - the angle of orientation of the major axis of the ellipsoid; it is measured between the OY' axis and the projection of the major axis onto the deformation plane.

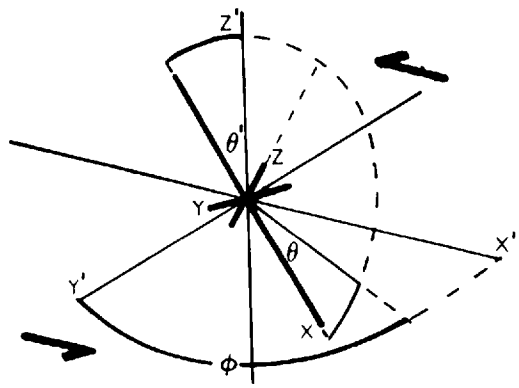
Z'
θ'
Z
Y
X'
θ
Y'
X
φ

(c) Motion of an ellipsoid of revolution

The equations of motion for an ellipsoid of revolution cannot be determined as easily as the two dimensional examples considered above and, instead of deriving an independent solution, recourse will be had to Jeffery's (1922) results.

Referring to figure 20, Jeffery's equation connecting the angle of orientation φ and the amount of simple shear is identical with IV.18 above (Jeffery, 1922, equation 48). Moreover, the plunge of the major semi-axis of the ellipsoid changes with orientation φ according to the equation

$$\tan^2\theta' = a^2b^2/[k^2(a^2\cos^2\varphi + b^2\sin^2\varphi)]$$

(Jeffery, 1922, equation 49) where $\theta' = 90^\circ - \theta$ is the complement of the plunge, θ, and k is a constant of integration. This equation can be written

$$\cot\theta = \cot\theta_i/\sqrt{1 - e^2\sin^2\varphi} \quad \ldots.(IV.19)$$

where θ_i is the plunge when $\varphi = 0^\circ$, $\cot\theta_i$ is the constant of integration and the axial ratio a/b is always calculated with b equal to unity.

(d) Significance and experimental verification of the equations of motion

In this section the significance of the equations derived above, together with the results obtained from experiments performed to check them, will be discussed.

i) Two dimensional particles

Dealing with the two dimensional particles first, the relevant equations for a disc and an ellipse are

$$\gamma_s = 2\varphi \quad \ldots..(IV.9)$$

and

$$\tan\varphi = (a/b)\tan[ab\gamma_s/(a^2 + b^2)] \quad \ldots.(IV.18)$$

Note that IV.18 reduces to IV.9 if a = b.

The graphs of these equations are plotted in figure 21 for different values of a : b and for φ ranging from -90° to 90°. From the graphs it is clear that the disc will rotate at a constant rate during the shearing but that the angular velocity for the ellipses varies from a maximum when $\varphi = 0^{\circ}$ (i.e. at right angles to the shear direction) to a minimum when $\varphi = \pm 90^{\circ}$ (parallel to the shear direction). Moreover, the tendency for the ellipses to rotate out of the direction of shearing decreases with increasing eccentricity of the particle and a very large shear indeed is required to rotate a 5 : 1 ellipse a significant amount.

This conclusion is clearly shown in another way by considering the differential form of equation IV.17 which can be written

$$d\varphi/d\gamma_s \equiv [a^2/(a^2 + b^2)][1 - e^2\sin^2\varphi] \quad ...(IV.17a)$$

If $\varphi = 0^{\circ}$, $d\varphi/d\gamma_s = a^2/(a^2 + b^2)$ ....(IV.17b)

If $\varphi = 90^{\circ}$, $d\varphi/d\gamma_s = b^2/(a^2 + b^2)$ ....(IV.17c)

Substituting values for the particle axial ratio a/b in equations IV.17b and IV.17c gives the following results:

a/b	$d\varphi/d\gamma_s$ ($\varphi=0^{\circ}$)	$d\varphi/d\gamma_s$ ($\varphi=90^{\circ}$)
1.3	0.639	0.373
1.5	0.692	0.308
2.0	0.800	0.200
3.0	0.900	0.100
4.0	0.941	0.059
5.0	0.990	0.010

From this table it is obvious that once in the $\varphi = 90^{\circ}$ position, very eccentric ellipses require a large amount of shear to displace them.

A number of experiments were performed in the simple shear

Figure 21 Rotation of two dimensional particles during simple shear. Solid graphs are plotted from the theoretical equations IV.9 and IV.18. The dashed curves are for the mean experimental results listed in Appendix I, tables I to VI The axial ratios of the particles represented by the curves are:

A - 1 : 1, B - 1.01 : 1, C - 3 : 1,
D - 2.70 : 1, E - 4 : 1, F - 3.66 : 1
G - 5 : 1, H - 4.71 : 1, I - 1.33 : 1
J - 1.36 : 1, K - 2 : 1, L - 1.94 : 1

φ - the angle of orientation of the major axis of the particle with respect to the OY' flow axis.

γ_s - amount of simple shear

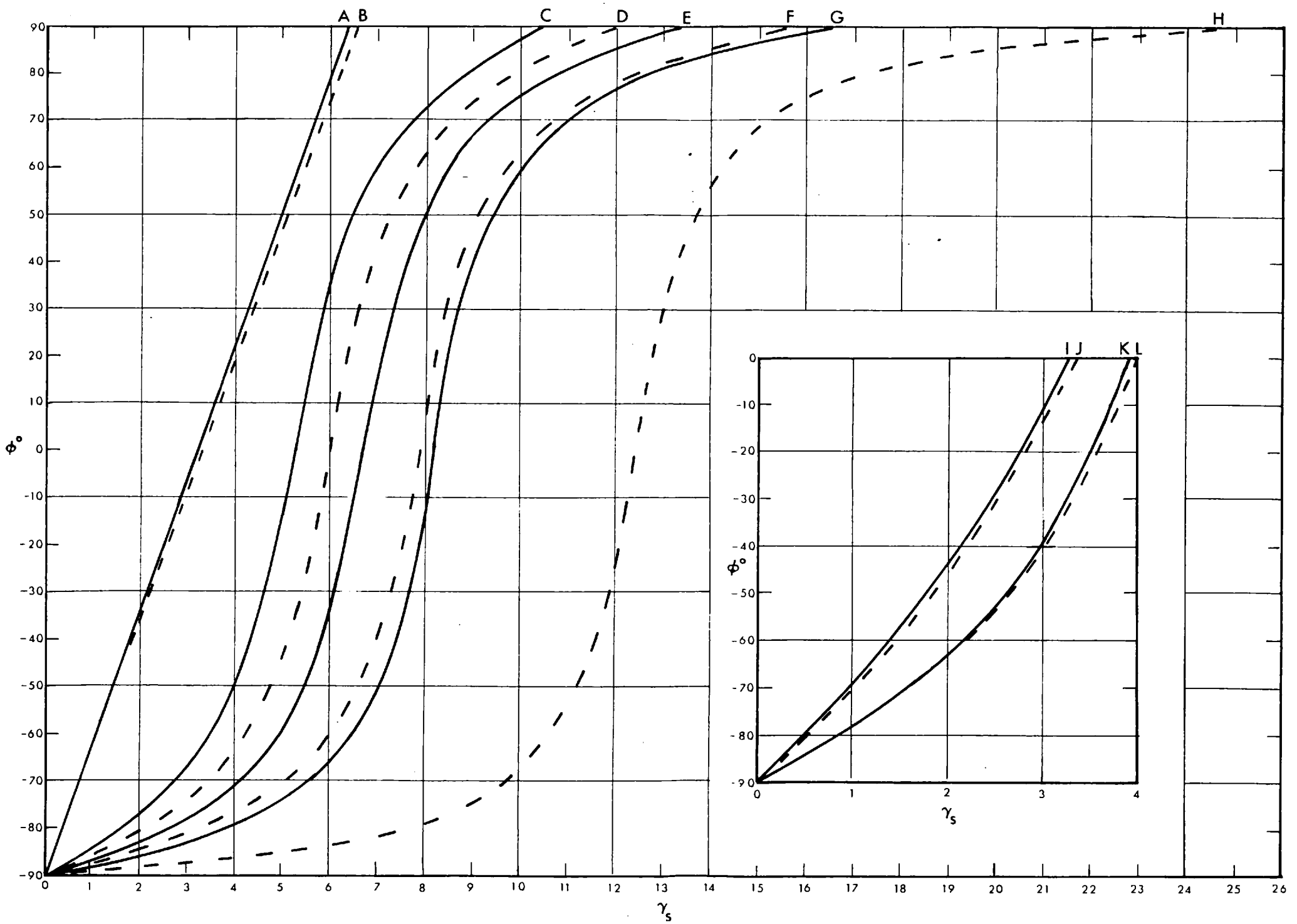
A B C D E F G H
I J K L
90 80 70 60 50 40 30 20 10 0 -10 -20 -30 -40 -50 -60 -70 -80 -90
0 1 2 3 4 5 6 7 8 9 10 11 12 13 14 15 16 17 18 19 20 21 22 23 24 25 26
$\phi°$
γ_s
0 -10 -20 -30 -40 -50 -60 -70 -80 -90
0 1 2 3 4
$\phi°$
γ_s

box on circular and elliptical particles to test these equations. The results of these experiments were treated statistically and mean graphs of rotation against simple shear were constructed for each particle. These graphs are also shown in figure 21. The method of constructing the graphs is given in Appendix I with the statistical data.

Comparison of the theoretical and experimental graphs shows that they have the same shapes but that generally the equations predict a more rapid rotation than that observed experimentally. The agreement between the curves for circular particles is good but with increasing eccentricity the ellipses do not rotate out of, or into, the shearing direction ($\varphi = \pm 90^{\circ}$) as readily as expected.

This retardation in the zone of small rotations is quite possibly due to errors in measurement. For example, referring to table IV (a : b = 2.7) in Appendix I, it is seen that the range in measurement of an initial rotation of 2° from $\varphi = -90^{\circ}$ is 1.5°, which is greater than the discrepancy between the theoretical and experimental curves. This initial discrepancy will naturally be magnified with increasing shear and rotation. Differences between theory and experiment are even more likely to occur with ellipses of greater axial ratio than 2.7, as the initial rotations will be equal to, or less than, the range of experimental error.

However, if the differences were solely due to errors in measurements, some experimental results should show more rapid rotation than that predicted theoretically. This was not observed in any of the experiments from which the graphs in figure 21 were calculated, which suggests that other errors not considered in the treatment of the results may have been introduced during the experiments, possibly in the measurement of γ_s.

Nevertheless, it is felt that the good agreement between the theoretical and experimental curves for the disc and the

Figure 22 Stereographic plots of equation IV.19 showing the variation of plunge, θ, with orientation, ϕ, for the following ellipsoids of revolution:
A - 1.33 : 1 : 1, B - 1.5 : 1 : 1,
C - 2 : 1 : 1, D - 4 : 1 : 1.
Also plotted in figure D are results of experiments carried out in the simple shear apparatus on 4 : 1 : 1 ellipsoids. The detailed results are listed in table VII, Appendix I.

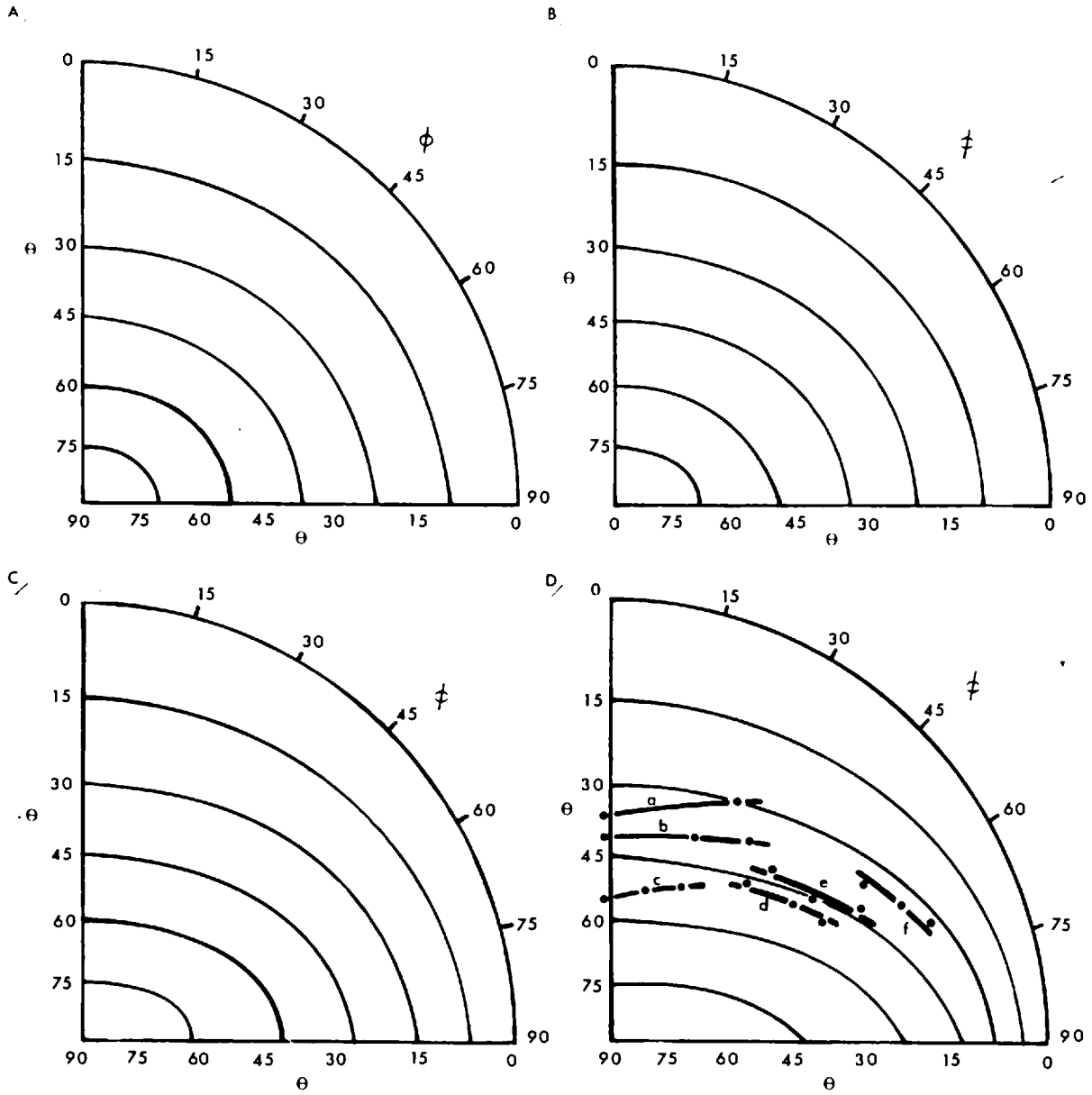
A
B
C
D
0
15
30
45
60
75
90
θ
φ
a
b
c
d
e
f

less eccentric ellipses, and the fact that the curves have the same shape, indicate that the equations are probably correct.

ii) Three dimensional particles

The equations describing the motion of ellipsoids of revolution during simple shear are

$$\tan \varphi = (a/b)\tan [ab\gamma_s/(a^2 + b^2)] \quad ...(IV.18)$$

$$\cot \theta = \cot \theta_i/\sqrt{1 - e^2\sin^2\varphi} \quad ...(IV.19)$$

Equation IV.18 has been discussed in detail above for two dimensional particles and here gives the change in orientation φ of the major axis of the ellipsoid, as measured in the deformation plane. Equation IV.19 correlates the change in the angle of plunge of the major axis with the change in φ.

Together, the two equations imply that during simple shear, an ellipsoid of revolution, plunging at some angle to the deformation plane, will rotate in a spherical elliptical orbit about the Z' axis, perpendicular to the deformation plane. This is clearly brought out in figure 22 in which IV.19 is plotted on quadrants of stereonets for ellipsoids of different eccentricity. From the graphs, it is seen that the plunge of the major axis decreases from a maximum along $\varphi = 0^\circ$ to a minimum along $\varphi = 90^\circ$. Moreover, the rate of change of plunge increases with increasing particle eccentricity.

The equations were tested experimentally using the 4 : 1 : 1 glass ellipsoids and the simple shear apparatus, the changes in plunge being calculated from equation III.14. These results are plotted in figure 22D and agree fairly well with those predicted theoretically, especially when it is remembered that there is a relatively large error involved in the determination of the plunge.

iii) Other experiments on two dimensional particles in the simple shear apparatus

In addition to predicting the motion of particles during simple shear, the equations IV.9, IV.18 and IV.19 also imply that the physical conditions under which the experiments are carried out do not affect the particle behaviour, provided that the initial assumption of a slow-moving, viscous fluid for the matrix and a resultant small Reynolds Number for the experiments, is met. To verify this conclusion, several experiments were performed to examine the effect, on particle rotations, of the size of the particle, the viscosity of the matrix and the rate of shear at which the deformation takes place.

The results of these experiments are listed in tables II, III and IV. From table II, it is clear that the amount of rotation during shear is independent of the size of the particles, as shown by the wetted surface area. Similarly, the data in table III show that an 84-fold increase in the viscosity coefficient of the matrix has no effect on the particle rotation; nor does a ten-fold increase in the rate of shear (table IV).

Therefore, it can be concluded that the size of the particle, the viscosity of the matrix and the rate of shear do not affect the behaviour of the particles. Moreover, provided that the Reynolds Number for the experiments is always small, this conclusion should apply to other experiments on rigid and non-rigid particles in both types of apparatus.

Table II Rotation of elliptical particles of different sizes during $0.7\gamma_s$ shear in a 30% matrix solution, at a constant shear rate.

a/b	A	φ°	a/b	A	φ°
1.96	2.60	29, 30	1.92	5.33	29, 30
2.85	4.14	33, 32	2.70	5.76	33, 33
3.66	5.28	33, 33	3.84	10.43	33, 33
4.71	2.37	34, 34	4.39	5.74	34, 35

a/b is the axial ratio of the particle; A is the surface area in cm^2; φ is measured from the position $\varphi = 0^\circ$.

Table III Rotation of particles embedded in ethyl cellulose - benzyl alcohol matrix solutions, with different viscosities, during $1\gamma_s$ simple shear.

Solution	φ_1°	φ_2°	φ_3°
A	27.0	11.0	5.0
B	27.5	10.5	-
C	27.5	11.5	5.0
D	28.0	11.0	4.0

A - 15% matrix solution; $\mu = 10^3$ poise.
B - 25% matrix solution; $\mu = 10^4$ poise
C - 30% matrix solution; $\mu = 2.9 \cdot 10^4$ poise
D - 35% matrix solution; $\mu = 8.4 \cdot 10^4$ poise

φ_1 - rotation of a particle with axial ratio of 0.99
φ_2 - rotation of a particle with axial ratio of 1.94
φ_3 - rotation of a particle with axial ratio of 2.70
φ is always measured from the position $\varphi = 90^\circ$.

Table IV Rotation of elliptical particles in a 30% ethyl cellulose solution during $0.75\gamma_s$ shear at different shear rates.

a/b	φ_a^o	φ_b^o	φ_c^o	φ_d^o
1.01	21	20	20	17
1.92	31	31	30	29
2.70	33	33	33	33
3.66	34	34	34	35
4.49	35	35	35	36

a/b is the particle axial ratio; φ is measured from $\varphi = 0^o$.

φ_a - rotation during shear at a rate of $0.0013\gamma_s$ sec^{-1}

φ_b - rotation during shear at a rate of $0.00053\gamma_s$ sec^{-1}

φ_c - rotation during shear at a rate of $0.00026\gamma_s$ sec^{-1}

φ_d - rotation during shear at a rate of $0.00013\gamma_s$ sec^{-1}

C. THE BEHAVIOUR OF RIGID PARTICLES DURING DEFORMATION BY PURE SHEAR

(a) Derivation of the general equations of motion

The motion of rigid particles during deformation by pure shear can be determined using Jeffery's (1922) basic equations as follows:

The undisturbed motion of the fluid in the neighbourhood of a particle is described by the general equations:

$$u = \underline{a}x + \underline{h}y + \underline{g}z + \eta z - \nu y$$
$$v = \underline{h}x + \underline{b}y + \underline{f}z + \nu x - \xi z \quad \ldots(IV.20) \quad \text{(Jeffery, equation 2)}$$
$$w = \underline{g}x + \underline{f}y + \underline{c}z + \xi y - \eta x$$

The terms $u = dx/dt$, $v = dy/dt$, $w = dz/dt$ are the undisturbed velocity components for each point in the fluid parallel to the X, Y, Z axes; $\underline{a}$, $\underline{b}$, $\underline{c}$, $\underline{f}$, $\underline{g}$, $\underline{h}$, ξ, η, ν are components of distortion and rotation of the fluid.

The general equations of motion for any ellipsoid subjected only to forces exerted upon it by any fluid motion are given by

$$(b^2 + c^2)\omega_1 = b^2(\xi + \underline{f}) + c^2(\xi - \underline{f})$$
$$(c^2 + a^2)\omega_2 = c^2(\eta + \underline{g}) + a^2(\eta - \underline{g}) \quad \ldots(IV.21) \quad \text{(Jeffery, eqn. 37)}$$
$$(a^2 + b^2)\omega_3 = a^2(\nu + \underline{h}) + b^2(\nu - \underline{h})$$

where a, b, c are the lengths of the semi-axes of the ellipsoid, and ω_1, ω_2, ω_3 are the respective rates of rotation of the ellipsoid about its own X, Y, Z axes.

To determine the components of distortion and rotation during a pure shear deformation, differentiate equations IV.2 with respect to time. This gives

$$u = l_1u' + m_1v' + n_1w'$$
$$v = l_2u' + m_2v' + n_2w' \quad \ldots(IV.22)$$
$$w = l_3u' + m_3v' + n_3w'$$

Substituting equations IV.5 into IV.22 results in

$$u = Cl_1x' - Cm_1y'$$
$$v = Cl_2x' - Cm_2y'$$
$$w = Cl_3x' - Cm_3y'$$

and using transformations IV.1 the equations of undisturbed fluid motion near the particle with respect to the particle coordinate axes become

$$u = Cl_1(l_1x + l_2y + l_3z) - Cm_1(m_1x + m_2y + m_3z)$$
$$v = Cl_2(l_1x + l_2y + l_3z) - Cm_2(m_1x + m_2y + m_3z)$$
$$w = Cl_3(l_1x + l_2y + l_3z) - Cm_3(m_1x + m_2y + m_3z) \quad \ldots(IV.23)$$

These equations are equivalent to IV.20 and equating coefficients the terms for the components of distortion and rotation are obtained. They are:

$$\underline{a} = C(l_1^2 - m_1^2),\ \underline{b} = C(l_2^2 - m_2^2),\ \underline{c} = C(l_3^2 - m_3^2)$$
$$\underline{f} = C(l_2l_3 - m_2m_3),\ \underline{g} = C(l_1l_3 - m_1m_3)$$
$$\underline{h} = C(l_1l_2 - m_1m_2),\ \xi = \eta = \nu = 0$$

Substituting these values into IV.21 results in the equations of motion of any ellipsoid during a pure shear deformation;

$$(b^2 + c^2)\omega_1 = C(b^2 - c^2)(l_2l_3 - m_2m_3)$$
$$(c^2 + a^2)\omega_2 = C(c^2 - a^2)(l_1l_3 - m_1m_3) \quad \ldots(IV.24)$$
$$(a^2 + b^2)\omega_3 = C(a^2 - b^2)(l_1l_2 - m_1m_2)$$

(b) Motion of a two dimensional particle

The motion of a two dimensional particle lying in the deformation plane is equivalent to that of an ellipsoid with one axis, Z say, permanently parallel to the Z' axis of the pure shear flow, as in figure 23. The direction cosines between the two sets of coordinate axes are

$$l_1 = \cos\varphi', \quad l_2 = \cos(90 + \varphi'), \quad l_3 = 0$$
$$m_1 = \cos(90 - \varphi'), \quad m_2 = \cos\varphi', \quad m_3 = 0$$
$$n_1 = n_2 = n_3 = 0$$

Therefore, equations IV.24 reduce to

$$(b^2 + c^2)\omega_1 = 0 \quad \text{i.e. } \omega_1 = 0$$
$$(c^2 + a^2)\omega_2 = 0 \quad \text{i.e. } \omega_2 = 0 \quad \ldots(IV.25)$$
$$(a^2 + b^2)\omega_3 = -C(a^2 - b^2)\sin 2\varphi'$$

It has been shown that C is equivalent to the rate of natural strain, $\dot{\bar{\varepsilon}}$. Also, ω_3 is the spin about the particle Z axis (i.e. $d\varphi'/dt$). Hence IV.25 can be written

$$(1/\sin 2\varphi')d\varphi'/dt = -[(a^2 - b^2)/(a^2 + b^2)]d\bar{\varepsilon}/dt$$

If the time factor is eliminated, this can be integrated

$$\int_{\varphi_i'}^{\varphi_f'} d\varphi'/\sin 2\varphi' = -[(a^2 - b^2)/(a^2 + b^2)]\int_0^{\bar{\varepsilon}} d\bar{\varepsilon} \quad (IV.26)$$

where φ_i' and φ_f' are the initial and final particle orientations. Carrying out the integration gives

$$\ln\tan\varphi_f' - \ln\tan\varphi_i' = [(a^2 - b^2)/(a^2 + b^2)](-2\bar{\varepsilon}) \quad \ldots(IV.27)$$

The relationship between the strain ellipse axial ratio and the natural strain for a pure shear is

$$2\bar{\varepsilon} = \ln\sqrt{\lambda_1/\lambda_2} \quad \ldots(IV.28)$$

Using this relationship and the angle φ between the major axis

Figure 23 Motion of an ellipse, or an ellipsoid with its Z axis parallel to the Z' flow direction, during a pure shear deformation.

Figure 24 The system of Euler angles, θ', φ', ψ, used to fix the position of the axes of an ellipsoid of revolution during a pure shear deformation.

23

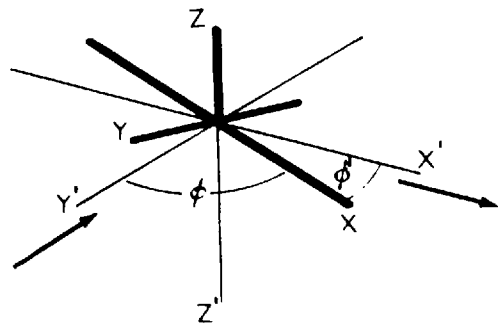

24

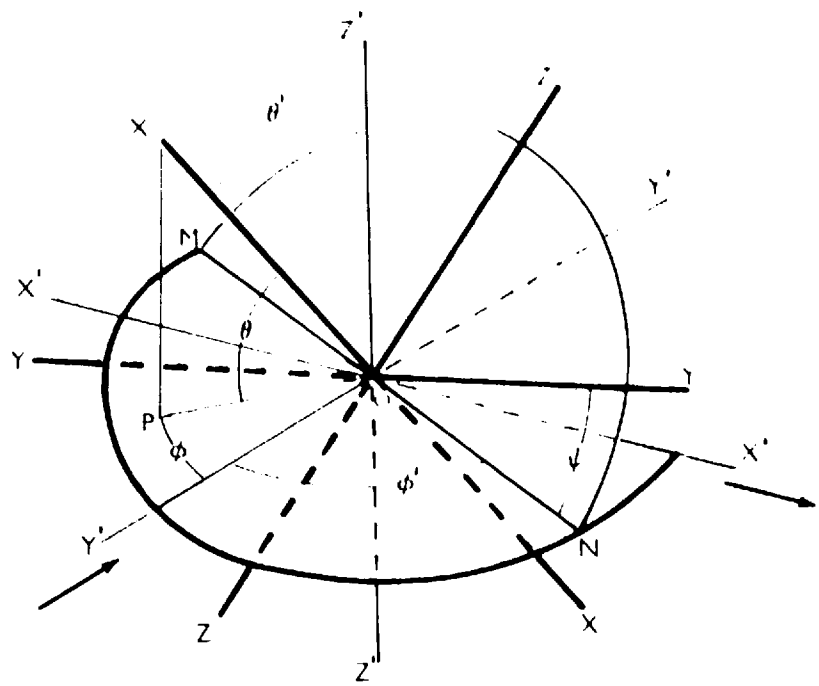

of the particle and the OY' flow direction, to define the particle position, instead of the angle φ', IV.27 becomes

$$\ln \cot \varphi_f = \ln \cot \varphi_i + [(a^2 - b^2)/(a^2 + b^2)] \cdot \ln \sqrt{\lambda_2/\lambda_1} \quad \ldots(IV.29)$$

This equation relates the initial and final particle positions to the amount of pure shear deformation. The significance of the equation will be discussed in detail after the equations describing the behaviour of ellipsoidal particles have been derived.

(c) Motion of an ellipsoid of revolution

Now consider the more general case of an ellipsoid of revolution aligned at any orientation to the fluid flow. The position of the ellipsoid with reference to the fixed axes of flow can be described completely by a system of three angles such as the Euler angles illustrated in figure 24. In the diagram, the origins of the moving and fixed axes coincide at O; and the X'Y' plane (the deformation plane) and the YZ plane intersect in some line ON (the line of nodes) which is perpendicular to the XZ'Z plane. The Euler angles are:

θ' - the angle between the X and Z' axes; it can have values between 0° and 180°.

φ' - the angle between Y' and ON; it can have values between 0° and 360°.

ψ - the angle between the Y axis and ON; it also can have values between 0° and 360°.

In terms of these angles, the angular velocities about the X, Y, Z axes are, respectively:

$$\omega_1 = \dot{\varphi}' \cos \theta' + \dot{\psi}$$

$$\omega_2 = \dot{\varphi}' \sin \theta' \cdot \sin \psi + \dot{\theta}' \cos \psi \quad \ldots(IV.30a)$$

$$\omega_3 = \dot{\varphi}' \sin \theta' \cdot \cos \psi - \dot{\theta}' \sin \psi$$

Similarly, the direction cosines between the two sets of coordinate axes become:

$$
\begin{aligned}
l_1 &= -\sin\theta'\cdot\cos\varphi' \\
l_2 &= \cos\psi\cdot\sin\varphi' + \cos\theta'\cdot\sin\psi\cdot\cos\varphi' \\
l_3 &= -\sin\psi\cdot\sin\varphi' + \cos\theta'\cdot\cos\psi\cdot\cos\varphi' \\
m_1 &= \sin\theta'\cdot\sin\varphi' \qquad \ldots(\text{IV.30b}) \\
m_2 &= \cos\psi\cdot\cos\varphi' - \cos\theta'\cdot\sin\psi\cdot\sin\varphi' \\
m_3 &= -\sin\psi\cdot\cos\varphi' - \cos\theta'\cdot\cos\psi\cdot\sin\varphi' \\
n_1 &= \cos\theta',\ n_2 = \sin\theta'\cdot\sin\psi,\ n_3 = \sin\theta'\cdot\cos\psi
\end{aligned}
$$

If the particle is an ellipsoid of revolution about the X axis, the YZ plane is circular and at any instant during the deformation, the Y axis can be considered to coincide with the line of nodes, ON; i.e. $\psi = 0$. Then equations IV.30 become

$$
\begin{aligned}
&\omega_1 = \dot{\varphi}'\cos\theta' + \dot{\psi},\ \omega_2 = \dot{\theta}',\ \omega_3 = \dot{\varphi}'\sin\theta' \\
&l_1 = -\sin\theta'\cdot\cos\varphi',\ l_2 = \sin\theta', \\
&l_3 = \cos\theta'\cdot\cos\varphi',\ m_1 = \sin\theta'\cdot\sin\varphi', \qquad \ldots(\text{IV.31}) \\
&m_2 = \cos\varphi',\ m_3 = -\cos\theta'\cdot\sin\varphi' \\
&n_1 = \cos\theta',\ n_2 = 0,\ n_3 = \sin\theta'
\end{aligned}
$$

Substituting IV.31 into equations IV.24 and remembering that b = c for an ellipsoid of revolution, results in the following equations of motion:

$$
\begin{aligned}
&2b^2(\dot{\varphi}'\cos\theta' + \dot{\psi}) = 0 \\
&(a^2 + b^2)\dot{\theta}' = -(a^2 - b^2)C(-\sin\theta'\cdot\cos\theta'\cdot\cos^2\varphi' \\
&\qquad\qquad + \sin\theta'\cdot\cos\theta'\cdot\sin^2\varphi') \\
&(a^2 + b^2)\dot{\varphi}'\sin\theta' = (a^2 - b^2)C(-\sin\theta'\cdot\cos\varphi'\cdot \\
&\qquad\qquad \sin\dot{\varphi}' - \sin\theta'\cdot\cos\varphi'\cdot\sin\varphi')
\end{aligned}
$$

These equations can be rearranged and reduced to

$$\dot{\varphi}'\cos\theta' + \dot{\psi} = 0 \qquad \ldots(\text{IV.32})$$

$$\dot{\varphi}'/\sin 2\varphi' = -[(a^2 - b^2)/(a^2 + b^2)]\dot{\bar{\varepsilon}} \quad \ldots(IV.33)$$

$$2\dot{\theta}'/\sin 2\theta' = [(a^2 - b^2)/(a^2 + b^2)]\cos 2\varphi' \cdot \dot{\bar{\varepsilon}} \quad \ldots(IV.34)$$

Dividing IV.33 by IV.34 results in the relationship:

$$\dot{\varphi}' \cot 2\varphi' = -2\dot{\theta}'/\sin 2\theta' \quad \ldots.(IV.35)$$

Equation IV.32 implies that there is no spin about the X axis of the ellipsoid.

Equation IV.33 can be written

$$\int_{\varphi_i'}^{\varphi_f'} d\varphi'/\sin 2\varphi' = -[(a^2 - b^2)/(a^2 + b^2)] \int_0^{\bar{\varepsilon}} d\bar{\varepsilon}$$

which on integration gives

$$\ln \tan \varphi_f' - \ln \tan \varphi_i' = [(a^2 - b^2)/(a^2 + b^2)](-2\bar{\varepsilon})$$

Using equations IV.28 and substituting the angle φ for φ' (see figure 24), this becomes

$$\ln \cot \varphi_f = \ln \cot \varphi_i + [(a^2 - b^2)/(a^2 + b^2)] \cdot \ln \sqrt{\lambda_2/\lambda_1} \quad \ldots.(IV.36)$$

To find the variation of θ' with φ', integrate IV.35.

$$\int_{\theta_i'}^{\theta_f'} d\theta'/\sin 2\theta' = \int_{\varphi_i'}^{\varphi_f'} \cot 2\varphi' \cdot d\varphi'$$

Therefore

$$\ln \tan \theta_f' - \ln \tan \theta_i' = -(1/2)(\ln \sin 2\varphi_f' - \ln \sin 2\varphi_i')$$

i.e. $$\tan \theta_f'/\tan \theta_i' = \sqrt{\sin 2\varphi_i'/\sin 2\varphi_f'}$$

Referring to figure 24, it is seen that θ' is the complement of the angle of plunge, θ, of the major axis of the ellipsoid. In terms of this angle, θ, and the angle φ, the above equation can be written

$$\cot \theta_f / \cot \theta_i = \sqrt{\sin 2\varphi_i / \sin 2\varphi_f} \quad \ldots(IV.37)$$

This equation is meaningless if the initial direction of plunge is 0° or 90°. For these two cases, equation IV.34 must be used. For $\varphi = 0^\circ$, i.e. $\varphi' = 90^\circ$, IV.34 is

$$2\dot{\theta}'/\sin 2\theta' = -[(a^2 - b^2)/(a^2 + b^2)]\dot{\varepsilon}$$

which, on integration and rearranging in terms of the plunge and the axial ratio of the strain ellipse, becomes

$$\ln \cot \theta_f = \ln \cot \theta_i + (1/2)[(a^2 - b^2)/(a^2 + b^2)] \cdot \ln \sqrt{\lambda_2/\lambda_1} \quad \ldots.(IV.38a)$$

Similarly, for $\varphi = 90^\circ$, the change in plunge is

$$\ln \cot \theta_f = \ln \cot \theta_i - (1/2)[(a^2 - b^2)/(a^2 + b^2)] \cdot \ln \sqrt{\lambda_2/\lambda_1} \quad \ldots.(IV.38b)$$

The equations IV.36, IV.37 and IV.38 describe the change in plunge and orientation of any ellipsoid of revolution during pure shear.

(d) Significance and experimental verification of the equations of motion

The significance of the equations derived above to describe the motion of rigid particles in a viscous matrix during a pure shear deformation will now be discussed.

i) Two dimensional particles

The relevant equation for a two dimensional particle lying in the deformation plane is

$$\ln \cot \varphi_f = \ln \cot \varphi_i + [(a^2 - b^2)/(a^2 + b^2)] \cdot \ln \sqrt{\lambda_2/\lambda_1} \quad \ldots(IV.29)$$

If $\varphi_i = 0^\circ$, i.e. the major axis of the ellipse is parallel to the Y' flow axis,

$$\ln \cot \varphi_f = \infty \text{ and } \varphi_f = 0^\circ$$

for all finite amounts of strain.

Similarly, if $\varphi_i = 90^\circ$, i.e. the major axis is parallel to the X' flow axis,

$$\ln \cot \varphi_f = -\infty \quad \text{and} \quad \varphi_f = 90^\circ$$

for all finite amounts of strain.

Therefore, the two positions of elliptical axes parallel to the flow or strain axes are stable.

Furthermore, if a = b, i.e. the particle is circular, $\varphi_f = \varphi_i$ and the particle does not rotate during the straining.

To show the effect of pure shear on ellipses not aligned parallel to either of the deformation axes, equation IV.29 is plotted graphically in figure 25 for ellipses with axial ratios of 2 : 1 and 5 : 1, assuming different initial angles of φ. The graphs show that with increasing deformation, the long axes of the ellipses rotate towards the u' flow direction, i.e. the direction of elongation, but become parallel to it only after an infinite amount of strain. The result of increasing particle eccentricity is more rapid rotation towards the u' direction.

Also plotted in these figures are the results obtained experimentally for ellipses in the irrotational strain box. From these graphs, it is seen that the particles follow the same type of curves as predicted but rotate too rapidly. Nevertheless, they do not rotate into the direction of elongation, which agrees with the theory.

The reason why the ellipses rotate more rapidly than the theory predicts is probably connected with the box not imparting a true pure shear and, especially, with the fact that the strain in the box is not uniform throughout. The dashed experimental curves in figures 25 correlate rotation with the axial ratio of the strain ellipse calculated theoretically for the pure shear transformation. However, if rotation is plotted against the axial ratio for the local strain ellipses around the particle, measured from the experimental graph in

Figure 25 Rotation of (A) 2 : 1 and (B) 5 : 1 elliptical particles during pure shear.

The solid graphs are plotted from equation IV.29; the dashed experimental curves correlate rotation and the axial ratio of the strain ellipse for a finite pure shear transformation in the irrotational strain box; the black dots are experimental points relating rotations and the local strain ellipse axial ratios, measured from the graph D in figure 10.

The detailed experimental results are listed in table VIII, Appendix I.

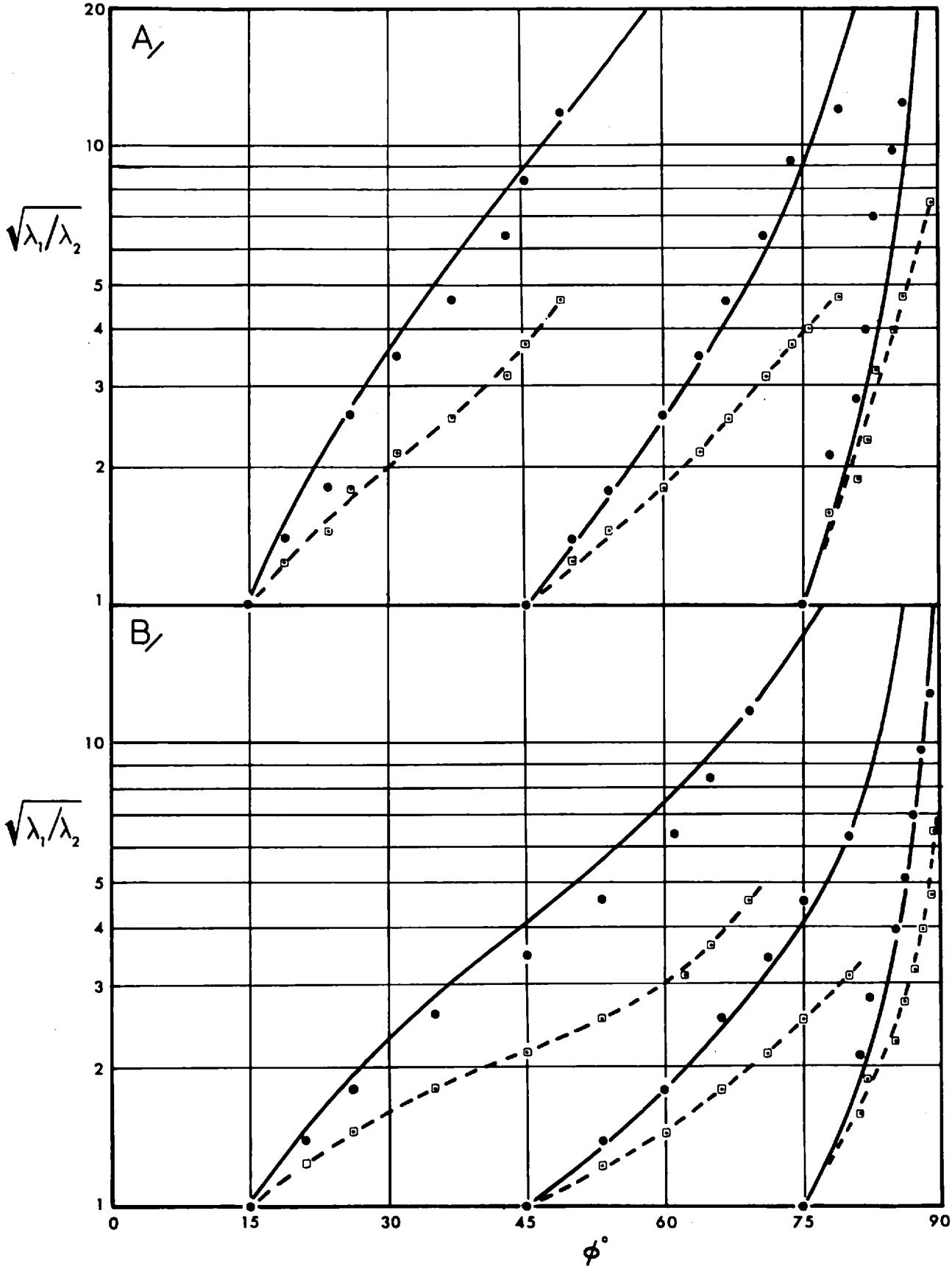
A/
B/
$\sqrt{\lambda_1/\lambda_2}$
$\sqrt{\lambda_1/\lambda_2}$
20
10
5
4
3
2
1
10
5
4
3
2
1
0
15
30
45
60
75
90
ϕ°

figure 10, the agreement between theoretical and experimental results is much better, thereby providing good evidence that equation IV.29 is correct.

ii) Three dimensional particles

The equations describing the motion of an ellipsoid of revolution are

$$\ln \cot \varphi_f = \ln \cot \varphi_i + [(a^2 - b^2)/(a^2 + b^2)] \cdot \ln \sqrt{\lambda_2/\lambda_1} \quad \ldots(IV.36)$$

$$\cot \theta_f / \cot \theta_i = \sin 2\varphi_i / \sin 2\varphi_f \quad \ldots(IV.37)$$

$$\ln \cot \theta_f = \ln \cot \theta_i \pm (1/2)[(a^2 - b^2)/(a^2 + b^2)] \cdot \ln \sqrt{\lambda_2/\lambda_1} \quad \ldots(IV.38)$$

Equation IV.36 is the same as the equation for the rotation of two dimensional particles during pure shear, which is discussed above and plotted in figure 25.

The change in plunge of the ellipsoids orientated in the stable positions ($\varphi = 0^\circ$, $\varphi = 90^\circ$) is given by equations IV. 38. The graphs of these equations are shown in figure 26 for 2 : 1 : 1 and 4 : 1 : 1 ellipsoids. The plunge of particles with their major axes parallel to the direction of shortening increases during deformation, while that of those parallel to the direction of elongation decreases. The more eccentric the particle, the more rapid is the rate of change in the angle of plunge.

The change in plunge for ellipsoids in positions other the stable ones, is given by equation IV.37. If $\theta_i = 0^\circ$ or 90°, then $\theta_f = 0^\circ$ or 90° for all changes in φ. However, for other values of θ_i, the plunge increases to a maximum at $\varphi = 45^\circ$ and then decreases as the particle rotates towards $\varphi = 90^\circ$. This is clear from the graphs of equation IV.37 which are plotted in figure 27 for different values of θ_i.

These conclusions were checked experimentally in the irrotational strain box using the 4 : 1 : 1 glass ellipsoids and the results are also plotted in figures 26 and 27. There

Figure 26 The change in plunge of (A) 2 : 1 : 1 and (B) 4 : 1 : 1 ellipsoids orientated in the stable positions at different initial angles of plunge, during pure shear. The solid graphs are calculated from equation IV.38a, the thick dashed graphs from IV.38b.

The black dots in (B) are experimental points determined in the irrotational strain box on a 4 : 1 : 1 ellipsoid, initially plunging at 25° along the direction of shortening. The light, dashed curves parallel to the theoretical graph for this ellipsoid, demarcate a zone of experimental error of $\pm 3^{\circ}$ in the plunge.

The data for the experimental points are listed in table IX, Appendix I.

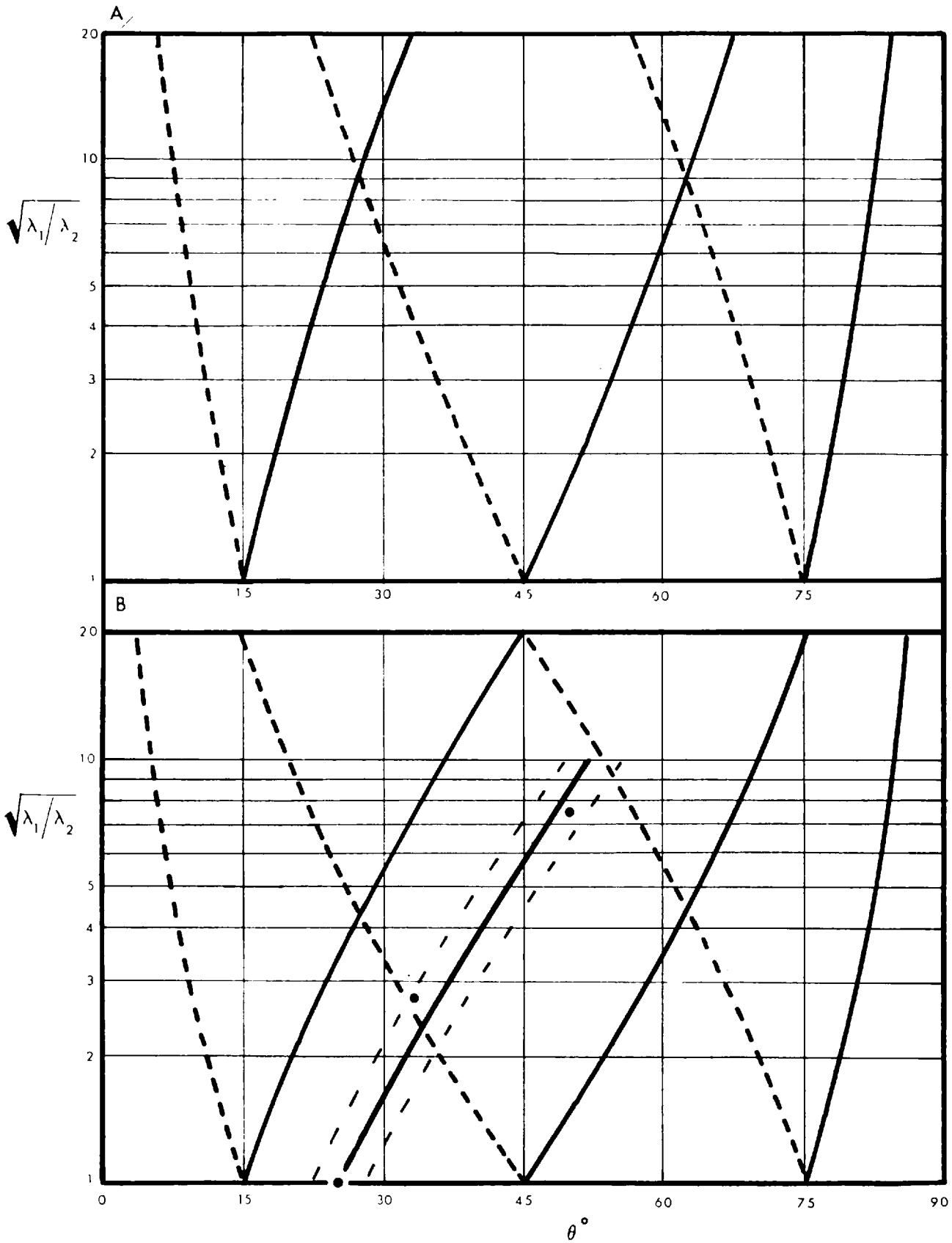
A
B
20
10
5
4
3
2
1
$\sqrt{\lambda_1/\lambda_2}$
15
30
45
60
75
0
90
θ°

Figure 27 The change in orientation, ϕ, and plunge, θ, of ellipsoids, during pure shear, calculated from equation IV.37. The dashed curves, A, B, C, D, are plotted from results obtained on a 4 : 1 : 1 glass ellipsoid in the irrotational strain box. The data for the experimental points are listed in table IX, Appendix I.

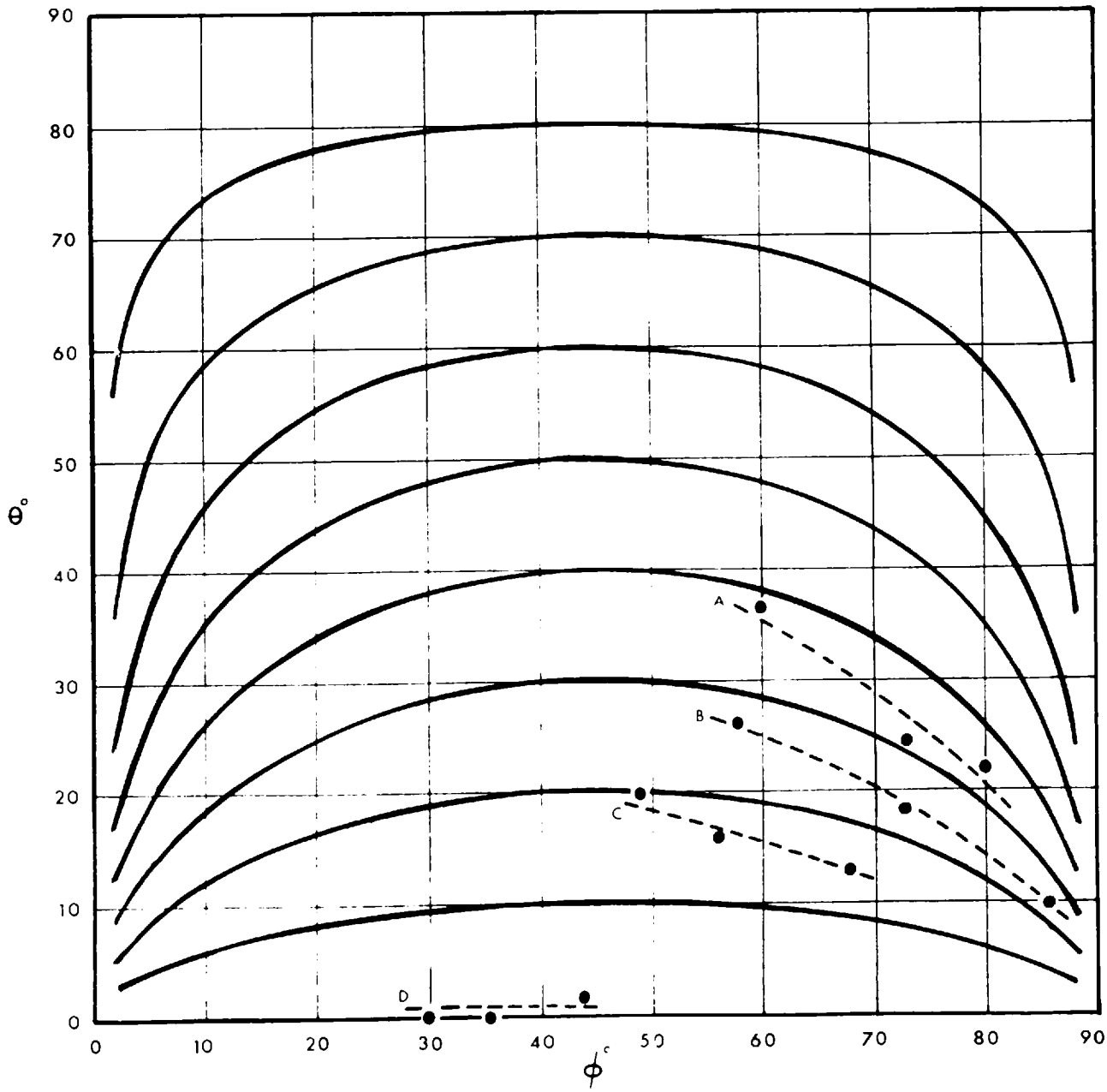
90
80
70
60
50
40
30
20
10
0
θ°
0
10
20
30
40
50
60
70
80
90
φ°
A
B
C
D

is fairly good agreement between the theoretical and experimental graphs but the curves for the simultaneous variation in plunge and rotation suggest that the plunge may change more rapidly than predicted. However, this is more likely to be due to the changes in the fluid level and the surface area of the matrix during straining. Note that the theoretical finite strain, not the local strain, is used to plot the results; this is because the glass ellipsoids are much smaller than the two dimensional ellipses and so are not greatly affected by the end effects in the apparatus.

Note also that when using equation IV.36 to calculate the change in orientation, for an ellipsoid plunging at some angle θ to the deformation plane, the major and minor axial lengths of the elliptical cross-section in the deformation plane must be used for the values of a and b, and not the axes of the ellipsoid itself. Assuming that b = 1, these values vary with the plunge according to the equation;

$$\bar{a} = 1/\sqrt{1 - e^2\cos^2\theta} \quad \ldots(IV.39)$$

where $\bar{a}$ is the ratio of the major and minor axes in the elliptical cross-section. When $\theta = 0^\circ$, $\bar{a} = a$; when $\theta = 90^\circ$, $\bar{a} = 1$.

Figure 28 Pure shear deformation of a non-rigid elliptical particle which has its axes parallel to the strain axes.

u', v' - fluid velocity components in the matrix.

u, v - fluid velocity components in the particle.

a_i, b_i - semi-axial lengths of the particle before deformation.

μ, μ' - viscosity coefficients inside and outside the particle.

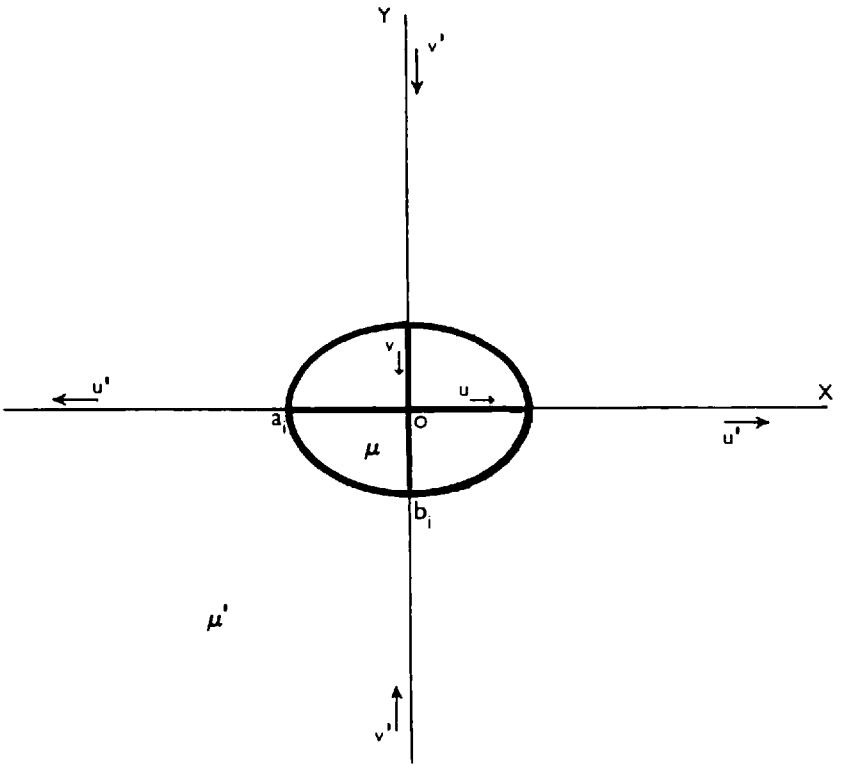
Y
v'
v
u'
u
X
a_i
O
μ
u'
b_i
μ'
v'

D. THE DEFORMATION OF NON-RIGID PARTICLES DURING PURE SHEAR

(a) Introduction

This section deals with the deformation, during pure shear, of a single circular or elliptical non-rigid particle embedded in a fluid matrix. Both matrix and particle are assumed to be Newtonian bodies and have viscosity coefficients μ' and μ respectively. The analysis is developed in two dimensions and the particle lies in the deformation plane with its axes parallel to the pure shear flow axes. In other words, the X, Y and X', Y' coordinate axes coincide and can be considered as a single system of coordinates X, Y. The components of fluid velocity parallel to these X, Y axes are, respectively, u' and v' in the matrix and u and v in the particle. The difference in the fluid velocities inside and outside the particle is a function of the viscosity ratio, $R = \mu/\mu'$.

Referring to figure 28, the particle is described, in its initial form, by the equation

$$x^2/a_i^2 + y^2/b_i^2 = 1 \quad \ldots(IV.40)$$

where a_i and b_i are the original semi-axial lengths and $a_i = 1/b_i$.

During deformation of the particle-matrix system by pure shear, the particle changes shape into another ellipse

$$x^2/a^2 + y^2/b^2 = 1 \quad \ldots(IV.41)$$

where, because the area remains constant during pure shear, $a = 1/b$.

This ellipse indicates the strain in the particle, if the initial shape is known, but it does not give the strain ellipse for the pure shear deformation of the particle-matrix system as a whole. The equation of this finite strain ellipse is

$$x^2/\lambda_1 + y^2/\lambda_2 = 1 \quad \ldots(IV.42)$$

where λ_1 and λ_2 are the principal quadratic elongations of

the strain, $\sqrt{\lambda_1}$ and $\sqrt{\lambda_2}$ are the semi-axial lengths and $\sqrt{\lambda_1/\lambda_2} = 1$.

It is the object of the analysis in this section to find a relationship between the change in particle shape, as given by equation IV.41, and the finite pure shear strain, as given by IV.42. To do this, the method developed by Taylor (1932, 1934) to determine the deformation of small drops of one liquid in another, is used.

First, the components of fluid velocity inside and outside the particle are calculated in general terms by means of Lamb's (1932) method of spherical harmonic analysis. These components of velocity must be equal at the boundary between the particle and the matrix because there is assumed to be no slipping at the particle-matrix interface. In addition, it is also assumed that there is continuity of stresses across the interface. Using these assumptions, and the fact that the area of the elliptical particle remains constant, the constants in the terms for the velocity components can be determined, and, hence, the velocity components in the particle and the matrix and at the boundary between the two. Knowing the boundary velocity conditions, the change in shape of the particle during the deformation can be found and directly related to the amount of strain in the particle-matrix system.

(b) The general equations for the velocity components

A general method for analyzing the slow motion of viscous, incompressible fluids has been developed by Lamb (1932, pp. 594-597) in terms of spherical harmonic functions. The method assumes that the components of fluid velocity can be considered as consisting of three types of terms describing the pressure distribution in the fluid, an irrotational motion and a vortex motion. The vortex motion terms disappear when considering any two dimensional flow and the components of

velocity, $\bar{u}$, $\bar{v}$, can be described by the general equations

$$\bar{u} = \frac{1}{\bar{\mu}} \sum \left[\frac{r^2}{2(2n+1)} \frac{\partial p_n}{\partial \bar{x}} + \frac{n r^{2n+3}}{(n+1)(2n+1)(2n+3)} \frac{\partial}{\partial \bar{x}} \frac{p_n}{r^{2n+1}} \right] + \sum \left[\frac{\partial \varphi_n}{\partial \bar{x}} \right] \qquad \ldots(IV.43a)$$

$$\bar{v} = \frac{1}{\bar{\mu}} \sum \left[\frac{r^2}{2(2n+1)} \frac{\partial p_n}{\partial \bar{y}} + \frac{n r^{2n+3}}{(n+1)(2n+1)(2n+3)} \frac{\partial}{\partial \bar{y}} \frac{p_n}{r^{2n+1}} \right] + \sum \left[\frac{\partial \varphi_n}{\partial \bar{y}} \right] \qquad \ldots(IV.43b)$$

in which $\bar{x}$ and $\bar{y}$ refer to the rectangular coordinate axes, $r^2 = x^2 + y^2$ and $\bar{\mu}$ is the coefficient of viscosity of the fluid. The terms in the first square bracket concern the pressure distribution, $p = \sum p_n$, in the fluid, where p_n is a solid harmonic function of degree n. The terms in the second square bracket represent the irrotational motion existing in a field of uniform pressure. The function φ_n is also a solid harmonic function of degree n and, moreover, because it describes an irrotational fluid motion, can be considered as the velocity potential of the flow. The velocity potential is related to the velocity components by the equations

$$\bar{u} = \partial\varphi/\partial\bar{x}, \quad \bar{v} = \partial\varphi/\partial\bar{y} \qquad \ldots.(IV.44)$$

(c) Choice of functions φ_n and p_n for the flows in the particle and the matrix

To find the velocity components $\bar{u}$ and $\bar{v}$ for any particular flow, suitable functions for p_n and φ_n must be chosen and substituted into equations IV.43. The choice of these functions is arbitrary and is normally made by trial and error, depending upon the type of flow and the solution required. In the present case, one of the functions φ'_n, for the flow in the matrix, can be obtained using the relationship IV.44.

In the matrix, the equations for the pure shear flow are

$$u' = \dot{\bar{\varepsilon}}x, \quad v' = -\dot{\bar{\varepsilon}}y \quad \ldots.(IV.5a)$$

Substituting these in IV.44 gives

$$\partial\varphi'/dx = \dot{\bar{\varepsilon}}x, \quad \partial\varphi'/\partial y = -\dot{\bar{\varepsilon}}y$$

and this pair of partial differential equations has a solution

$$\varphi'_2 = (\dot{\bar{\varepsilon}}/2)(x^2 - y^2) \quad \ldots.(IV.45a)$$

This is one of the required functions. Corresponding with it, there must be a complementary solid harmonic function to satisfy the general relationship

$$\varphi'_n = r^{2n+1}.\varphi'_{-n-1} \qquad \text{(Lamb, 1932, p. 111)}$$

i.e. $$\varphi'_{-3} = B_{-3}\rho^5(x^2 - y^2)/r^5 \quad \ldots(IV.45b)$$

where B_{-3} is a constant determined by the boundary conditions and $\rho = b/\sqrt{1 - e^2\cos^2\alpha'}$ gives the length of any line in an ellipse which has α' as its polar angle.

The choice of the other required functions for φ_n and p_n is made in a similar manner. Taylor (1932) has shown that the appropriate forms to give a satisfactory solution are

$$p'_{-3} = \mu A_{-3}\rho^3(x^2 - y^2)r^5 \quad \ldots(IV.45c)$$

for the pressure distribution outside the particle; and

$$\varphi_2 = B_2(x^2 - y^2), \; p_2 = \mu A_2\rho^{-3}(x^2 - y^2) \quad \ldots(IV.46)$$

for the irrotational flow and pressure inside the particle. The constants A_{-3}, B_2, A_2 are again determined by the boundary conditions. In Taylor's original functions, the radius of the drop appeared, instead of the length ρ, because he was working with small drops assumed to remain spherical.

Substituting the equations IV.45 into IV.43 gives the components of velocity outside the particle as

$$u' = (1/2)A_{-3}\rho^3 x(x^2 - y^2)/r^5 +$$
$$B_{-3}\rho^5[-5x(x^2 - y^2)/r^7 + 2x/r^5] + \dot{\bar{\varepsilon}}x$$
$$v' = (1/2)A_{-3}\rho^3 y(x^2 - y^2)/r^5 + \qquad \ldots(IV.47)$$
$$B_{-3}\rho^5[-5y(x^2 - y^2)/r^7 - 2y/r^5] - \dot{\bar{\varepsilon}}y$$

Similarly, from IV.46 and IV.43, the velocity components inside the particle are

$$u = A_2\rho^{-2}[(5/21)xr^2 - (2/21)x(x^2 - y^2)] + 2B_2x$$
$$v = A_2\rho^{-2}[(-5/21)yr^2 - (2/21)y(x^2 - y^2)] - 2B_2y \qquad \ldots(IV.48)$$

(d) Determination of the components of stress in the particle and the matrix

It is also necessary to know the components of stress inside and outside the particle. These can be obtained from relationships derived by Lamb (1932, pp. 596-597) for the components of stress, σ_{rx}, σ_{ry}, σ_{rz}, across a unit area of the surface of a sphere. The general two dimensional expression for $\bar{\sigma}_{rx}$ is

$$r\bar{\sigma}_{rx} = \sum\left[\frac{n-1}{2n+1} r^2 \frac{\partial p_n}{\partial \bar{x}} + \frac{2n^2+4n+3}{(n+1)(2n+1)(2n+3)} r^{2n+3}.\right.$$
$$\left.\frac{\partial}{\partial \bar{x}} \frac{p_n}{r^{2n+1}}\right] + 2\mu\sum\left[(n-1)\frac{\partial \varphi_n}{\partial \bar{x}}\right]$$

There is a similar expression for $\bar{\sigma}_{ry}$.

Taylor (1932) has shown that these reduce outside the particle to

$$r\sigma_{rx}/\mu' = A_{-3}\rho^3[x/r^3 - 4x(x^2 - y^2)/r^5] -$$
$$8B_{-3}\rho^5[2x/r^5 - 5x(x^2 - y^2)/r^7] + 2\dot{\bar{\varepsilon}}x$$
$$\ldots(IV.49a)$$

$$r\sigma_{ry}/\mu' = A_{-3}\rho^3[-y/r^3 - 4y(x^2 - y^2)/r^5] - 8B_{-3}\rho^5[-2y/r^5 - 5y(x^2 - y^2)/r^7] - 2\dot{\varepsilon}y \qquad \ldots(IV.49b)$$

and inside the particle to

$$r\sigma_{rx}/\mu = A_2\rho^{-2}(16/21)r^2x - (19/21)x(x^2 - y^2) + 4B_2x \qquad \ldots(IV.50a)$$

$$r\sigma_{ry}/\mu = A_2\rho^{-2}(16/21)r^2y - (19/21)y(x^2 - y^2) - 4B_2y \qquad \ldots(IV.50b)$$

(e) Determination of the constants A_2, A_{-3}, B_2, B_{-3}

The following conditions at the boundary $r = \rho$ can be used to determine the constant terms in equations IV.47 and IV.48;

1/ Continuity of velocity; i.e. $u = u'$, $v = v'$.

2/ Constant area of the particle. The area of the elliptical particle is given by the formula

$$A = \pi ab$$

Differentiating this with respect to time gives the rate of change in the area during deformation

$$\dot{A} = \pi(\dot{a}b + \dot{b}a)$$

Therefore, for constant area

$$\dot{a}b + \dot{b}a = 0$$

Also, at the boundary $r = \rho$ along the X and Y axes, respectively,

$$\dot{a} = u, \quad \dot{b} = v$$

3/ Continuity of normal stresses.

1/ At $r = \rho$, IV.47 and IV. 48 reduce to

$$u' = [(1/2)A_{-3} - 5B_{-3}]x(x^2 - y^2)/(x^2 + y^2) + (2B_{-3} + \dot{\varepsilon})x$$

$$v' = [(1/2)A_{-3} - 5B_{-3}]y(x^2 - y^2)/(x^2 + y^2) - (2B_{-3} + \dot{\bar{\varepsilon}})y$$

$$u = (-2/21)A_2x(x^2 - y^2)/(x^2 + y^2) + [2B_2 + (5/21)A_2]x$$

$$v = (-2/21)A_2y(x^2 - y^2)/(x^2 + y^2) - [2B_2 + (5/21)A_2]y$$

Therefore, $u = u'$ and $v = v'$ if

$$(1/2)A_{-3} - 5B_{-3} = (-2/21)A_2 \quad ...(IV.51)$$

and

$$2B_{-3} + \dot{\bar{\varepsilon}} = 2B_2 + (5/21)A_2 \quad ....(IV.52)$$

2/ Along the X and Y coordinate axes at the boundary between the particle and the matrix, the rates of change in the lengths of particle axes are equivalent to the components of fluid velocity parallel to the axes. In other words, at $r = \rho$

$$\dot{a} = u, \ \dot{b} = v, \ a = x, \ b = y.$$

Therefore, equations IV.48 can be written

$$\dot{a} = (5/21)A_2a - (2/21)A_2a(a^2 - b^2)\rho^{-2} + 2B_2a$$

$$\dot{b} = (-5/21)A_2b - (2/21)A_2b(a^2 - b^2)\rho^{-2} - 2B_2b$$

Therefore

$$\dot{a}b + \dot{b}a = (-4/21)A_2ab(a^2 - b^2)\rho^{-2} = 0$$

if

$$A_2 = 0 \quad ...(IV.53)$$

3/ At $r = \rho$, equations IV.49 reduce to

$$\sigma_{rx} = \mu'(A_{-3} - 16B_{-3} + 2\dot{\bar{\varepsilon}})x/\rho - 4\mu'(A_{-3} - 10B_{-3})x(x^2 - y^2)/\rho^3$$

$$\sigma_{ry} = \mu'(-A_{-3} + 16B_{-3} - 2\dot{\bar{\varepsilon}})y/\rho - 4\mu'(A_{-3} - 10B_{-3})y(x^2 - y^2)/\rho^3$$

and equations IV.50 to

$$\sigma_{rx} = \mu[(16/21)A_2 + 4B_2]x/\rho - (19/21)\mu A_2 y(x^2 - y^2)/\rho^3$$

$$\sigma_{ry} = \mu[(-16/21)A_2 - 4B_2]y/\rho - (19/21)\mu A_2 y(x^2 - y^2)/\rho^3$$

Therefore, for continuity of stress

$$\mu'(A_{-3} - 16B_{-3} + 2\dot{\bar{\varepsilon}}) = \mu[(16/21)A_2 + 4B_2]$$

$$4\mu'(A_{-3} - 10B_{-3}) = (19/21)\mu A_2$$

i.e. $$\mu'(5A_{-3} - 56B_{-3} + 2\dot{\bar{\varepsilon}}) = \mu[(35/21)A_2 + 4B_2]. \quad \ldots.(IV.54)$$

Solving equations IV.51 - IV.54 gives the required values of the constants;

$$A_{-3} = 10B_{-3} = -10\dot{\bar{\varepsilon}}(R - 1)/(2R + 3)$$

$$A_2 = 0, \quad B_2 = (5/2)\dot{\bar{\varepsilon}}/(2R + 3) \quad \ldots(IV.55)$$

where $R = \mu/\mu'$ is the viscosity ratio.

(f) Derivation of the equations for the change in shape of the particle

If the above values for the constants are substituted into equations IV.47 and IV.48, the components of velocity inside and outside the particle are found to be

$$u' = \dot{\bar{\varepsilon}}[(R - 1)/(2R + 3)][-5\rho^3 x(x^2 - y^2)/r^5 + 5\rho^5 x(x^2 - y^2)/r^7 - 2\rho^5 x/r^5] + \dot{\bar{\varepsilon}}x \quad ..(IV.56a)$$

$$v' = \dot{\bar{\varepsilon}}[(R - 1)/(2R + 3)][-5\rho^3 y(x^2 - y^2)/r^5 + 5\rho^5 y(x^2 - y^2)/r^7 + 2\rho^5 y/r^5] - \dot{\bar{\varepsilon}}y$$

$$u = [(5/2)\dot{\bar{\varepsilon}}/(2R + 3)]x$$

$$v = [(-5/2)\dot{\bar{\varepsilon}}/(2R + 3)]y \quad \ldots(IV.56b)$$

When $r = \rho$, these expressions become

$$u = u' = [5\dot{\bar{\varepsilon}}/(2R + 3)]x$$
$$v = v' = -[5\dot{\bar{\varepsilon}}/(2R + 3)]y \qquad \ldots(IV.57)$$

To obtain the change in shape of the particle, introduce the polar coordinates $x = \rho\cos\alpha'$, $y = \rho\sin\alpha'$, where $\rho = b/\sqrt{1 - e^2\cos^2\alpha'}$ and α' is the polar angle, into IV.57. Then

$$u = [5\dot{\bar{\varepsilon}}/(2R + 3)][b/\sqrt{1 - e^2\cos^2\alpha'}]\cos\alpha' \qquad ..(IV.58)$$
$$v = -[5\dot{\bar{\varepsilon}}/(2R + 3)][b/\sqrt{1 - e^2\cos^2\alpha'}]\sin\alpha'$$

Along the line $\alpha' = 0^o$, $\rho = a$ and $u = da/dt$ at the boundary of the particle. Therefore

$$da/dt = [5/(2R + 3)]ad\bar{\varepsilon}/dt$$

i.e. $$da/a = [5/(2R + 3)]d\bar{\varepsilon}$$

This equation can be integrated between limits as follows:

$$\int_{a_i}^{a} da/a = [5/(2R + 3)]\int_{0}^{\bar{\varepsilon}} d\bar{\varepsilon}$$

The result is

$$\ln (a/a_i) = [5/(2R + 3)]\bar{\varepsilon} \quad \ldots(IV.59)$$

Similarly, along the line $\alpha' = 90^o$, $\rho = b$ and $v = db/dt$. Therefore

$$\ln (b/b_i) = -[5/(2R +3)]\bar{\varepsilon} \quad \ldots.(IV.60)$$

To get the change in axial ratio of the particle during the deformation, subtract IV.60 from IV.59:

$$\ln (a/a_i) - \ln (b/b_i) = 10\bar{\varepsilon}/(2R + 3)$$

i.e. $$a/b = (a_i/b_i)\exp[10\bar{\varepsilon}/(2R + 3)]$$

In terms of the relationship IV.28 between the axial ratio of the pure shear strain ellipse and the natural strain, this equation can be written

$$\ln (a/b) = \ln (a_i/b_i) + [5/(2r +3)]\ln \sqrt{\lambda_1/\lambda_2}$$
$$\ldots(IV.61)$$

Figure 29 Variation in the axial ratio of a non-rigid circular particle during pure shear, as given by equation IV.61.

a/b - particle axial ratio.

$\sqrt{\lambda_1/\lambda_2}$ - axial ratio of the pure shear strain ellipse.

R - viscosity ratio between the particle and the matrix.

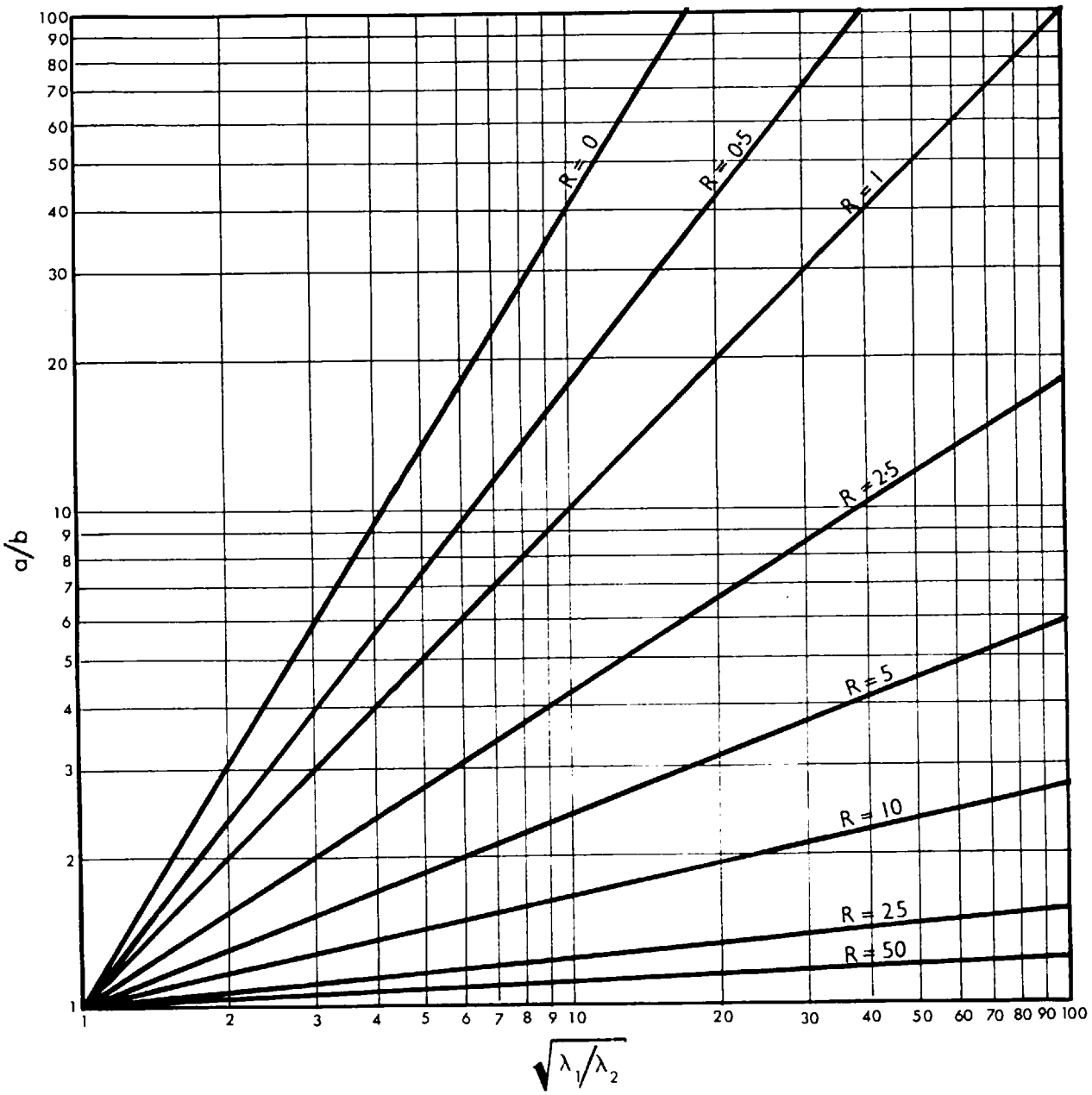
a/b
100
90
80
70
60
50
40
30
20
10
9
8
7
6
5
4
3
2
1
R = 0
R = 0·5
R = 1
R = 2·5
R = 5
R = 10
R = 25
R = 50
1
2
3
4
5
6
7
8
9
10
20
30
40
50
60
70
80
90
100
$\sqrt{\lambda_1/\lambda_2}$

(g) Significance and experimental verification of the equation for the change in shape of the particle

Equation IV.61 gives the change in axial ratio of an elliptical particle embedded in a viscous matrix, during a pure shear deformation of the particle-matrix system, assuming that the particle has its axes aligned parallel to the strain axes and allowing for a difference in the viscosities of the particle and the matrix. The effect of increasing viscosity contrast between the particle and the matrix is clearly to reduce the change in shape of the particle. For example, if the particle is rigid, $R = \infty$ and there is no change in particle shape for all finite amounts of strain. If $R = 1$, the particle has the same viscosity as the matrix and acts as a strain ellipse during the deformation. For values of R between 0 and 1, the particles are less viscous than the matrix and deform more rapidly than the particle-matrix system.

These considerations are clearly illustrated in figure 29, in which equation IV.61 is expressed graphically, assuming an initially circular particle and different values of R. The most striking feature of these graphs is the marked effect an increase in R has in reducing the change in shape of the particle during a certain amount of finite strain. It is clear that for values of R greater than 10, the particle-matrix system has to experience very large strains to achieve a significant increase in the particle axial ratio.

To test the validity of the above theoretical conclusions, several experiments were carried out in the irrotational strain box, using ethyl cellulose solutions of known viscosities to represent both particles and matrix. The results are plotted graphically in figures 30a-30f, together with the relevant theoretical graphs.

From these graphs, it is obvious that the conclusions drawn about the importance of the viscosity ratio in controlling the particle deformation are correct. Moreover, there

Figure 30 Variation in the axial ratios of initially circular, non-rigid particles during finite pure shear transformations in the irrotational strain box.

The solid straight lines are calculated from IV.61; the dashed lines parallel to them demarcate the zone of experimental error assuming errors of $\pm$ 0.5 mm in measurement of the axial lengths and $\pm$ 0.5° in the apical angle from which the strain ellipse axial ratios are calculated.

Crosses indicate points which satisfied the conditions of constant area; the dots show points which did not.

Experiments were performed using particles with large (1.7 cm) and small (1.1 cm) diameters. However, the results did not vary significantly with the size of the particle.

a/b - particle axial ratio.

$\sqrt{\lambda_1/\lambda_2}$ - axial ratio of the strain ellipse for the finite pure shear transformation.

a) R = 1, b) R = 2.5, c) R = 5

d) R = 7.5, e) R = 10, f) R = 15

The detailed experimental results are listed in table X, Appendix I.

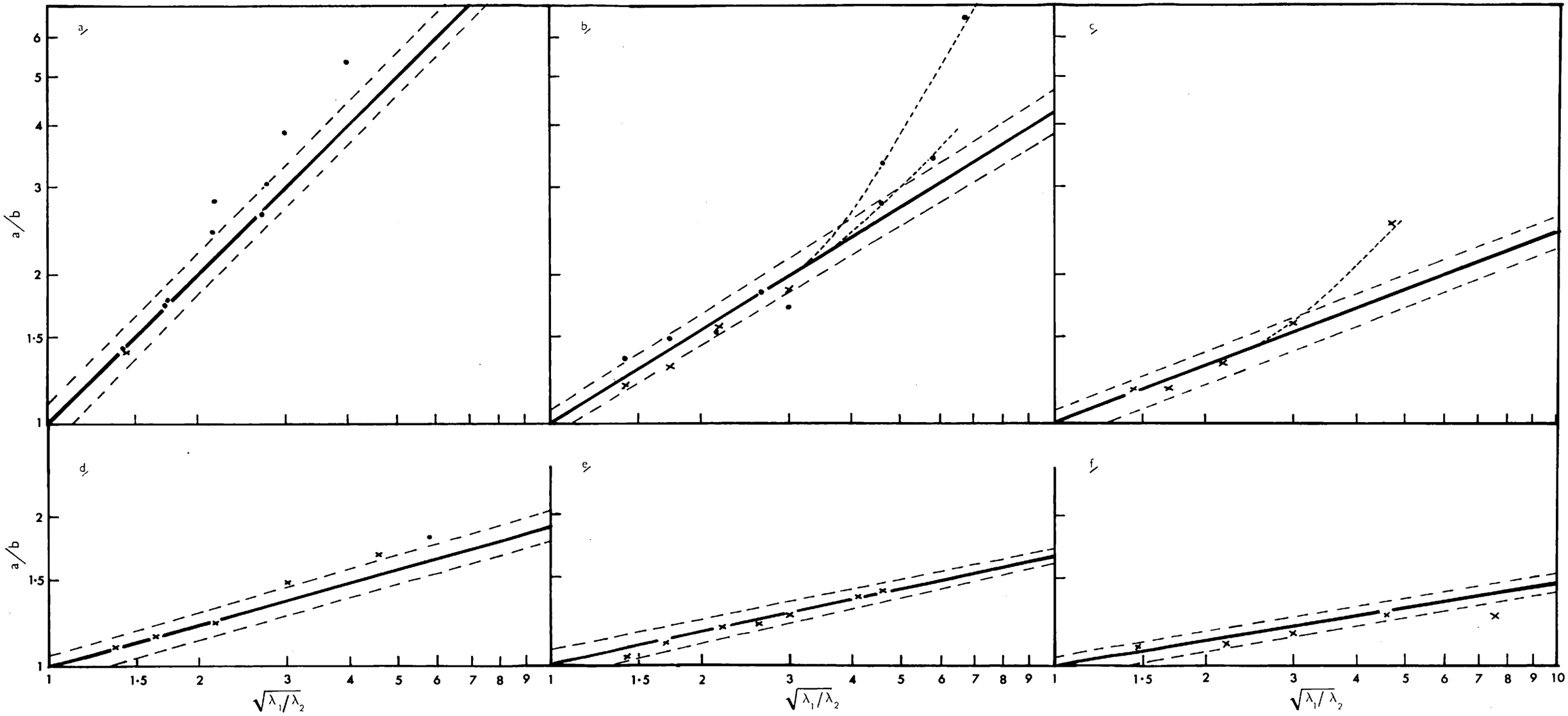
a
b
c
d
e
f
a/b
6
5
4
3
2
1·5
1
1·5
2
3
4
5
6
7
8
9
10
$\sqrt{\lambda_1/\lambda_2}$

is good agreement between the theory and experimental results until the particle axial ratio reaches a value of about 2 : 1. However, beyond this point, the particles deform more rapidly than expected.

It was at first thought that this increase in the rate of elongation of the particle was due to end effects in the apparatus, as discussed in chapter III, and so, to overcome this, smaller particles were used in the experiments. However, the results showed no significant difference when compared with those for larger particles.

Another possible explanation is that the molecular structure of the ethyl cellulose - benzyl alcohol solution forming the particle becomes anisotropic with increasing deformation and the solution, therefore, becomes less viscous. This would cause a reduction in R with a corresponding increase in the rate of particle deformation. However, one would also expect the viscosity of the matrix to change in the same way, but it apparently does not do so to the same extent.

It is therefore not possible to decide definitely why the particles deform more rapidly than expected. The reason may be connected with the experiments not being performed in a true pure shear field; it may be that the properties of the materials being used change after a large strain; or the boundary conditions assumed in obtaining the theoretical solution may not hold after a large change in the particle shape.

E. PURE SHEAR DEFORMATION OF AN ELLIPTICAL PARTICLE WITH ITS AXES NOT NECESSARILY PARALLEL TO THE STRAIN AXES

(a) Introduction

The theory developed in the previous section applies only to circular particles or ellipses orientated parallel to the deforming stresses. If the axes of the ellipse are not coincident with the stress directions, the deformation will result in a rotation as well as a change in shape. To find an analytical solution to this problem is extremely difficult. However, a numerical solution has been developed from the assumption that, for infinitesimal strains, the effect on the particle can be considered as a pure shear deformation followed by a rigid body rotation. The rotational component will disappear once the particle is aligned parallel to either of the strain axes. The total finite strain is obtained by summing the infinitesimal strains. The method is outlined below.

(Note - the notation used in this and the following section need not necessarily conform with that used elsewhere in the thesis. This is mainly because only alphanumeric symbols can be used in the language used for programming. Where symbols are used in a different sense, they are defined either in the text or in a diagram.)

(b) Initial conditions

The initial position of the elliptical particle, which lies in the deformation plane, is shown in figure 31a. As before, X', Y' are the pure shear strain axes and X, Y are axes fixed parallel to the major and minor particle axes and rotating with them. The initial lengths of the particle axes are $2a_i$ and $2b_i$. With respect to the X, Y axes, the equation of the ellipse is:

$$x^2/a_i^2 + y^2/b_i^2 = 1$$

Figure 31 Diagrams to illustrate the numerical method of calculating the pure shear deformation of a non-rigid ellipse with its axes not parallel to the strain axes.

a) Initial position of the ellipse.

a_i, b_i - major and minor semi-axial lengths of the particle.

φ_i - angle between the major axis of the particle and the Y' pure shear axis.

μ, μ' - viscosities of the particle and matrix, respectively.

b) Infinitesimal pure shear strain ellipse.

a_o, b_o - semi-axial lengths of the ellipse.

c) Particle after superimposition of the infinitesimal strain ellipse.

a_1, b_1 - new semi-axial lengths of the particle.

$\lambda'_x C$, $\lambda'_y D$ - points of intercept of the ellipse on the X' and Y' axes.

θ - angle between the particle major axis and the X' pure shear axis.

d) Mohr circle construction for the ellipse in figure c.

A_1, B_1 - principal reciprocal quadratic elongations.

e) Position of the ellipse in figure c after the rigid body rotation component.

φ_f - final angle between the major particle axis and the Y' pure shear axis.

a/

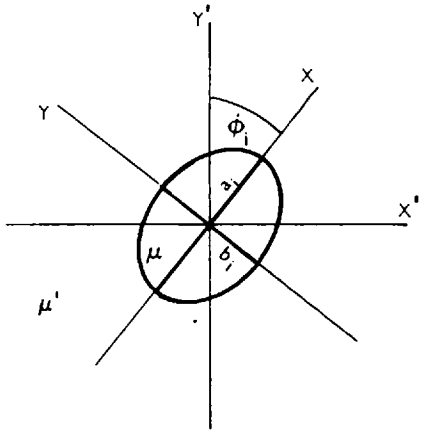
Y'
X
Y
ϕ_i
a_1
X'
μ
b_1
μ'

b/

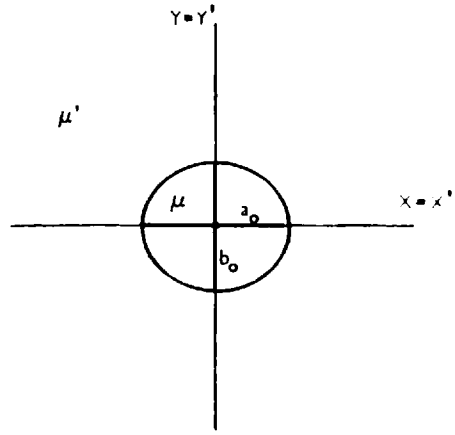
Y=Y'
μ'
μ
a_o
X=X'
b_o

d/

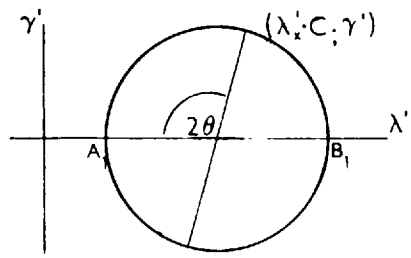
Y'
$(\lambda'_x \cdot C : Y')$
2θ
λ'
A_1
B_1

c/

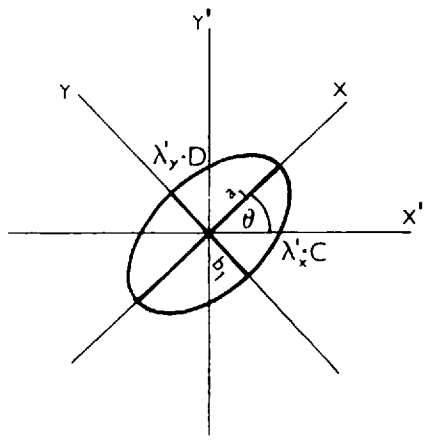
Y'
Y
X
$\lambda'_y \cdot D$
a_1
θ
X'
$\lambda'_x : C$
b_1

e/

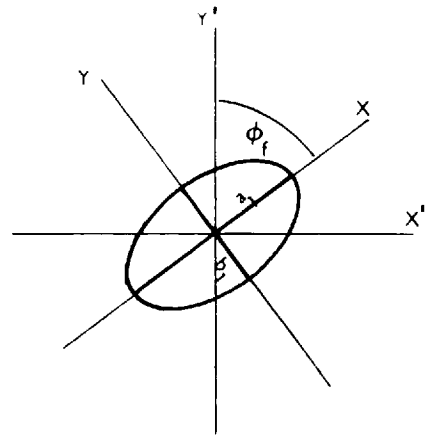
Y'
Y
X
ϕ_f
a_1
X'
b_1

This can be written

$$Ax^2 + By^2 = 1 \quad \ldots(IV.62)$$

where $A = 1/a_i^2$, $B = 1/b_i^2$ $\ldots(IV.62a)$

With respect to the X', Y' coordinate axes, this equation becomes

$$x'^2(A\sin^2\varphi_i + B\cos^2\varphi_i) - 2x'y'(B - A)\sin\varphi_i \cdot \cos\varphi_i + y'^2(A\cos^2\varphi_i + B\sin^2\varphi_i) = 1$$

which can be simplified to

$$\lambda_x' x'^2 - 2\gamma' x' y' + \lambda_y' y'^2 = 1 \quad \ldots(IV.63)$$

where

$$\lambda_x' = A\sin^2\varphi_i + B\cos^2\varphi_i$$
$$\lambda_y' = A\cos^2\varphi_i + B\sin^2\varphi_i \quad \ldots(IV.63a)$$
$$\gamma' = (B - A)\sin\varphi_i \cdot \cos\varphi_i$$

The following invariant properties, which will hold throughout the deformation of the ellipse, can be formulated in terms of A, B, λ_x', λ_y' and γ'.

$$J_1 = \lambda_x' + \lambda_y' = A + B$$
$$J_2 = \lambda_x'\lambda_y' - \gamma'^2 = AB \quad \ldots(IV.64a)$$

and A and B can be expressed as functions of J_1 and J_2:

$$A, B = (J_1 \mp \sqrt{J_1^2 - 4J_2})/2 \quad \ldots(IV.64b)$$

(c) Calculation of the infinitesimal strain ellipse for a pure shear

Consider a circular particle of unit radius and the same viscosity, and viscosity ratio with the matrix, as the ellipse IV.62. This circle is deformed into the infinitesimal strain ellipse by a pure shear applied parallel to the X', Y' axes, as in figure 31b. The equation of this infinitesimal strain ellipse is:

$$x'^2/a_o^2 + y'^2/b_o^2 = 1$$

This can be written

$$Cx'^2 + Dy'^2 = 1 \quad ...(IV.65)$$

where $C = 1/a_o^2$, $D = 1/b_o^2$ ...(IV.65a)

are the principal reciprocal quadratic elongations.

In terms of the viscosity ratio between the particle and the matrix, the lengths of the semi-axes of the strain ellipse are given by equations IV.59 and IV.60, i.e.:

$$a_o = \exp[5\bar{\varepsilon}/(2R + 3)] \quad ...(IV.66)$$
$$b_o = \exp[-5\bar{\varepsilon}/(2R + 3)]$$

and the equation of the axial ratio of the ellipse is

$$\ln (a_o/b_o) = [5/(2R + 3)](2\bar{\varepsilon}) \quad ...(IV.67)$$

(d) Superposition of the strain ellipse on the particle

The effect of superimposing the strain ellipse on the particle ellipse is given by the transformations

$$x_1' = a_o x', \quad y_1' = b_o y' \quad ...(IV.68)$$

Substituting IV.68 in IV.63 results in the equation

$$\lambda_x'(x_1'/a_o)^2 - 2\gamma' x_1' y_1'/a_o b_o + \lambda_y'(y_1'/b_o)^2 = 1$$

This can be rearranged to

$$\lambda_x' Cx'^2 - 2\gamma' x' y' + \lambda_y' Dy'^2 = 1 \quad ...(IV.69)$$

using the fact that for pure shear CD = 1.

Equation IV.69 represents the new elliptical shape of the particle, shown in figure 31c. To calculate the semi-axial lengths (a_1, b_1) of this ellipse, equations IV.64 are used as follows:

The invariant terms of the ellipse are

$$J_1 = C(A\sin^2\varphi_i + B\cos^2\varphi_i) + D(A\cos^2\varphi_i + B\sin^2\varphi_i)$$
$$J_2 = C(A\sin^2\varphi_i + B\cos^2\varphi_i)D(A\cos^2\varphi_i + B\sin^2\varphi_i)$$
$$- (B - A)\sin\varphi_i \cdot \cos\varphi_i \quad ....(IV.70)$$

The terms on the right hand sides of these equations are substituted for J_1 and J_2 in IV.64 to obtain two new reciprocal quadratic elongations:

$$A_1, B_1 = (J_1 \mp \sqrt{J_1^2 - 4J_2})/2$$

from which the semi-axial lengths of the ellipse are given by

$$a_1 = 1/A_1, \quad b_1 = 1/B_1 \quad ....(IV.71)$$

To find the new orientation, φ, of the particle major axis, consider the Mohr construction (see Brace, 1961) of the ellipse IV.69, as shown in figure 31d. From this diagram

$$\tan 2\theta = \gamma'/[(A_1 + B_1)/2 - \lambda_x' C]$$

which, by making use of J_1 (IV.64a), can be written

$$\tan 2\theta = \gamma'/[(\lambda_x' C + \lambda_y' D)/2 - \lambda_x' C]$$

i.e. $$\tan 2\theta = 2\gamma'/(\lambda_y' D - \lambda_x' C)$$

After some rearrangement and reduction, this becomes

$$\tan 2\theta = 2(B - A)\sin\varphi_i.\cos\varphi_i/[B(D\sin^2\varphi_i - C\cos^2\varphi_i) - A(C\sin^2\varphi_i - D\cos^2\varphi_i)] \quad ..(IV.72)$$

from which the angle θ can be obtained. The required orientation φ is the complement of this angle; i.e.

$$\varphi = 90^\circ - \theta \quad ....(IV.73)$$

(e) Addition of the rigid body rotation

For particles with R not equal to 1, a rigid body rotation accompanying the infinitesimal pure shear, has to be added to the orientation given by IV.73. To find the final orientation after this rigid body rotation, use is made of equation IV.29 of the rigid particle theory, which in terms of the present notation can be written

$$\ln \cot \varphi_f = \ln \cot \varphi + [(a_1^2 - b_1^2)/(a_1^2 + b_1^2)] \cdot (-2\bar{\varepsilon})$$

i.e. $$\cot \varphi_f = \cot \varphi / \exp[2\bar{\varepsilon}(B_1 - A_1)/(B_1 + A_1)] \quad ..(IV.74)$$

(f) Computation and significance of the results

A programme to do the above calculations has been written in FORTRAN IV for the IBM 7090 computer. The flow diagram of this programme is shown in figure 32. The data fed into the computer are values of R and the initial axial lengths (λ_1, λ_2) and orientation (φ_i) of the ellipses. The calculations are then carried out in the following order:

1/ A subprogramme DEFORM computes the reciprocal quadratic elongations, C and D, for specific values of R and $\bar{\varepsilon}$. The size of the increment $\bar{\varepsilon}$ depends on the value of R; if R = 1, a large value of $\bar{\varepsilon}$ can be chosen, because there is no rigid body rotation involved in the deformation and the programme merely solves the superposition of two ellipses; if R is not equal to one, $\bar{\varepsilon}$ is very small.

2/ A subprogramme UNITY converts the axial lengths of the particle to reciprocal quadratic elongations A and B such that AB = 1. This makes the invariant J_2 always equal to 1.

3/ A subprogramme AXES calculates the strain invariants and computes the new semi-axial lengths (RTA, RTB) and axial ratio (ARATIO) of the deformed ellipse; sums the infinitesimal strains $\bar{\varepsilon}$ to obtain the finite natural strain (STRAIN) and converts this to the axial ratio (ELLIPS) of the finite strain ellipse.

4/ The angle θ is then calculated and the new orientation φ of the major axis is found.

5/ If R is not equal to 1, a subprogramme SBROTN computes the rigid body rotation and the final orientation φ_f.

By a series of DO-LOOPS, these calculations are repeated for successive increments of $\bar{\varepsilon}$ until the total finite strain experienced by the particle-matrix system, reaches a set value, or the particle major axis becomes oriented very close to $\varphi = 90^\circ$.

Figure 32 Flow diagram of the programme to compute the pure shear deformation of non-rigid ellipses, not aligned parallel to the strain axes.

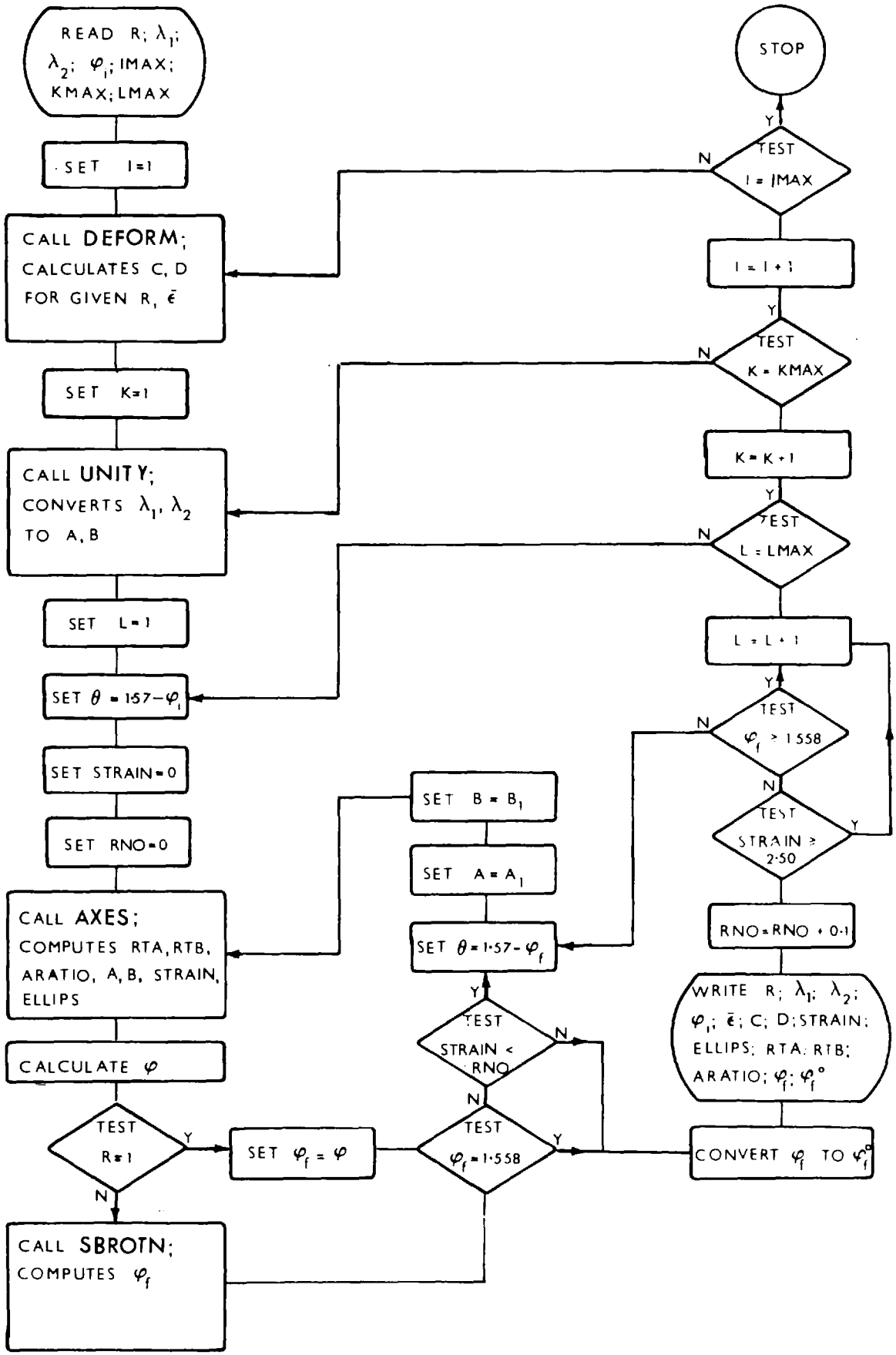
READ R; λ_1; λ_2; φ_1; IMAX; KMAX; LMAX
SET I=1
CALL DEFORM; CALCULATES C, D FOR GIVEN R, $\bar{\epsilon}$
SET K=1
CALL UNITY; CONVERTS λ_1, λ_2 TO A, B
SET L=1
SET $\theta = 1{\cdot}57 - \varphi_1$
SET STRAIN=0
SET RNO=0
CALL AXES; COMPUTES RTA, RTB, ARATIO, A, B, STRAIN, ELLIPS
CALCULATE φ
TEST R=1
Y
N
SET $\varphi_f = \varphi$
CALL SBROTN; COMPUTES φ_f
SET B = B_1
SET A = A_1
SET $\theta = 1{\cdot}57 - \varphi_f$
TEST STRAIN < RNO
N
Y
TEST $\varphi_f = 1{\cdot}558$
N
Y
CONVERT φ_f TO φ_f°
TEST $\varphi_f > 1{\cdot}558$
N
Y
TEST STRAIN ≥ 2·50
N
Y
RNO=RNO + 0·1
WRITE R; λ_1; λ_2; φ_1; $\bar{\epsilon}$; C; D; STRAIN; ELLIPS; RTA; RTB; ARATIO; φ_f; φ_f°
L = L + 1
TEST L = LMAX
N
Y
K = K + 1
TEST K = KMAX
N
Y
I = I + 1
TEST I = IMAX
N
Y
STOP

Figure 33 Pure shear deformation paths for R = 1 ellipses which do not have their particle axes parallel to the strain axes. The dashed curves are contours of the pure shear natural strain; the contour interval is $\bar{\varepsilon}$ = 0.1 units.

a/b - particle axial ratio.

Φ - angle between the Y' strain axis and the major axis of the particle.

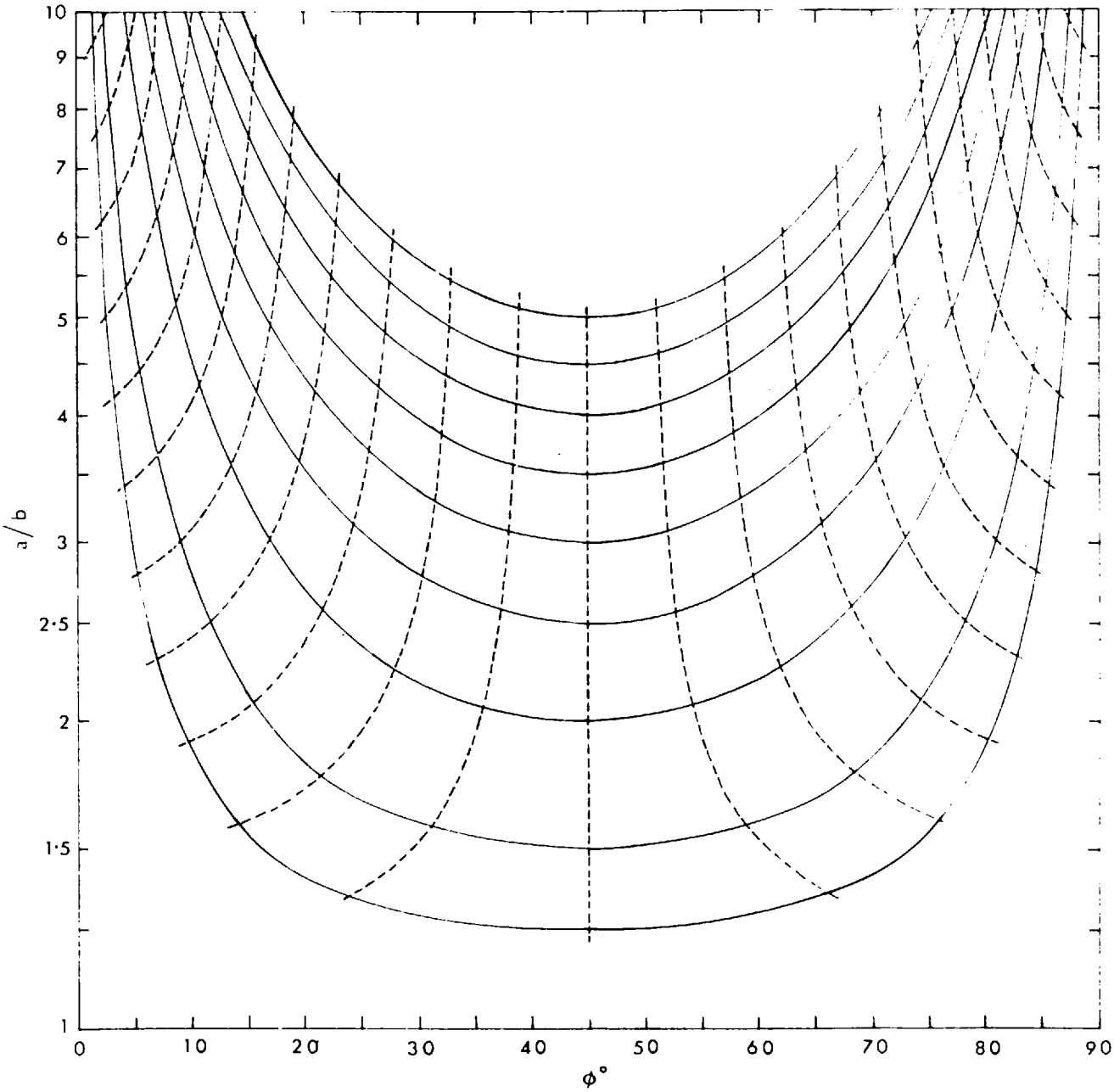
10
9
8
7
6
5
4
3
2·5
2
1·5
1
a/b
0
10
20
30
40
50
60
70
80
90
φ°

The results obtained from the computer were plotted graphically as in figure 33, which shows the changes, with deformation, of the shape and orientation of ellipses of any axial ratio for R = 1. The solid curves in this figure are the deformation paths followed by a particular ellipse while being strained. The dashed curves are contours of natural strain with a contour interval of $\bar{\varepsilon}$ = 0.1. Both sets of curves are symmetrical about $\varphi = 45^{\circ}$.

All ellipses which have initial orientations between 0° and 45° become less eccentric during deformation and rotate towards the direction of elongation. However, when the orientations of the major axes pass through $\varphi = 45^{\circ}$, the particles enter into the field of elongation and become more eccentric as they rotate towards $\varphi = 90^{\circ}$. All the particle major axes approach very near to this final position but only become parallel to it after an infinite amount of strain.

One interesting conclusion which may be drawn from the graphs is that the initial shape differences between particles is altered during the deformation. For example, consider particles with initial axial ratios 2 : 1 and 4 : 1, orientated along $\varphi = 15^{\circ}$. The following table shows the approximate changes in shape and position during deformation.

$\bar{\varepsilon}$	A	φ_A°	B	φ_B°	A/B
0	4.0	15	2.0	15	2.00
0.1	3.4	22	1.7	24	2.00
0.2	3.0	32	1.5	37	2.00
0.3	2.9	43	1.5	53	1.90
0.4	3.0	55	1.7	66	1.75
0.5	3.3	65	2.0	75	1.65

However, the change is not as marked for particles initially oriented at $\varphi = 45^{\circ}$. This is shown by the following data.

$\bar{\varepsilon}$	A	φ_A^o	B	φ_B^o	A/B
0	3.0	45	1.5	45	2.00
0.1	3.1	56	1.6	61	1.95
0.2	3.5	66	1.8	71	1.95
0.3	4.0	73	2.1	78	1.90
0.4	4.8	79	2.6	82	1.85
0.5	5.8	82	3.2	85	1.80

Similarly, the reduction in the ratio of individual particle shapes will be less marked as the initial orientations approach $\varphi = 90^o$, and along this direction there will be no change in the ratio A/B during the deformation.

The effect of an increase in the viscosity ratio between the particle and the matrix is well illustrated in figures 34a, b. These graphs show the changes, during deformation, of the shape and orientation of initially 2 : 1 ellipses, aligned at $\varphi = 45^o$, for different values of R.

In figure 34a, the change in axial ratio of the particle is plotted against the natural strain and it is clear that, with increasing R, there is a rapid decrease in the deformation experienced by the particle. Similarly, there is a reduction in the changes in orientation of the major axes of the ellipses with increasing R, during the early stages of the pure shear (figure 34b). However, because all the ellipses rotate towards the $\varphi = 90^o$ position, these initial differences are reduced with increasing strain and, eventually, after an infinite amount of pure shear, all ellipses will have their major axes parallel to $\varphi = 90^o$.

The combined effect of these changes in shape and orientation are shown in figure 35. These graphs are the deformation paths of the ellipses and show clearly the marked effect an increase in R has on the behaviour of the particle.

Figure 34 Graphs to show the effect of increasing viscosity ratio, R, on the pure shear deformation of 2 : 1 ellipses, initially at 45^{o} to the strain axis.

a) The change in axial ratio (a/b) with natural strain ($\bar{\varepsilon}$).

b) The change in orientation (φ), of the particle major axis with respect to the Y' pure shear axis, with natural strain ($\bar{\varepsilon}$).

The numerals next to the curves indicate the value of the viscosity ratio, R, used to calculate the graphs.

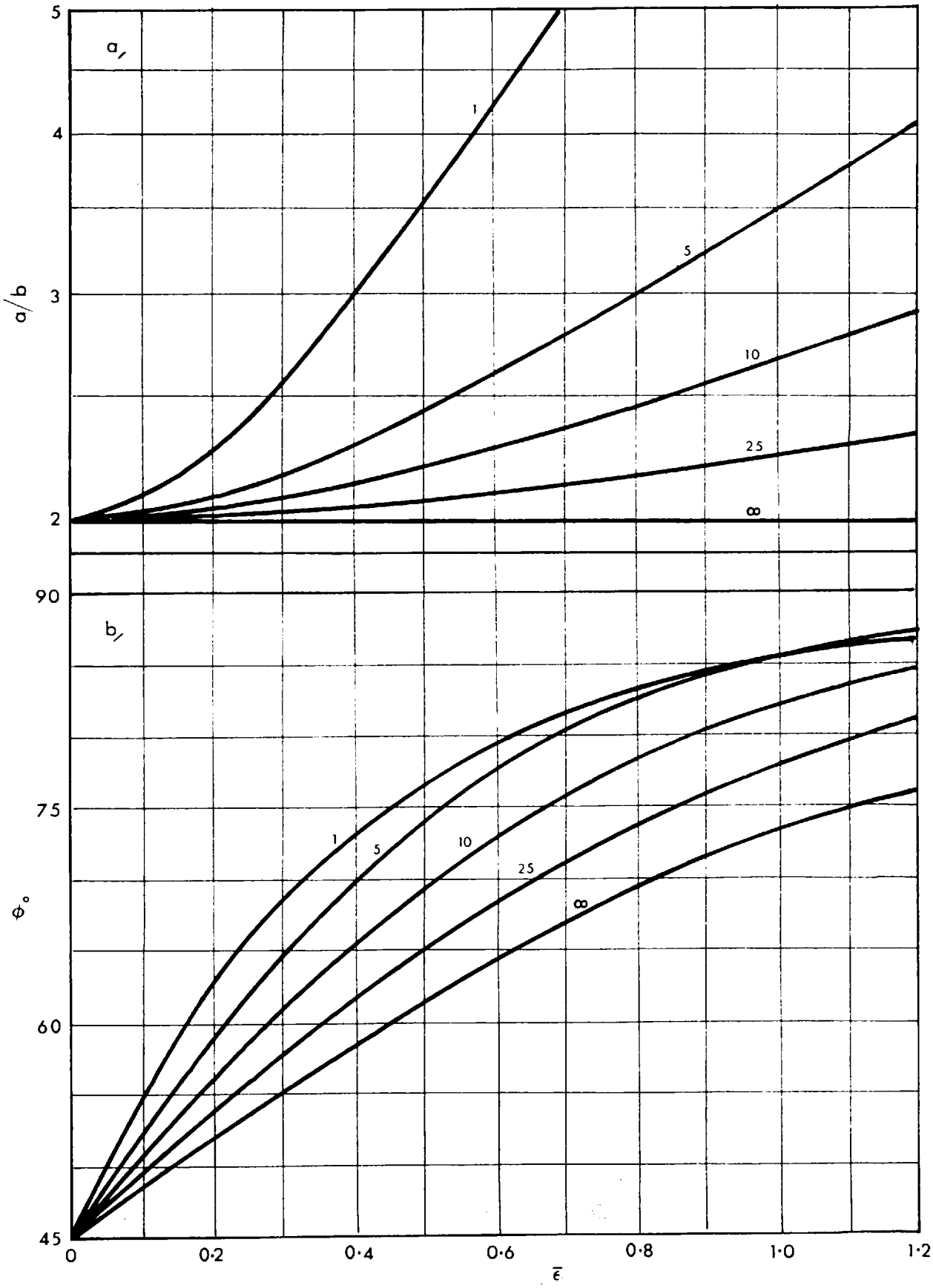
a/
b/
a/b
φ°
$\bar{\epsilon}$
1
5
10
25
∞
5
4
3
2
90
75
60
45
0
0·2
0·4
0·6
0·8
1·0
1·2

Figure 35 Pure shear deformation paths for initially 2 : 1 ellipses, aligned at $\varphi = 45^{\circ}$ to the Y' strain axis.

The graphs combine the results shown in figures 34a, b and were computed numerically using the indicated values of the viscosity ratio, R. Each point on the curves represents an interval of 0.1 $\bar{\varepsilon}$ in the natural strain of the pure shear.

a/b - particle axial ratio.

φ - orientation of the major particle axis with respect to the Y' pure shear axis.

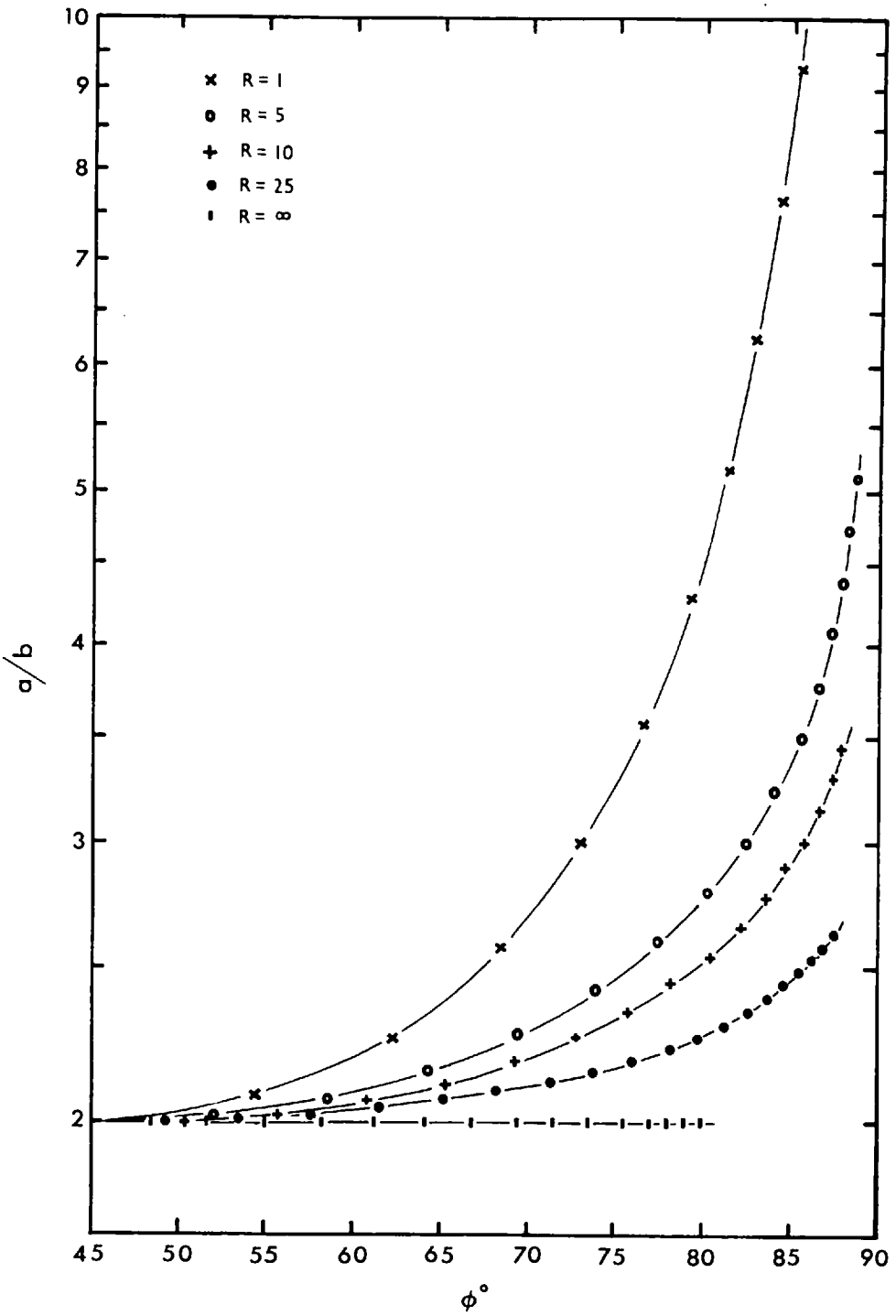
R = 1
R = 5
R = 10
R = 25
R = ∞
a/b
φ°
10
9
8
7
6
5
4
3
2
45
50
55
60
65
70
75
80
85
90

F. SIMPLE SHEAR DEFORMATION OF NON-RIGID CIRCULAR PARTICLES

(a) Introduction

The problem of the deformation of non-rigid particles is similar to that discussed in the previous section and is also difficult to solve. Taylor (1934) found a solution for very small drops of one fluid suspended in another. This analysis indicated that the drops would deform and rotate into the shearing direction. Experiments showed that once in this position, the deformed drops remained there and kept a constant shape.

To solve the problem for larger particles, the present writer has had to develop a numerical solution similar to that described above for ellipses in pure shear. The method uses the fact that a simple shear deformation is essentially a pure shear combined with a rotation (Nadai, 1950, p. 149). The pure shear component acts along axes at 45° to the shear-direction (figure 36a) and the natural strain describing it is given by equation III.10, which for infinitesimal strains reduces to

$$\bar{\varepsilon} = \gamma_s/2 \quad \ldots(IV.75)$$

Similarly, the rigid body rotation component of an infinitesimal simple shear is $\gamma_s/2$ or $\bar{\varepsilon}$ radians.

(b) Initial deformation of the particle

Referring to figure 36a, the equation of the initially circular particle with respect to its own X, Y axes is:

$$x^2 + y^2 = 1$$

Deform this circle through a very small amount of shear, γ_s. The associated pure shear changes the circle to the infinitesimal strain ellipse in figure 36b. It has the equation:

$$x^2/a_o^2 + y^2/b_o^2 = 1 \quad \ldots(IV.76)$$

Figure 36 Diagrams to illustrate the numerical method for determining the simple shear deformation of an initially circular, non-rigid particle.

a) Initial position.

X'', Y'' - axes of simple shear.

X', Y' - axes of associated pure shear.

X, Y - particle axes.

μ, μ' - viscosities of particle and matrix, respectively.

The particle has unit radius.

b) Infinitesimal pure shear deformation of the particle.

a_o, b_o - major and minor semi-axial lengths of the elliptical particle.

φ - orientation of the major axis of the ellipse to the Y'' simple shear axis.

c) Infinitesimal rigid body rotation of the ellipse through an angle $\bar{\varepsilon}$ radians

a/

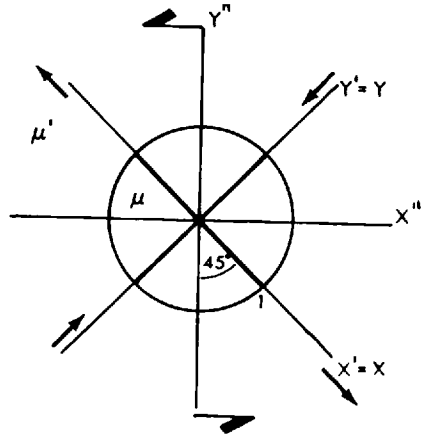

b/

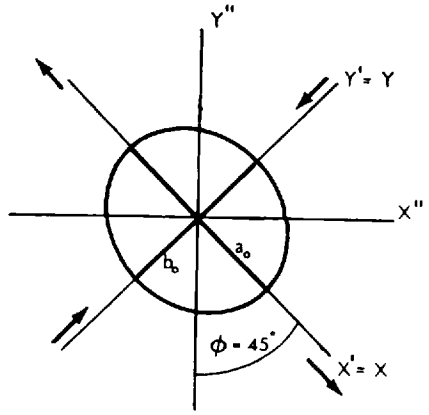

c/

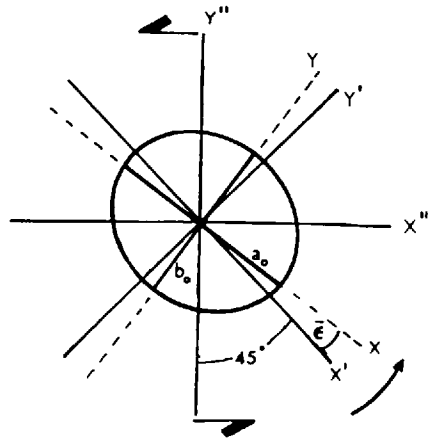

which is the same as IV.65 and, hence, has reciprocal quadratic elongations C and D. The orientation of the major axis of the ellipse with respect to the simple shear Y'' axis is $\varphi_i = 45^\circ$.

Similarly, in terms of the viscosity ratio R between the particle and the surrounding matrix, the lengths of the semi-axes and the axial ratio are given by equations IV.66 and IV.67.

After the pure shear, the ellipse is rotated through $\bar{\varepsilon}$ radians. The transformation equations for this are

$$x = x'\cos\bar{\varepsilon} + y'\sin\bar{\varepsilon}$$
$$y = -x'\sin\bar{\varepsilon} + y'\cos\bar{\varepsilon} \qquad \ldots(IV.77)$$

Substituting IV.77 into IV.76 gives

$$(x'\cos\bar{\varepsilon} + y'\sin\bar{\varepsilon})^2/a_o^2 + (-x'\sin\bar{\varepsilon} + y'\cos\bar{\varepsilon})^2/b_o^2 = 1$$

which is the equation of the ellipse in figure 36c, with reference to the X', Y' pure shear axes. This equation can be rearranged into the same form as equation IV.63, i.e.:

$$\lambda_x' x'^2 - 2\gamma' x'y' + \lambda_y' y'^2 = 1 \qquad \ldots(IV.78)$$

where
$$\lambda_x' = A\cos^2\bar{\varepsilon} + B\sin^2\bar{\varepsilon}$$
$$\lambda_y' = A\sin^2\bar{\varepsilon} + B\cos^2\bar{\varepsilon} \qquad \ldots(IV.78a)$$
$$\gamma' = (B - A)\sin\bar{\varepsilon}\cdot\cos\bar{\varepsilon}$$

and
$$A = 1/a_o^2, \quad B = 1/b_o^2$$

With reference to the Y'' simple shear axis, the new orientation of the ellipse is $\varphi = \pi/4 + \bar{\varepsilon}$ radians.

(c) Superposition of the next infinitesimal pure shear

The infinitesimal strain ellipse for the pure shear component of the next increment in simple shear is described by equation IV.76. Superposing this ellipse on IV.78 is carried out by the transformations

$$x_1' = a_o x, \quad y_1' = b_o y$$

and results in the equation of a new ellipse:

$$\lambda_x' C x'^2 - 2\gamma' x' y' + \lambda_y' D y'^2 = 1$$

This is the same ellipse as IV.69 and, following the same procedure as before, its semi-axial lengths a_1, b_1 and orientation θ can be calculated from

$$a_1, b_1 = \sqrt{[2/(J_1^2 \mp \sqrt{J_1^2 - 4J_2})]} \quad \ldots(IV.79)$$

$$\tan 2\theta = 2(B - A)\sin \bar{\varepsilon}.\cos \bar{\varepsilon}/[B(D\cos^2\bar{\varepsilon} - C\sin^2\bar{\varepsilon}) - A(C\cos^2\bar{\varepsilon} - D\sin^2\bar{\varepsilon})] \quad \ldots(IV.80)$$

(d) Addition of the rigid body rotation component

To apply the solid body rotation, an angle $\bar{\varepsilon}$ must be added to θ. Then, the new angle between the particle major axis and the pure shear axes is

$$\omega = \theta + \bar{\varepsilon} \quad \ldots(IV.81)$$

The final orientation, φ, of the major particle axis with respect to the Y' coordinate of the simple shear is

$$\varphi = \pi/4 + \omega \quad \ldots(IV.82)$$

Figure 37 Flow diagram of the programme to compute the simple shear deformation of non-rigid discs.

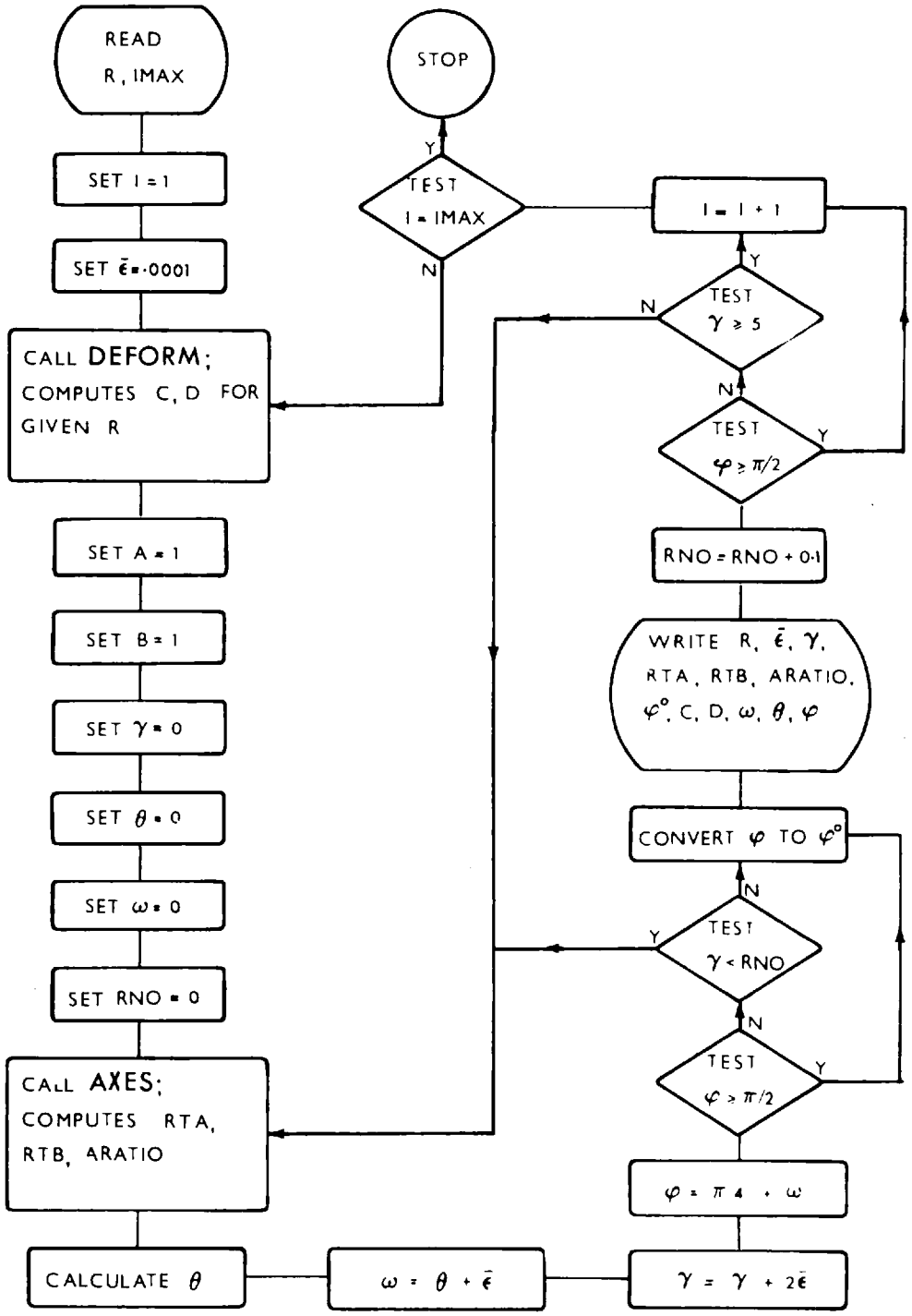
READ
R, IMAX
SET I = 1
SET $\bar{\epsilon}$ = ·0001
CALL DEFORM;
COMPUTES C, D FOR
GIVEN R
SET A = 1
SET B = 1
SET γ = 0
SET θ = 0
SET ω = 0
SET RNO = 0
CALL AXES;
COMPUTES RTA,
RTB, ARATIO
CALCULATE θ
$\omega = \theta + \bar{\epsilon}$
$\gamma = \gamma + 2\bar{\epsilon}$
$\varphi = \pi/4 + \omega$
TEST
$\varphi \geq \pi/2$
N
Y
TEST
$\gamma < RNO$
N
Y
CONVERT φ TO φ°
WRITE R, $\bar{\epsilon}$, γ,
RTA, RTB, ARATIO,
φ°, C, D, ω, θ, φ
RNO = RNO + 0·1
TEST
$\varphi \geq \pi/2$
N
Y
TEST
$\gamma \geq 5$
N
Y
I = I + 1
TEST
I = IMAX
Y
N
STOP

Figure 38 Simple shear deformation paths for initially circular, non-rigid particles with different viscosity ratios. The solid curves are deformation paths and were calculated numerically using the relevant value of R. The dashed curves are lines of equal simple shear, the value of γ_s for each line is indicated next to it.

a/b - particle axial ratio.

ϕ - orientation of the particle major axis, with respect to the Y' simple shear axis.

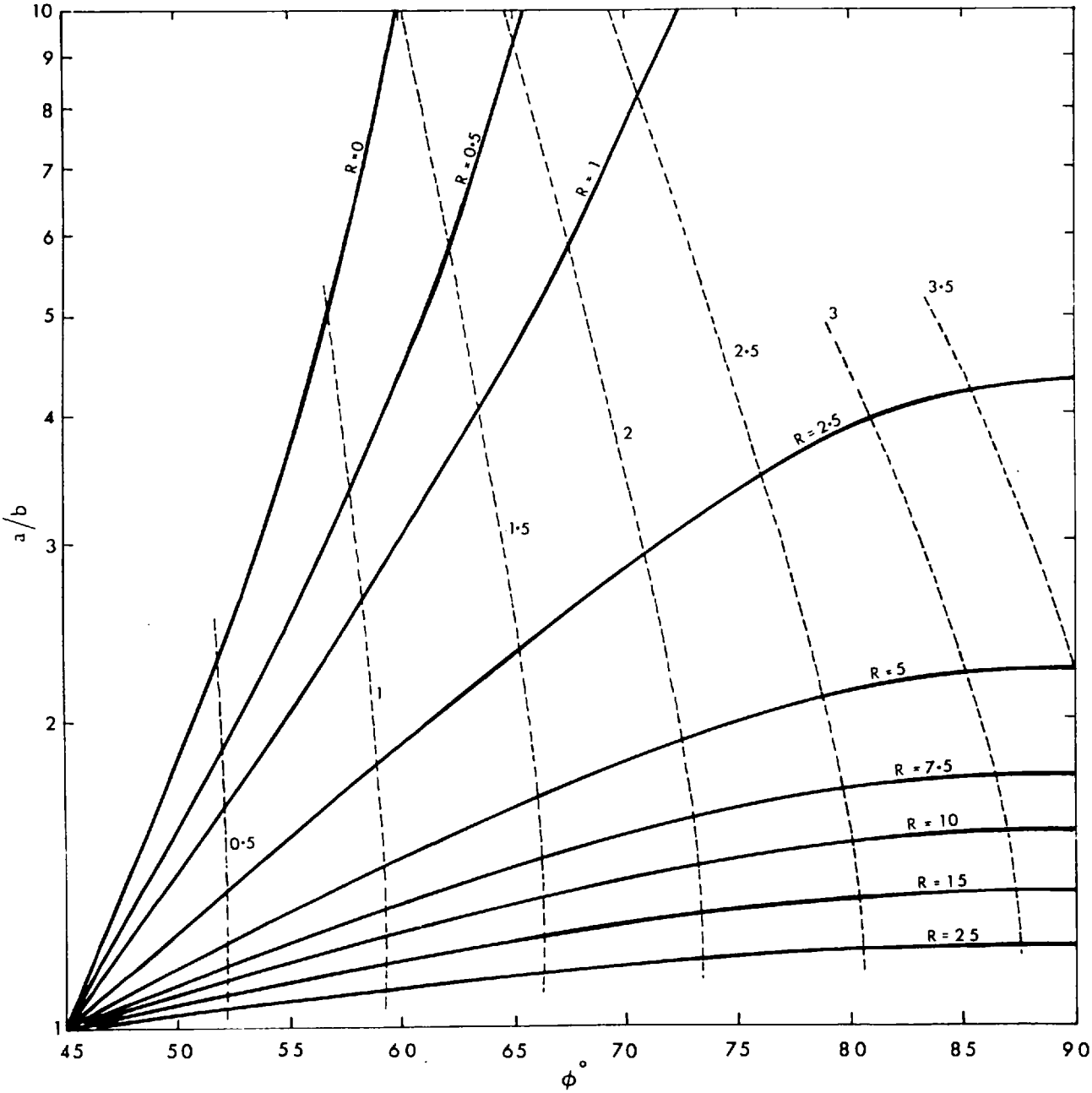
a/b
φ°
R=0
R=0·5
R=1
R=2·5
R=5
R=7·5
R=10
R=15
R=25
0·5
1
1·5
2
2·5
3
3·5
10
9
8
7
6
5
4
3
2
1
45
50
55
60
65
70
75
80
85
90

(e) Computation and significance of the results

The calculations outlined above are carried out for succesive small increments of shear. The flow diagram for the programme is drawn in figure 37. Values of R are fed into the computer and the computations are then performed in the same manner as outlined in the previous section, for ellipses deforming in pure shear.

The results obtained from the computer are plotted graphically in figure 38. The solid graphs are deformation paths for initially circular particles with different values of R. The dashed curves are lines of equal simple shear, with a contour interval of 0.5 γ_s. From these deformation paths, it is clear that, for a given amount of shear, an increase in R results in a smaller change in shape and a greater rotation.

It is possible to check the reliability of the method of computing these deformation paths by comparing the data obtained for R = 1, with that calculated from the theoretical equations for the geometry of simple shear (equations III.3 and III.4):

$$\sqrt{\lambda_1/\lambda_2} = [\sqrt{(\gamma_s/2)^2 + 1} + \gamma_s/2]/[\sqrt{(\gamma_s/2)^2 + 1} - \gamma_s/2]$$

and $$\varphi = \pi/4 + (1/2)\tan^{-1}(\gamma_s/2)$$

This is done in the table below.

γ_s	$\sqrt{\lambda_1/\lambda_2}$ num	φ^o num	$\sqrt{\lambda_1/\lambda_2}$ th	φ^o th
0	1.00	45.00	1.00	45.00
1	2.62	58.29	2.62	58.28
2	5.83	67.50	5.83	67.50
3	10.91	73.16	10.91	73.16
4	17.94	76.72	17.94	76.72
5	26.95	79.10	26.97	79.10

It is clear that the results obtained numerically correspond remarkably well with the correct theoretical values.

Figure 39 Experimental and theoretical deformation paths for particles deforming by simple shear.

The continuous curves are calculated theoretically and the light, dashed curves parallel to them indicate the zone of error, assuming errors of ± 0.5 mm in measurement of the axial lengths, and $\pm 2^{\circ}$ in the orientation of the major particle axis.

Cutting these curves at right angles are the dashed lines of equal simple shear; the value of γ_s for each line is indicated next to it.

The values of R for the theoretical curves and the experiments are as follows:

A) R = 1, B) R = 2.5, C) R = 5

D) R = 7.5, E) R = 10, F) R = 15.

The experimental points indicate the particle axial ratio (a/b) and the orientation of its major axis (ϕ), after 0.25 γ_s or 0.5 γ_s units of shear. The breaks in the experimental curves are due to repositioning of the particle at the end of each run in the simple shear box.

The crosses indicate results obtained during one set of experiments, the dots are the results of another set. The detailed experimental results are listed in table XI, Appendix I.

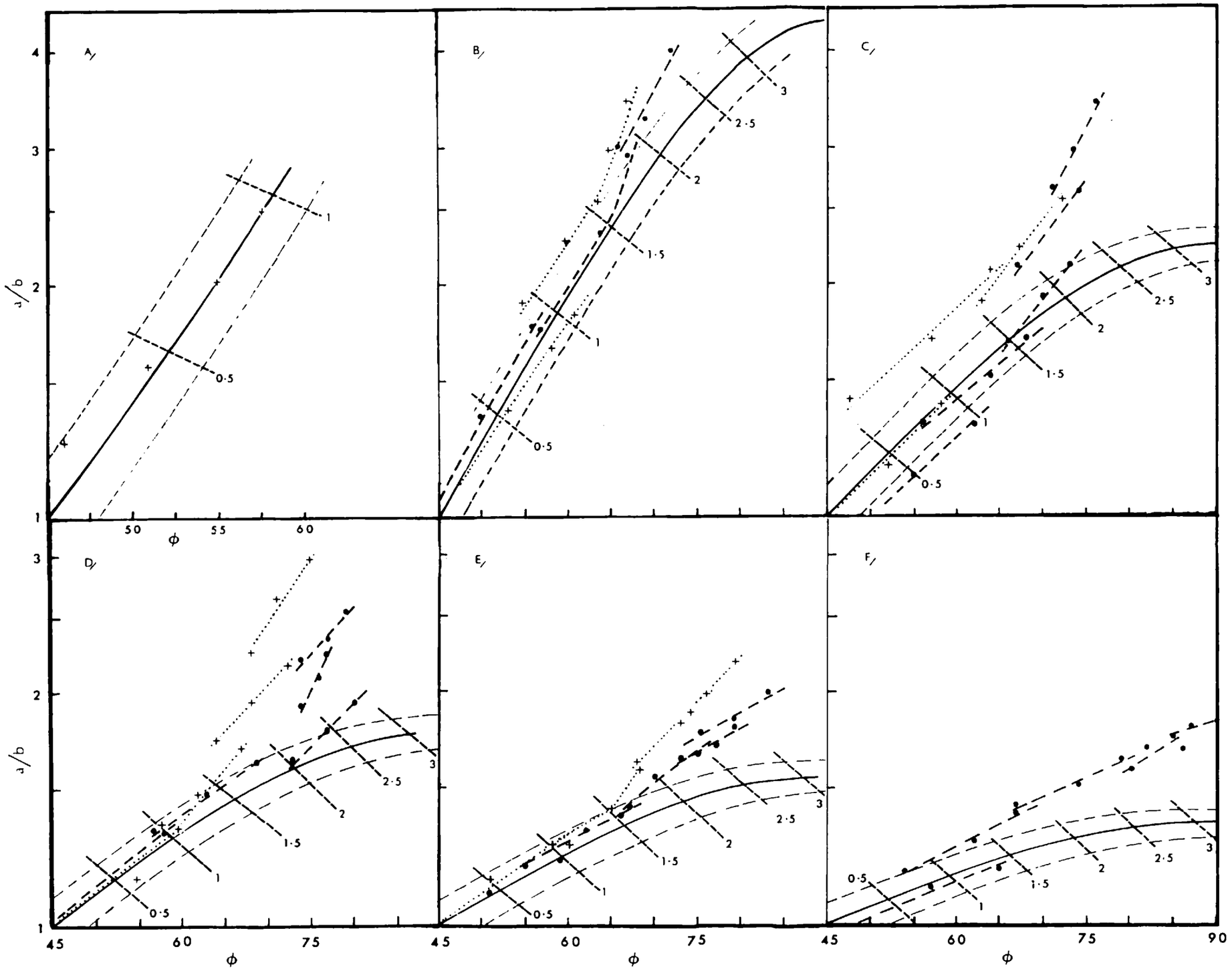
A/
B/
C/
D/
E/
F/
a/b
ϕ
0·5
1
1·5
2
2·5
3
50
55
60
45
60
75
90

(f) Experimental checks on the deformation paths

Several experiments were carried out in the simple shear box on the deformation of initially circular, non-rigid particles. The results of these experiments are plotted graphically in figures 39A - 39F, with the relevant theoretical deformation paths and contours of equal shear. The light, dashed curves parallel to the deformation paths demarcate the zone of experimental error, assuming that, at the end of each run, the particles are rotated into the exact equivalent positions However, it is clear from the experimental curves that this has not happened and there is obviously an error introduced during the repositioning of the particles. Each experimental point indicates the axial ratio and orientation of the particle major axis after a certain amount of simple shear. Normally measurements were taken after a shear of 0.5 γ_s, though for the R = 1 and some of the R = 2.5 experiments, the interval was 0.25 γ_s.

The results obtained on particles with viscosity ratios of R = 1 and R = 2.5 agree very well with the theoretical deformation paths. The more viscous particles also deform as predicted during the early stages of the deformation. However, with increasing γ_s, the particles elongate more rapidly and rotate more slowly than expected. This may correspond with the similar rapid elongation observed during the deformation of particles in pure shear, and may also be attributed to the particles becoming anisotropic with increasing deformation.

Nevertheless, it is evident that with increasing viscosity ratio between the particle and the matrix, there is a marked decrease in the change in shape and a corresponding increase in the rate of rotation.

G. THE DEFORMATION OF SYSTEMS CONTAINING A LARGE NUMBER OF PARTICLES EMBEDDED IN A VISCOUS MATRIX

(a) Introduction

The behaviour of systems containing a large number of particles in a viscous matrix, during simple and pure shear deformations, will now be discussed in the light of the previously developed equations of motion for single particles, assuming that the Newtonian conditions for which those equations were derived still hold. This assumption is generally valid for suspensions of particles up to quite large concentrations (30 per cent, Moore, 1965, p.20). However, at higher concentrations or, if the particles are asymmetrical in shape, at relatively low concentrations, the rheological properties of the suspensions may change to those of a non-Newtonian body with variable viscosity. This effect is important, especially if the particles are non-rigid and are changing shape during the deformation.

In the following section, the behaviour of systems of rigid particles is discussed, assuming the equations for isolated particles can be applied to them. In general, the individual particles should behave as predicted, provided that the concentration of particles is not so great that they come into contact with one another. If the particles are ellipsoidal, they develop preferred orientations which will affect the mean viscosity of the particle-matrix system.

Then, systems of non-rigid particles are considered. It is obvious that the mean viscosity of such a system and, hence, the viscosity ratio which controls the particle deformation, will vary with the number of particles present. An equation to calculate this variation in the viscosity ratio with particle concentration is derived and then checked experimentally. The preferred orientations which may be developed during the deformation of the particles will also affect the mean viscosity of the system; these too are discussed, though only in general terms.

(b) Systems of rigid particles

i) Simple shear

In the section dealing with rigid ellipsoids in a simple shear field, it was shown that an isolated particle rotated in a spherical elliptical orbit about the Z' axis. The rate of rotation varied from a maximum, when the particle was aligned along the $\varphi = 0^{\circ}$ direction, to a minimum, along $\varphi = 90^{\circ}$. Simultaneously, the angle of plunge of the particle major axis decreased from a maximum to a minimum value. Thus the particle would take a greater time to pass through the X'Z' plane at $\varphi = 90^{\circ}$ than it would through any other point on its orbit, and, because the plunge of its long axis is a minimum along this direction, the particle major axis would approach parallelism with the X' direction of the simple shear.

Assuming that the individual particles in a multiparticle system being deformed by simple shear behaved in this manner, one would expect a preferred orientation of particle long axes to be set up parallel to the X' flow direction. The degree of this preferred orientation will clearly depend on the ellipsoidal axial ratios and should be best developed for the more eccentric particles. Moreover, once it is set up, the degree of preferred orientation should remain statistically constant despite the fact that particles will be entering and leaving the zone of orientation continuously.

Mason and Manley (1956) have calculated from Jeffery's (1922) equations that, once this statistical equilibrium position has been reached, the integral distribution function giving the fraction of particles having an orientation between $\varphi = 0^{\circ}$ and $\varphi = \varphi^{\circ}$ is

$$P(\varphi) = (1/2\pi)\tan^{-1}[\tan\varphi/(a/b)] \quad \ldots(IV.83)$$

where φ ranges between 0 and 2π.

These workers were not able to define a similar function $P(\theta)$ for the equilibrium distribution of plunges along the

shearing direction, though they did show experimentally that this distribution was set up for highly elongate particles ($a/b > 20$) after a great amount of shear (more than 2300 rotations per particle).

At high particle concentrations, it is possible in a simple shear field for one particle to approach sufficiently close to another for their rotation fields to interact. Mason and Manley (1956) found that the effect of this interaction was to change the orbits of the particles and they suggested that, eventually, this would result in a steady state distribution of orientations and plunges. In other words, the particles would achieve stable positions parallel to some direction in the flow field. The writers do not specify what direction this is but from the fact that the statistical preferred orientation is set up parallel to the X' axis, one would expect the stable position to be in this direction, as well. However, Jeffery (1922) postulated that in a simple shear flow field, ellipsoids should adopt a stable orientation with their major axes parallel to the Z' flow axis. He could suggest no mechanism whereby this stable position could be achieved but proposed it because it would satisfy the requirements of minimum energy in the system and would reduce the viscosity to a minimum.

ii) Pure shear

The equations of motion of a single ellipsoidal particle during a pure shear deformation show that a particle will, in general, rotate towards the direction of elongation of the strain. At the same time, the plunge of the particle's major axis increases until it is orientated along the $\varphi = 45^{\circ}$ direction, after which it decreases as the rotation proceeds further. No rotation occurs during the deformation, if the particle is oriented parallel to either of the strain axes. However, the plunge of the major axis of a particle in this position will either increase, along the direction of compression, or decrease, along the direction of elongation.

The rate at which changes in orientation and plunge occur increases with increasing particle eccentricity. Moreover, the general result of these combined motions will be that the particle tends to become parallel to the X' strain axis and to lie in the deformation plane. This will not happen, of course, if the particle is aligned along the direction of compression, in this case, the particle will tend to lie parallel to the Z'axis.

Assuming that these equations of motions are applicable to the individual particles in a multi-particle system, it is clear that during a pure shear deformation the majority of the particles rotate towards the direction of elongation. This results in a preferred orientation of particle major axes being set up parallel to this direction. At first, the degree of this preferred orientation depends upon the shape of the particles, because the more eccentric ones rotate faster. However, with continuing strain, this factor becomes unimportant as particles of all shapes approach the end position.

In addition to the major zone of concentration of particles around the X' axis, those particles initially aligned along the direction of shortening, develop a lesser zone of preferred orientation parallel to the Z' axis.

The theoretical equations governing the particle motions predict that complete parallelism between particle major axes and the X' or Z' flow direction will only occur after an infinite amount of pure shear. Therefore, the degree of preferred orientation is always increasing and will never reach a position of statistical equilibrium. For this reason, it is not possible to calculate an integral distribution function corresponding to IV.83 for simple shear.

The effect of particle interactions in systems containing a high concentration of particles during pure shear has not, so far as the writer is aware, been investigated, either experimentally or theoretically. However, from the results

obtained by Mason and Manley (1956) for simple shear deformations, one would expect interactions to change the orientations and plunges of the particles concerned. If the plunge were increased, this could eventually lead to the particles approaching the stable position with their major axes parallel to the Z' axis. Similarly, if plunges were decreased, the probable end position would be parallel to the X' axis. Thus, the effect of the interactions may be to enhance the development of the preferred orientations.

iii) Viscosity of solutions of rigid particles

To determine the effect of the presence of a number of particles on the viscosity of the particle-matrix system, consider first a single particle suspended in a uniformly flowing fluid. The presence of the particle causes a disturbance in the flow in the region immediately surrounding it. This disturbance increases the resistance of the fluid to the flow deformation and, hence, increases the viscosity coefficient. If more than one particle is present, the region of disturbance depends on the volume and number of the particles and, therefore, the mean viscosity of a suspension will depend on the volume concentration of the particles. Einstein (1906, 1911) derived the following equation to describe this effect for suspensions of rigid spheres.

$$\mu_m = \mu'(1 + kC_v) \quad \ldots(IV.84)$$

where μ_m is the viscosity of the suspension; μ' the viscosity of the continuous phase (i.e. the matrix); C_v the volume concentration of the dispersed phase (i.e. the particles); and k is a constant which describes the interference with the flow and, theoretically, has a value of 2.5.

For suspensions of ellipsoids of revolution, Jeffery (1922) suggested a similar equation but k could vary in value 2.5 to infinity, depending upon the eccentricity of the particles. This increase in k is due to the fact that an

ellipsoidal particle will sweep through a volume much greater than its own, as it rotates in the fluid and, hence, will produce a greater region of disturbance in the flow.

Both Einstein and Jeffery assumed that the suspensions were so dispersed that the distance between the particles was infinitely great compared to their diameters. If, however, the particle concentration increases so that the modification in the flow produced by one particle extends into the field of a neighbouring particle, the resistance to flow (and hence the constant k) is increased still more.

To allow for this effect, Happel (1957) introduced an interaction factor, Φ, which was proportional to the volume concentration of the particles, C_v. Using this factor and assuming that the particle interference fields interact at even the greatest dilutions, Einstein's equation IV.84 for suspensions of rigid spheres becomes

$$\mu_m = \mu'(1 + 5.5\Phi C_v) \quad \ldots(IV.85)$$

The above discussion shows that the mean viscosity depends upon the volume of fluid disturbed during the rotation of the particles. This volume will obviously decrease as the degree of preferred orientation of the particles increases and the viscosity of the system should, therefore, decrease accordingly. The minimum value of the viscosity will be reached when the particles achieve a stable position, or the statistical equilibrium degree of preferred orientation is set up.

(c) Systems of non-rigid particles

i) Simple shear

The results of the theoretical and experimental work on the deformation of single non-rigid particles during simple shear show that the particle will deform and rotate towards the X' flow direction. A particle with the same viscosity as the matrix will require an infinite amount of shear before it becomes parallel to the X' flow axis. However, with increasing viscosity contrast, the change in shape of the particle decreases and the rate of rotation increases. Consequently, a relatively viscous particle (R = 15, say) may rotate into, and through, the shearing direction, quite rapidly.

It follows from these arguments that, in systems containing a large number of non-rigid particles, one would expect a preferred orientation to be set up parallel to the X' flow axis. For particles with a high viscosity contrast to the matrix and which rotate through the shearing direction quite easily, this preferred orientation will be one of statistical equilibrium, as described above for rigid particles. However, it is unlikely that less viscous particles will be able to rotate out of the shearing direction, once they are parallel to it, because of the large amount of shear required. Therefore, these particles will develop a stable preferred orientation. It is possible that for very low viscosity ratios, the particle major axes may not become parallel to the shearing direction; nevertheless, they still should have their long axes parallel to each other, if they were originally of similar shape.

ii) Pure shear

The theory for a single non-rigid particle in pure shear shows that, if its axes are aligned parallel to either of the strain axes, the particle will be elongated in the direction of elongation of the strain ellipse. If its axes are not initially parallel to the strain axes, the

particle rotates towards the direction of elongation. Simultaneous with the rotation, the axial ratio of the particle decreases until an orientation of $\varphi = 45^{\circ}$ is reached, after which it increases. Thus, the end result is for the particle to approach parallelism with the direction of elongation and to increase in eccentricity. The rates of rotation and elongation increase as the viscosity ratio between the particle and the matrix is reduced.

Applying these observations to systems containing a large number of particles, it is clear that during pure shear a preferred orientation will be set up parallel to the direction of elongation of the strain. Initially, the degree of this preferred orientation will be greatest for the least viscous particles but, because all particles rotate towards the same direction, this difference will disappear as the strain continues. However, the less viscous particles will always be much more eccentric in shape than the more competent particles.

iii) <u>The viscosity of systems containing non-rigid particles</u>

It was shown in the section on rigid particles that the mean viscosity of a particle-matrix system is proportional to the volume concentration of the particles. This effect is very important for systems of non-rigid particles, because the deformation of the individual particles depends on the viscosity ratio between the particle and the system. In the single particle theory, the viscosity of the system was assumed to be that of the matrix solution. However, this is obviously not valid in multi-particle systems and so an attempt will be made to correct for the effect of the particle concentration.

Einstein (1906, 1911) in his work on the viscosity of suspensions of rigid spheres, showed that the mean viscosity depended only on the solid harmonic function p'_3, appearing in the equation of fluid velocity IV.43. Using this fact, Taylor (1932) extended Einstein's analysis to suspensions of

small fluid drops held approximately spherical by surface tension forces. His resultant equation was

$$\mu_m = \mu'[1 + (1/2)C_v(5R + 2)/(R + 1)] \quad ...(IV.86)$$

The same procedure can be followed to determine the viscosity of systems containing larger particles, not necessarily affected by surface tension forces.

From equation IV.45c it is clear that p'_{-3} is proportional to the constant A_{-3} which, in turn, has a value given by

$$A_{-3} = -5[(R - 1)/(2R + 3)](2\dot{\bar{\varepsilon}}) \quad ...(IV.55)$$

For rigid spheres with $R = \infty$, this equation reduces to

$$A_{-3} = -2.5(2\dot{\bar{\varepsilon}})$$

where the number 2.5 is the value of the coefficient k appearing in the Einstein equation IV.84. Hence, for fluid spheres not subject to surface tension forces, k = 2.5 must be replaced in equation IV.84 by

$$k = 5(R - 1)/(2R + 3)$$

i.e. the Einstein equation is modified to

$$\mu_m = \mu'[1 + 5C_v(R - 1)/(2R + 3)] \quad ...(IV.87)$$

This equation agrees with that obtained by Hashin (quoted by Reiner, 1960b, p. 214) for the analogous problem in elasticity theory; i.e. the increase in the shear modulus of one elastic material by the presence of spherical inclusions of another.

The increase in viscosity due to the interaction between regions of disturbance in the flow around the particles has not been considered in deriving IV.87. To allow for this effect, it will be assumed that Happel's interaction factor for rigid spheres is also valid for non-rigid particles. Inserting this into IV.87 results in the following equation

$$\mu_m = \mu'[1 + 5\Phi C_v(R - 1)/(2R + 3)] \quad ...(IV.88)$$

Figure 40 Graphs of equation IV.89, showing the variation in viscosity ratio with particle concentration.

R_m - viscosity ratio between the individual particle and the particle-matrix system.

C_v - volume concentration of the particles in the system

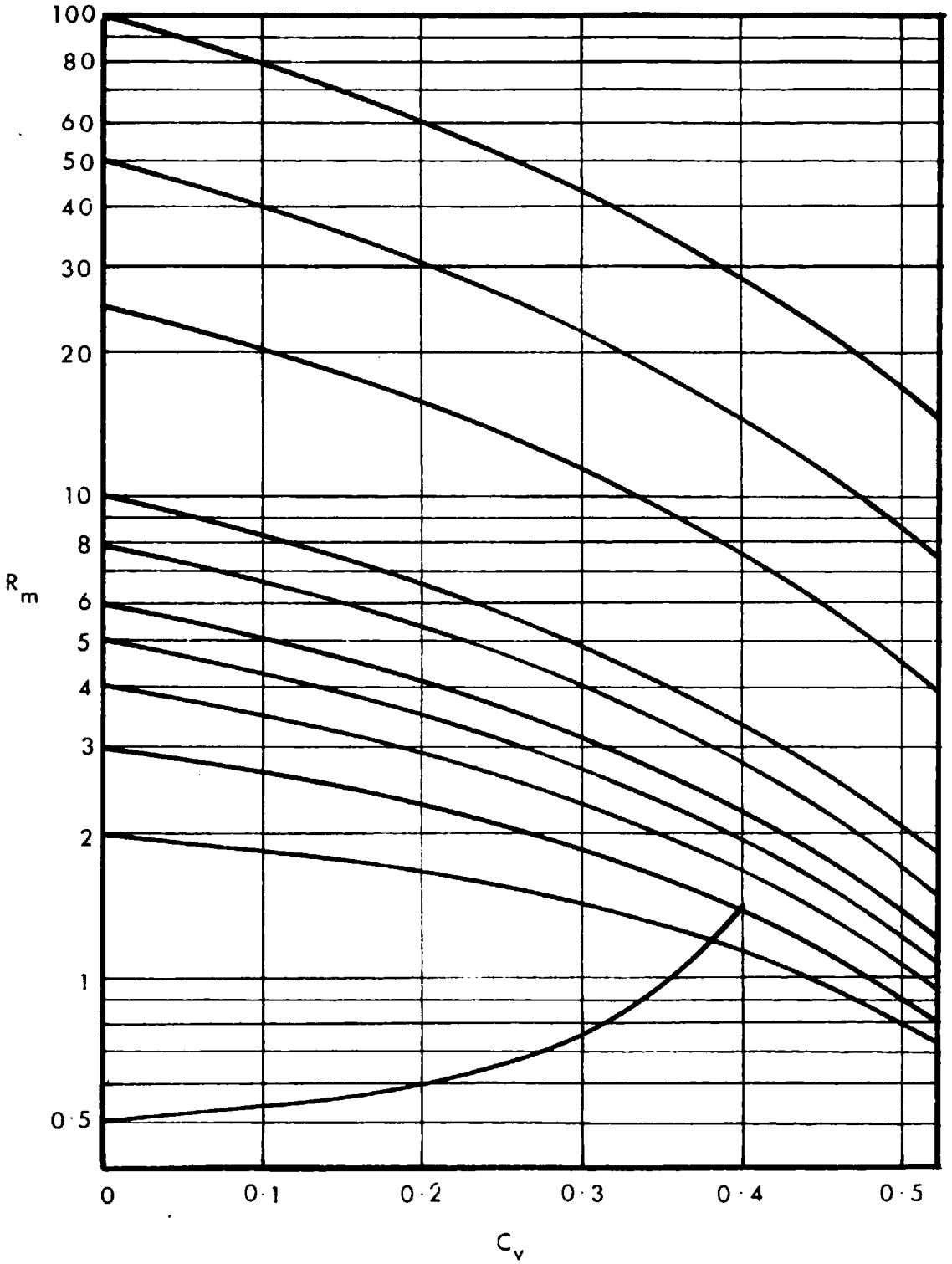
100
80
60
50
40
30
20
10
8
6
5
4
3
2
1
0·5
R_m
0
0·1
0·2
0·3
0·4
0·5
C_v

which gives the viscosity of the particle-matrix system.

In calculating the deformation of the individual particles, it is the viscosity ratio

$$R_m = \mu/\mu_m$$

which is the controlling factor. To obtain R_m, IV.88 can be modified to

$$R_m = R/[1 + 5\Phi C_v(R - 1)/(2R + 3)] \quad ...(IV.89)$$

from which it appears that R_m is always less than R, if $R > 1$, and it decreases with increasing Φ and C_v.

The decrease in R_m with increasing particle concentration is well shown in figure 40, in which equation IV.89 is plotted graphically for different initial values of R_m. To calculate these graphs, the numerical values of Φ at different concentrations C_v, as tabulated by Happel (1957, table I. Note that Happel uses the symbol ψ for Φ) were used. Concentrations greater than $C_v = 0.5$ were not considered because above this level friction effects due to interparticle contacts become large and the resistance to shear very much greater than predicted; i.e. R_m is greatly decreased.

From the graphs in figure 40, several conclusions can be drawn. First, it is obvious that significant reductions in the viscosity ratio, controlling deformation of the individual particles, can be achieved by increasing the particle concentration. In this way, it is apparently possible for R_m to become less than 1; i.e. a particle-matrix system can have a viscosity greater than the particles alone, because of the interaction between the disturbed regions of flow around the particles. If R is initially less than 1, R_m increases in value with C_v and may become greater than 1. However, for such values of R, there is a concentration for which R_m becomes negative, according to equation IV.89. This shows that the equation does not hold realistically over a wide range of values.

Figure 41 The effect of increasing volume concentration on particle deformation.

A) Theoretical deformation paths for initially circular particles deforming during simple shear.

Experimental points 1 to 6 give the mean particle axial ratio (a/b) and orientation (φ) after 1 γ_s shear, for different particle volume concentrations (C_v). The data for each point is listed in table XII, Appendix I.

The zone of experimental error is indicated by the dashed curves parallel to the $\gamma_s = 1$ contour; the assumed errors are ± 0.5 mm in the axial lengths and $\pm 3^o$ in the orientation.

B) Theoretical and experimental variation of viscosity ratio, R_m, and particle concentration, C_v. The solid curves are calculated from equation IV.89; the dashed curve is the experimental one. Points 1 to 6 relate the value of R_m to C_v. R_m was determined from figure A, by extrapolating from points 1 to 6 onto the $\gamma_s = 1$ curve.

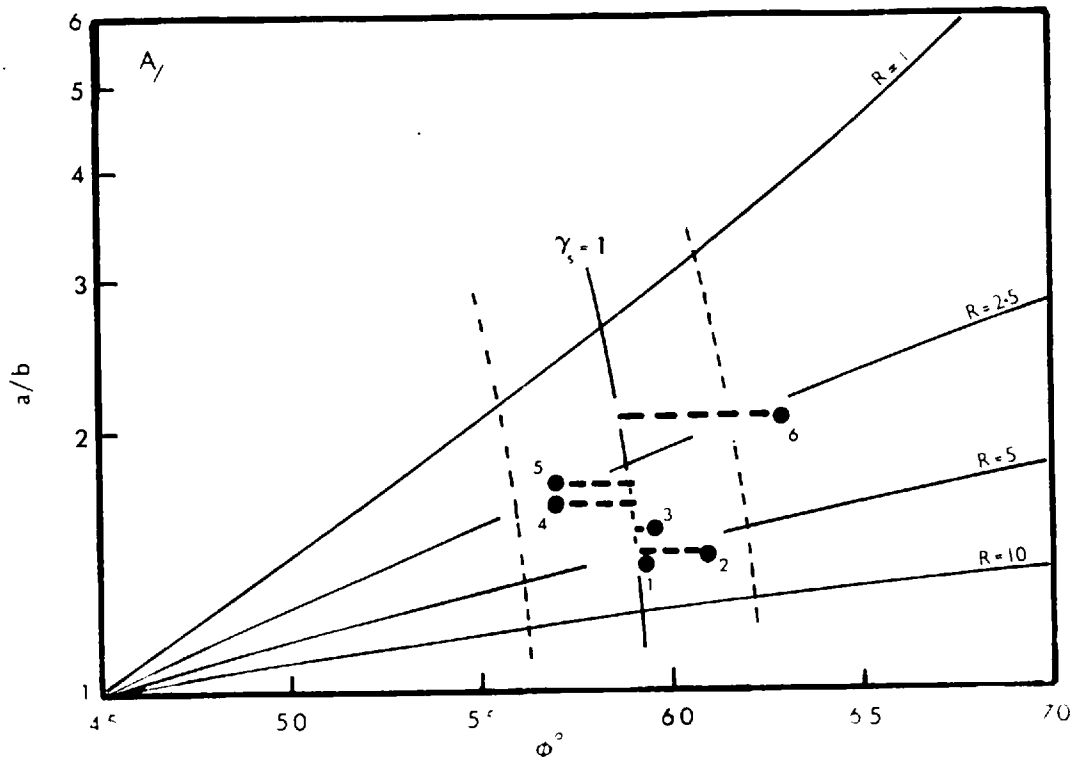
A/
a/b
R = 1
R = 2·5
R = 5
R = 10
$\gamma_s = 1$
1
2
3
4
5
6
50
60
70
Φ°

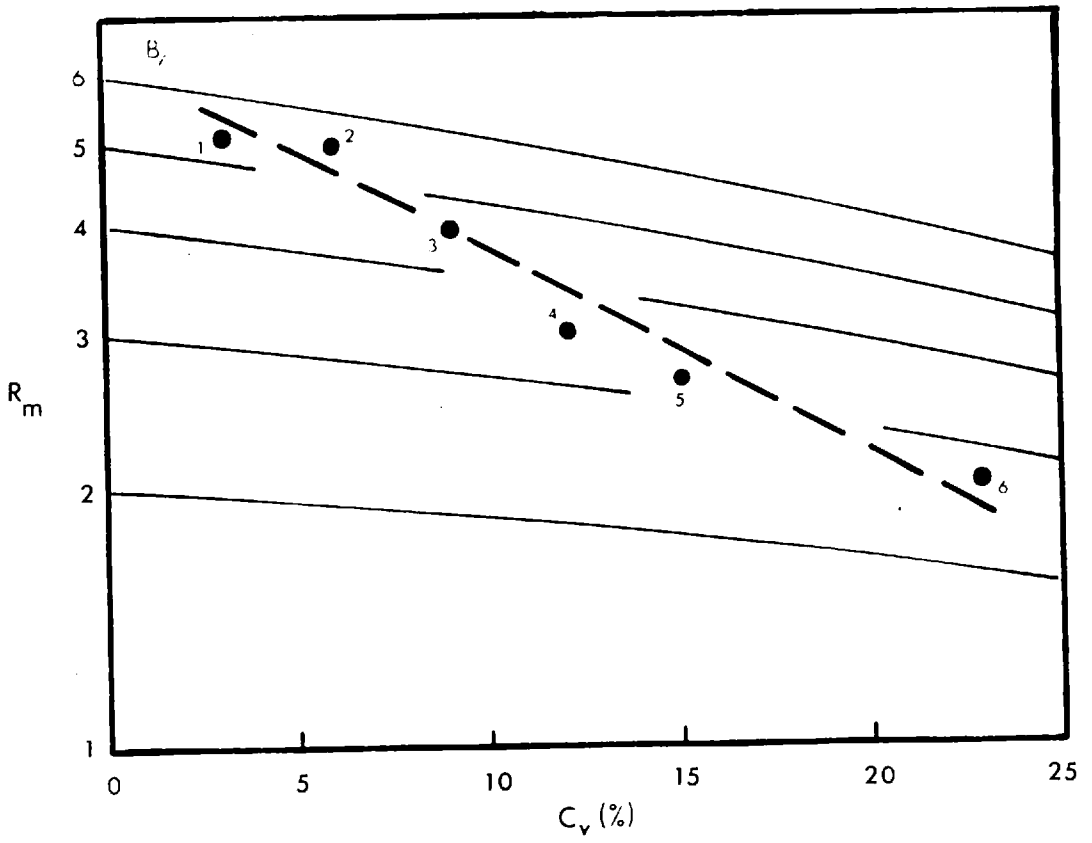
B/
R_m
1
2
3
4
5
6
0
5
10
15
20
25
C_v (%)

iv) Experiments to observe the effect of increasing concentration on particle deformation

A series of experiments were carried out in the simple shear box to observe the increase in particle deformation with increasing concentration and, in particular, to check equation IV.89. The particle-matrix systems used had a viscosity ratio of R = 5 at C_v = 0 and the concentration range covered was 3 to 23 per cent.

From photographs of the deformed particles, a mean axial ratio and orientation of the major axis was determined at each concentration. These were then plotted on the theoretical deformation paths for particles deforming during simple shear (figure 41A). It is clear from this graph that there is a significant increase in the particle axial ratio with increasing concentration. The change in angle of orientation is very erratic but allowing for the large range in measured values and the experimental error, ϕ appears to remain relatively constant.

To find the value of R_m at each concentration, the experimental points are extrapolated back to the γ_s = 1 contour. Then, the value of the viscosity ratio at these points is R_m for the particular concentration. These values of R_m and C_v are plotted in figure 41B for comparison with the theoretical curves. The results show that the experimentally determined values of R_m decrease much more rapidly, with increasing concentration, than expected.

It is not surprizing that there is this discrepancy between the experiment and the theory. The discussion on equation IV.90 showed that it was unrealistic over large ranges of R. Moreover, Happel (1957) suggested the interaction factor Φ to explain the viscosity of suspensions of rigid spheres. The particles in the present experiments are non-rigid and become elliptical during the deformation and so

it is quite probable that the boundary conditions used to obtain Φ may no longer hold. However, both the theoretical curves and the experimental results emphasize that the viscosity ratio decreases rapidly with increasing volume concentration of the particles. This is important when estimating the deformation of systems containing a large number of particles. Furthermore, it is suggested that the curves in figure 40 can be used to estimate R_m, if C_v is known, provided that it is realized that this value of R_m may be too high.

H. STRAINS DEVELOPED IN THE MATRIX AROUND A SINGLE PARTICLE DURING DEFORMATION BY PURE OR SIMPLE SHEAR

(a) Introduction

In this section, the variations in strain throughout the matrix, during the deformation of a particle-matrix system, are considered. It is obvious that since a particle causes a region of disturbance to be set up in the uniform flow field, the deformation in the matrix immediately surrounding the particle will be different from that experienced by material outside the region of disturbance. However, it is very difficult to calculate theoretically this variation in the strain. Considering a pure shear, for example, one would have to solve equations IV.56 for the fluid velocities outside the particle for different values of x and y. Hence, the stream lines around the particle could be constructed and from these the required strains could be obtained.

An easier method than this is to calculate the strains experimentally from the distortion of rectangular grids, stamped onto the surface of the matrix. This is the approach adopted here and the results obtained are described in the following subsection. Moreover, from the initial and final shape of a grid, the displacement vectors of the matrix during the deformation can be constructed. These are important because they reflect the type of deformation which has occurred. They are also discussed in the following section.

Figure 42 The major and minor semi-axes of the local strain ellipses, developed around a rigid disc of diameter 2.5 cm, during 0.5 γ_s simple shear.

$\sqrt{\lambda_1}, \sqrt{\lambda_2}$ - major and minor semi-axes of the strain ellipse for the simple shear deformation.

The magnitude and orientation of the local strain axes were determined from the distortion at each point of a rectangular grid, using the Mohr construction.

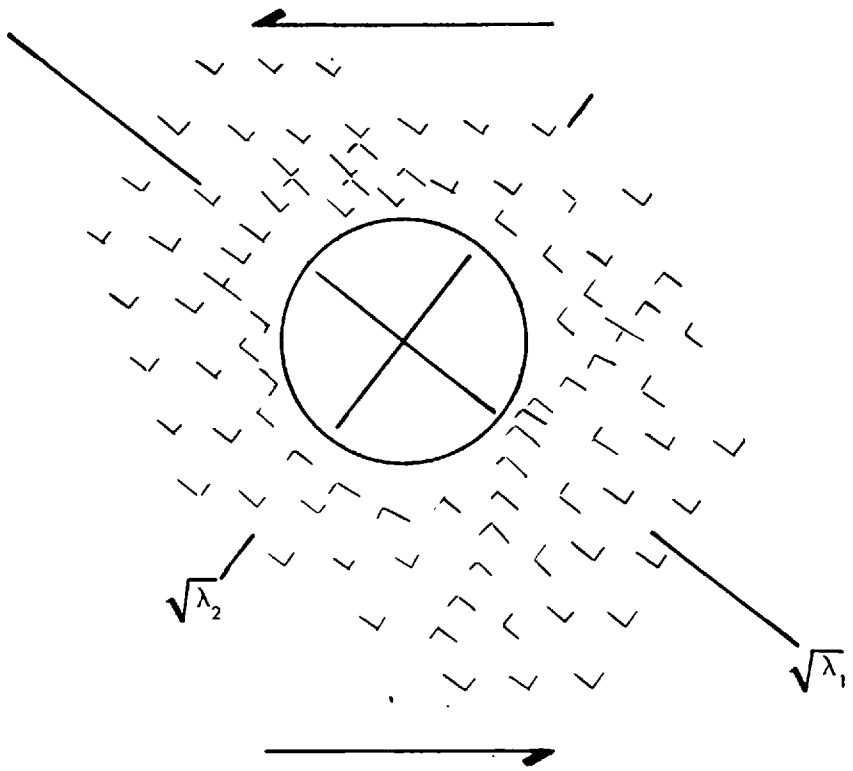
$\sqrt{\lambda_2}$
$\sqrt{\lambda_1}$

(b) Strains and movement directions in the matrix

The strains in the matrix were determined from a distorted rectangular grid by using the Mohr construction (see Brace, 1961). At each point on the grid, the changes in the right angle and the initial lengths of the lines were measured. These observations were then used to construct a Mohr circle, from which could be determined the orientation and magnitude of the maximum and minimum principal strains at the point. The method is tedious and time-consuming and the calculations have only been carried out completely for the strains developed around a rigid disc, during 0.5 γ_s simple shear. The resultant diagram is illustrated in figure 42.

Examination of this figure shows that the strain due to the presence of the particle is greatest in the matrix immediately surrounding it, and that this zone of disturbance extends for a distance approximately equal to the radius of the disc. Within this zone, the axial ratios of the local strain ellipses are generally greater than those elsewhere in the matrix. Moreover, the principal strain axes are deflected from the mean orientation towards a line, which passes through the centre of the disc and is parallel to the major principal axis of the strain ellipse for the simple shear. However, apart from these observations, it does not appear that the disc has significantly affected the strain in the matrix.

Diagrams showing the movement of the matrix, during deformation of the particle-matrix system, are in many ways more meaningful than those showing the actual strains around the particle. These diagrams are easily constructed by joining the initial and final positions of all points on the rectangular grid. They, therefore, show the direction and magnitude of the movement in the matrix.

In figures 43 and 44, several such movement diagrams are

Figure 43 The displacements in the matrix around a particle during a pure shear transformation in the irrotational strain box.

The diagrams on the left are of the distorted rectangular grids; those on the right show the displacement vectors obtained from the initial and final positions of all points on the grids. The dotted ends of the vectors are the initial positions.

All diagrams are for the same amount of strain, namely $\sqrt{\lambda_1/\lambda_2} = 2.60$

The viscosity ratios are as follows:

A, B - R = 2.5; C, D - R = 5;

E, F - R = 10; G, H - rigid disc;

I, J - rigid 2 : 1 ellipse.

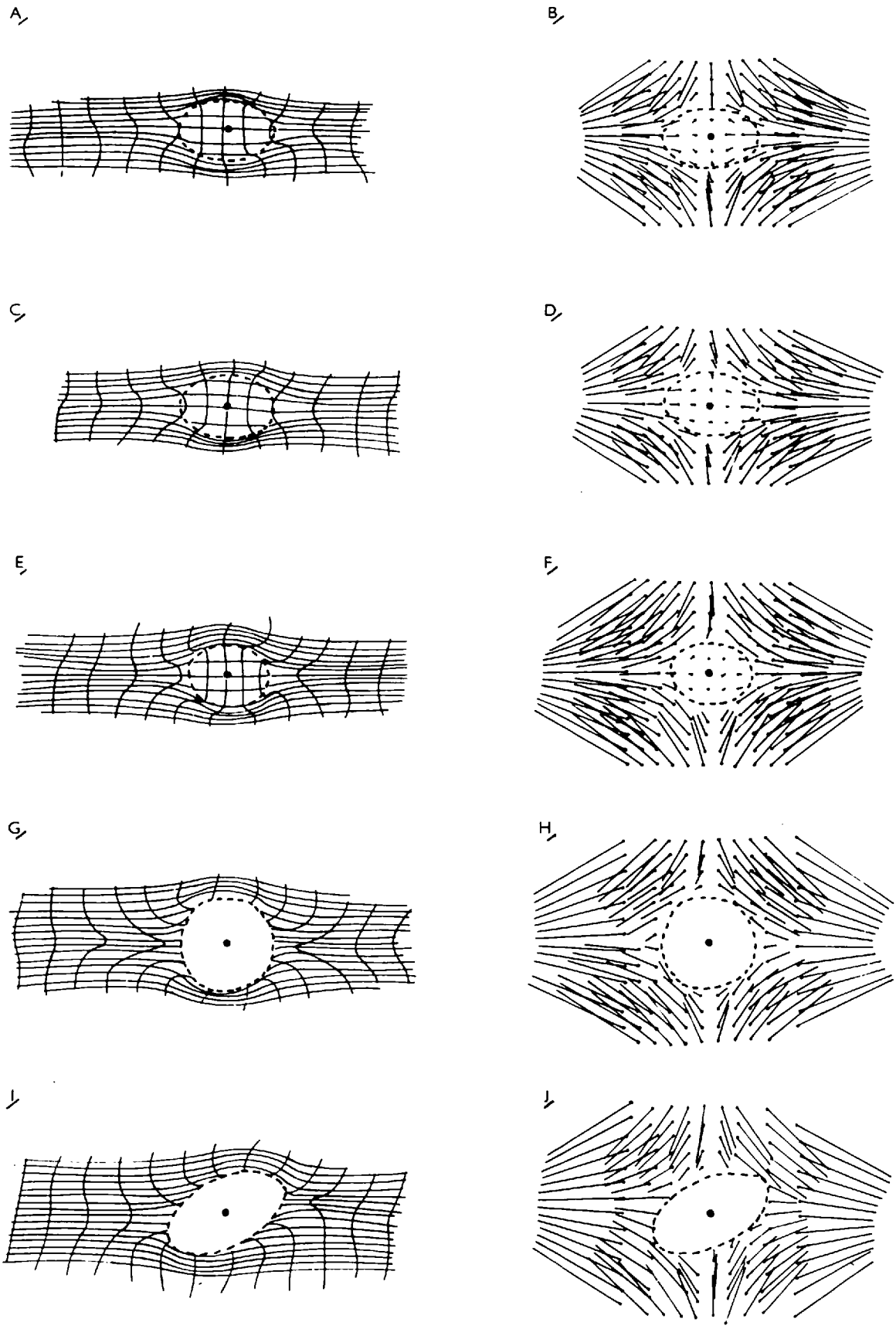
A
B
C
D
E
F
G
H
I
J

shown, together with the distorted grids from which they were constructed. These figures clearly illustrate the hyperbolic and laminar flow fields for pure and simple shear, respectively. Moreover, it appears that the distortion in the flow field around the particle depends on the viscosity ratio. For particles with R = 2.5, the disturbance in the flow is slight and dies out very rapidly. However, with increasing R, the distortion in the movement vectors increases and is quite marked for the rigid particles. The areal extent of the region of disturbance appears to depend, in part, on the type of deformation. In simple shear, the disturbance dies out quickly and has generally disappeared within a distance equal to one particle radius. However, the distorted grids around the particles in the irrotational strain box, suggest that the disturbance affects a much greater area in this type of deformation. For example, the distortion extends along the direction of elongation for at least a distance equal to the length of the major axis of the particle.

It is possible that the distortion of the matrix around the particle could be used to estimate the viscosity ratio between the particle and the matrix. Flow or movement lines around the particles with the same order of viscosity as the matrix, should only be slightly refracted. Around the more viscous particles, however, the refraction should be more marked. In this way, an estimate of the value of R can be made.

Figure 44 The displacements in the matrix around a particle during simple shear.

The diagrams on the left illustrate the distorted rectangular grids; those on the right show the displacement vectors obtained from the initial and final positions of all points on the grids. The dotted ends of the vectors are the initial positions.

The viscosity ratios between each particle and the matrix, and the amount of deformation are as follows:

A, B - R = 2.5, 1 γ_s shear.
C, D - R = 5, 1 γ_s shear.
E, F - R = 10, 1 γ_s shear.
G, H - rigid disc, 0.5 γ_s shear.
I, J - rigid 2 : 1 ellipse, 0.5 γ_s shear.

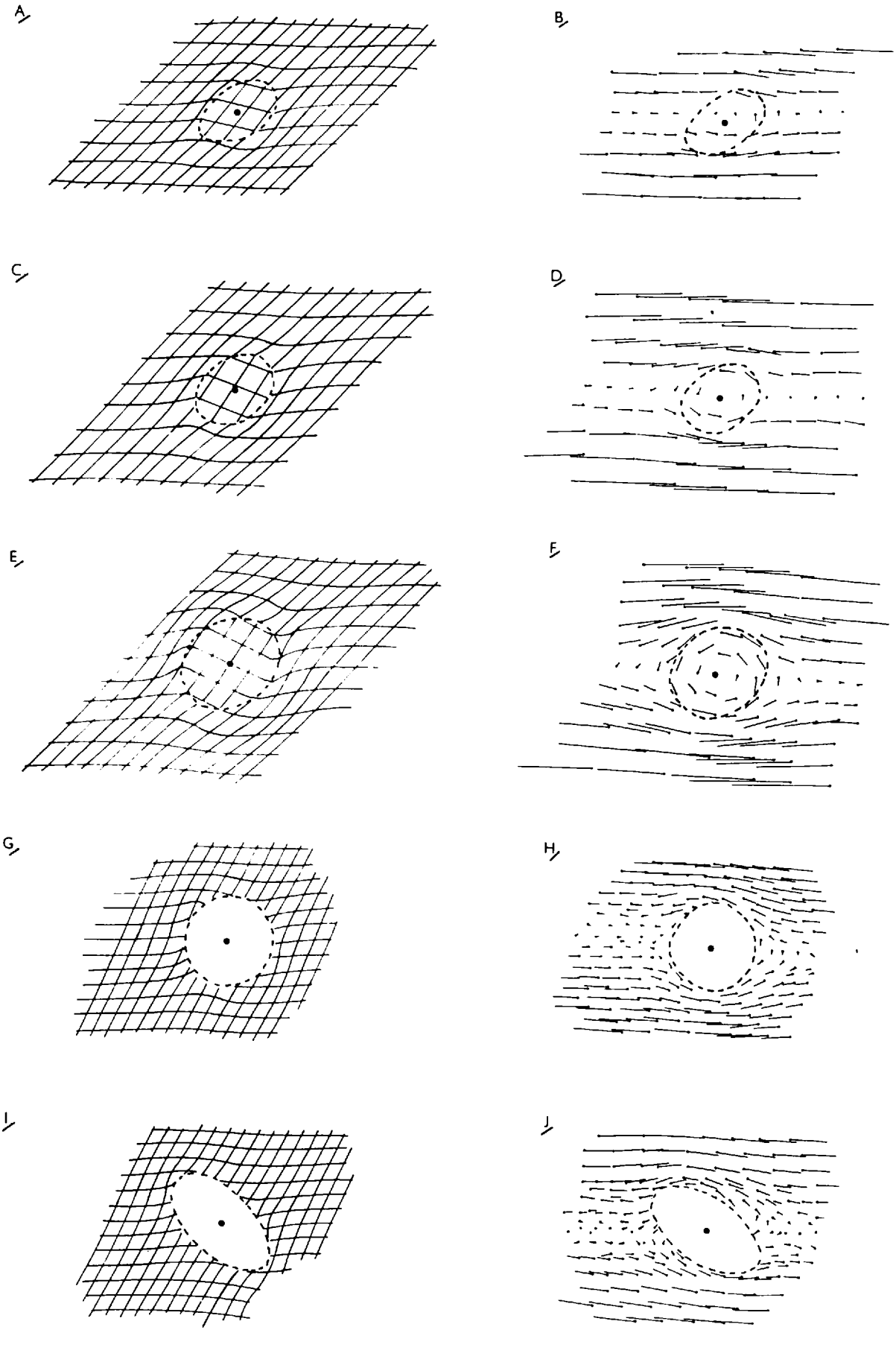
A
B
C
D
E
F
G
H
I
J

CHAPTER V GEOLOGICAL APPLICATIONS

A. ROTATED CRYSTALS AS QUANTITATIVE STRAIN INDICATORS

(a) Isolated crystals

i) Previous work

Rotated crystals of minerals such as garnet, albite, kyanite, staurolite, chloritoid and magnetite have often been used as criteria for shearing movements along suitable surfaces such as schistosity, cleavage and bedding planes. Rotation may be indicated by distortion of the material around the crystal or by helicitic structures within the grains. These latter structures may be planar, indicating crystal growth prior to the shearing, or curved in a spiral form suggesting that growth and movement were contemporaneous. The spiral forms have been described as "snowball" or "pin-wheel" structures in the literature (e.g. Flett, 1912, p. 111; Knopff and Ingerson, 1938, p.35).

The first person, known to the present writer, to use rotated porphyroblasts for determining quantitative amounts of slip or shear strain in a rock was Schmidt (1918) who suggested the simple model of a sphere rotating between two rigid planes, as in figure 45. According to this model, the amount of shear is related to the angle of rotation by the equation

$$\gamma_s = \phi \text{ radians} \quad \ldots \text{ (V.I)}$$

Becke (1924), Mugge (1930) and in recent years Osberg (1952 p.93) and Zwart (1960, 1963) are among the many workers who have used this formula. The equation provides only a minimum value for the amount of simple shear and allowances have to be made for factors such as slipping between the particle and the boards, which may retard the rotation. Zwart (1963, p.345) for example, found the maximum angle of rotation of porphyroblasts in a series of Pyrenean schists to be 90°, indicating a shear of approximately 1.6 units. To this amount he added 2 units to allow for what he termed the breaking effect of frictional drag and a further 2 units to

Figure 45 The model of a sphere between two rigid planes, suggested by Schmidt (1918) to determine quantitative amounts of shear from rotated porphyroblasts. (After Spry, 1963)

A) Initial position; the circle has unit radius.

B) Final position, after the top plane has moved to the left and the bottom plane to the right and the sphere has rotated through an an angle of $\varphi = \gamma_s/2$ radians. The total slip between the points a and b is 2φ; the planes are two units apart. Therefore, the amount of simple shear is

$$\gamma_s = \tan \delta = \varphi$$

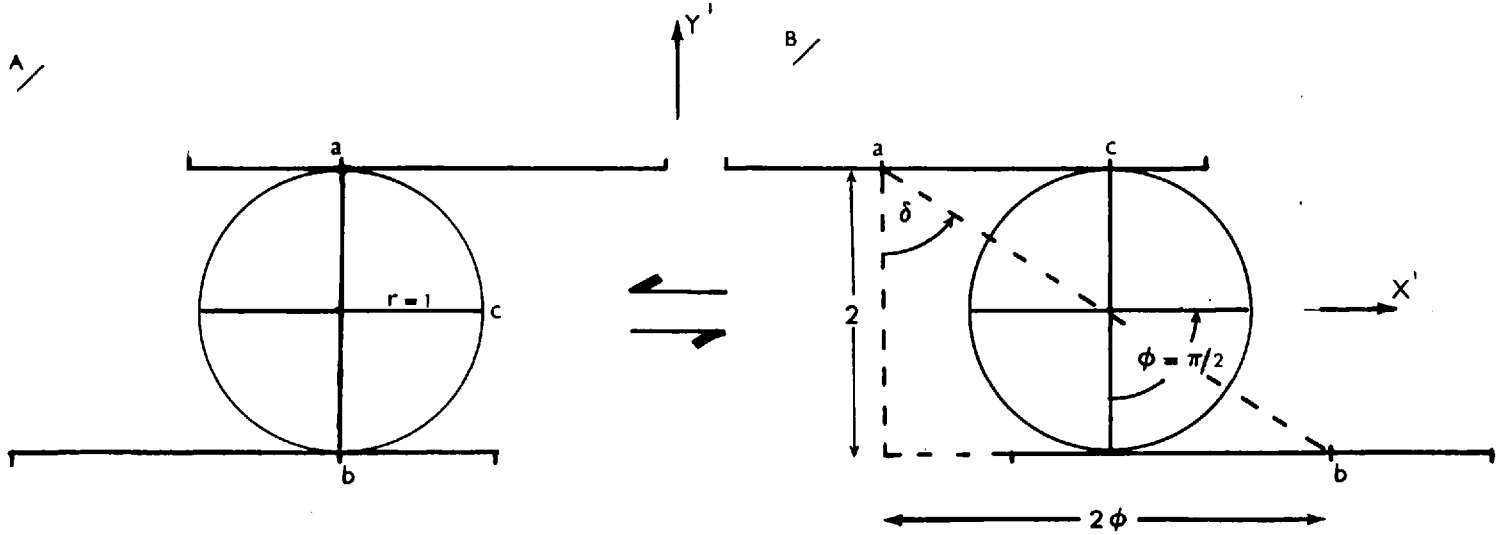
A
B
Y'
X'
a
b
c
r = 1
a
c
δ
2
φ = π/2
b
2φ

compensate for the retardation due to flattening. Therefore, the total shearing strain was found to be roughly γ_s = 6.

Nobody, so far as the writer is aware, has allowed for the effect of eccentricity of the crystal shape in making quantitative calculations of strain. Obviously, when using crystals of minerals such as garnet, which may approximate to a sphere, the shape factor is unimportant. However, Zwart (1960, p.178) in discussing orientations of andalusite, staurolite and cordierite porphyroblasts, notes that round or square crystals are rotated more than those which are elliptical in shape and highly elongate ones show no rotation at all.

Spry (1963) reviews most of the work dealing with rotated porphyroblasts and suggests that instead of the Schmidt formula, a more accurate method for calculating the shear strain from "snowball" garnets is to measure the visible length of the spiral path formed by the inclusions in the crystals. The shearing causing the rotation is approximately 30 per cent greater than this length. The method is supposed to give a value for γ_s almost twice as large as that obtained from the Schmidt equation. However, in comparing the two methods, Spry (1963, table on p.220) has miscalculated by a factor of two, the shear according to equation V.I and by correcting this it is found that the Schmidt model gives a slightly greater value for the shear than does the spiral length.

An explanation for the occurrence of equidimensional porphyroblasts which have apparently been rotated in a pure shear flattening field was suggested by Ramsay (1962, pp.322-324). Because the particles are circular in shape, they must remain stationary during this type of deformation but any external planar features not parallel to either of the strain axes rotate passively, thus causing the angular difference between the internal helicitic trails and the external schistosity.

Plate III Photomicrograph of two rotated garnet porphyroblasts (x 15)

(Reproduced by permission of Mr. Tom Sibbald.)

a) Diagram to show the method of measuring the angle of rotation between the innermost portion of the snowball trails (S_i) and the mean direction of the external schistosity (S_e).

A/

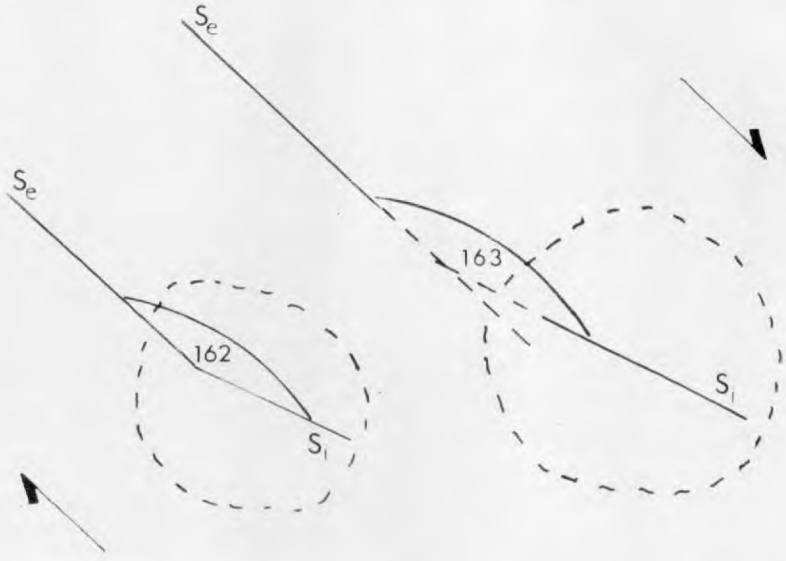

The angular rotation is determined by Wettstein's (1886, p.33) formula

$$\tan \varphi_f = \tan \varphi_i \sqrt{\lambda_1/\lambda_2} \quad ....(V.2)$$

Note that rotations of more than 90^o cannot be obtained in this way.

ii) The suggested viscous model

The model proposed in this thesis, namely rigid particles embedded in a viscous fluid, is in the writer's opinion a more realistic one than those discussed above and removes to a great extent the need for arbitrary guesswork about retarding forces. In a simple shear deformation, the necessary equations to calculate the amounts of strain are

$$\tan \varphi = (a/b)\tan[ab\gamma_s/(a^2 + b^2)] \quad ....(IV.18)$$

for elliptical particles and

$$\gamma_s = 2\varphi \quad ....(IV.9)$$

for circular ones. Equation IV.9 is similar to the Schmidt formula but gives twice the value of γ_s for a specific rotation φ.

The equation for describing the particle rotation in a pure shear field is

$$\ln \cot \varphi_f = \ln \cot \varphi_i + [(a^2 + b^2)/(a^2 + b^2)] \cdot \ln \sqrt{\lambda_2/\lambda_1} \quad ...(IV.29)$$

Note that rotation cannot exceed 90^o and that for circular particles the equation reduces to $\varphi_i = \varphi_f$, i.e. there is no rotation. External schistosity in the matrix also rotates during pure shear according to equation V.2.

Therefore, to calculate the amount of strain, the axial ratio of the crystal is measured and the angle between the internal and external schistosity planes or between the major axis of the particle and the external schistosity. These values are then substituted into one of the above equations,

Table V Quantitative estimates of the amount of simple shear in a rock, made from rotated crystals.

Reference	Porphyroblast	φ^{o}	A	B	C
Schmidt (1918)	Graphite	155	2.70	-	5.40
	Garnet	173	3.04	-	6.08
Osberg (1952)	Albite	90	1.57	-	3.14
Spry (1963)	Raglan garnet	144	2.50	2.20	5.00
	Schichallion garnet	144	2.50	2.44	5.00
Zwart (1963)	Andalusite, garnet, staurolite, etc.	90	6.00*	-	3.14

φ^{o} - angle of rotation measured between the internal and external schistosities, assuming that shearing has occurred along the schistosity planes.

A - shear calculated according to equation V.1 (Schmidt model).

B - shear calculated according to Spry's method of measuring the spiral length. The unit shear is then calculated by dividing the measured length by the diameter of the porphyroblast.

C - shear calculated according to equation IV.9 (viscous model).

* - includes allowances for retarding forces.

depending upon the type of deformation, and the strain is calculated.

To illustrate the technique, consider the two garnet crystals shown in plate III. The garnets contain curved inclusion trails indicating that they have grown during rotation. The crystals are approximately circular and the angle between the innermost portion of the trail and the mean direction of the external schistosity is 162^{o}. Because this is greater than 90^{o}, the rock has probably experienced a simple shear deformation. Therefore, from equation IV.9, the amount of simple shear is $\gamma_s = 5.6$.

The data of other workers has been recalculated in a similar manner and the results are listed, together with the original estimates, in table V.

iii) Use of a large number of crystals

Obviously, when working in the field, as much data as possible should be obtained about the rotations of individual crystals together with their relative positions to each other and in the host rock as a whole. In this way it should be possible to obtain a picture of the general movement pattern during the deformation.

Zwart (1963) examined schists ranging from Cambro - Ordovician to Lower Devonian in age from the Central Pyrenees and measured 300 rotated crystals in samples covering the whole area. The maximum rotation was 90^{o}; smaller angles than this were attributed to the elliptical shape of the crystals but were not used in the calculations. Zwart concluded that the rocks had been sheared by an amount of $6\ \gamma_s$ but probably much more information about the shearing movements could have been obtained by considering all the measurements together with particle shapes and positions.

Figure 46 A minor fold from the Stgir Schists, Switzerland, containing garnet porphyroblasts (Numbers 1 - 9) which have an internal schistosity not parallel to the external schistosity.

Scale - actual size.

(Reproduced from Chadwick, 1965, fig. 59, by permission of Dr. Brian Chadwick.)

a, b) Graphs showing the variation of thicknesses T and t for the lithological units I and II, around the fold. T is measured parallel to the axial plane; t is measured perpendicular to the layering.

A.P. - axial plane.

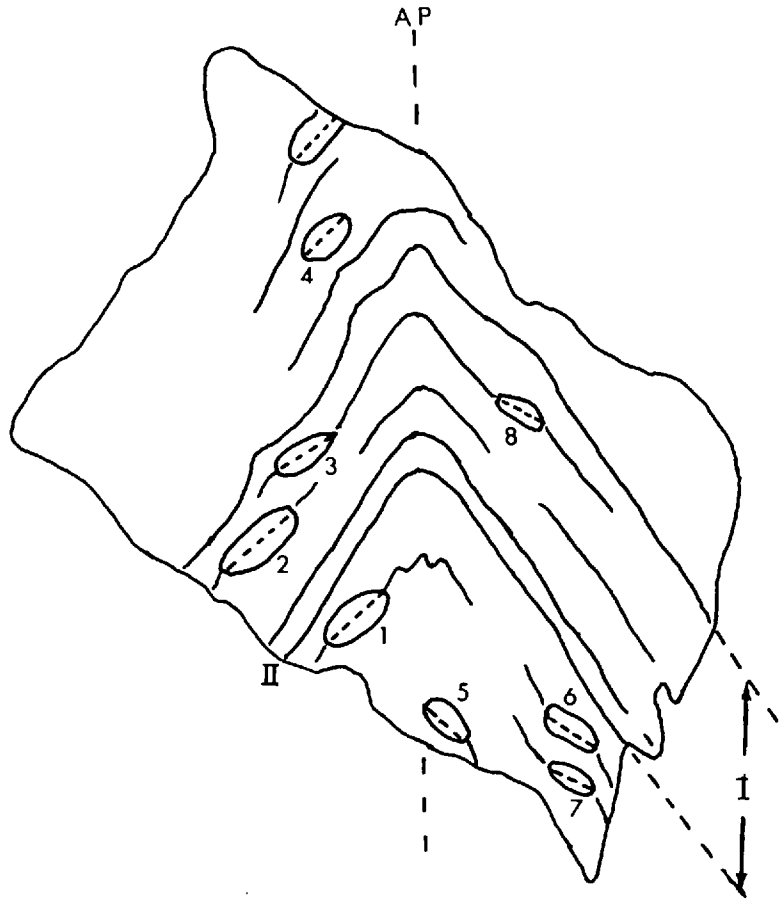
AP
4
3
2
1
8
II
5
6
7
I

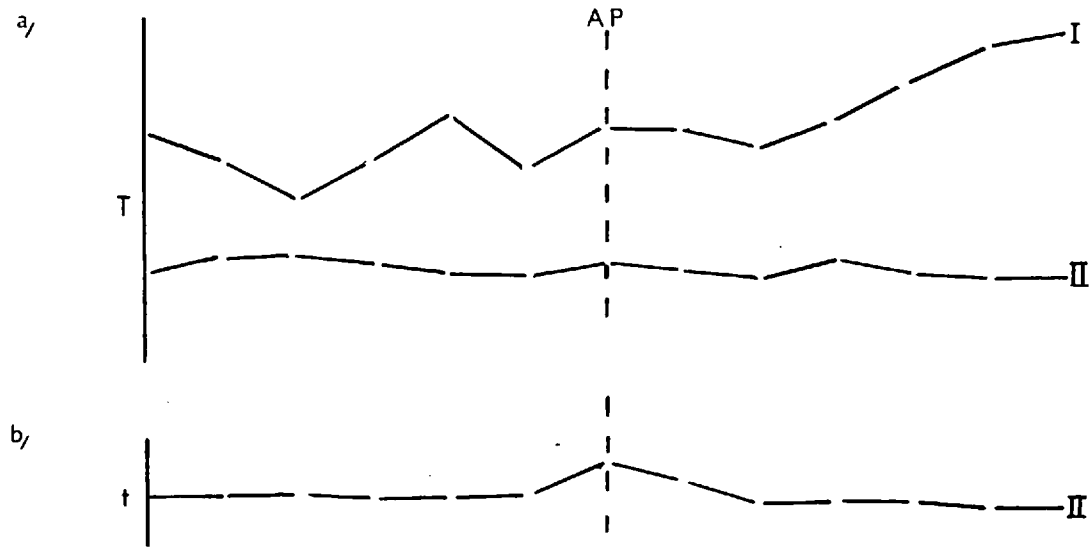
a/
AP
I
T
II
b/
t
II

(b) The variation in rotation of crystals about a fold

The differences in rotation experienced by crystals distributed around some geological structures is readily understood when considering folding. Moreover, the sense of rotation can help to decipher the folding mechanism and the amount of rotation can give a quantitative estimate of the strains involved.

Again, it is Zwart who has done most work in this field. In his 1960 paper (pp. 178-179), he uses the sense and amount of rotation to deduce two types of deformation in the rocks he was discussing: early shear folding followed by later concentric folding. In a very recent paper, Zwart and Oele, (1966) describe magnetite crystals rotated about axes parallel to the fold axis and use them to interpret the type of deformation in an over-turned anticline in the Rocroi massif. The argument is vague but from the sense of rotation, which appears to be connected with shearing movements along cleavage planes developed in the phyllitic rocks during compression, it is concluded that the folds are of a flattened flexure type. These results are also compared with a similar-type fold (described by Langheinrich, 1964) in which pyrite crystals are rotated in the opposite sense.

Instead of discussing the above examples in detail, the potential of using rotated crystals to analyze folding will be demonstrated using data taken from the fold represented in figure 46. This diagram shows the profile section of a minor fold from Stgir Schists, Lukmanier, Switzerland. The rock is a garnet schist and contains porphyroblasts which are unusual in that they are not equidimensional in shape but have axial ratios between 2 : 1 and 2.5 : 1. The schistosity trails enclosed in the crystals are planar, indicating pre-deformational growth under static conditions; they lie at different angles to the external schistosity but are parallel to the major axes of the crystals.

Figure 47 Diagrams to illustrate a similar fold mechanism for the formation of the fold in figure 46.

a) Initial position

b) A similar fold formed by shearing parallel to the axial plane.

φ - angle of orientation of the major axis of the crystal.

φ' - angle of dip on the limbs of the fold.

c) The variation in simple shear about the fold in figure 46, assuming that it was formed by a similar fold mechanism.

The numbers plotted next to each porphyroblast are the amount of γ_s as calculated from the present position of the crystal using equation IV.18. The maximum shear on the limbs is calculated from equation V.3. The relevant data required for the calculations are listed below.

Garnet	Axial ratio	φ^o	γ_s
1	2 : 1	39	0.96
2	2.4 : 1	40	0.96
3	2.5 : 1	32	0.71
4	2 : 1	45	1.15
5	2 : 1	43	1.09
6	2 : 1	36	0.87
7	2 : 1	30	0.70
8	2.3 : 1	30	0.67

Maximum γ_s from the dip of the limbs = 1.43
(Angle of dip = 55^o)

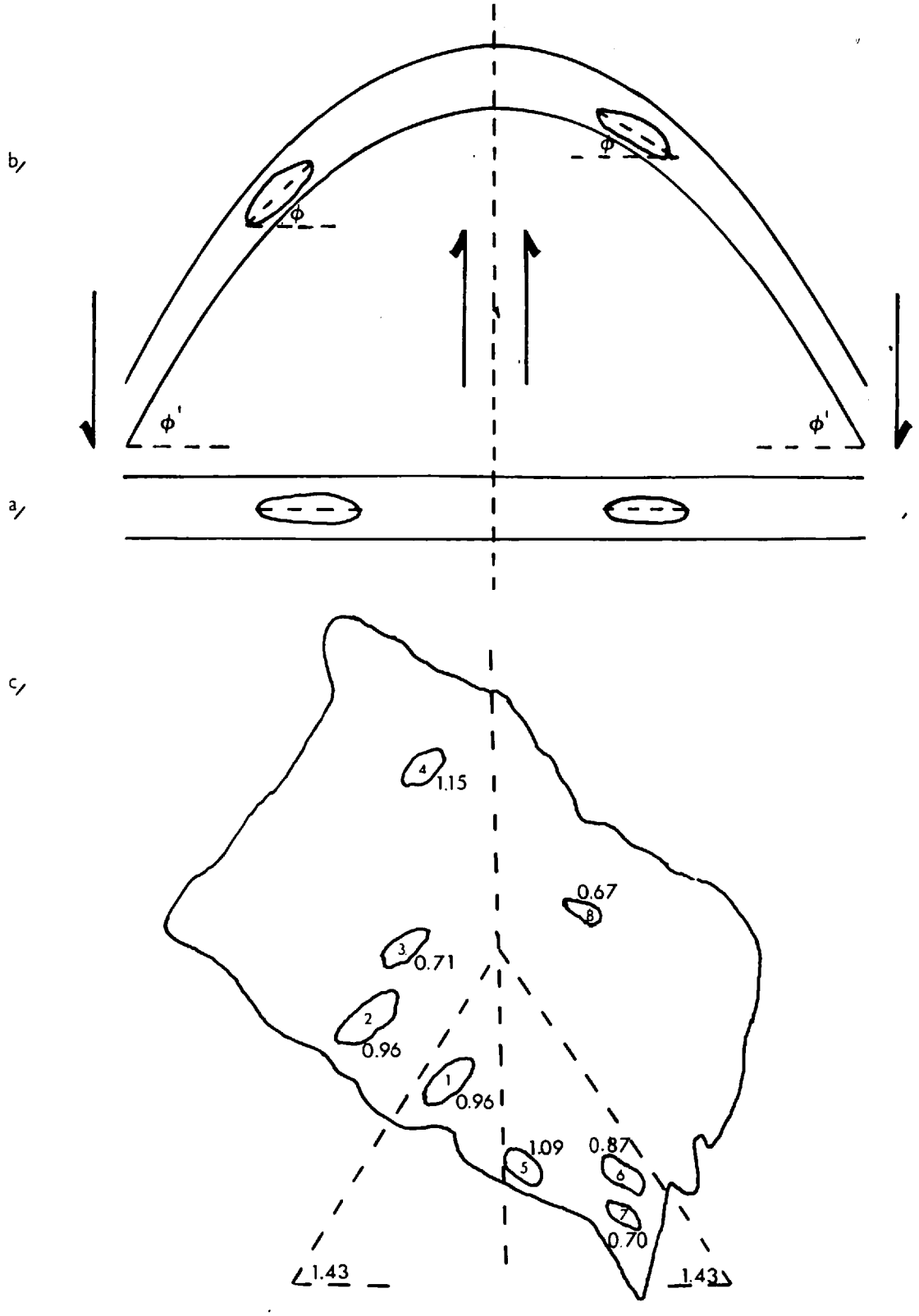
b/
a/
c/
ϕ
ϕ
ϕ'
ϕ'
4
1.15
0.67
8
3
0.71
2
0.96
1
0.96
1.09
5
0.87
6
7
0.70
1.43
1.43

To get an initial idea of the mechanics of formation of the fold, the conventional methods as described by Ramsay (1962) were used. These involve measuring thicknesses parallel to the axial plane (T) and perpendicular to the bedding plane (t) for different lithological units. Figures 46a, b show the change in these parameters about the fold. The thickness T is relatively constant along layer II but is distorted in layer I by the presence of the rigid crystals. The values for t are approximately constant except for a marked increase about the axial plane.

The constant value for T in layer II suggests that the fold may be of a similar-type, which agrees with the conclusions reached by Chadwick (1965, p. 129) for folds of this age in the Lukmanier region. However, the fact that t is much greater in the hinge of the fold than it is on the limbs indicates a flattened flexure type of fold (Ramsay, 1962, p. 316). The relative positions of the porphyroblasts around the fold can be used as follows to determine which of the folding mechanisms is more likely to have operated.

Consider first the possibility that the fold is a similar fold, formed by shearing parallel to the present axial plane and let the initial position be as in figure 47a. The bulk of the rock is assumed to be in a homogenous, viscous condition and the rigid crystals lie with their long axes parallel to the layering, which behaves passively during the deformation. To form the fold, differential shearing movements are applied symmetrically about the axial plane and at right angles to the layering, as in figure 47b. The position of any particle relative to the layering now gives a measure of the amount of shearing strain it has experienced. Ideally one would expect the maximum shear on the limbs of the fold and zero shear at the hinge. Hence, with reference to figure 47b, the dip on the flanks of the fold, φ', indicates the maximum shearing strain during the deformation. The value

of the maximum shear is given by the equation

$$\gamma_{s\ max} = \tan \varphi' \quad ...(V.3) \quad \text{(Nadai, 1950, p. 146)}$$

Using this model and assuming that the axes of rotation are parallel to the fold axis, the shear around each garnet has been calculated from equation IV.18. The results are plotted in figure 47c and there appears to be no systematic variation in the shear around the fold. Crystals in the hinge zone indicate values for γ_s similar to those on the limbs. Moreover, all the γ_s values calculated from the crystals are significantly less than the maximum shear indicated by the dip of the limbs. This almost certainly implies that the model of an ideal similar fold is not correct.

To analyze the fold in terms of the flattened flexure model, it is first necessary to determine the amount of flattening. This is done using the graphs published by Ramsay (1962, fig. 7). The thickness t is measured at a point on the fold, expressed as a fraction of the thickness in the hinge and plotted against the dip at the point of measurement. Only two such points could be obtained for the present fold because of its straight limbs. However, both these points fell on the graph for 50 per cent flattening.

The next step in the procedure is to unflatten the fold by this amount. This was carried out for the writer by Mr. F. Hudleston whose help is gratefully acknowledged. The resultant fold is shown in figure 48a. The limbs are still straight and dip at approximately 35°. During the unflattening, the porphyroblasts rotate and their new positions are calculated from IV.29 using the known values of φ_f and a strain ellipse axial ratio of 2 : 1. The new orientations are also plotted in figure 48a. It is clear that all the porphyroblasts now lie with their major axes dipping at a slightly lower angle than the bedding. They could have reached this position as a result of slip along the bedding planes during the initial folding.

Figure 48 a) The appearance of the fold in figure 46 after unflattening by an amount of 50 per cent.

The limbs now dip at 35^{o} and the new orientations of the porphyroblasts are as follows:

Garnet	φ^{o}	Garnet	φ^{o}
1	28	5	31
2	27	6	26
3	21	7	21
4	33	8	20

b) Diagram to illustrate the bedding plane slip along the straight-limbed section of the fold during the initial folding. γ_s is the amount of simple shear during the bedding plane slip

a/

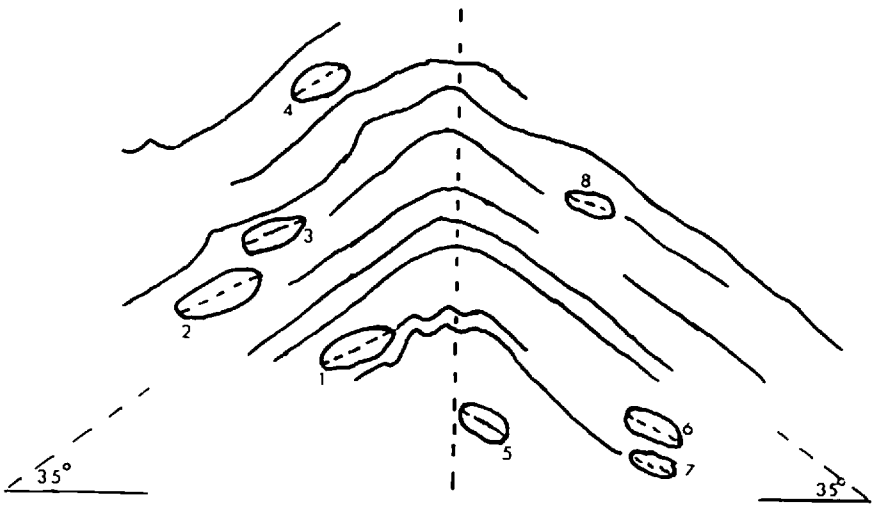

b/

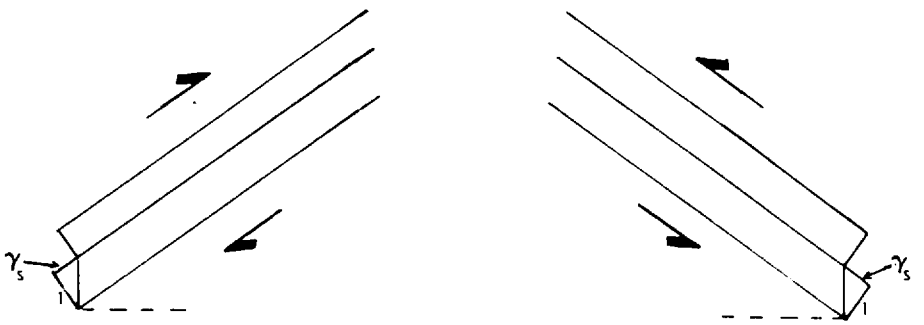

The amount of this slip along the straight portion of the limbs is given by the tangent of the angle of dip of the limbs (see fig. 48b) i.e. for the present fold $\gamma_s = 0.70$ along the limbs.

Because the fold consists mainly of the straight limbs, unfolding it so that the layers become horizontal involves applying a simple shear of this magnitude in the opposite sense to that shown in figure 48b. The porphyroblasts rotate during this shearing and their final orientations can be calculated from equation IV.18. The results are as follows :

Garnet	θ^o	Garnet	θ^o
1	+1	5	+5
2	-2	6	-1
3	-7.5	7	-5
4	+6	8	-7.5

The angle θ lies between the major axis of the porphyroblast and the layering. Positive angles are measured in an anti-clockwise sense; negative angles in a clockwise sense.

The calculations show that the porphyroblasts were oriented before folding with their major axes approximately parallel to, or at low angles to, the layering. It was previously mentioned that the internal schistosity was parallel to the major axis of the porphyroblasts. Therefore unflattening and unfolding has restored an approximate parallelism between the internal and external schistosities. This strongly suggests that the flattened flexure fold model is correct.

B. THE DEVELOPMENT OF PREFERRED ORIENTATIONS IN ROCKS

It was shown in the section on deformation of particle-matrix systems containing a large number of particles that during pure and simple shear deformations preferred orientations of the particle major axes would be set up. This is obviously of great importance in

the development of preferred orientations of porphyroblasts, pebbles and other particles in igneous and metamorphic rocks. Indeed, Jeffery's (1922) theory on the motion of ellipsoids has often been quoted as an explanation for the development of preferred orientations of minerals (e.g. Knopff and Ingerson, 1938, pp.135-136: Turner and Weiss, 1963, pp. 323-325) and recently there has appeared a paper by Bhattacharyya (1966) who uses Jeffery's equations and the experimental results of Mason and his co-workers (e.g. Mason and Bartok, 1959) to explain parallelism between mineral lineations and flow directions in rocks. Orientations of stones in till have been explained in a similar way by Glen, Donner and West (1957) who have also constructed a rose diagram for the long axes of 2 : 1 : 1 ellipsoids illustrating the stable preferred orientation parallel to the shearing direction.

However, so far as the present writer is aware, no one has attempted to correlate the degree of preferred orientation of the particles with the amount of finite strain, as Flinn (1962, pp. 399-400) has done for preferred orientations of lines and planes in a homogenous material. An attempt to do this is made in the following sections, using the equations previously derived to describe the behaviour of the particles. First, rigid ellipsoids are considered and the changes, during pure and simple shear, of initially random and regular distributions of plunges of particles are examined and related to the finite strain. Then, preferred orientations of non-rigid ellipses, developed during pure shear, are discussed and the changes in shape and orientation related to the strain.

(a) Rigid particles

The rigid particles are assumed to be 2 : 1 : 1 ellipsoids. The initial distributions of the plunges of the major axes of those particles with respect to the

Figure 49 Stereographic projections of the plunges of the major axes of 2 : 1 : 1 ellipsoids. (Lower hemisphere, Wulff net)

a) Random diagram, 100 points.

b) Regular diagram, 88 points.

φ - orientation between the particle major axis and the OY' axis, measured in the X'Y' deformation plane.

X', Y', Z' - strain axes.

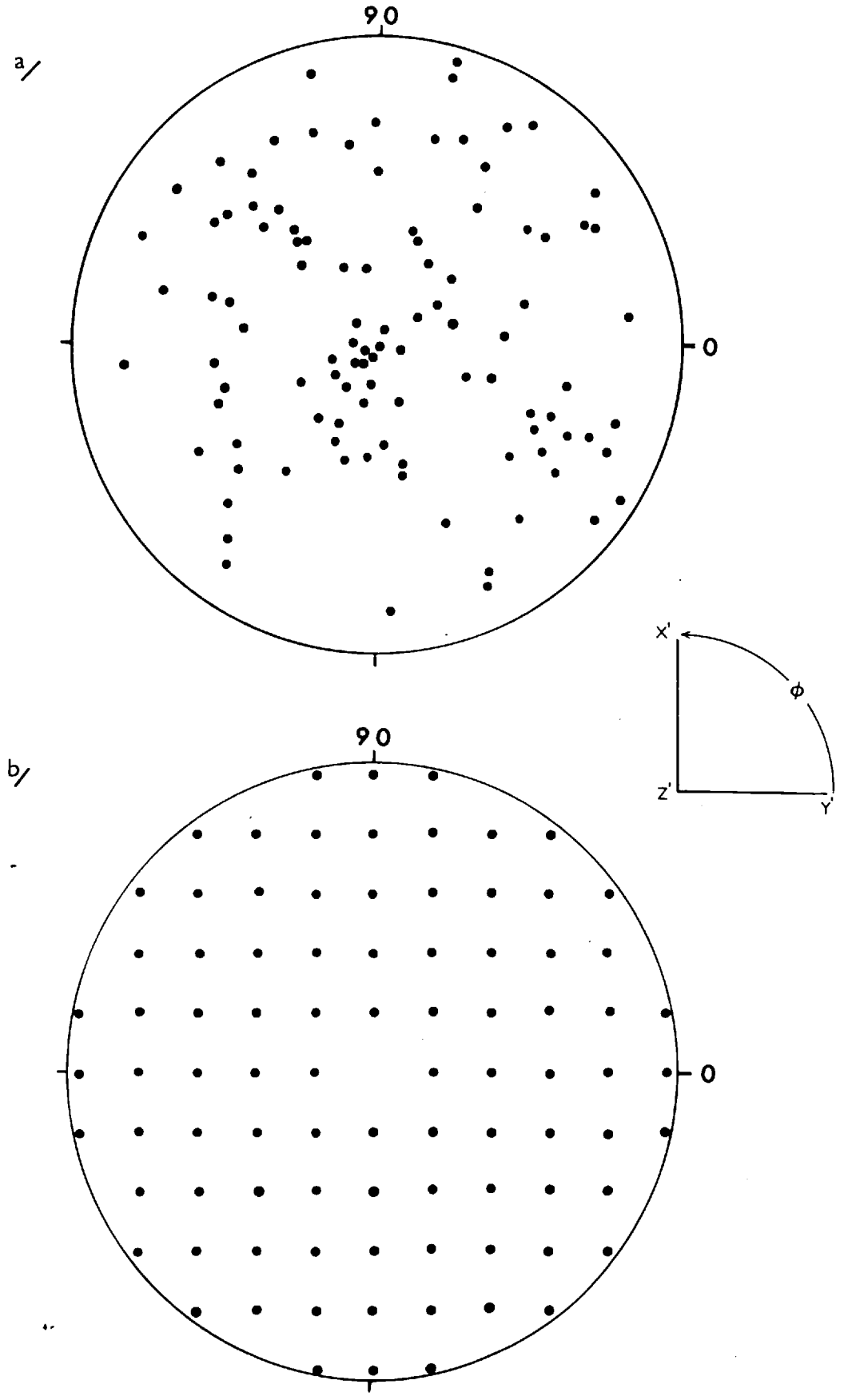
a/
90
0
X'
φ
Z'
Y'
b/
90
0

deformation planes are shown in figures 49a, b for randoms and regular orientations respectively.

The random diagram was constructed from tables of random numbers. The first number appearing in a column was taken as the plunge of the major axis and the second number as the direction of plunge. Numbers greater than 90 were ignored. In this way 25 random points were allocated to each quadrant of the stereonet. The diagram, so obtained, contained several areas of concentration of plunges; the most marked of these is about the Z' strain axis.

The regular diagram was prepared by placing the tracing paper over a piece of centimetre graph paper and selecting points at regular intervals. Consequently, there are no areas of concentration of plunges on this diagram.

The changes in the position of these points during deformation of the systems were calculated as follows. First, the axial ratio of the elliptical cross-section in the deformation plane was calculated for the particle from equation IV.39. Then, using this axial ratio, the change in orientation ψ during a definite amount of strain was calculated from either equation IV.18 or IV.36, depending upon the type of deformation. The change in plunge θ during the rotation was determined from equations IV.19 or IV.37. The axial ratio at this angle of plunge was then checked to see whether it had changed sufficiently to affect the amount of rotation significantly. If this did happen, the calculation was repeated for a smaller increment of strain. Normally, increments of $0.5\,\gamma_s$ or $0.5\,\bar{\varepsilon}$ were used. All the calculations could be done rapidly by reading off rotations from graphs such as those in figures 21, 22, 25, 26 and 27.

The effect of a simple shear deformation on the particle distributions is illustrated in figures 50a - 50f

Figure 50 Stereographic projections showing the changes in the initially random and regular distributions of plunges of particle major axes (figures 49a, b) during simple shear. The amounts of simple shear for each diagram are

a, b) $\gamma_s = 1$; c, d) $\gamma_s = 2$

e, f) $\gamma_s = 3$.

ϕ - angle of orientation between the particle major axis and the OY' axis.

X', Y', Z' - axes of simple shear.

(Lower hemisphere, Wulff net projections)

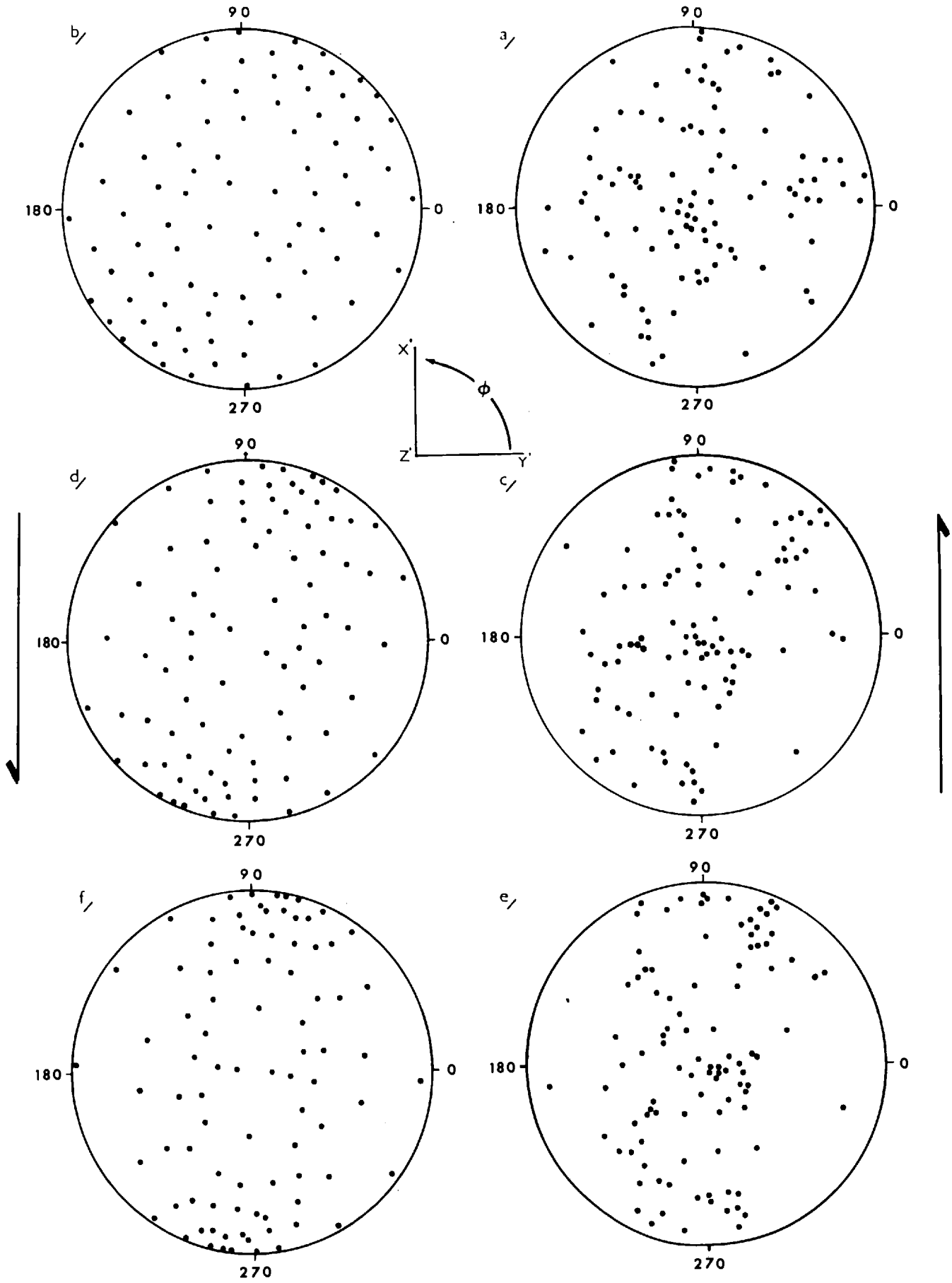
b/
90
180
0
270
a/
90
180
0
270
X'
Z'
Y'
ϕ
d/
90
180
0
270
c/
90
180
0
270
f/
90
180
0
270
e/
90
180
0
270

Figure 51 Stereographic projections showing the changes in the initially random and regular distributions of plunges of particle major axes (figures 49a, b) during pure shear. The axial ratios of the strain ellipses for each diagram are

a, b) $\sqrt{\lambda_1/\lambda_2} = 2.7$

c, d) $\sqrt{\lambda_1/\lambda_2} = 5.7$

e, f) $\sqrt{\lambda_1/\lambda_2} = 11.0$

φ - angle of orientation between the particle major axis and the OY' axis.

X', Y', Z' - axes of pure shear

(Lower hemisphere, Wulff net projections)

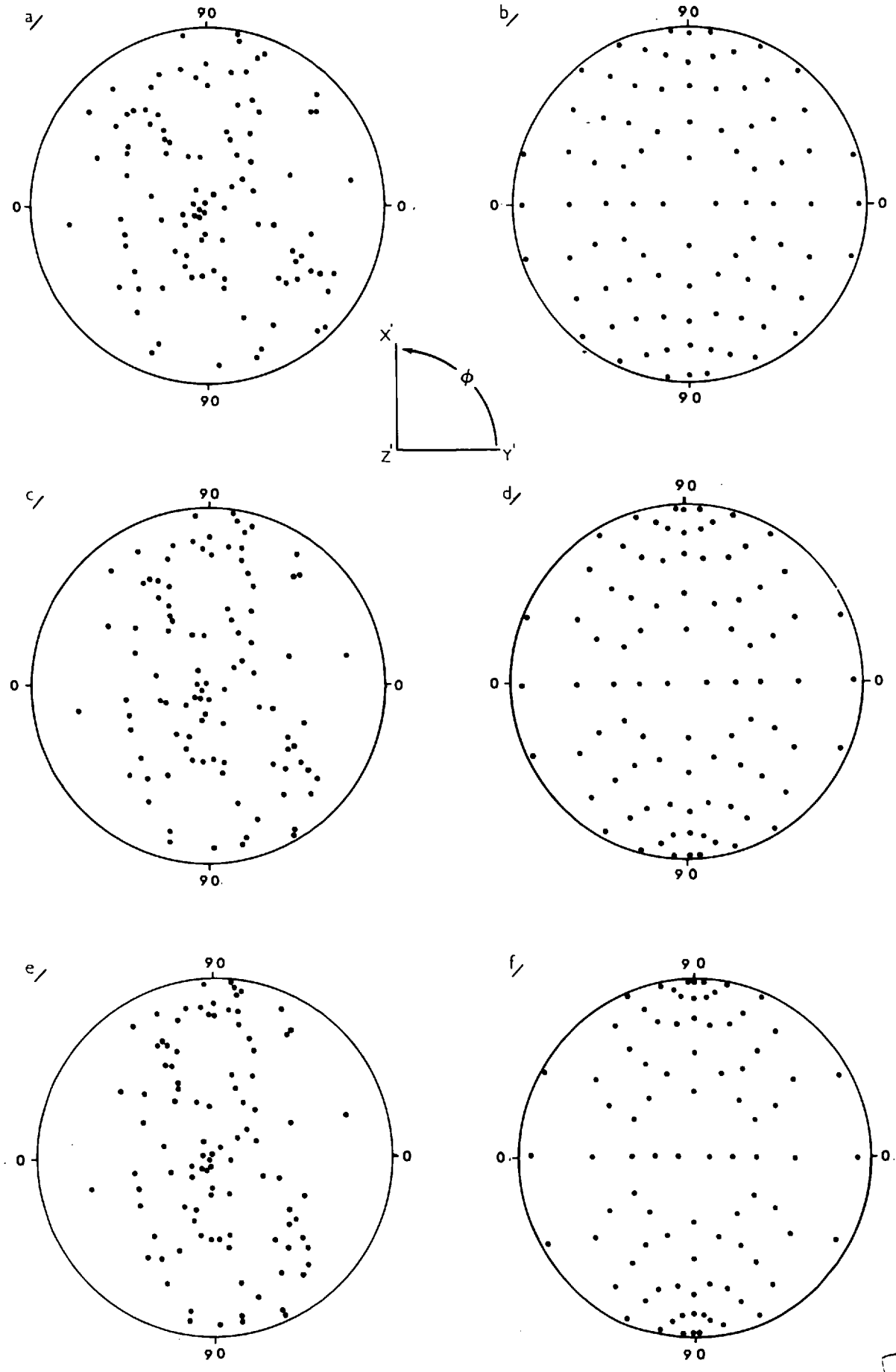
a/
b/
c/
d/
e/
f/
90
0
X'
Y'
Z'
ϕ

for values of γ_s = 1, 2 and 3. These stereographic plots show that, as predicted in the theoretical discussion, a significant preferred orientation is built up gradually and the direction of this orientation rotates toward the shearing direction ($\varphi = 90^\circ$). This is the direction of the stable degree of preferred orientation; it has not quite been reached after a shear of $3\gamma_s$ but the intensity of orientation is near its maximum value.

The changes in the initial distributions of the particle major axes during pure shear are shown in figures 51a - 51f. The applied strain ellipses have axial ratios of 2.7, 5.7 and 11. It is clear from the figures that, as predicted theoretically, a significant preferred orientation of major axes is built up parallel to the direction of elongation of the strain ellipse and that the degree of this preferred orientation increases with increasing deformation.

The pure shear strain ellipses have axial ratios approximately equal to the strains during simple shear of $1\gamma_s$, $2\gamma_s$ and $3\gamma_s$. Therefore direct comparison between figures 50 and 51 is possible. To facilitate this comparison, contour diagrams have been prepared for the plunges after $\gamma_s = 3$ and $\sqrt{\lambda_1/\lambda_2} = 11$ deformation. These diagrams are shown in figures 52. The degree of maximum concentration is approximately the same for both types of deformation though the zone of concentration is smaller in the pure shear diagrams, illustrating well the tendency to form a point concentration of major axes parallel to the direction of elongation. The development of minor preferred orientations about the Z' axis during both types of deformation is well brought out in the plots of the initially regular distributions. However, in the random diagrams, this orientation is hidden by the initial preferred orientation parallel to the Z' axis.

Figure 52 Contour diagrams of figures 50e, f; 51e, f showing the concentrations of particle major axes which are developed during simple shear (figs. a, b) and pure shear (figs. c, d).

The amount of simple shear is $3\gamma_s$; the pure shear strain ellipse has an axial ratio $\sqrt{\lambda_1/\lambda_2} = 11.0$

The contour intervals are 0 - 1%; 2 - 4%; 5 - 7%; > 7%.

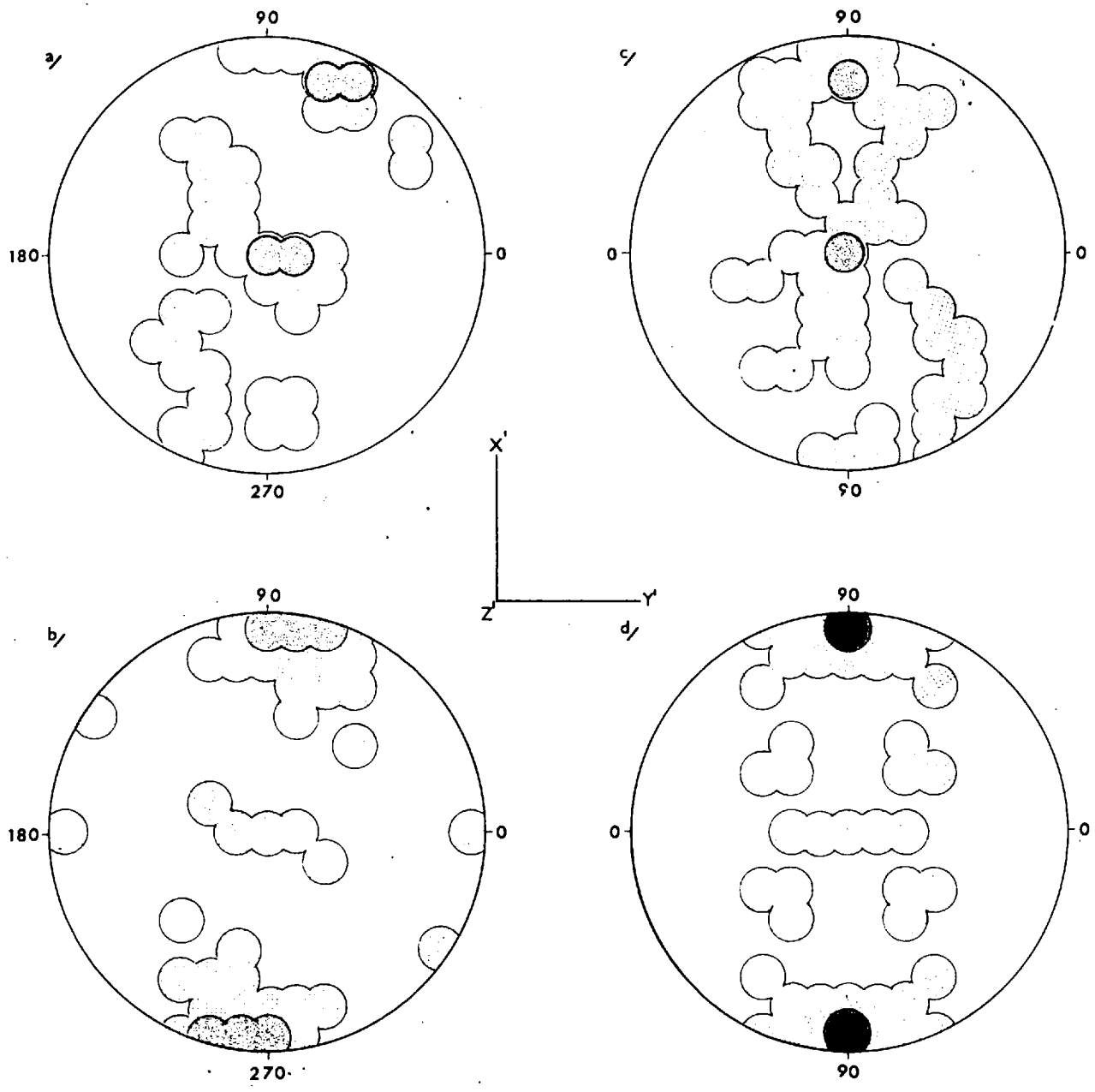
a/
90
180
0
270
c/
90
0
0
90
X'
Z'
Y'
b/
90
180
0
270
d/
90
0
0
90

It is clear from figures 50 and 51 that there is a definite correlation between the degree of preferred orientation and the amount of deformation. Therefore, it should be possible to estimate the magnitude of a pure shear deformation from the final degree of preferred orientation, provided that the initial fabric is known. In simple shear, however, the maximum preferred orientation may be set up early in the deformation and not be changed appreciably by later shearing. Therefore, only a minimum value for the shear strain can be obtained. However, if the zone of preferred orientation has not reached its stable position, a more exact estimate of the strain can be made. Non-parallelism between the shearing direction and the zone of maximum concentration of particle axes would indicate that the stable orientation has not yet been set up.

(b) Non-rigid particles

The theory describing the behaviour of non-rigid particles has only been worked out in two dimensions and, therefore, it is not possible to discuss the effect of changes in plunge of particle long axes. Nevertheless, significant conclusions about the development of preferred orientations can be drawn from the two dimensional examples of ellipses changing shape and rotating in the deformation plane.

Dealing with the pure shear deformation first, deformation paths for non-rigid ellipses with different viscosity ratios to the matrix have been shown previously in figures 33 and 35. From graphs such as these, it is possible to construct diagrams showing changes in shape and orientation for assemblages of ellipses of known axial ratio and positions. This has been done for R = 1 particles with initial axial ratios of 2 : 1 and major axes orientated

Figure 53 Diagrams to show the development of preferred orientations during pure shear of initially 2 : 1 ellipses, with viscosity ratio R = 1.

The lengths of the lines 1 - 7 give the axial ratio of the ellipses and their directions give the orientation, φ, of the major axes to the Y' pure shear axis. Lines which end in dashes are too long to fit in the diagram.

The strain ellipse axial ratios are

a) $\sqrt{\lambda_1/\lambda_2} = 1$; b) $\sqrt{\lambda_1/\lambda_2} = 2.7$

c) $\sqrt{\lambda_1/\lambda_2} = 5.7$; d) $\sqrt{\lambda_1/\lambda_2} = 11.0$

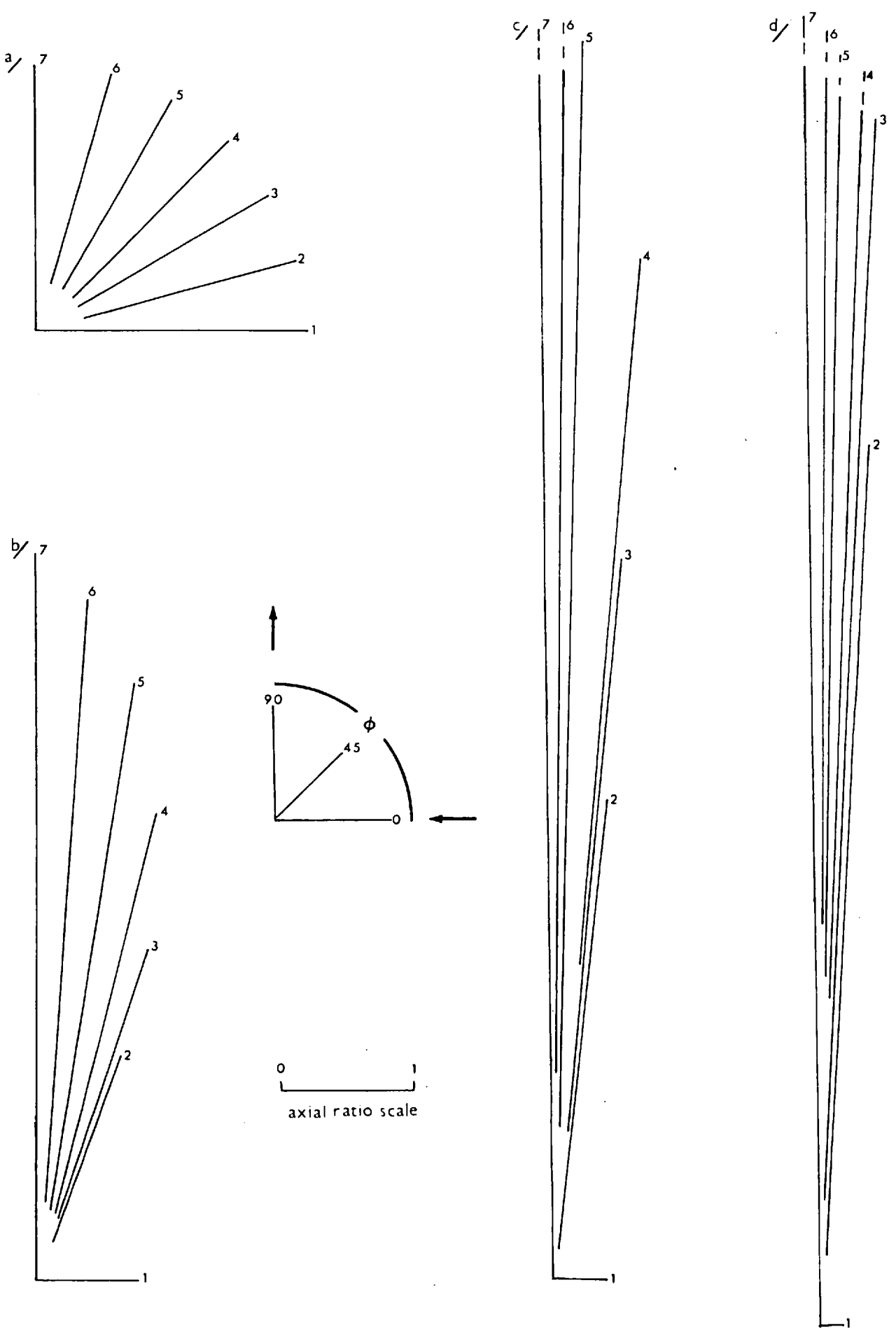
a
7
6
5
4
3
2
1
b
7
6
5
4
3
2
1
c
7
6
5
4
3
2
1
d
7
6
5
4
3
2
1
90
φ
45
0
0
1
axial ratio scale

at $\varphi = 0^{\circ}$, 15°, 30°, 45°, 60°, 75° and 90° (see figure 53a). The changes in shape and orientations of these ellipses during pure shear were determined from figure 33 and are plotted in figures 53b, c, d. The lengths of lines 1 to 7 in these figures give the axial ratio of the ellipse and their direction gives the orientation of the major axis with respect to the strain axes after the relevant amount of pure shear.

The axes of ellipses 1 and 7 do not rotate. The eccentricity of 1 decreases until eventually its axial ratio becomes equal to unity. Further deformation makes the initial major axis the minor axis and the ellipse is elongated along the $\varphi = 90^{\circ}$ direction. The eccentricity of ellipse 7 increases continually. Ellipses 2 to 6 all rotate rapidly towards the direction of elongation of the pure shear. While φ is less than 45° their eccentricity decreases but once passed this direction they elongate. Thus the effect of the pure shear deformation is to build up very rapidly a marked preferred orientation of particle long axes about the major strain axis.

Similar diagrams for ellipses with a viscosity ratio to the particle-matrix system of $R_m = 5$ are shown in figure 54. As expected, the effect of the increase in the viscosity ratio is to retard the rotation and change in shape of the ellipses. Nevertheless there is still a marked degree of preferred orientation developed about the direction of elongation.

The development of preferred orientations of non-rigid particles during simple shear cannot be examined in such detail because the theory has been developed for initially circular particles only. However, it was shown in the theoretical discussion on multiparticle systems that a preferred orientation of particle long axes should develop parallel to the shearing direction in the same way as for rigid particles, provided there is a competence

Figure 54 Diagrams to show the preferred orientations developed during the pure shear deformation of initially 2 : 1 ellipses, with viscosity ratio R = 5.

The lengths of lines 1 - 7 give the particle axial ratios and their directions give the orientation, Φ, of the major axes to the Y' pure shear axis.

The axial ratios of the strain ellipses are

a) $\sqrt{\lambda_1/\lambda_2} = 1$; b) $\sqrt{\lambda_1/\lambda_2} = 2.7$

c) $\sqrt{\lambda_1/\lambda_2} = 5.7$; d) $\sqrt{\lambda_1/\lambda_2} = 11.0$

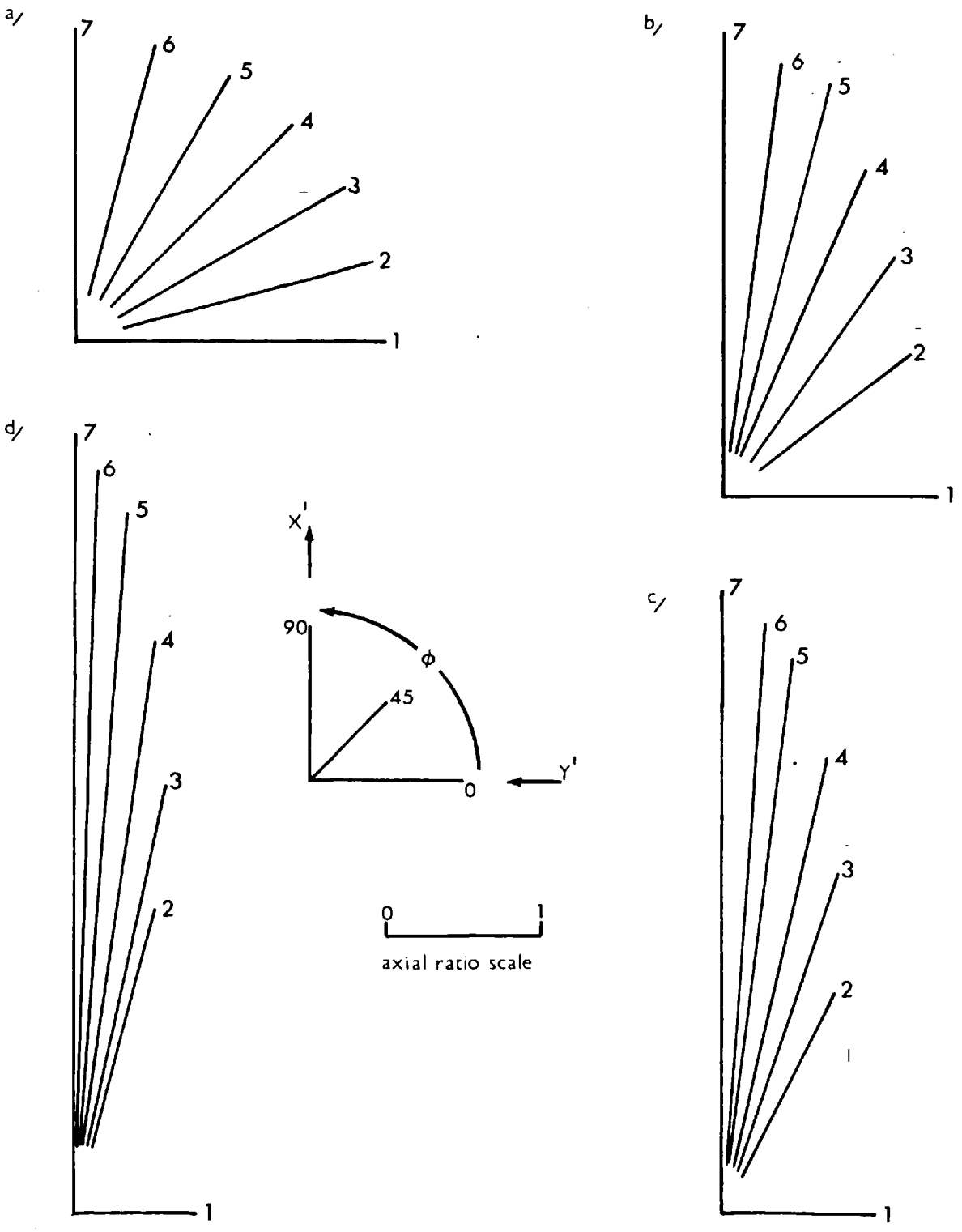
a/
7
6
5
4
3
2
1
b/
7
6
5
4
3
2
1
d/
7
6
5
4
3
2
1
X'
90
φ
45
0
Y'
0
1
axial ratio scale
c/
7
6
5
4
3
2
1

difference between the particles and the matrix. Once established, the degree of this preferred orientation should remain approximately constant despite continuing deformation. Moreover, because no deforming forces act parallel to the shearing direction, ellipses in the zone of preferred orientation will not undergo any further changes in shape.

C. THE USE OF DEFORMED PEBBLES AS QUANTITATIVE STRAIN INDICATORS

The problems associated with the use of deformed pebbles to calculate finite strain in rocks include lack of knowledge about the original pebble shapes, the relative competence differences between particles and matrix and the orientation of particles with respect to the deforming forces. It is common practice to consider these factors and make allowance for them when working on deformed conglomerates and there are available several papers and theses in which quantitative amounts of strain have been discussed (e.g. Mehnert, 1959; Oftedahl, 1948; Flinn 1956; Pavenson-Smith, 1962; Higgins, 1964; Hossack, 1965.) However, because the allowances made are to a greater or lesser extent arbitrary, the final results are necessarily subjective. Obviously, it will be impossible to remove completely all the arbitrary assumptions required for the determination of finite strain from changes in pebble shape. Nevertheless, in this section methods of surmounting some of the difficulties involved will be discussed and it is hoped that they will provide for better estimates of strain.

(a) Competence difference factor

The theory developed in this thesis provides a method for assessing the importance

of and a means of overcoming the second of the above-mentioned difficulties, namely the competence difference between particle and matrix. If the rocks have deformed under conditions in which they behave as viscous fluids, then the theory indicates that to obtain significant particle deformation, the particle-matrix viscosity ratio cannot be too large, preferably of the order of 10 : 1 or less. Moreover, if it is possible to determine this ratio, graphs such as those illustrated in figure 29 can be used to calculate the finite strain in the rock, from the deformed pebble axial ratio, whereas in the papers cited above the strain in the pebbles only has been determined.

It would be foolish, however, to suggest that the actual determination of the viscosity ratio is an easy matter. The viscous behaviour of rocks has been discussed in chapter II and values of viscosity coefficients obtained experimentally for different rock types under varying conditions were listed in table 1. Examination of these results shows variation in viscosity coefficients between 10^{15} and 10^{22} poise, which implies that R is several orders of magnitude greater than that permitted for particle deformation. However, most of these determinations were made at relatively low temperatures and pressures and it is quite likely that under conditions which are more realistic geologically, such as those required for regional metamorphism, coefficients of viscosity for different rock types would decrease and possibly tend to the same order of magnitude. Nevertheless, it must be concluded that the available experimental data on rock viscosities is unlikely to be of much use in calculating R.

A more fruitful approach is the examination of the actual rocks themselves with regard to assessing the strain in the individual components. It was pointed out in the theoretical section on the strains developed in the matrix, that the distortion around a particle could

Table VI Composition and axial ratios of deformed pebbles

Pebble type	Axial ratio	Reference
Quartz (volcanic)	1 : 1 to 2 : 1	Mehnert (1939)
Coarse quartzite	5 : 1	
Fine quartzite	8 : 1	
Dense greywacke	10 : 1 to 12 : 1	
Greywacke schist and shale	18 : 1	
Quartz	6 : 1	Higgins (1964)
Quartz-biotite-gneiss	10 : 1	
Augen gneiss	10 : 1	
Schist and amphibolite	19 : 1	
Granite	8.6 : 3.1 : 1.1	Walton et al (1964)
Quartzite	13.8 : 3.4 : 1.0	
Granite	2.3 : 1.0	Tavener-Smith (1962)
Quartzite	9 : 1.0	

be used to estimate roughly the viscosity ratio. Thus pebbles around which the schistosity or sedimentary layering is only slightly distorted, would have had a low viscosity contrast to the matrix. Around the more competent pebbles the refraction should be more marked.

It is possible to determine approximate viscosity ratios between different rock types under deformation conditions from published data on the shapes of pebbles of different compositions in the same deformed conglomerate. The first person known to the writer to describe differences in deformation of pebbles of different composition was Mehnert (1939, pp. 250 - 255) in his paper on the Wiesenthaler metaconglomerate. This information has been supplemented recently by Higgins (1964, pp. 167 - 169) from observations on the Lebendun conglomerate in Switzerland. The results of these two workers and others who have reported similar data are summarized in table VI.

To calculate the viscosity ratios between different rock types from the deformed pebble shapes it will be assumed that the pebbles were originally spherical. This is almost certainly not true but it is necessary because of lack of knowledge about the initial shapes. (This point will be discussed in more detail in the following section.) It is also assumed that pebbles in the same conglomeratic layer have experienced the same applied strain.

From the previous theory, the relevant equation for the deformation of pebble A is

$$\log (a/b)_A = [5/(2R_A + 3)] \log \sqrt{\lambda_1/\lambda_2} \quad \ldots(IV.61)$$

$$= [5\mu_m/2\mu_A + 3\mu_m)] \log \sqrt{\lambda_1/\lambda_2}$$

where μ_A is the viscosity of the pebble, μ_m the viscosity of the surrounding conglomeratic material; $R_A = \mu_A/\mu_m$.

Similarly for pebble B

$$\log (a/b)_B = [5\mu_m/(2\mu_B + 3\mu_m)] \log \sqrt{\lambda_1/\lambda_2}$$

Therefore

$$\log (a/b)_A/\log (a/b)_B = (2\mu_B + 3\mu_m)/(2\mu_A + 3\mu_m)$$

This equation can be arranged to

$$\mu_B/\mu_A = \log (a/b)_A/\log (a/b)_B - (3/2R_A)[1 - \log (a/b)_A/\log (a/b)_B] \quad ..(V.4)$$

which gives the viscosity ratio between pebbles of different composition under deformation conditions.

For example, substituting Wahnert's measurements on quartzite and shale pebble axial ratios in V.4 results in

$$\mu_{qte}/\mu_{sh} = 1.255/0.903 - (3/2R_{sh})(1 - 1.255/0.903)$$

$$= 1.4 + 0.6/R_{sh}$$

Assume $1 < R_{sh} < 100$, i.e. the shale pebble is more competent than the matrix. Then

$$1.4 < \mu_{qte}/\mu_{sh} < 2$$

which indicates that the viscosity ratio of quartzite to shale under metamorphic deformation conditions is of the theoretically predicted order of magnitude. Similar calculations have been made for the viscosity ratios between other rock types using the data listed in Table VI. The results are given in table VII.

Note that in carrying out the calculations, B has always been taken as the more competent rock type (as indicated by the pebble axial ratios). Slightly different results are obtained if A is taken to have the greater

Table VII Viscosity ratios calculated from the deformed pebble shapes listed in table VI.

Pebble types	Viscosity ratio	Source reference
Volcanic quartz/ fine quartzite	3 - 6	Mehnert (1939)
Coarse quartzite/ fine quartzite	1.3 - 1.75	
Fine quartzite/ greywacke	1.15 - 1.4	
Greywacke/shale	1.2 - 1.5	
Fine quartzite/ shale	1.4 - 2	
Quartz/gneiss	1.3 - 1.75	Higgins (1964)
Gneiss/schist	1.3 - 1.7	
Quartz/schist	1.65 - 2.6	
Granite/quartzite	1.2 - 1.55	Walton et al (1964)
Granite/quartzite	2.6 - 5	Tavener-Smith (1962)

Table VIII Viscosity ratios for different rock types relative to a shale or schist matrix.

Rock type	Viscosity ratio	Source reference
Shale	1.0	Mehnert (1939)
Greywacke	1.2 - 1.5	
Fine quartzite	1.4 - 2.0	
Coarse quartzite	1.8 - 3.5	
Volcanic quartz	4.2 - 12.0	
Schist	1.0	Higgins (1964)
Gneiss	1.3 - 1.7	
Quartz	1.7 - 2.6	

viscosity ratio because the arbitrary limits assumed for R_A now apply to the more competent of the pebble types. In view of the assumption made, these values should only be used as a guide. Recalculations based on as many pebble measurements as possible should obviously be made as more data become available.

The data of Mehnert and Higgins in table VII can be rearranged to give the viscosity ratio for individual rock types relative to a shale or schist matrix. The results are listed in table VIII.

The concentration of pebbles in the conglomerates from which the measurements are made does not affect the ratios obtained because these compare only the viscosities of the two pebble rock types. However, when using the viscosity ratios to calculate strain in another conglomerate in which pebble B occurs in matrix A, the pebble concentration must obviously be considered, because with increasing number of pebbles the mean viscosity of the conglomerate is increased and hence the viscosity ratio R_m is decreased.

(b) Initial shape factor

It is difficult to make allowance for the initial shape of the particles but a qualitative idea can at least be obtained. Reference to standard texts on sedimentary rocks (e.g. Twenhofel, 1932, pp. 202 - 210) shows that the following factors are among those which affect the final pebble shapes: Original form of the rock fragment; the structure and texture of the pebble material; the durability of the material during abrasion; the distance travelled by the pebble before deposition; and the environments through which it passes and in which it is finally deposited.

Of these factors, the first three can be directly

correlated with the rock type and they control, to a certain extent, the final pebble form. For example, Wentworth (1922) has shown that flat, discoidal pebbles in a beach conglomerate were originally flat in shape and that roller-shaped forms were derived from initially elongate fragments. The shapes of the initial fragments are obviously related to the structure and texture of the rock material and one would expect laminated rocks to give rise to flat pebbles and homogenous, non-schistose rocks such as quartzite to result in spheroidal forms. Thus when working in a deformed conglomerate a qualitative idea of the original shape can be obtained from the composition of the pebble.

Quantitative corrections for original shape can only be made using data obtained from measurements on undeformed pebbles of a similar composition and environmental history to the deformed ones. It does not seem to matter whether those measurements are made on recent pebbles (as Flinn, 1956, did) or on undeformed extensions of the deformed conglomerate (as Oftedahl, 1948, did). Because of this observation, it should be feasible to define standard initial pebble shapes for the different rock types when sufficient data from undeformed pebble beds has been obtained.

Knowledge of the initial shape is important when calculating quantitative amounts of finite strains and if ignored can lead to erroneous conclusions. For example, examination of Rohnert's (1959) and Higgins's (1964) results in table VI shows that those pebbles which were probably derived from massive, homogenous rocks such as quartzite are much less eccentric than those derived from laminated material such as shales, gneisses and schists. In the discussion on the effect of the relative competence of rock types, this difference in eccentricity

was explained by the quartzites or granites having a greater viscosity than the schists. Now, it appears that part of the difference is probably due to the more ellipsoidal initial shape of the laminated pebbles. Therefore, one ought to recalculate the viscosity ratios given in table VII allowing for an initial particle shape. However in view of the scanty data and tenuous assumptions on which the calculations are made, this seems unnecessary at the moment.

(c) Initial orientation factor

Initial shape is particularly important when considering the orientation of the particles with respect to the deforming forces. As shown previously in the section on the development of preferred orientations, pebbles with their major axes parallel to the direction of shortening will become less eccentric in shape while those aligned parallel to the direction of elongation will increase in ellipticity.

With this in mind, Higgins (1964, pp. 173 - 183) and Hossack (1965, pp. 65 - 72) have constructed diagrams showing the final shapes of initially ellipsoidal pebbles, depending on their orientation to the stress field and it is evident that a wide range of pebble shapes can result in this manner. However, in the opinion of the writer, these diagrams are misleading because they tend to emphasise the possible discrepancies in pebble shape and ignore the more important fact that most of the pebbles will be rapidly reoriented into the direction of elongation and will become very much more eccentric.

Therefore, to overcome initial orientation effects, the zone of greatest preferred orientation of the pebble major axes should be found. This direction of orientation is most likely to be parallel to the direction of

elongation, if the stress field causing the deformation was an irrotational one. Then, the most eccentric pebbles in this zone should be used for any finite strain determinations because they will probably have been aligned closest to the direction of elongation during the deformation.

D. A PROCEDURE FOR ANALYZING DEFORMED CONGLOMERATES

On the basis of the above discussion the following procedure is suggested for the determination of finite strain in deformed conglomerates.

1) Record the maximum, intermediate and minimum axial lengths, the trend and plunge of the major axes, the composition of the pebbles and the surrounding matrix, and the relative concentration of pebbles to matrix.

2) Find the direction of the zone of maximum preferred orientation of the pebbles and from such factors as the symmetry of the pebble shapes, the presence or absence of rotated particles and the major regional structures, decide whether the rocks have undergone a rotational or irrotational deformation.

3) To overcome the initial orientation factor use the data from pebbles aligned parallel to the direction of greatest preferred orientation and showing maximum eccentricity.

4) From the composition of the pebbles and matrix try to estimate the viscosity ratio R, using the relationships given in tables VII and VIII.

5) Also from the composition or from measurements on undeformed pebbles, try to estimate the original shape of the pebbles.

6) Using the graphs in figure 40, determine the viscosity ratio R_m from the concentration of pebbles in the conglomerate.

7) Allowing for a mean initial shape and the viscosity ratio, use the theoretical graphs in figure 29 or equation IV.61 to obtain the finite strain in the rock from the deformed pebble axial ratio.

8) Repeat for pebbles of different composition, if possible.

9) The finite strain can be checked by determining the degree of preferred orientation and comparing it with those theoretically predicted in figures 53 and 54.

E. COMMENTS ON SOME DEFORMED CONGLOMERATES

Since Hitchcock, Hitchcock and Hagers' (1861) account of elongated and parallel pebbles in deformed conglomerates in Vermont, a large number of reports on pebble deformations and preferred orientations in conglomerates has been published in the geological literature. Most of the observers supplying this data have been content merely to record pebble shapes and parallelism of major axes to some structural direction in the host rocks, but occasionally, use has been made of the pebbles to deduce information about the type of deformation that has acted on the rock. In this section two well-known conglomerates, which have been examined in detail by other workers, will be discussed in the light of the observations made above on pebble deformation and the development of preferred orientations.

(a) The Bygdin conglomerate, Norway.

This conglomerate occurs in the Valdres Sparagmite of Central Norway. After deposition of these sediments they were overthrust by a large nappe and deformed and metamorphosed. A schistosity was developed in the rocks and pebbles now lie with their major and intermediate axes in the schistosity plane. In addition the major axes are oriented parallel to a pronounced lineation which is assumed to indicate the direction of thrusting.

Oftedahl (1948) concluded that the pebble deformation was due to a simple shearing parallel to the schistosity planes during the thrusting of the nappe over the conglomerates. To explain the fact that the pebbles now lie in the schistosity plane, he had to postulate an additional external rotation, occurring simultaneously with the shearing but of unknown origin. From the above discussion of particles deformed during simple shear, it is clear that a viscosity contrast between pebbles and matrix would account for the additional rotation in the assumed plane of shearing and the development of the preferred orientation. However, this preferred orientation would be a statistical one and not all the pebbles need have their major axes parallel to it.

From the observations of other workers (eg. Strand, 1944; Flinn, 1961; Hossack, 1965) it is clear that the type of deformation involved is more complicated than that proposed by Oftedahl. The intensity of deformation increases away from the thrust plane as would be expected from a component of simple shear along the thrust (Flinn, 1961) but the morphology of the pebbles, which vary in shape between flattened pancakes, rod-like cigars and triaxial ellipsoids, cannot be explained by this mechanism alone. Flattening perpendicular to the thrust plane is the dominant type of pebble deformation according to Hossack, and Flinn reports that it is particularly prominent adjacent to the thrust plane Moreover it is an irrotational type of deformation, and the previous discussion on particles deforming in pure shear showed that a rapid development of preferred orientation was possible in irrotational deformations. This would help explain why the pebbles lie in the schistosity plane.

Therefore, in addition to the shearing set up by the overthrusting of the nappe it seems as though compressional forces have been at least partly responsible for the deformation of the conglomerates and the associated development

of preferred orientations. This is probably still too simple a picture of what has actually happened because both Flinn and Hossack have shown from pebble symmetries that the type of deformation varies throughout the area.

(b) The Funzie Conglomerate, Shetland

The structure and deformation of theFunzie conglomerate has been discussed in detail by Flinn (1956) who also showed in later papers (1959, 1961) that it was similar in genesis, style of deformation and metamorphism but not in constituent materials, to the Norwegian conglomerates described above.

In the Funzie conglomerate, pebbles occurring immediately below the thrust plane have, as in the Bygdin conglomerate, a flattened pancake form. These pebbles grade into triaxial ellipsoids with the intermediate axes equal to the diameter of the sphere of equivalent volume. With increasing distance beneath the thrust plane, the intermediate pebble axes show a shortening of 10 per cent relative to the diameter of the equivalent sphere.

The most significant aspect of the conglomerate is the systematic variation in pebble shape over the area. The variation is due to an increase in deformation across the region, reflected by increasing elongation and a greater degree of preferred orientation of the elongated axis. For example, in the northern, least deformed part of the area the standard deviation of the trend of pebble major axes is 16°, and in the southern, highly deformed region, it is only 5°. These general observations are strikingly similar to those predicted in figures 53 and 54 for pebbles deforming in pure shear.

Flinn, in his discussion, rejects pure shear as a deformation mechanism for the conglomerate partly because of the petrofabric girdles formed by the mica flakes in the pebbles and partly because there appears to have been

deformation along all three strain axes. If a pure shear mechanism had operated there would have been no shortening along the intermediate pebble Y axis.

However, both shear and the triaxial "einengung" deformation proposed by Flinn are irrotational strains, and so one would expect the pebbles to behave in roughly the same way in both kinds of deformation field. Moreover, the observed reduction along the intermediate strain axis is small (10 per cent). Assuming that this can be ignored, the deformation becomes equivalent to a pure shear. Therefore, the present shapes and orientations of the pebbles can be used to determine quantitatively the strain experienced by the rocks, provided that adequate allowance is made for initial pebble shapes and competence differences. In view of the close correspondence between the theoretical predictions and Flinn's field observations, an attempt will be made to perform this calculation.

The original shape can be estimated from pebbles observed in modern beach deposits. Flinn provides data on mean axial lengths for quartzite pebbles from a beach in Shetland (table 1, p. 488, locality BA). Using this information, the mean ratio of maximum to minimum pebble axes is approximately 2:1. It is also stated in the paper that the pebbles are probably more competent than the matrix. For the sake of convenience a viscosity ratio R=5 will be assumed. The pebbles in the original conglomerate probably also had an initial degree of preferred orientation; this is difficult to estimate, but if it is ignored the initial situation is similar to that in figure 54.

In Flinn's zone of minimum deformation (zone VI) the ratio of maximum to minimum pebble axes varies as follows.

Locality	Axial Ratio	Locality	Axial Ratio
C25	2.9	C34	2.9
C26	3.0	C35	2.8
C27	2.9		

(Localities are plotted on figure 2 in Flinn's paper; axial ratios are given in table 1)

No data is given in the tables on the variation in the trend of the major pebble axes but in the next least deformed zone, the standard deviation of the trend is 16^{o} (table 2, locality C30).

In the area of maximum deformation (zone II) the pebble shapes are as follows:

Locality	Axial ratio	Locality	Axial ratio
C10	7.5	C12	5.0
C11	5.8		

The standard deviation in the trend of the major axis is 5^{o}.

Figure 54 predicts a theoretical maximum pebble axial ratio of 3:1 and a range in preferred orientation of $\pm$ 50^{o} after a finite strain of 2.7:1. A pebble axial ratio of 5:1 with a range of preferred orientation of $\pm$ 15^{o} is obtained after an 11:1 pure shear. The range in the preferred orientations would probably be less if an initial sedimentary fabric is taken into account.

Therefore, if the assumptions are correct, the Funzie conglomerate has experienced a pure shear type of deformation of which the strain ellipse axial ratio increased from approximately 3:1 in the least deformed area to 11:1 in the most deformed part.

SUMMARY AND CONCLUSIONS

1) This thesis is an analysis of rock deformation, assuming that a rock can be considered as an inhomogenous viscous fluid. In detail, the model is a body of homogenous viscous matrix in which are embedded much smaller, spheroidal or ellipsoidal particles. The particles may be rigid or non-rigid, with a coefficient of viscosity greater than, equal to, or less than that of the matrix. Both the matrix and the non-rigid particles are assumed to be Newtonian bodies.

2) Published work on the viscous flow of rock is reviewed to try and define the conditions under which the assumption of Newtonian flow is valid. It appears that rocks in a molten state are probably Newtonian fluids. However, at temperatures below the melting point, rock only conforms to a Newtonian body if it is subjected to deforming stresses for a long time, or if the rate of strain is very slow. Increases in temperature and pressure enhance the Newtonian flow and it is suggested that rock deforms as a Newtonian body during regional metamorphism. The type of flow during the deformation is generally laminar.

3) In the theoretical section, the changes in shape and position of the particles during deformation of the particle-matrix system, is examined using the theory of slow-moving viscous fluids. The types of flow considered are equivalent to pure shear and simple shear deformations.

4) The equations of motion for a single, rigid ellipsoid in a viscous matrix during simple shear are

$$\tan \varphi = (a/b)\tan[ab\gamma_s/(a^2 + b^2)] \quad \ldots(IV.18)$$

$$\cot \theta = \cot \theta_1/\sqrt{1 - e^2\sin^2 \varphi} \quad \ldots(IV.19)$$

The equations give the change in orientation, φ, and plunge, θ, of the major axis of the ellipsoid, during a finite simple shear, γ_s. They indicate that the particle will rotate in a spherical elliptical orbit about an axis perpendicular to the

deformation plane. The rate of rotation is greatest when the major axis is at right angles to the shear direction, and least when it is parallel to the shear direction. The plunge decreases from a maximum at right angles to the shear direction to a minimum parallel to it.

5) The equivalent equations of motion during a pure shear deformation are

$$\ln \cot \varphi_f = \ln \cot \varphi_i + [(a^2 - b^2)/(a^2 + b^2)] \cdot \ln \sqrt{\lambda_2/\lambda_1} \quad \ldots(IV.36)$$

$$\cot \theta_f / \cot \theta_i = \sqrt{\sin 2\varphi_i / \sin 2\varphi_f} \quad \ldots(IV.37)$$

$$\ln \cot \theta_f = \ln \cot \theta_i \pm (1/2)[(a^2 - b^2)/(a^2 + b^2)] \cdot \ln \sqrt{\lambda_2/\lambda_1} \quad \ldots.(IV.38)$$

The equations imply that there is no change in orientation φ of the particle major axis, if this axis is parallel to either of the strain axes. In these positions, the plunge of the axis either increases, if the axis is parallel to the direction of shortening in the system, or decreases if it is parallel to the direction of elongation.

At other orientations, particles rotate so that they tend to lie with their major axes parallel to the direction of elongation, although they only achieve this position after an infinite amount of strain. Simultaneous with this rotation, the plunge of the major axis increases, at first, and then decreases, so that the particle tends to lie with its major axis in the deformation plane, though, again, this position is only reached after an infinite pure shear.

6) The equation for the change in shape of a non-rigid, elliptical particle, which lies in the deformation plane for pure shear and has its axes parallel to the strain axes, is

$$\ln (a/b) = \ln (a_i/b_i) + [5/(2R + 3)] \ln \sqrt{\lambda_1/\lambda_2} \quad \ldots.(IV.61)$$

The equation implies that R, the viscosity ratio between the

particle and the matrix, greatly affects the deformation of the particle, during pure shear of the particle-matrix system. If R is less than 1, the particle changes shape more rapidly than the pure shear strain ellipse; if R is equal to 1, the particle is equivalent to the strain ellipse; if R is greater than 1, the particle changes shape more slowly than the strain ellipse. With increasing R, the amount of finite strain required to cause a significant change in the particle shape increases very rapidly.

7) The pure shear deformation of non-rigid particles not aligned parallel to the pure shear axes is analyzed numerically. The results show that these particles deform and rotate, simultaneously, towards the direction of elongation. The change in shape and rate of rotation decrease with an increase in the viscosity ratio. The end position parallel to the direction of elongation is only reached after an infinite amount of pure shear.

8) The simple shear of non-rigid particles lying in the deformation plane is also solved numerically. Only circular particles are considered. The results show that particles deform and rotate simultaneously. With increase in R, the change in shape decreases and the rotation increases, during a given amount of simple shear.

9) The equations of motion for the rigid particles and the changes in shape of non-rigid particles, during simple shear and pure shear, are checked experimentally in the simple shear box and the irrotational strain box. Solutions of ethyl cellulose in benzyl alcohol are used for the matrix and non-rigid particles. The rigid particles are made of aluminium or glass.

The results for the rigid particles agree satisfactorily with theory. Non-rigid particles deform as predicted until they have an axial ratio of approximately 2 : 1, after which they elongate more rapidly than expected.

10) The behaviour of systems containing a large number of particles is discussed in the light of the results for a single particle.

During simple shear, a preferred orientation of particle major axes is set up parallel to the shearing direction. Because the particles rotate continuously, this preferred orientation remains statistically constant.

In pure shear, a major zone of preferred orientation is set up parallel to the direction of elongation; simultaneously, a minor preferred orientation is developed parallel to the axis perpendicular to the deformation plane.

The number and volume of particles present in the matrix affect the mean viscosity of the particle-matrix system and, also, the viscosity ratio, which controls the particle deformation. This variation of viscosity ratio with concentration of particles is given by the equation

$$R_m = R/[1 + 5\Phi C_v(R - 1)/(2R + 3)] \quad ...(IV.89)$$

where R_m is the ratio of the viscosity of an individual particle to the viscosity of the particle-matrix system; Φ is a factor which allows for the interaction between regions of disturbance in the flow around the particles; and C_v is the volume concentration of the particles. The results of experiments to check this equation suggested that the ratio R_m changes even more rapidly than predicted.

11) The strains developed in the matrix around a particle were examined experimentally and diagrams, which show the displacement of the matrix during the deformation, were constructed. These clearly illustrate the symmetry of the flow field. Moreover, the distortion in the flow around the particle can be used to estimate the value of the viscosity ratio between the particle and the matrix.

12) Geological applications of the theory.

a) Previous work on the use of rotated crystals as strain indicators is reviewed and it is suggested that the model of

a particle rotating in a viscous fluid is a more realistic one than those previously used. Calculations of the amount of simple shear are made from the rotation of porphyroblasts in metamorphic rocks, using the equation

$$\gamma_s = 2\varphi \text{ radians} \quad \ldots(IV.9)$$

b) The use of rotated porphyroblasts in analyzing folds is discussed. A minor fold, which from conventional measuring techniques could be either a similar-type fold or a flattened flexure fold, is examined. The present orientation of the porphyroblasts, with respect to the schistosity, indicates that the fold is a flattened flexure fold.

c) The development of preferred orientations in rocks is discussed. Diagrams showing the changes in initially random and regular distributions of particles, during simple and pure shear deformations, are constructed and the degree of the preferred orientation is related to the amount of finite strain.

d) The use of deformed pebbles to estimate strain is discussed. The shapes of pebbles of different composition, in the same deformed conglomerate, are used to estimate viscosity ratios between different rock types, during deformation. Knowing this ratio, equation IV.61 can be used to relate the pebble shape to the axial ratio of the finite strain ellipse.

The shape of the pebbles is important. If it is not possible to correct for this by making measurements on undeformed pebbles, it is suggested that the composition of the deformed pebble can be used to obtain a rough idea of the initial shape: homogenous, non-schistose rocks should give rise to round pebbles; schistose rocks to flat pebbles.

The initial orientation of the pebble axes is also important, because the change in shape of the pebbles depends upon the orientation of their axes to the strain axes. In an irrotational strain field, it is possible to overcome this by using pebbles lying parallel to the direction of greatest

preferred orientation, because this direction is most likely to be closest to the direction of elongation.

e) A procedure is suggested for analyzing deformed conglomerates.

f) The results obtained by previous workers on the Bygdin and Funzie conglomerates are discussed in the light of the theory developed in this thesis. By assuming a pure shear deformation of the Funzie conglomerate, the variation in the finite strain between the least and most deformed outcrops is calculated from the present pebble shapes and orientations.

- - - - -

REFERENCES

ANDRADE E.N. da C. (1934). A theory on the viscosity of liquids. Phil. Mag., 17, 497-511, 698-732.

BALK R. (1937). Structural behaviour of igneous rocks. Mem. geol. Soc. Amer., 5, 177 pp..

BARTOK W. AND MASON S.G. (1958). Particle motions in sheared suspensions, VII. Internal circulation in fluid droplets (theoretical). J. Colloid Sci., 13, 293-307.

BARTOK W. AND MASON S.G. (1959). Particle motions in sheared suspensions, VIII. Singlets and doublets of fluid spheres. J. Colloid Sci., 14, 13-26.

BECKE F. (1924). Struktur und Kluftung. Fortschr. Min. Krist. Petr., 9, 185.

BECKER G.F. (1904). Experiments on schistosity and slaty cleavage. Bull U.S. geol. Surv., No. 241, 34 pp.

BECKER R. (1925). Uber die Plastizitat Amorpher und Kristalliner fester Korper. Z. Phys., 26, 919.

BELL R.T. AND CURRIE J.B. (1964). Photoelastic experiments related to structural geology. Proc. geol. Ass. Canada, 15, 33-51.

BHATTACHARYYA D.S. (1966). Orientation of mineral lineation along the flow direction in rocks. Tectonophysics, 3, 29-33.

BIRCH F., SCHAIRER J.F. AND SPICER H.C. (1942). Handbook of physical constants. Spec. Pap. geol. Soc. Amer., No. 36, 325 pp.

BRACE W.F. (1961). Mohr construction in the analysis of large geologic strain. Bull. geol. Soc. Amer., 72, 1059-1080.

CAREY S.W. (1953). The rheid concept in geotectonics. J. geol. Soc. Austr., 1, 67-117.

CERF R. (1951). Recherches theorique et experimentales sur l'effet Maxwell des solutions de macromolecules deformables. I and II. J. Chim. Phys., 48, 59-84, 85-105.

CHADWICK B. (1965). The structural and metamorphic geology of the Lukmanier region, Ticino-Grisons, Switzerland. Unpublished Ph.D. thesis, University of London.

CHARLESWORTH H.A.K. AND LAMBERT R. St. J (1964). Recumbent folding in metamorphic terraines. Bull. Canad. Petrol. Geol., 12, 831-846.

CLOOS E. (1946). Lineation. Mem. geol. Soc. Amer., 18, 122 pp.

CLOOS E. (1947). Oolite deformation in the South Mountain fold, Maryland. Bull. geol. Soc. Amer., 58, 843-918.

CLOOS E. (1955). Experimental analysis of fracture patterns. Bull. geol. Soc. Amer., 66, 241-256.

DANE E.B. AND BIRCH F. (1938). The effect of pressure on the viscosity of boric anhydride glass. J. Appl. Phys., 9, 669-674.

DONATH F.A. (1963). Fundamental problems in dynamic structural geology. In Donelly T.W. (Ed). The Earth Sciences - problems and progress in current research. University of Chicago Press, for William Rice University, pp. 83-103.

DORN J.E. (1957). The spectrum of activation energy for creep. In Creep and Recovery (Seminar), Amer. Soc. for Metals, Cleveland, pp. 255-283.

EINSTEIN A. (1906). Eine neue Bestimmung der Molekuldimension. Ann. der Physik, 19, 289-306.

EINSTEIN A. (1911). Berichtingung "Eine neue Bestimmung der Molekuldimension." Ann. der Physik., 34, 591-592.

FLETT J.S. (1912). In Geology of Ben Wyvis, Carn Chuinneag, Inchbae and the surrounding country. Mem. geol. Surv. Scotland, 93, p. 111.

FLINN D. (1956). On the deformation of the Funzie conglomerate, Fetlar, Shetland. J. Geol., 64, 480-505.

FLINN D. (1959). On certain geological similarities between North-East Shetland and the Jotunheim area of Norway. Geol. Mag., 96, 473-481.

FLINN D. (1961). On deformation at thrust planes in Shetland and the Jotunheim area of Norway. Geol. Mag., 98, 245-256.

FLINN D. (1962). On folding during three dimensional progressive deformation. Quart. J. geol. Soc. Lond., 98, 385-434.

FRIEDMAN I., LONG W. AND SMITH R.L. (1963). Viscosity and water content of rhyolite glass. J. geophys. Res., 68, 6523-6535.

GIGNOUX M. (1950). Comment les geologues des Alpes francaises concorvent la tectonique d'ecoulement. Geol. en Mijnbouw, 12, 342-346.

GLEN J.W., DONNER J.J. AND WEST R.G. (1957). On the mechanism by which stones in till become oriented. Amer. J. Sci., 255, 194-205.

GOODIER J.N. (1934). An analogy between the slow motions of a viscous fluid in two dimensions and systems of plane stress. Phil. Mag. (7), 17, 554-576, 800-803.

GORANSON R.W. (1940). Fracture and flow in stressed solids. Trans. Amer. geophys. Un., 21, 698-700.

GORDON R.B. (1965). Diffusion creep in the earths mantle. J. geophys. Res., 70, 2413-2418.

GRIGGS D.T. (1936). Deformation of rocks under high confining pressures. J. Geol., 44, 541-577.

GRIGGS D.T. (1939). Creep of rocks. J. Geol., 47, 225-251.

GRIGGS D.T. (1940). Experimental flow of rocks under conditions favouring recrystallization. Bull. geol. Soc. Amer. 51, 1001-1022.

GRIGGS D.T. AND HANDIN J. (Eds.) (1960). Rock deformation (a symposium). Mem. geol. soc. Amer., 79, 382 pp.

GZOVSKY M.V. (1959). The use of scale models in tectonophysics. Int. Geol. Rev., 1, 31-47.

HANDIN J. AND HAGER R.V. (1958). Experimental deformation of sedimentary rocks under confining pressure: Tests at high temperature. Bull. Amer. Ass. Petrol. Geol., 42, 2892-2934.

HAPPEL J. (1957). Viscosity of suspensions of uniform spheres. J. Appl. Phys., 28, 1288-1291.

HASKELL N.A. (1937). On the possibility of viscous behaviour in crystalline rocks under dynamometamorphic conditions. Gerlands Beitr. Geophysik, 49, 387-392.

HAUGHTON S. (1856). On slaty cleavage and the distortion of fossils. Phil. Mag., 12, 409-421.

HAUL R.A.W. AND STEIN L.H. (1955). Diffusion in calcite crystals on the basis of isotopic exchange with carbon dioxide. Trans. Faraday Soc., 51, 1280-1290.

HEARD H.C. (1963). Effect of large changes in strain rate in the experimental deformation of Yule marble. J. Geol., 71, 162-195.

HEIM A. (1878). Untersuchungen uber den Mechanismus der Gebirgsbildung. 2 vols. (Quoted by Cloos, 1946, p. 56)

HIGGINS A.K. (1964). The structural and metamorphic geology of the area between Nufenenpass and Basodino Tessin, S. Switzerland. Unpublished Ph.D. thesis, University of London.

HITCHCOCK E., HITCHCOCK C.H. AND HAGER A.D. (1861). Report on the geology of Vermont, Vol. 1, pp. 34 etc..

HOSSACK J.R. (1965). Structural analysis of the Bygdin area, Southern Norway. Unpublished Ph.D. thesis, University of Edinburgh.

JAEGER J.C. (1962). Elasticity, fracture and flow. 2nd. ed. Metheun & Co., Ltd., London, 208 pp.

JAHNKE E. AND EMDE E. (1943). Tables of functions with formulae and curves. Enlarged revised edition. Dover, New York.

JEFFERY G.B. (1922). The motion of ellipsoidal particles immersed in a viscous fluid. Proc. Roy. Soc. A, 102, 161-179.

KNOPFF E.B. AND INGERSON E. (1938). Structural petrology. Mem. geol. Soc. Amer., 270 pp.

LAMB H. (1932). Hydrodynamics. 6th. ed. Cambridge University Press, 738 pp.

LANGHEINRICH G. (1964). Vergleichende Untersuchungen uber das Verhaltnis der Schieferung zur Faltung unter Berucksichtigung des Stockwerkproblems. Neues Jb. Geol. Palaont., 120, 41-80.

LE COMTE P. (1965). Creep in rock salt. J. Geol., 73, 469-484.

McKENNELL R. (1960). The measurement and control of viscosity and related flow properties. Instrument Manual, Section XI, 3-46; Ferranti Ltd., Manchester.

MASON S.G. AND BARTOK W. (1959). The behaviour of suspended particles in laminar shear. In Rheology of Disperse Systems, Pergamon Press, London, New York, pp. 16-48

MASON S.G. AND MANLEY R.St. J. (1956). Particle motions in sheared suspensions, IV. Orientatations and interactions of rigid rods. Proc. Roy. Soc. A., 238, 117-131

MEHNERT K.R. (1939). Die Meta- Konglomerate des Wiesenthaler Gneiszuges im sachsischen Erzgebirge. Miner. petrogr. Mitt., 50, 194-272.

MISRA A.K. (1962). An investigation of time dependent deformation or "creep" in rocks. Unpublished Ph.D. thesis, University of Sheffield.

MISRA A.K. AND MURRELL S.A.F. (1965). An experimental study of the effect of temperature and stress on the creep of rocks. Geophys. J., 9, 509-535.

MOORE F. (1965). Rheology of ceramic systems. Maclaren & Sons, Ltd., London, 78 pp.

MUGGE O. (1930). Bewegungen von porphyroblasten. Neues Jb. Miner., B-B 61A, 469-510.

MURRELL S.A.F. AND MISRA A.K. (1962). Time dependent strain or "creep" in rocks and similar non-metallic materials. Trans. Instn. Min. Metall., 71, 353-378.

NADAI A. (1950). Theory of flow and fracture of solids, Vol. 1, 2nd ed. McGraw-Hill Book Company, Inc., New York, Toronto, London, 572 pp.

NADAI A. (1963). Theory of flow and fracture of solids, Vol. 2. McGraw-Hill Book Company, Inc., New York, Toronto, London, 705 pp.

NAUMANN C.F. (1839). Ueber den Linear-Parallelismus oder die Streckung mancher Gebirgssteine. Arch. f. Min. Geog. Bergbau und Huttenck, Karsten, 12, 23-38.

NICHOLS R.L. (1939). Viscosity of lava. J. Geol., 47, 290-302.

OFTEDAHL C. (1948). Deformation of quartz conglomerates in Central Norway. J. Geol., 56, 476-487.

OROWAN E. (1965). Convection in a non-Newtonian mantle, continental drift, and mountain building. In A symposium on continental drift. Phil. Trans., 258A, 284-313.

OSBERG P.H. (1952). The Green Mountain anticlinorium in the vicinity of Rochester and East Middlebury, Vermont. Bull. Vermont geol. Surv., No. 5, 127 pp.

OSOKINA D.N., GZOVSKY M.V., VINOGRADOV G.V. AND PAVLOV V.I. (1960). Optical polarization studies of plastic deformation using solutions and gels of ethyl cellulose. Kolloidnyi Zh., 22, 434-441; English translation: Colloid J. 22, 439-445.

PAI S-I. (1956). Viscous flow theory, I - Laminar flow. D. van Nostrand & Co., Princeton, N.J., 384 pp.

PHILLIPS J. (1843). On certain movements in the parts of stratified rocks. Brit. Ass. Adv. Sci., meeting at Cork, Aug., 1843, pp. 60-61.

PRICE N.J. (1964). A study of time-strain behaviour of coal measure rocks. Int. J. Rock Mech. Min. Sci., 1, 277-303.

RAMBERG H. (1959). Evolution of ptygmatic folding. Norsk. Geol. Tidsskr., 39, 99-151.

RAMSAY J.G. (1962). The geometry and mechanics of formation of "similar" type folds. J. Geol., 70, 309-327.

REINER M. (1960a). Lectures on theoretical rheology. 3rd. ed. North-Holland Publishing Company, Amsterdam, 158 pp.

REINER M. (1960b). Deformation, strain and flow. H.K. Lewis & Co., Ltd., London, 347 pp.

REUSCH H. (1887). Geologische Beobachtungen in einen regional-metamorphosierten Gebiet am Hardangerfjord in Norwegen. Neues Jb. Miner., B-B 5, 52-67.

ROBERTSON E.C. (1964). Viscoelasticity of rocks. In Judd W.R. (Ed.). State of stress of the earth's crust. American Elsevier Publishing Company, Inc., pp. 181-233.

ROUX A.J.A. AND DENKHAUS H.G. (1954). An analysis of the problem of rock bursts in deep level mining. Part 2. J. Chem. Met. Min. Soc. S. Afr., 55, 103-124.

RUMSCHEIDT F.D. AND MASON S.G. (1961). Particle motions in sheared suspensions, XI. Internal circulation in fluid droplets (experimental). J. Colloid. Sci., 16, 210-237.

SANDER B. (1930). Gefugekunde der Gesteine. Julius Springer, Wien, 352 pp.

SANDER B. (1950). Einfuhrung in die Gefugekunde der Geologischen Korper, II teil. Springer Verlag, Wien und Innsbruck, 409 pp.

SCHMIDT W. (1918). Bewegungspuren in Porphyroblasten krystalliner Schiefer. S.B. Akad. Wiss. Wien, Abt 1, 127, 293-310.

SCROPE G.P. (1825). Consideration on volcanoes. W. Phillips, London, 270 pp.

SHARPE D. (1846). On slaty cleavage. Quart. J. geol. Soc. Lond., 3, 74-104.

SHAW H.R. (1963). Obsidian - H_2O viscosities at 1000 to 2000 bars in the temperature range 700° to 900°C. J. geophys. Res., 68, 6337-6343.

SORBY H.C. (1853). On the origin of slaty cleavage. Edinburgh New Phil.J. 10, 137-147.

SORBY H.C. (1855). On slaty cleavage as exhibited in the Devonian limestones of Devonshire. Phil. Mag. (4), 11, 20-37.

SPRY A. (1953). Flow structure and laminar flow in bostonite dykes at Armidale, New South Wales. Geol. Mag., 90, 248-256.

SPRY A. (1963). The origin and significance of snowball structure in garnets. J. Petr., Oxford, 4, 211-222.

STRAND T. (1944). Structural petrology of the Bygdin conglomerate. Norsk. Geol. Tidsskr., 24, 14-31.

TAVENER-SMITH R. (1962). A deformed Katanga conglomerate in Northern Rhodesia. Trans. geol. Soc. S. Afr., 65(I), 177-195.

TAYLOR G.I. (1932). The viscosity of a fluid containing small drops of another fluid. Proc. Roy. Soc. A., 138, 41-48.

TAYLOR G.I. (1934). The formation of emulsions in definable fields of flow. Proc. Roy. Soc. A., 146, 501-523.

TREVALYAN B.J. AND MASON S.G. (1951). Particle motions in sheared suspensions, I. Rotations. J. Colloid Sci., 6, 345-367.

TURNER F.J. AND WEISS L.E. (1963). Structural analysis of metamorphic tectonites. McGraw-Hill Book Company, Inc., New York, Toronto, London, 545 pp.

TWENHOFEL W.H. (1932). Treatise on sedimenatation, 2nd. ed., Williams and Wilkins, Baltimore, 926 pp.

VOLAROVICH M.P. AND KORCEMKIN L.I. (1937). Der Zusammenhang zwischen der Viskositat geschmolzer Gesteine und den Aziditatskoeffizienten nach F.J. Loewinson-Lessing. Dokl. Akad. Nauk. SSSR, 17, 417-422.

WALTON M., HILLS A. AND HANSEN E. (1964). Compositionally zoned granitic pebbles in three metamorphic conglomerates. Amer. J. Sci., 262, 1-25.

WENTWORTH C.K. (1922). The shape of beach pebbles. Prof. Pap. U.S. geol. Surv. 131-C, 75-83.

WETTSTEIN A. (1886). Uber den Fischfauna des Tertiaren Glarnerschiefers. Abh. der Schweiz, Pal. Ges., 13, 101 pp.

ZHARKOV V.N. (1960). Viscosity of the interior of the earth. In Magnitskii V.A. (Ed.). Problems of theoretical seismology and physics of the earth's interior. Proc. Geophys. Inst. im O.Yu. Schmidt, No. 11, 29-49. Translated by Israel programme for Scientific Translations, 1963.

ZWART H.J. (1960). Relation between folding and metamorphism in the Central Pyrenees and their chronological succession. Geol. en Mijnbouw, 22, 163-180.

ZWART H.J. (1963). Metamorphic history of the Central Pyrenees. Pt. II. Valle de Aran. Leidse Geol. Mededel., 28, 323-376.

ZWART H.J. AND OELE J.A. (1966). Rotated magnetite crystals from the Rocroi massif (Ardennes). Geol. en Mijnbouw, 45, 70-74.

APPENDIX I THE EXPERIMENTAL RESULTS

a) The rotation of two dimensional particles during simple shear

i) Calculation of the mean experimental curves in figure 21

For each experiment performed, a graph relating the rotation, φ, to the finite simple shear, γ_s, was constructed. In this way, several graphs were obtained for each particle used in the experiments. The mean experimental curve was then calculated as follows:

1) From the origin ($\varphi_i = -90^\circ$, $\gamma_s = 0$) the rotation during a set amount of shearing ($\gamma_s = 0.5$ or 1.0) was read from all the experimental graphs for a particular ellipse.

2) The mean rotation ($\bar{x}_1$) was then determined and the new particle orientation ($\varphi_f \equiv \varphi_i + \bar{x}_1$).

3) Starting at this value of $\varphi_i' = \varphi_f$, the rotation during another increment of shear was read from the graphs and the mean value ($\bar{x}_2$) calculated.

4) $\bar{x}_2$ was then added to φ_i' to get the new mean orientation, φ_f'.

5) Starting at this value $\varphi_i'' = \varphi_f'$, the mean rotation ($\bar{x}_3$), during a further increment of shear, was found. Hence, a new orientation, φ_f'', was calculated.

6) The procedure was repeated until φ_f was equal to zero.

7) The mean curves were then plotted for φ ranging from -90° to $+90^\circ$, using the fact that they should be symmetrical about $\varphi = 0^\circ$.

ii) Statistical results for the mean experimental curves in figure 21

Table I Curve B; particle with axial ratio = 1.01 : 1.

Number of readings, n = 33

Mean rotation during 1 γ_s shear, $\bar{x} = 27.5^\circ$

Standard deviation, s = 0.762

Coefficient of variation, v = 1.71%

Range, w = 1°.

Table II Curve J; particle with axial ratio 1.36 : 1.

γ_s	$-\varphi_i^o$	$-\varphi_f^o$	$\bar{x}^o$	n	s	v%	w^o
0.5	90.0	80.5	9.5	8	0.50	5.3	1.5
1.0	80.5	70.0	10.5	8	0.59	5.6	2.0
1.5	70.0	58.5	11.5	8	1.12	9.7	3.5
2.0	58.5	45.5	13.0	8	1.00	7.7	3.5
2.5	45.5	30.0	15.5	8	0.71	4.6	2.5
3.0	30.0	13.0	17.0	8	0.92	5.4	3.0
3.5	13.0	-5.0	18.0	8	0.75	4.2	2.5

Table III Curve L; particle with axial ratio = 1.94 : 1 (mean of ellipses with axial ratios 1.92 and 1.96)

γ_s	$-\varphi_i^o$	$-\varphi_f^o$	$\bar{x}^o$	n	s	v%	w^o
0.5	90.0	84.5	5.5	7	0.47	8.5	1.5
1.0	84.5	78.5	6.0	8	0.61	10.2	1.5
1.5	78.5	72.0	6.5	8	0.47	7.2	1.0
2.0	72.0	64.0	8.0	8	0.64	8.0	2.0
2.5	64.0	54.0	10.0	8	0.61	6.1	2.0
3.0	54.0	40.5	13.5	7	0.43	3.2	1.0
3.5	40.5	22.5	18.0	7	0.47	2.6	1.5
4.0	22.5	0.5	22.0	8	0.97	4.4	3.0

Table IV Curve D; particle with axial ratio 2.70 : 1.

γ_s	$-\varphi_i^o$	$-\varphi_f^o$	$\bar{x}^o$	n	s	v%	w^o
0.5	90.0	88.0	2.0	7	0.59	29.5	1.5
1.0	88.0	85.5	2.5	7	0.39	15.5	1.0
1.5	85.5	83.0	2.5	7	0.46	18.5	1.5
2.0	83.0	80.5	2.5	7	0.42	16.9	1.0
2.5	80.5	77.5	3.0	7	0.33	10.9	1.0
3.0	77.5	74.0	3.5	7	0.33	9.4	1.0
3.5	74.0	69.5	4.5	7	0.59	13.1	1.0
4.0	69.5	63.5	6.0	7	0.57	9.4	1.5
4.5	63.5	55.0	8.5	7	0.80	9.4	2.5
5.0	55.0	43.0	12.0	7	0.91	7.5	2.5
5.5	43.0	25.5	17.5	7	1.30	7.4	3.5
6.0	25.5	0.0	25.5	7	1.10	4.3	4.0

Table V Curve F; particle with axial ratio = 3.66 : 1

γ_s	$-\varphi_i^o$	$-\varphi_f^o$	$\bar{x}^o$	n	s	v%	w^o
0.5	90.0	88.5	1.5	5	0.59	39.4	1.5
1.0	88.5	87.0	1.5	5	0.39	25.8	1.0
1.5	87.0	85.5	1.5	5	0.45	30.0	1.0
2.0	85.5	84.0	1.5	5	0.45	30.0	1.0
2.5	84.0	82.5	1.5	5	0.45	30.0	1.0
3.0	82.5	81.0	1.5	5	0.45	30.0	1.0
3.5	81.0	79.0	2.0	5	0.39	19.5	0.5
4.0	79.0	76.5	2.5	5	0.55	21.9	1.5
4.5	76.5	74.0	2.5	5	0.55	21.9	1.5
5.0	74.0	70.5	3.5	5	0.39	11.1	1.0
5.5	70.5	66.0	4.5	5	0.67	14.9	2.0
6.0	66.0	60.0	6.0	5	0.93	15.4	2.0
6.5	60.0	51.0	9.0	5	0.71	7.8	2.0
7.0	51.0	38.5	12.5	5	0.67	5.4	2.0
7.5	38.5	18.0	20.5	5	1.14	5.6	3.5
8.0	18.0	-7.5	25.5	5	1.02	4.0	3.0

Table VI Curve H; particle with axial ratio = 4.71 : 1

γ_s	$-\varphi_i^o$	$-\varphi_f^o$	$\bar{x}^o$	n	s	v%	w^o
0.5	90.0	89.5	0.5	4	0	0	0
1.0	89.5	89.0	0.5	4	0	0	0
1.5	89.0	88.5	0.5	4	0	0	0
2.0	88.5	88.0	0.5	4	0	0	0
2.5	88.0	87.5	0.5	4	0	0	0
3.0	87.5	87.0	0.5	4	0	0	0
3.5	87.0	86.5	0.5	4	0.25	50.0	0.5
4.0	86.5	86.0	0.5	4	0.25	50.0	0.5
4.5	86.0	85.5	0.5	4	0.25	50.0	0.5
5.0	85.5	85.0	0.5	4	0.25	50.0	0.5
5.5	85.0	84.5	0.5	4	0.25	50.0	0.5
6.0	84.5	83.5	1.0	4	0.35	35.0	0.5
6.5	83.5	82.5	1.0	4	0.35	35.0	0.5
7.0	82.5	81.5	1.0	4	0.25	25.0	0.5
7.5	81.5	80.5	1.0	4	0.25	25.0	0.5
8.0	80.5	79.0	1.5	4	0.35	23.6	1.0
8.5	79.0	77.0	2.0	4	0.50	25.0	1.0
9.0	77.0	74.5	2.5	4	0.61	24.5	1.5
9.5	74.5	71.5	3.0	4	0.61	20.4	1.5
10.0	71.5	67.5	4.0	4	0.35	8.8	0.5
10.5	67.5	62.0	5.5	4	0.50	9.1	1.0
11.0	62.0	53.5	8.5	4	0.35	4.2	0.5
11.5	53.5	42.0	11.5	4	0.25	2.2	0.5
12.0	42.0	22.0	20.0	4	0.50	2.5	1.0
12.5	22.0	-5.0	27.0	4	0.35	1.3	1.0

b) The rotation of 4 : 1 : 1 ellipsoids in simple shear.

Table VII Results for the experimental curves in figure 22D.

	a)		b)		c)		d)		e)		f)	
γ_s	φ^o	θ^o	φ^o	θ^o	φ^o	θ^o	φ^o	θ^o	φ^o	θ^o	φ^o	θ^o
0	-2	36	-2	41	-3	55	41	40	44	35	58	23
0.5	28	28	23	37	13	52	56	36	55	31	65	18
1.0	-	-	35	33	24	48	61	33	63	25	70	15

c) The rotation of two dimensional particles in the irrotational strain box.

Table VIII Results for the experimental curves in figure 25

		2 : 1		4 : 1	
$\sqrt{\lambda_1/\lambda_2}$ th	$\sqrt{\lambda_1/\lambda_2}$ exp	φ^o	φ^o	φ^o	φ^o
1.00	1.00	15.0	45.0	15.0	45.0
1.25	1.40	19.0	50.0	21.0	53.0
1.45	1.80	23.5	54.0	26.0	60.0
1.80	2.60	26.0	60.0	35.0	66.0
2.15	3.50	31.0	64.0	45.0	76.0
2.55	4.60	37.0	67.0	53.0	75.0
3.20	6.20	43.0	71.0	62.0	80.0
3.70	8.40	45.0	74.0	65.0	-
4.60	12.00	49.0	79.0	69.0	-
1.00	1.00	75.0		75.0	
1.60	2.15	78.0		81.0	
1.90	2.85	81.0		82.0	
2.30	4.00	82.0		85.0	
2.65	5.10	83.0		86.0	
3.30	7.00	85.0		87.0	
4.00	9.80	86.0		88.0	
4.75	13.00	89.0		89.0	

d) The rotation of 4 : 1 : 1 ellipsoids in the irrotational strain box.

Table IX Results for the experimental curves in figures 26 and 27.

	26)		27A)		27B)		27C)		27D)	
$\sqrt{\lambda_1/\lambda_2}$	φ^o	θ^o	φ^o	θ^o	φ^o	θ^o	φ^o	θ^o	φ^o	θ^o
1.00	0	25	60	37	58	26	49	20	30	0
2.75	0	33	73	25	73	18	56	16	35	0
7.60	0	50	80	22	86	10	68	13	44	3

e) The deformation of non-rigid particles in the irrotational strain box

Table X Results for the experimental curves in figures 30a-f.

	$\sqrt{\lambda_1/\lambda_2}$	a_i/b_i	A_i	a/b	A	a/b^+
a/	1.42	1.02	10.4	1.46	12.3	1.43
	1.74	0.95	19.1	1.67	25.4	1.77
	2.16	0.95	19.1	2.34	24.0	2.46
	2.75	1.02	16.7	2.77	19.5	2.72
	3.00	1.03	16.0	4.00	17.7	3.88
	4.00	0.94	9.6	5.00	12.8	5.32
	1.42	1.03	15.6	1.44	14.8	1.40
	1.74	1.01	20.2	1.73	24.4	1.71
	2.16	1.00	13.0	2.82	14.9	2.82
	2.75	1.00	11.9	3.05	16.1	3.05
b/	1.42	1.00	23.0	1.35	25.0	1.35
	1.74	0.99	24.3	1.48	26.0	1.49
	2.16	1.06	23.5	1.63	28.0	1.54
	2.72	1.00	29.7	1.84	35.6	1.84
	3.00	1.05	33.4	1.80	41.3	1.71
	4.60	0.99	24.2	2.77	34.0	2.80
	5.80	1.00	24.0	3.44	31.2	3.44
	1.42	0.99	10.7	1.17	10.5	1.19
	1.74	0.99	11.4	1.28	12.2	1.30
	2.16	0.96	11.4	1.52	11.1	1.58
	3.00	0.97	11.6	1.81	12.2	1.86
	4.60	1.03	11.2	3.44	13.8	3.35
	5.80	1.00	13.0	6.66	13.0	6.66
c/	1.42	0.97	11.9	1.12	11.9	1.16
	1.70	1.00	10.3	1.18	10.7	1.18
	2.16	0.97	11.2	1.30	11.7	1.33
	3.00	1.03	11.2	1.67	11.3	1.62
	4.60	0.98	11.0	2.52	11.1	2.56
	5.90	1.00	13.0	2.62	12.8	2.62
d/	1.42	0.97	11.4	1.08	11.7	1.11
	1.74	0.97	11.2	1.12	11.5	1.16
	2.16	1.01	11.1	1.25	11.3	1.23
	3.00	1.00	13.0	1.69	13.9	1.69
	4.60	1.00	11.2	1.84	11.0	1.84
	5.80	1.00	12.5	1.49	13.9	1.49

a_i/b_i - initial axial ratio

a/b - final axial ratio

a/b^+ - final axial ratio, corrected for initial shape.

A_i, A - initial and final area factors

Table X, continued.

	$\sqrt{\lambda_1/\lambda_2}$	a_i/b_i	A_i	a/b	A	a/b^+
e/	1.42	1.05	33.0	1.10	33.0	1.04
	1.74	1.00	35.0	1.11	36.0	1.11
	2.16	1.00	21.5	1.19	22.0	1.19
	2.60	0.99	38.0	1.21	39.0	1.22
	3.00	0.96	34.0	1.22	33.5	1.27
	4.10	1.00	36.5	1.38	38.5	1.38
	4.60	0.97	35.0	1.37	34.5	1.42
f/	1.42	1.00	23.0	1.09	23.0	1.09
	2.16	1.00	24.0	1.10	24.0	1.10
	3.00	1.02	23.5	1.18	24.0	1.15
	4.60	0.98	24.5	1.25	24.5	1.27
	7.50	1.07	22.5	1.30	23.0	1.22

f) The deformation of non-rigid particles in the simple shear box

Table XI Results for the experimental curves in figures 39A-F

	γ_s	a/b	φ^o	a/b^+	a/b	φ^o	a/b^+
A/	0	1.00	45	1.00			
	0.25	1.27	46	1.27			
	0.50	1.59	51	1.59			
	0.75	2.04	55	2.04			
	1.00	2.52	58	2.52			
B/	0	1.01	45	1.00	1.00	45	1.00
	0.50	1.40	53	1.38	1.35	50	1.35
	0.75	1.67	58	1.64	-	-	-
	1.00	1.86	61	1.83	1.76	56	1.76
	1R	1.92	55	1.89	1.75	57	1.75
	1.25	2.30	60	2.27	-	-	-
	1.50	2.60	64	2.56	2.33	64	2.33
	1.75	3.02	65	2.97	-	-	-
	2.00	3.48	67	3.43	2.94	67	2.94
	2R	-	-	-	3.02	66	3.02
	2.50	-	-	-	3.28	69	3.28
	3.00	-	-	-	4.00	72	4.00

R indicates that the particle has been repositioned

Table XI, continued.

	γ_s	a/b	φ^o	a/b^+	a/b	φ^o	a/b^+
C/	0	0.99	45	1.00	1.00	45	1.00
	0.50	1.16	52	1.17	1.14	55	1.14
	1.00	1.39	58	1.40	1.32	62	1.32
	1R	1.40	48	1.42	1.33	56	1.33
	1.50	1.68	57	1.70	1.52	64	1.52
	2.00	2.06	64	2.08	1.70	66	1.68
	2R	1.87	63	1.89	1.68	66	1.68
	2.50	2.21	69	2.23	1.93	70	1.93
	3.00	2.55	72	2.57	2.12	73	2.12
	3R	-	-	-	2.11	67	2.11
	3.50	-	-	-	-	-	-
	4.00	-	-	-	2.63	74	2.63
	4R	-	-	-	2.65	71	2.65
	4.50	-	-	-	2.97	73	2.97
	5.00	-	-	-	3.42	76	3.42
D/	0	1.01	45	1.00	0.98	45	1.00
	0.50	1.18	54	1.16	-	-	-
	1.00	1.37	58	1.35	1.29	58	1.32
	1R	1.35	60	1.33	1.30	57	1.32
	1.50	1.51	62	1.48	1.45	63	1.48
	2.00	1.70	66	1.68	1.59	69	1.62
	2R	1.75	64	1.73	1.59	73	1.62
	2.50	1.98	68	1.94	1.75	77	1.78
	3.00	2.19	72	2.16	1.90	80	1.94
	3R	2.24	68	2.20	1.88	74	1.92
	3.50	2.68	71	2.64	2.04	76	2.08
	4.00	2.98	75	2.94	2.18	77	2.22
	4R	-	-	-	2.15	74	2.22
	4.50	-	-	-	2.30	77	2.34
	5.00	-	-	-	2.48	79	2.54

Table XI, continued.

	γ_s	a/b	φ^o	a/b^+	a/b	φ^o	a/b^+
E/	0	1.00	45	1.00	1.00	45	1.00
	0.50	1.15	51	1.15	1.10	51	1.10
	1.00	1.27	60	1.27	1.21	59	1.21
	1R	1.27	58	1.27	1.19	55	1.19
	1.50	1.42	65	1.42	1.33	62	1.33
	2.00	1.60	68	1.60	1.42	67	1.42
	2R	1.62	68	1.62	1.39	66	1.39
	2.50	1.82	74	1.82	1.56	70	1.56
	3.00	-	-	-	1.66	75	1.66
	3R	1.89	74	1.89	1.64	74	1.64
	3.50	2.00	76	2.00	1.70	77	1.70
	4.00	2.18	79	2.18	1.79	79	1.79
	4R	-	-	-	1.77	75	1.77
	4.50	-	-	-	1.84	79	1.84
	5.00	-	-	-	1.99	83	1.99
F/	0	1.04	45	1.00			
	0.50	1.17	57	1.13			
	1.00	1.22	66	1.18			
	1R	1.23	54	1.19			
	1.50	1.35	62	1.29			
	2.00	1.45	67	1.39			
	2R	1.49	67	1.43			
	2.50	1.57	74	1.51			
	3.00	1.70	79	1.63			
	3R	1.66	80	1.59			
	3.50	1.76	82	1.69			
	4.00	1.75	86	1.68			
	4R	1.82	85	1.80			
	4.50	1.87	87	1.80			
	5.00	1.90	90	1.83			

g) The effect of increasing volume concentration on particle deformation

Table XII Results for the experimental points in figures 41

Point	C_v%	a/b	range	φ^o	range	R_m
1	3	1.44	0.04	59	1	5
2	6	1.45	0.12	61	2	5
3	9	1.55	0.19	60	5	4
4	12	1.68	0.21	57	6	3
5	15	1.73	0.23	57	10	2.75
6	23	2.07	0.82	63	6	2